6TH INTERNATIONAL MAAR CONFERENCE - ABSTRACTS

CHANGCHUN, CHINA

JULY 30 - AUGUST 3, 2016

Edited by **Jiaqi Liu**

INTECH

INTECH
open science | open minds

6th International Maar Conference - Abstracts
http://dx.doi.org/10.5772/64766
Edited by Jiaqi Liu

Published by InTech
Janeza Trdine 9, 51000 Rijeka, Croatia

© The Editor(s) and the Author(s) 2016
The moral rights of the editor(s) and the author(s) have been asserted.
All rights to the book as a whole are reserved by InTech. The book as a whole (compilation) cannot be reproduced, distributed or used for commercial or non-commercial purposes without InTech's written permission. Enquiries concerning the use of the book should be directed to InTech's rights and permissions department (permissions@intechopen.com).
Violations are liable to prosecution under the governing Copyright Law.

Individual manuscripts of this publication are distributed under the terms of the Creative Commons Attribution 3.0 Unported License which permits commercial use, distribution and reproduction of the individual manuscripts, provided the original author(s) and source publication are appropriately acknowledged. More details and guidelines concerning content reuse and adaptation can be found at http://www.intechopen.com/copyright-policy.html.

Notice
Statements and opinions expressed in the manuscripts are these of the individual contributors and not necessarily those of the editors or publisher. No responsibility is accepted for the accuracy of information contained in the published manuscripts. The publisher assumes no responsibility for any damage or injury to persons or property arising out of the use of any materials, instructions, methods or ideas contained in the book. Review of the content was conducted by the 6th International Maar Conference.

Cover: InTech Design Team
Photo: Zhensheng Yu

First published July, 2016

6th International Maar Conference - Abstracts, Edited by Jiaqi Liu
p.cm.
Print ISBN: 978-953-51-2540-2
Online ISBN: 978-953-51-2541-9

Previous IMC's

International Maar Conference
Daun, Germany, 2000

Second International Maar Conference
Lajosmizse, Hungary, 2004

Third International Maar Conference
Malargüe, Argentina, 2009

Fourth International Maar Conference
Auckland, New Zealand, 2012

Fifth International Maar Conference
Querétaro, Mexico, 2014

Conference Supporters

International Association of Volcanology and Chemistry of Earth´s Interior (IAVCEI)

International Association of Sedimentologists (IAS)

National Natural Science Foundation of China (NSFC)

Chinese Academy of Sciences (CAS)

Institute of Geology and Geophysics, Chinese Academy of Sciences (IGGCAS)

Guangzhou Institute of Geochemistry, Chinese Academy of Sciences (GIGCAS)

State Key Laboratory of Isotope Geochemistry, Guangzhou Institute of Geochemistry, Chinese Academy of Sciences

Jilin University

Arxan National Geopark Administration, Inner Mongolia

Zhalantun National Scenic Area Management Committee, Inner Mongolia

Longwan National Nature Reserve Administration, Jilin Province

Jingyu National Nature Reserve Administration, Jilin Province

Changbai Mountain Protection and Development Zone of Jilin Province

Scientific Committee

J. Liu, Chair
J. Negendank, Co-Chair
G.C. Núñez, Co-Chair
J. Marti, Co-Chair
Y. Xu, Co-Chair

Members

B. van Wyk de Vries
B. Zimanowsk
B. Zolitschka
F. Goff
G. Valentine
G. Chu
H. Kitagawa
I. Smith
J. Han
K. Nemeth
M.N. Guilbaud
M. Koziol
M. Ort
M. Stein
P. Rioual
R. Cas
S. Rasskazov
S. Leroy
Y. Erel
Y.S. Lee
Y.K. Sohn
Y. Zhang

Organizing Committee

J. Liu, Chair
X. Han, Co-Chair
F. Sun, Co-Chair
Y. Chai, Co-Chair
F. Wu, Co-Chair
K. Nemeth, Co-Chair
B. Zhou, Co-Chair

Members

J. Xiao
Q. Liu
Q. Yang
W. Xu
Y. Zhao
Z. Guo
Z. Zhou

Secretary

J. Wu
C. Lan
J. Che

Abstract-making panel

W. Baek, Republic of Korea
X. Bolós, Spain
C. Chen, China
S. Chen, China
X. Chen, China
Y. Choi, Republic of Korea
G. Chu, China
S. Cronin, New Zealand
L. Ding, China
E. Duarte, Costa Rica
J. Gao, China
S. Go, Republic of Korea
I. Gravis, New Zealand
Q. Jin, Republic of Korea
Z. Guo, China
V. Khomich, Russia
G. Kim, Republic of Korea
H. Kitagawa, Japan
W. Klöckner, Germany
W. Lee, Republic of Korea
Y. Lee, Republic of Korea
L. Li, China
T. Li, China
J. Liu, China
A. Moatari-Kazerouni, Iran
K. Németh, New Zealand
C. Oh, Republic of Korea
M. Park, Republic of Korea
S. Rasskazov, Russia
P. Reynolds, Australia
P. Rioual, China
V. Sakhno, Russia
I. Seghedi, Romania
C. Siebe, México
I. Smith, New Zealand
C. Sohn, Republic of Korea
C. Sun, China
K. Tao, China
R. van Niekerk, New Zealand
G. Ventura, Italy
M. van Wyk de Vries ,UK
H. Wang, China
J. Wu, China
D. Xu, China
M. Yu, China
S. Zaarur, Israel
M. Zhang, China
L. Zhang, China
B. Zhao, China
W. Zhou, China
B. Zolitschka, Germany

Contents

Preface

We cordially welcome you to the Sixth International Maar Conference (6IMC) and look forward to hosting you in Changchun, China. We anticipate an exciting week of scientific exchanges, renewing friendships and making new friends.

The IMC has been held five times. The 1IMC was held in Daun, Germany, 2000. Four years later, the 2IMC was held in Hungary. In 2009, the 3IMC shifted to the Southern Hemisphere; Argentina hosted the 3IMC in Malargüe. The 4IMC is held in Auckland, New Zealand, in 2012. Mexico hosted the 5IMC in Querétaro, 2014.

The 6IMC on maar-diatreme volcanism and associate processes is held in Asia for the first time. Changchun sits in the hinterlands of the Song Liao Plain of Northeast China. It is the capital city of Jilin Province, which is the nearest big city away from maar-concentrated distribution area in China. The 6IMC is a scientific event supported by the International Association of Volcanology and Chemistry of the Earth Interior (IAVCEI) and is enthusiastically supported by the International Association of Sedimentologists (IAS).

The Changchun Conference is also officially supported by the National Natural Science Foundation of China (NSFC), Chinese Academy of Sciences (CAS), Institute of Geology and Geophysics Chinese Academy of Sciences (IGGCAS), Guangzhou Institute of Geochemistry Chinese Academy of Sciences (GIGCAS), State Key Laboratory of Isotope Geochemistry of China, Jilin University, Arxan National Geopark Administration, Inner Mongolia, Zhalantun National Scenic Area Management Committee, Inner Mongolia, Longwan National Nature Reserve Administration, Jilin Province, Jingyu National Nature Reserve Administration, Jilin Province, Changbai Mountain Protection and Development Zone of Jilin Province.

Fifty-one authors from 15 countries presented 56 abstracts, which were reviewed by the Scientific Committee.

We hope you will find the 6IMC a memorable event and the Abstract Volume a useful collection and enjoy Changchun and surrounding.

With best wishes,

The Organizing and Scientific Committees

Measurement of Surface Deformation on Mt. Baekdu/Chanbai by Using Sentinel-1 SAR Interferometrty

Won-Kyung Baek[1,*], Hyung-Sup Jung[1], Min-Jeong Jo[2], Sung-Ho Chae[1], Nam-Ki Jeong[1], Sunmin Lee[1], and Daeseong Kim[1]

[1]*Deparment of Geoinformatics, University of Seoul, Seoul, Korea*
[2]*Department of Earth System Sciences, Yonsei University, Seoul, Korea*
*Corresponding author E-mail: bekwkz@uos.ac.kr

Keywords: SAR, InSAR, Mount Baekdu/Changbai

Mount Baekdu or Changbai, which is a stratovolcano, is an active volcano located on the border between Korea and China (Figure 1). Although some gentle volcanic movements were only observed recently, it is known that one of the most notable eruptions occurred around 1000 years ago whose volcanic ash was found on Hokkaido, Japan. Moreover, recently a significant magma storage was suggested, and accordingly the concerns of eruption and the necessity of periodic observation were gradually increased (Kim, 2002; Yun and Lee, 2012). However, the research of volcanic activities on Mount Baekdu has not been performed sufficiently. The reason is that Mount Baekdu is not a very accessible area.

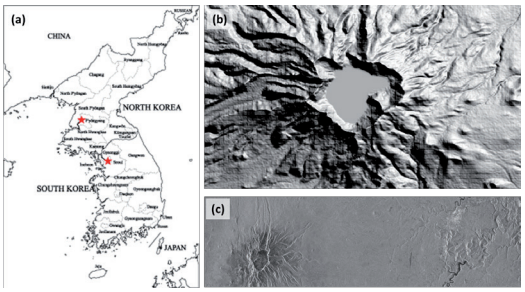

Figure 1. (a) Geological location of study area, Mount. Baekdu/Chanbai. (b) Shuttle Radar Topography Mission (SRTM) of study area. (c) Sentinel-1 amplitude image of the study area.

Meanwhile, satellite SAR interferometry (InSAR) has been successfully applied to measure ground surface deformation. Observation using InSAR was improved by mitigating error component from time-series deformation signal using the sufficient number of multitemporal SAR imagery. It is known that at least 20 images are needed to mitigate noise signal properly (Ferretti et al., 2001). Moreover, in case the portion of meaningful signal is small, additional images are needed. Therefore, sufficient data accumulation should be preceded to apply multitemporal approaches.

In this point of view, Sentinel-1 data could be utilized to apply the multitemporal approach. The first reason is that every data is distributed for free. And second reason is for its short revisit time. Even though Sentinel-1 has revisit time of 12 days now, Sentinel-1b could reduce it to 6 days by constellating two twin satellites. For these reasons, Sentinel-1 has an advantage of data accumulation to separate meaningful signal from error on a study area.

In spite of advantages of data accumulation, another factor reduces the number of available interferograms on a multitemporal approach. In case the data acquisition on the same orbit is separated for long time interval, it is difficult to build up interferogram between earlier group of data and later group of data because of temporal decorrelation.

In this study, we would observe time-series ground surface deformation of Mount Baekdu using multitemporal SAR interferometry. In this process, we adopted refined small baseline subset (SBAS) (Jung et al., 2008) to mitigate atmospheric effect. For the preliminary results, we used these 6 Sentinel-1 SAR data and processed 10 pairs of interferograms acquired from December 13, 2015 to Mar 30, 2016 (Figure 2). The data acquired before and after these periods were not proper to be utilized together since the temporal baseline was too long to maintain its coherence.

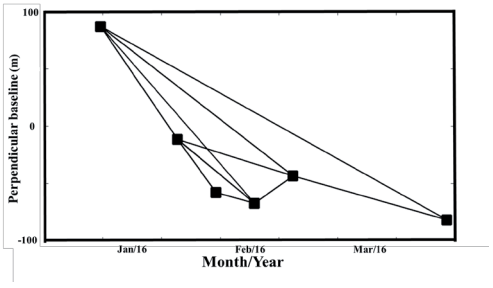

Figure 2. processed interferometric pairs.

As a preliminary result, we acquired time-series signal variation (Figure 3). However, it is hard to suggest that the results indicate time-series deformation, as severe atmospheric effect errors in interferograms were observed (Figure 4). Moreover, the number of data was not sufficient to separate the atmospheric effect. Especially, the area which has small deformation signal size announced an uplifting

of 1~2 cm/year. So to observe the study area, more than 20 SAR data should be utilized to separate error component properly. The blue area of Figure 4 means atmospheric effect and Figures4(a) and (c) show severe atmospheric pattern. And others were not too severe as compared to these two interferograms.

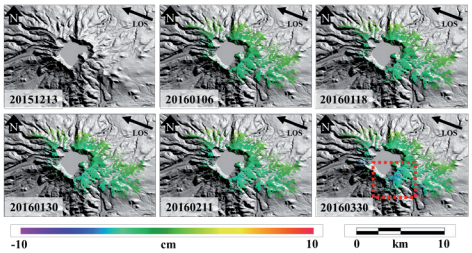

Figure 3. Time-series signal variation of the study area from 2015-12-13 to 2016-03-30.

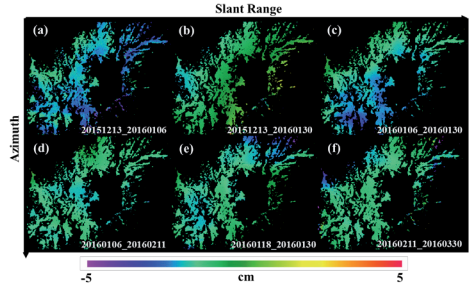

Figure 4. Some of the processed interferograms.

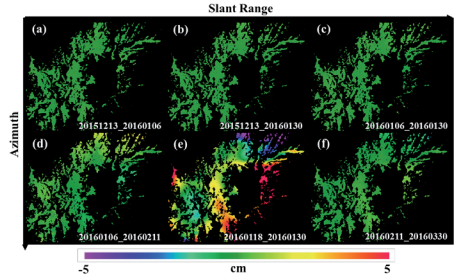

Figure 5. Atmospheric pattern extracted by refined SBAS.

This is the atmospheric effect estimation as a result of refined SBAS. Despite the pattern in the prior slides, the atmospheric effects pattern of the two pairs extracted from refined SBAS was not matched between the patterns of prior slides and this one. On the other hand, the atmospheric pattern of Figure 5(e) also did not match between the prior one and this one. The atmospheric effect of Figure 5(e) was overestimated since error component had been regarded as a deformation signal. We discussed that this mis-match was caused by the less number of SAR data, and we expected that the results would be improved by using sufficient number of data.

Mount Baekdu or Chanbai where located on the border between Korea and China, which erupted violently around 1000 years ago. After that, significant volcanic activities have not been observed. However, significant magma storage was suggested recently, and the concerns of eruption and necessity of periodic observation were gradually increased.

We carried out multitemporal ground deformation observation by applying the Sentinel-1 data set to refined SBAS. As a result, we get preliminary results and the time-series signal variations of mount Baekdu/Chanbai. However, the atmospheric effect extracted from time-series analysis was not estimated well because of insufficient number of processed SAR data. So, we planned the study for reducing atmospheric effect performed by accumulated data, as well as to overcome the gap of data acquisition caused by long temporal baseline.

Acknowledgments

This study was supported by “Research and Development for KMA Weather, Climate, and Earth system Services (NIMS 2016-3100)” of National Institute of Meteorological Sciences and by “Research and Development for Mid-career Researcher Program” through National Research Foundation of Korea (NRF-2015R1A2A2A01005018) grant funded by the Ministry of Education, Science and Technology (MEST).

References

Sung-Hyo, Y., Lee, J.H., 2012, Analysis of unrest sign of activity at the Baegdusan Volcano. J. Petrol. Soc. Korea 21(1), 1–12.

Kim, S.-W., 2003, Measurement of surface displacement of Mt. Baekdu and Busan area using L-band SAR interferometry, Doctorial thesis, Yonsei University of Seoul.

Zebker, H.A., Rosen, P., 1997, Atmospheric artifacts in interferometric SAR surface deformation and topographic maps. J. Geophys. Res. Solid Earth, 102, 7547–7563.

Ferretti, A., Prati, C., Rocca, F., 2001, Permanent scatterers in SAR interferometry. IEEE Trans. Geosci. Remote Sens., 39, 8–20.

Berardino, P., Fornaro, G., Lanari, R., Sansosti, E., 2002, A new algorithm for surface deformation monitoring based on small baseline differential SAR interferograms. IEEE Trans. Geosci. Remote Sens., 40, 2375–2383.

Jung, H.-S., Lee, C.-W., Park, J.-W. Kim, K.-D., Won, J.-S., 2008, Improvement of Small Baseline Subset (SBAS) Algorithm for measuring time-series surface deformations from differential SAR interferograms. Korean J. Remote Sens., 24, 165–177.

Grandin, R., 2015, Interferometric processing of SLC Sentinel-1 TOPS data. In Proceedings of FRINGE’15: Advances in the Science and Applications of SAR Interferometry and Sentinel-1 InSAR Workshop, Frascati, Italy, 23–27 March, 2015, Ouwehand L., Ed., ESA Publication SP-731. doi:10.5270/Fringe2015.116

Causes and Mechanisms of Phreatomagmatism in La Garrotxa Volcanic Field (NE Iberia)

Xavier Bolós[1,2,*], Llorenç Planagumà[3], Joan Martí[1], and Joan Bach[4]

[1]*Institute of Earth Sciences Jaume Almera, CSIC, Barcelona, Spain*
[2]*Institute of Geophysics, UNAM, Morelia, Michoacán, Mexico*
[3]*Tosca Environmental Services, Parc Natural de la Zona Volcànica de la Garrotxa, Olot, Spain*
[4]*Geology Department, Science Faculty, Autonomous University of Barcelona, Bellaterra, Spain*
*Corresponding author E-mail: xavier.bolos@gmail.com

Keywords: phreatomagmatism, hydrogeology, Garrotxa volcanic field

Hydromagmatic monogenetic landforms are the product of explosive interactions between magma and groundwater, surface water, or/and wet sediment, and give rise to morphologies and structures whose final forms depend on the nature of the eruption environments and styles present (Wohletz & Sheridan, 1983; Kokelaar, 1986; White & Ross, 2011; Nemeth & Kereszturi, 2015).

The morphology of phreatomagmatic volcanoes is attributable to differences in eruption intensities, explosion styles, and depositional processes, which are controlled by a number of variables including how magma and water interact, the amount and properties of the interacting fluids, the lithology and mechanical properties of conduit wall rocks, and vent geometry (Kokelaar, 1986; Sohn, 1996; White, 1996; White & Ross, 2011).

In the case study of La Garrotxa volcanic field (Figure 1), the phreatomagmatic events have been common and it is present in the deposits of the majority of volcanic eruptions of the region. This phenomenon results in a large variety of eruptive sequences and morphologies despite magma composition is homogeneous (Martí et al., 2011), mainly basanites and alkaline basalts.

This basaltic volcanic field contains over 50 cones including cinder and scoria cones, tuff rings, and maars, ranging in age from 0.7 Ma to early Holocene (Bolós et al., 2014). This volcanic region is related to the Neogene-Quaternary European Rift system and is the youngest representation of volcanism in the Iberian Peninsula. The selected studied area is located in the northern sector of the GVF, which contains most of the volcanic eruptions of the whole area, and corresponds to the Garrotxa Volcanoes Natural Park (Figure 1). Thick layers of Eocene sediments folded and faulted and Quaternary lava flows characterize the substrate.

Two main aquifers have been identified to interact with La Garrotxa magmas causing such a wide variety of phreatomagmatic episodes and eruption sequences. One aquifer is located at an average depth of a few hundred meters below the volcanic cones, while the other is much more shallower, just a few tens of meters below the surface.

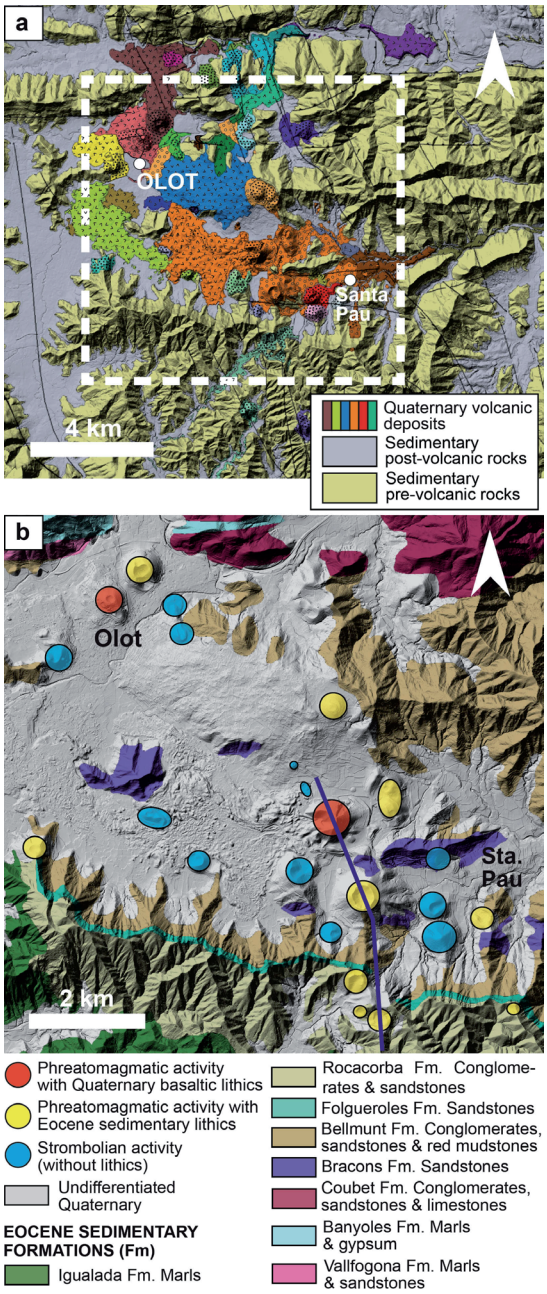

Figure 1. (a) Volcanic stratigraphy map of the studied area. (b) Geographical distribution of the volcanic vents from country rock lithics and mapping of the Eocene sedimentary formations. Blue line shows the cross-section of Figure 2.

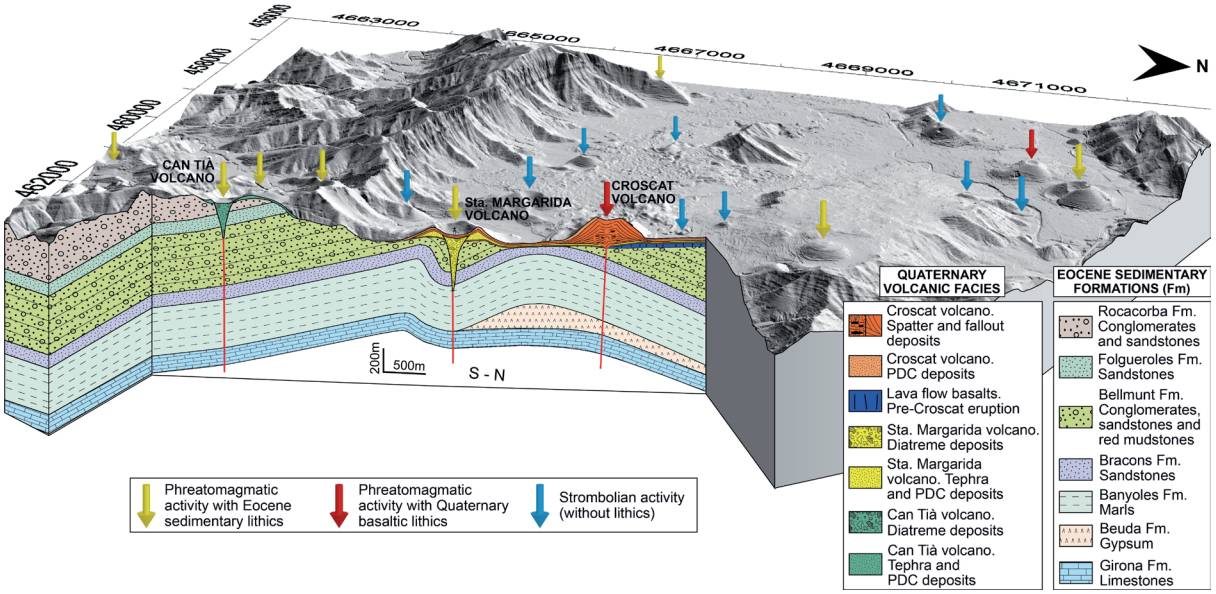

Figure 2. Geological cross-section in a 3D block diagram showing the geometry and depth of the diatremes and volcanic successions, as well as the sedimentary layers of the basement. The arrows show the location of the volcanoes divided in three main categories taking into account the presence/absence and their origin.

The deep aquifer corresponds to Eocene continental sediments, known as the Bellmunt Formation, built up of conglomerates, sandstones, and red mudstones, and the shallow aquifer corresponds to volcanic lava flows of Quaternary age (Figure 2).

In this work, we have analyzed 25 volcanoes and their deposits in an area of about 65 km^2 by describing their products and by identifying the volcanic successions that present country rock lithics. According to the obtained results we have divided these volcanoes in three main categories taking into account the lithics presence/absence and their origin.

The first group is that of volcanoes that present phreatomagmatic activity with basaltic lithics that come from the Quaternary aquifers. The second group contains Eocene sedimentary lithics and the third category does not present evidences of phreatomagmatic activity (Figures 1 and 2).

The way and timing in which such magma/water interaction occurred in La Garrotxa eruptions may differ considerably from one volcano to another. This contrasts with other monogenetic volcanic fields around the world, where eruptions seem to follow a more general pattern.

In conclusion, the different types of substrates results in aquifer diversity. Thus, the magma-water interaction provides a wide range of eruptive dynamics in a relatively small area. In the present case, the large diversity of eruption sequences observed should be explained by variations in the stratigraphy and structure of the shallow geological basement beneath each volcano and the hydraulic characteristics of each aquifer.

References

Bolós, X., Planagumà, L., & Martí, J. (2014). Volcanic stratigraphy and evolution of the Quaternary monogenetic volcanism in the Catalan Volcanic Zone (NE Spain). Journal of Quaternary Science.

Kokelaar, P. (1986). Magma-water interactions in subaqueous and emergent basaltic volcanism. Bulletin of Volcanology, 48, 275–289.

Martí, J., Planagumà, L., Geyer, A., Canal, E., & Pedrazzi, D. (2011). Complex interaction between Strombolian and phreatomagmatic eruptions in the Quaternary monogenetic volcanism of the Catalan Volcanic Zone (NE of Spain). Journal of Volcanology and Geothermal Research, 201(1), 178–193.

Németh, K., & Kereszturi, G. (2015). Monogenetic volcanism: personal views and discussion. International Journal of Earth Sciences, 104, 2131–2146. doi: 10.1007/s00531-015-1243-6.

Sohn, Y.K. (1996). Hydrovolcanic processes forming basaltic tuff rings and cones on Jeju Island, Korea. Geological Society of America Bulletin, 108, 1199–1211.

White, J.D.L. (1996). Impure coolants and interaction dynamics of phreatomagmatic eruptions. Journal of Volcanology and Geothermal Research, 74, 155–170. doi: http://dx.doi.org/10.1016/S0377-0273(96)00061-3.

White, J.D.L., & Ross, P.S. (2011). Maar-diatreme volcanoes: a review. Journal of Volcanology and Geothermal Research, 201, 1–29. doi: http://dx.doi.org/10.1016/j.jvolgeores.2011.01.010.

Wohletz, K.H., & Sheridan, M.F. (1983). Hydrovolcanic explosions: II. Evolution of basaltic tuff rings and tuff cones. American Journal of Science, 283, 385–413. doi: 10.2475/ajs.283.5.385.

Reconstruction of a Maar-Diatreme Features from Borehole Cores and Logging

Xavier Bolós[1,2,*], María José Jurado[1], Oriol Oms[3], Joan Martí[1], Bruno Gómez de Soler[4], Gerard Campeny[4], José Crespo[1], and Jordi Agustí[5]

[1]*Institute of Earth Sciences Jaume Almera, CSIC, Barcelona, Spain*
[2]*Institute of Geophysics, UNAM, Campus Morelia, Morelia, Michoacán, Mexico*
[3]*Geology Department, Science Faculty, Autonomous University of Barcelona, Campus Bellaterra, Bellaterra, Spain*
[4]*Institute of Human Paleocology and Social Evolution, Campus Sescelades URV, Tarragona, Spain*
[5]*ICREA, Institute of Human Paleocology and Social Evolution, Campus de Sescelades, Tarragona, Spain*
*Corresponding author E-mail: xavier.bolos@gmail.com

Keywords: maar-diatreme, wireline coring, geophysical measurements

Maar volcanoes expose shallower or deeper levels of their internal structure as a function of the degree of erosion. In the case study of El Camp dels Ninots maar-diatreme (CNMD; Catalan Volcanic Zone, Spain), the tephra ring has been largely eroded and the remaining volcanic deposits infilling the diatreme are hidden under a lacustrine sedimentary infill of the maar crater. The volcano shows hardly any exposure, so its study needs the application of direct (e.g., boreholes) and indirect subsurface exploration techniques such as surface geophysical methods.

Geophysical logging measurements are a powerful technique that helps to identify centimeter- to millimeter-size features on the borehole wall. Typically, such features include sedimentary structures or fractures, but its potential use goes far beyond these examples. We have successfully applied borehole imaging in a continental volcanic context particularly that of maar-diatreme structure of CNMD. This maar-diatreme is a Pliocene volcano located just SW of Caldes de Malavella village (Girona province, Spain). This volcanic structure belongs to the Catalan Volcanic Zone (CVZ), one of the volcanic provinces of the European Rift System (Martí et al., 1992) (Figure 1). The tectonic evolution of this volcanic region was controlled by a system of NW–SE extensional Neogene faults leading to the formation of several fault-bounded basins (Bolós et al., 2015). The faults bounding the La Selva Basin (Figure 1) contain maar-diatremes such as La Crosa de Sant Dalmai (Bolós et al., 2012) and the CNMD case study. Vehí et al. (1999) identified and described for the first time the morphology of the volcano, which had remained largely unknown since it hardly has any geomorphological evidence of the original tephra ring. More recently, Oms et al. (2015) have reported a detailed geological study of the maar structure based on several drill cores and nine electrical resistivity tomography cross-sections. The geology at CNMD area includes: (1) basement rocks (granites and few schists) of Late Carboniferous—Permian age and (2) Pliocene arkose sands, clays, and gravels of the La Selva Basin alluvial fan systems that may be up to 150 m thick.

According to the results obtained from gravity and electrical tomography data reported by Oms et al. (2015), we have performed two drill cores in the center of the diatreme in order to obtain the whole proximal (i.e., central) facies of the diatreme. A complete set of geophysical logging measurements including oriented ultrasonic borehole images was acquired.

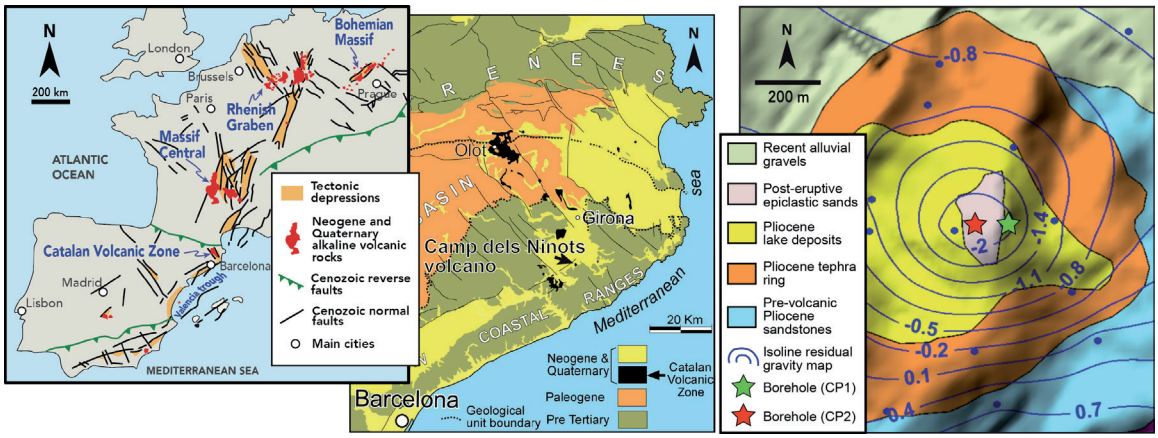

Figure 1. Geological settings of the Camp dels Ninots maar-diatreme (CNMD). Left: Location of the Catalan Volcanic Zone in the European Rift System (modified from Bolós et al., 2015). Center: Situation in the Catalan Volcanic Zone. Right: Geological map of the CNMD with indication of the isoline residual gravity map and location of CP1 and CP2 boreholes in the center of the gravimetric anomaly (modified from Oms et al., 2015).

Borehole images were processed in order to enhance geological and textural features. Borehole images displayed together with core images, allowed us to orient the cores and also to characterize in detail volcanic rocks facies and features (Figure 2).

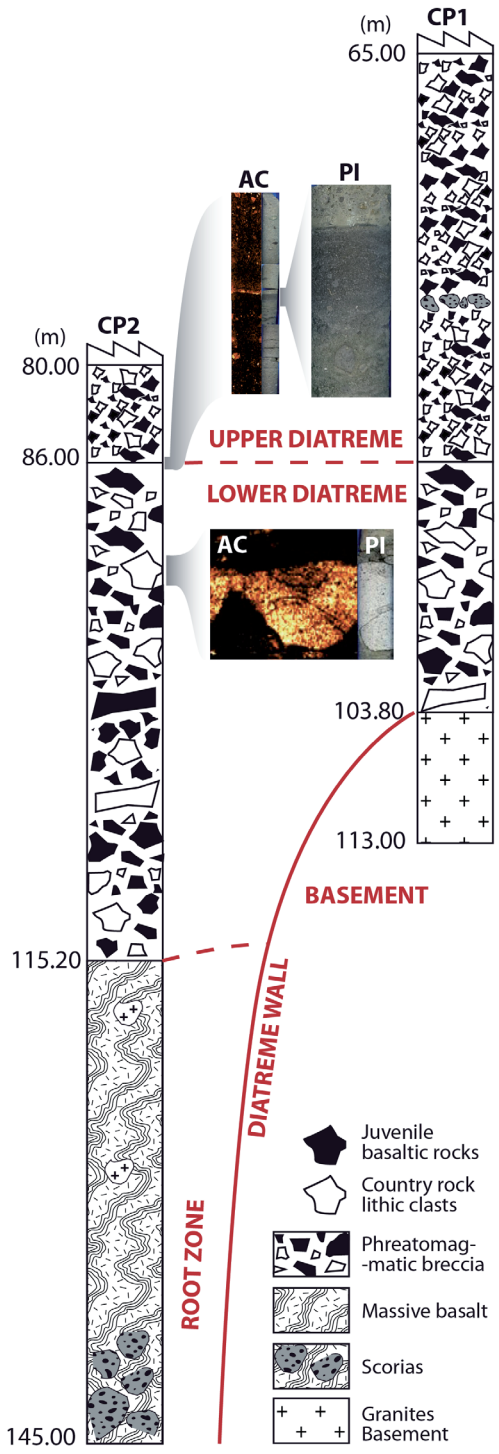

Figure 2. Cross-section with tentative correlation of the CP1-CP2 boreholes and details of the ultrasonic acoustic televiewer (AT) and core picture (PI) showing the identified facies types of the Camp dels Ninots maar-diatreme.

In conclusion, boreholes imaging and wirelines logging have been successfully applied to volcanic deposits and facies characterization. Moreover, we have achieved correlation between cores and borehole ultrasonic televiewer-oriented images. Borehole imaging techniques and logging data could be used for subsurface volcanic facies characterization especially in sections of low or no core recovery. On this high-quality borehole images detailed interpretations and measurements can be performed. The analysis of the boreholes reveals a progressive transition from fissure to diatreme, and overall evolution from Strombolian weak eruption styles to phreatomagmatic phases. Diatreme development was initiated by deep-quarrying explosive eruptions along a fissure to form the country rock-rich breccia.

Acknowledgments

Projects 2014-100575 from Departament de Cultura and SGR2014-901 from AGAUR (both from Catalan Government) financed the drilling campaigns. The Town Council of Caldes de Malavella provided logistics and Mr. Jaume Pla permitted us to work in his property. Borehole images were processed with the Techlog software (Schlumberger).

References

Bolós, X., Barde-Cabusson, S., Pedrazzi, D., Martí, J., Casas, A., Himi, M., and Lovera, R., 2012. Investigation of the inner structure of La Crosa de Sant Dalmai maar (Catalan Volcanic Zone, Spain). Journal of Volcanology and Geothermal Research, 247–248(0): 37–48.

Bolós, X., Martí, J., Becerril, L., Grosse, P., Planagumà, L., and Barde-Cabusson, S., 2015. Volcano-structural analysis of La Garrotxa Volcanic Field (NE Iberia): implications for the plumbing system. Tectonophysics. DOI: 10.1016/j.tecto.2014.12.013Cas

Martí, J., Mitjavila, J., Roca, E., and Aparicio, A., 1992. Cenozoic magmatism of the Valencia trough(western Mediterranean): relationship between structural evolution and volcanism. Tectonophysics, 203: 145–165.

Martí, J., Planagumà, L., Geyer, A., Canal, E., and Pedrazzi, D., 2011. Complex interaction between Strombolian and phreatomagmatic eruptions in the Quaternary monogenetic volcanism of the Catalan Volcanic Zone (NE of Spain). Journal of Volcanology and Geothermal Research, 201(1): 178–193.

Oms, O., Bolós, X., Barde-Cabusson, S., Martí, J., Casas, A., Lovera, R., Himi, M., Gómez de soler, B., Campeny Vall-Llosera, G., Pedrazzi, D., and Agustí, J. 2015. Structure of the Pliocene Camp dels Ninots maar-diatreme (Catalan Volcanic Zone, NE Spain). Bulletin of Volcanology, 77(11): 1–13.

Vehí, M., Pujadas, A., Roqué, C., and Pallí, L., 1999. Un edifice volcanic inèdit a Caldes de Malavella (La Selva, Girona): el Volcà del Camp dels Ninots. Quaderns de la Selva, 11. Centre d'Estudis Selvatan.

A Revised Age Model for the Lacustrine Records from Tianyang Maar Paleolake, South China

Cong Chen[1,*], Zhuo Zheng[1], Yongqiang Zong[2], Kangyou Huang[1], Xiaoqiang Yang[1], Shixiong Yang[1,3], and Shaohua Yu[1,4]

[1]*School of Earth Science and Geological Engineering, Sun Yat-sen Universtiy, Guangzhou, China*
Department of Earth Sciences, The University of Hong Kong, Hong Kong, SAR China
[3]*The Key Laboratory of Marine Hydrocarbon Resources and Environmental Grology, Qingdao Institute of Marine Geology, Ministry of Land and Resources, Qingdao, China*
[4]*The Key Laboratory of Marine Mineral Resources, Guangzhou Marine Geological Survey, Ministry of Land and Recources, Guangzhou, China*
*Corresponding author E-mail: chenc7@mail2.sysu.edu.cn

Keywords: age model, multiple dating methods, Bayesian age-depth modeling, Tianyang Maar Paleolake

Long-term records of past climate changes covering the last few glacial-interglacial (G-IG) cycles have been successfully reconstructed from marine sediments and ice cores. However, there are fewer long continental records of similar timescale, which impedes our understanding of past continental climate changes. One of the major reasons accounting for this dilemma is the difficulty in constructing reliable age models for long continental sediment sequences, especially long lacustrine sequences.

Developing age models for long lacustrine records is greatly challenging. Radiocarbon dating method is limited to the last 50 ka BP, other methods such as optically stimulated luminescence (OSL) and uranium-series dating usually accompany relatively high uncertainties, and well-dated tephra ashes and magnetic excursions are not common in most environments and depend on the availability of material (Shanahan et al., 2013). Besides, astronomical tuning is a widely used technique to build age models through correlating supposedly synchronous climatic event between records. But this approach may include potential problems such as circular reasoning and unrecognized chronological uncertainties (Blaauw, 2012), and cannot resolve some paleoclimate questions, such as lead and lag relationships between different areas (Colman et al., 2006). Despite the challenges mentioned above, we still could develop robust age models by combining multiple methods.

Tianyang Maar Paleolake provides an excellent opportunity to explore these issues. The Paleolake, located on the Leizhou Peninsula, lies at the modern northern limit of the intertropical convergence zone (ITCZ). Local climate is dominated by the complex ITCZ-Asian Monsoon (ITCZ-AM) circulation and seasonal typhoon activity. The sedimentary archive of the Paleolake is known to be ~224 m, representing the longest known terrestrial record in SE Asia. These advantages mentioned above make the Paleolake suitable for studying migration of ITCZ and evolution history of AM. In the 1970s and 1980s, a number of boreholes were drilled in the crater and studies on sedimentology, palynology, and geochemistry were carried out. These previous researches reported multidisciplinary data but at low resolution and indicated that the entire 224 m archive spanned four G-IG cycles based on palynochronology (Zheng and Lei, 1999). In order to realize the potential of the Tianyang Marr Paleolake archive, we drilled two new cores (TY08 and TY15) from the center of the crater. The two cores were drilled ~10 m apart to provide overlapping for any gap resulting from sampling process, and are used to construct a ~230 m composite record (TYC) based on the correlation of lithological evidence and magnetic susceptibility. The lithology of the upper ~40 m alternates between clayey silt beds and layers of silt and fine-coarse grain sands, but the lower part is dominated with diatomite (up to ~80%).

Unfortunately, our attempts to build an age-depth model for the entire ~230 m composite record failed due to the nonavailability of dating material. However, we still endeavor to develop a robust age-depth model for the upper ~40 m of the core TYC through multiple approaches. A total number of 18 samples (e.g., bulk organic matter and plant macrofossil) were selected from the upper ~40 m of the core TYC and dated via accelerator mass spectrometry (AMS) radiocarbon dating method. Previous researches suggested that the upper ~40 m of the archive belonged to MIS3 to present. However, our results reveal that the ages of sediments below ~8 m are already beyond the limit of radiocarbon (~50 ka BP), which make only 11 samples usable in the data set, and we attribute the discrepancy to limitations of conventional radiocarbon dating method used in previous

research. Moreover, we pick two samples from available clean sand layers between ~10 and ~25 m for optically stimulated luminescence dating. To construct a robust age-depth model using this absolute-date data set comprised of 11 AMS ^{14}C and 2 OSL samples, we employ Bayesian age-depth modeling approach implemented in the software program BACON 2.2 (Blaauw and Christen, 2011), which is usually used to radiocarbon-dated sequences. The methods employed by BACON are not bothered by outliers in many cases, and can substantially minish the error estimates with prior information taken into account. We successfully construct an age-depth model for the uppermost sediments from the Tianyang Maar Paleolake, and this model suggests age estimate of 367.87 ka with 95% confidence range of 41.27 ka at 40 m (Figure1). As illustrated in Figure 1, the uncertainties in the age-depth model is small, but slowly increase with depth because of relatively large age errors associated with these dating methods and the lower sample densities. It is worth noting that age estimates of sediments blow ~23 m are based on extrapolation of the age-depth model.

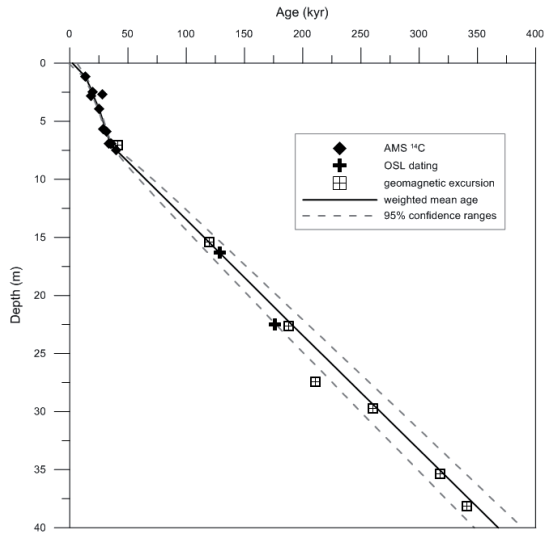

Figure 1. Bayesian age-depth model for the uppermost sediments from Tianyang Maar Paleolake, only using absolute dates, AMS ^{14}C and OSL dating (though geomagnetic excursions showed here).

In order to assess the reliability of this model and further improve it, we collect U-channel subsamples from core TY08 for paleomagnetic analysis using a 2G-755R superconducting magnetometer. A total of seven geomagnetic excursions are recognized based on inclination reversals and correlated with the known Brunhes chron excursions in Ocean Drilling Program cores (Lund et al., 2006). These excursions are ploted in the age-depth model and all but one well fall within the 95% confidence ranges, which implies that this model is reliable. We also suggest that these geomagnetic excursions should not be included in the data set, avoiding the trap of circular reasoning. Actually, though the age model is tightly constrained by ages of geomagnetic excursions because of their relatively small age errors, the model seems to change very little whether the data set include or exclude these geomagnetic excursions.

In the future, we will attempt to employ tephrochronology and Ar-Ar dating method to constrain the chronological framework and minimize uncertainties, so that we can confidently reconstruct regional paleoenvironment and compare local climate events with global signals based on multiple proxies (e.g., pollen and geochemistry).

Acknowledgments

The drilling of the TY08 core were financed by the international collaboration project between University of Hong Kong (HKU700109P), University of Durham, UK (NERC Radiocarbon Allocation 1423.1009), and Sun Yat-sen University, China (Fundamental Research Funds for the Central Universities: 111gjc13 and 101gzd08). The development of the chronology was supported by the National Natural Science Foundation of China (Grant No. 41230101 and 41472143).

References

Blaauw, M., Christen, J. A., 2011. Flexible paleoclimate age-depth models using an autoregressive gamma process. Bayesian Analysis, 6:457–474.

Blaauw, M., 2012. Out of tune: the dangers of aligning proxy archives. Quaternary Science Reviews, 36:38–49.

Lund, S., Stoner, J. S., Channell, J. E. T., Acton, G., 2006. A summary of brunhes paleomagnetic field variability recorded in ocean drilling program cores. Physics of the Earth & Planetary Interiors, 156:194–204.

Shanahan, T. M., Peck, J. A., Mckay, N., Heil, C. W., King, J., Forman, S. L., et al., 2013. Age models for long lacustrine sediment records using multiple dating approaches – an example from lake Bosumtwi, Ghana. Quaternary Geochronology, 15(1):47–60.

Variations in the Deep Asthenospheric Processes Beneath the Northeast Asian Marginal Region from Pre- to Postopening of the Japan Sea

Shuang-Shuang Chen* and Jia-Qi Liu

Institute of Geology and Geophysics, Chinese Academy of Sciences, Beijing, China

*Corresponding author E-mail: sschen@mail.iggcas.ac.cn

Keywords: basaltic magma, eastward asthenosphere, Northeast Asian

Deep asthenospheric processes and the dynamic mechanism of magmatism in the northeast Asian marginal region are of significant interest. We present the $^{87}Sr/^{86}Sr$ and $^{143}Nd/^{144}Nd$ versus age diagrams of basaltic rocks from the Japan Sea, the back-arc side of northeast Japan, north Hokkaido and southwest Hokkaido, and the Sikhote-Alin area (Figure 1; Fukase and Shuto, 2000; Kondo et al., 2000; Nohda, 2009; Nohda et al., 1988; Ohki et al., 1995; Shuto et al., 1993, 1997, 2004, 2006; Takanashi et al., 2011).

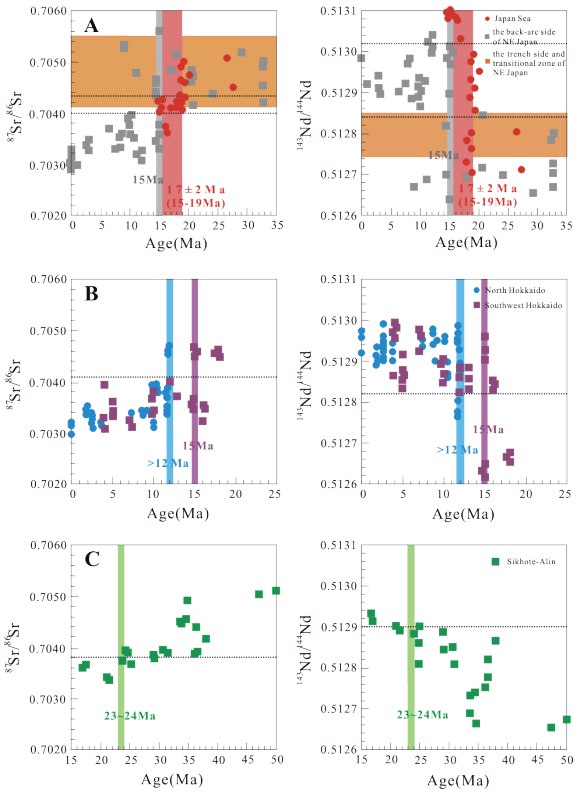

Figure 1. $^{87}Sr/^{86}Sr$ versus age and $^{143}Nd/^{144}Nd$ versus age diagrams of basaltic rocks from the Japan Sea, the trench side and transitional zone of NE Japan, the back-arc side of NE Japan (A), the north Hokkaido and southwest Hokkaido (B), and the Sikhote-Alin (C).

The significance of our study is that we found systematic and marked variations in the basaltic magma of the Sikhote-Alin area, the Japan Sea, the back-arc side of NE Japan, and SW Hokkaido and north Hokkaido from a slightly enriched isotopic signature to a depleted isotopic signature at 23–24, 15–19, 15, and >12 Ma, respectively. That is to say, the time period of the injections of asthenosphere into subcontinental lithospheric mantle occurred roughly at 23–24, 15–19, 15, and >12 Ma, in a trend indicating a eastward asthenosphere flow beneath the Northeast Asia continent (Figure 2).

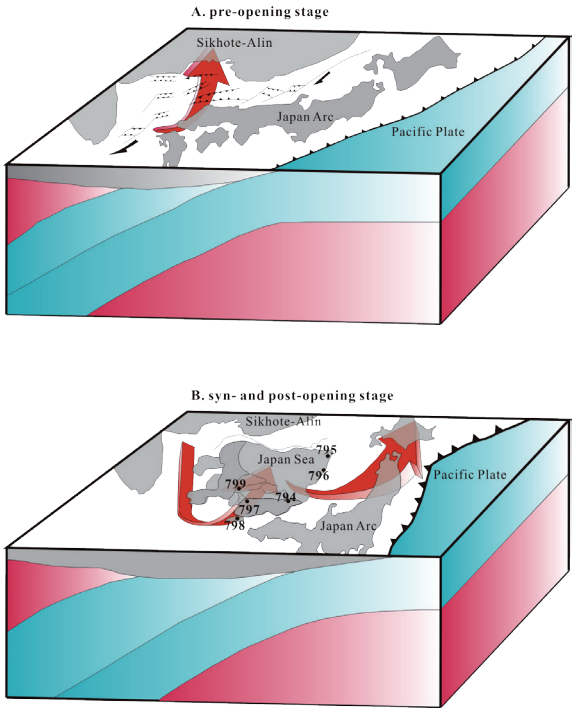

Figure 2. Skeptical models illustrating the structural changes that occurred beneath the northeast margin of the Asian continent during the preopening stage (A) and the syn- and postopening stage (B).

Additionally, the volcanoes in Northeast Asian continental margin are linearly and parallelly distributed in the Great Xing'an, the Songliao Basin,

the Talu-Yitong fault, the Penglai-Mishan fault, the Mt. Changbai, the Japan Sea, and the Japan Arc. Synthesizing these ages of the volcanism, we found that the intensive expansion of the Japan Sea gave rise to the closure of Songliao-Jizhong rift, accompanied by the closure of the Songliao rift, the extensional stress occurred in its both flanks. It is interesting to note that a similar situation occurred in the Japan Sea. The weakening of the "Japan Sea rift" resulted in the ceasation of volcanism in the central back-arc basin, but highlight the volcanic activities in its both flanks (–10 Ma, Japan Arc and NE China). Thus, we suggest that the synchronous and similar volcanism on both sides of the Japan Sea (i.e., the Japan Arc and NE China) is closely associated with the rift expansion and the back-arc spreading of the Japan Sea (Figure 3).

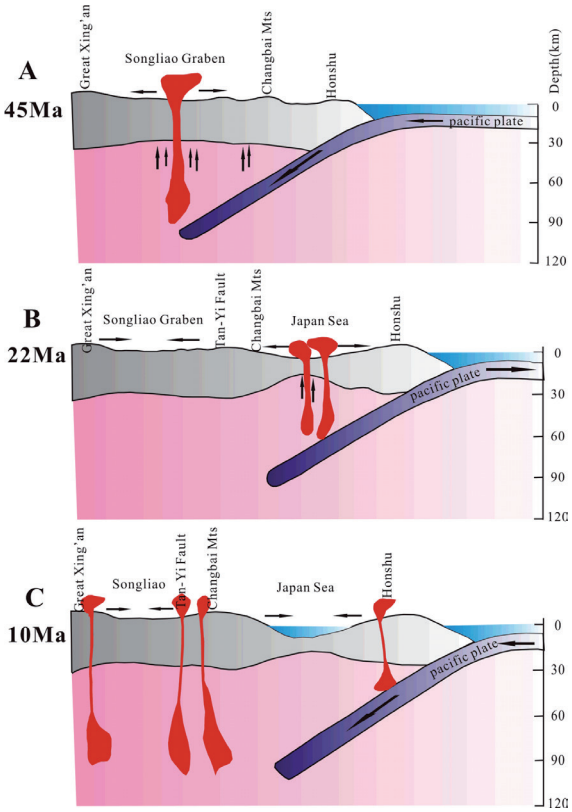

Figure 3. Schematic diagram illustrating the relationship between the development of East Asia continental rift system and the subduction of Western Pacifc Plate.

Acknowledgments

This work was supported by the National Natural Science Foundation of China (Grant code: 41476034, 41272369, 40802038, 41320104006, 41302102, and 15CX05007A).

References

Fukase, M., Shuto, K., 2000. Petrology of Oligocene volcanic rocks from the middle part of the Monzen Formation, Oga Peninsula, northeastern Japan (in Japanese with English abstract). The Journal of the Geological Society of Japan 106, 280–298.

Kondo, H., Shuto, K., Fukase, M., 2000. An AFC (assimilation and fractional crystallization) as the petrogenesis of andesites from the Pliocene Myojin-iwa Formation, the back-arc side of the Northeast Japan: combined major-and trace-element and Sr–Nd isotope constraints (in Japanese with English abstract). The Journal of the Geological Society of Japan 106, 426–441.

Nohda, S., 2009. Formation of the Japan Sea basin: reassessment from Ar–Ar ages and Nd–Sr isotopic data of basement basalts of the Japan Sea and adjacent regions. Journal of Asian Earth Sciences 34, 599–609.

Nohda, S., Tatsumi, Y., Otofuji, Y., Matsuda, T., Ishizaka, K., 1988. Asthenospheric injection and back-arc opening: isotopic evidence from Northeast Japan. Chemical Geology 68, 317–327.

Ohki, J.I., Shuto, K., Kagami, H., 1995. Middle Miocene bimodal volcanism by asthenospheric upwelling: Sr and Nd isotopic evidence from the back-arc region of the Northeast Japan arc. Oceanographic Literature Review 42(8).

Shuto, K., Ohki, J., Kagami, H., Yamamoto, M., Watanabe, N., Yamamoto, K., Anzai, N., Itaya, T., 1993. The relationships between drastic changes in Sr isotope ratios of magma sources beneath the NE Japan arc and the spreading of the Japan Sea back-arc basin. Mineralogy and Petrology 49, 71–90.

Shuto, K., Kato, S., Ohki, J., Kagami, H., Arato, H., Rezanov, A.L., 1997. Miocene bimodal volcanism in the Niigata oil and gas fields, northeast Japan—with special reference to the spreading of the back-arc basin (in Japanese with English abstract). Journal of the Japanese Association for Petroleum Technology 62, 45–58.

Shuto, K., Hirahara, Y., Ishimoto, H., Aoki, A., Jinbo, A., Goto, Y., 2004. Sr and Nd isotopic compositions of the magma source beneath north Hokkaido, Japan: comparison with the back-arc side in the NE Japan arc. Journal of Volcanology and Geothermal Research 134, 57–75.

Shuto, K., Ishimoto, H., Hirahara, Y., Sato, M., Matsui, K., Fujibayashi, N., Takazawa, E., Yabuki, K., Sekine, M., Kato, M., Rezanov, A.I., 2006. Geochemical secular variation of magma source during Early to Middle Miocene time in the Niigata area, NE Japan: Asthenospheric mantle upwelling during back-arc basin opening. Lithos 86, 1–33.

Takanashi, K., Shuto, K., Sato, M., 2011. Origin of Late Paleogene to Neogene basalts and associated coeval felsic volcanic rocks in Southwest Hokkaido, northern NE Japan arc: constraints from Sr and Nd isotopes and major-and trace-element chemistry. Lithos 125, 368–392.

Cryptotephra: A Powerful Tool for Independent Correlation and Precise Dating of Paleoclimate Records

Xuan-Yu Chen[1,2,3,4,*], Danielle McLean[3,5], Simon P.E. Blockley[3], Pavel E. Tarasov[6], Yi-Gang Xu[1], Jia-Qi Liu[7], and Martin A. Menzies[1,4]

[1]*State Key Laboratory of Isotope Geochemistry, Guangzhou Institute of Geochemistry, CAS, Guangzhou, China*
[2]*University of Chinese Academy of Sciences, Beijing, China*
[3]*Department of Geography, Royal Holloway University of London, Egham, Surrey, UK*
[4]*Department of Earth Sciences, Royal Holloway University of London, Egham, Surrey, UK*
[5]*Research Laboratory for Archaeology and the History of Art, University of Oxford, Oxford, UK*
[6]*Institute of Geological Sciences, Palaeontology, Free University Berlin, Berlin, Germany*
[7]*Key Laboratory of Cenozoic Geology and Environment, Institute of Geology and Geophysics, CAS, Beijing, China*
*Corresponding author E-mail: Xuanyu.Chen.2014@live.rhul.ac.uk

Keywords: cryptotephra, tephrochronology, tephrostratigraphy

Detailed reconstructions of past climate variability, especially the regional variations in response to abrupt climate change, require precise correlation between disparate environmental archives. However, chronological uncertainties, such as the modeling and calibration issues in radiocarbon dating, or the counting errors in ice-core or varved lake records, have hindered the direct comparison of any of these vital paleoclimate records. The emergence of cryptotephra research in the past two decades has witnessed the great potential that it can offer, for linking numerous individual sequences in a wide geographical area (e.g., Lowe et al., 2012; Lane et al., 2013; Lowe et al., 2015). As part of a regional tephrostratigraphic study of terrestrial and marine records in NE Asia, we report on the presence of late Holocene B-Tm tephra in Lake Kushu, Northern Japan, which is located more than 1100 km away from the source volcano (i.e., Changbaishan) that generated the cryptotephra deposit (Chen et al., 2016). The presented grain-specific glass chemistry, including for the first time, single-grain trace element data, for both proximal and distal deposits, allows the establishment of a robust proximal-distal correlation, which is then used to clarify the problematic proximal tephra stratigraphy. The high-resolution ice-core age of this widespread tephra (Sun et al., 2014) provides an absolute tie-point for testing and refining the Kushu radiocarbon chronology at the related time interval. Along with the presence of the B-Tm tephra in Central Japan (Lake Suigetsu: McLean et al., in preparation), Sea of Japan, and NE China (Lake Sihailongwan: Sun et al., 2015), it is now possible to synchronize these high-resolution climatic records across NE Asia (Figure 1), with direct reference to the Greenland ice-core records, providing constraints on the timing of late Holocene climatic events (e.g., Medieval Warm Period) over a wide geographical area. This highlights the significant potential for the ongoing research into the tephrostratigraphy of NE Asia, which is focused on the identification of more widely dispersed tephra/cryptotephra deposits that are suitable for independent correlation and precise dating of paleoclimate records.

References

Chen, X.-Y., Blockley, S.P.E., Tarasov, P.E., Xu, Y.-G., McLean, D., Tomlinson, E.L., Albert, P.G., Liu, J.-Q., Müller, S., Wagner, M., and Menzies, M.A., 2016. Clarifying the distal to proximal tephrochronology of the Millennium (B–Tm) eruption, Changbaishan Volcano, northeast China. Quaternary Geochronology, 33: 61–75.

Lane, C.S., Brauer, A., Blockley, S.P.E., and Dulski, P., 2013. Volcanic ash reveals time-transgressive abrupt climate change during the Younger Dryas. Geology, 41(12): 1251–1254.

Lowe, J., Barton, N., Blockley, S., Ramsey, C.B., Cullen, V.L., Davies, W., Gamble, C., Grant, K., Hardiman, M., Housley, R., Lane, C.S., Lee, S., Lewis, M., MacLeod, A., Menzies, M., Mueller, W., Pollard, M., Price, C., Roberts, A.P., Rohling, E.J., Satow, C., Smith, V.C., Stringer, C.B., Tomlinson, E.L., White, D., Albert, P., Arienzo, I., Barker, G., Boric, S., Carandente, A., Civetta, L., Ferrier, C., Guadelli, J.-L., Karkanas, P., Koumouzelis, M., Mueller, U.C., Orsi, G., Pross, J., Rosi, M., Shalamanov-Korobar, L., Sirakov, N., and Tzedakis, P.C., 2012. Volcanic ash layers illuminate the resilience of Neanderthals and early modern humans to natural hazards. Proceedings of the National Academy of Sciences of the United States of America, 109(34): 13532–13537.

Lowe, J.J., Ramsey, C.B., Housley, R.A., Lane, C.S., and Tomlinson, E.L., 2015. The RESET project: constructing a European tephra lattice for refined synchronisation of environmental and archaeological events during the last c. 100 ka. Quaternary Science Reviews, 118: 1–17.

McLean, D., Albert, P.G., Nakagawa, T., and Smith, V.C., in preparation. Identification of the Millennium (B-

Tm) eruption at Lake Suigetsu, Japan: synchronization of hemispheric wide paleoclimate archives.

Sun, C., Plunkett, G., Liu, J., Zhao, H., Sigl, M., McConnell, J.R., Pilcher, J.R., Vinther, B., Steffensen, J.P., and Hall, V., 2014. Ash from Changbaishan Millennium eruption recorded in Greenland ice: implications for determining the eruption's timing and impact. Geophysical Research Letters, 2013GL058642.

Sun, C.Q., You, H.T., He, H.Y., Zhang, L., Gao, J.L., Guo, W.F., Chen, S.S., Mao, Q., Liu, Q., Chu, G.Q., and Liu, J.Q., 2015. New evidence for the presence of Changbaishan Millennium eruption ash in the Longgang volcanic field, Northeast China. Gondwana Research, 28(1): 52–60.

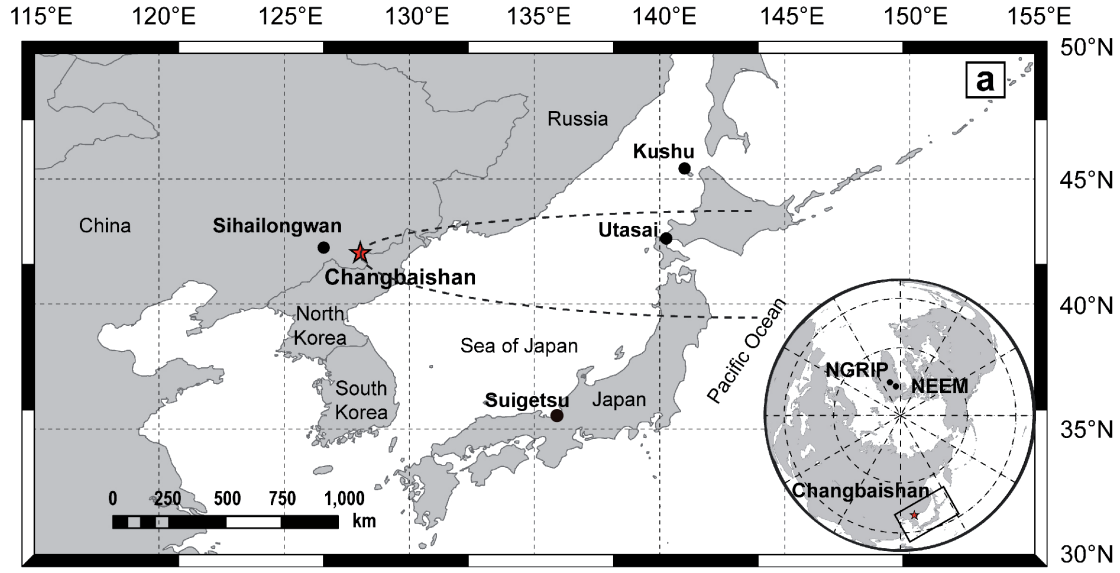

Figure 1. A map showing the location of the Changbaishan volcano that produced the B-Tm tephra and other distal archives where the tephra has been recorded. The dashed line shows the previously reported distribution of B-Tm according to Machida and Arai (1983), which now can be updated due to the advent of cryptotephra techniques.

Extraction of Volcanic Ash Information Using the Polar Orbit and Geostationary Satellite Imagery: A Case Study of Sakurajima Volcano

Yoon-Ho Choi*, Won-jin Lee, Hyojin Yang, Sun-Cheon Park, and DukKee Lee

National Institute of Meteorological Sciences, Jeju, Republic of Korea

*Corresponding author E-mail: koala1015@korea.kr

Keywords: Landsat 8, COMS, ash cloud, Sakurajima, cloud shadow

Volcanic ash consists of various rock fragments and its particle is less than 2 mm. After the eruption, the volcanic ash spreads over thousands of kilometers by the effect of wind. The falling volcanic ash affects not only the natural environment but also human health and activities such as agriculture and transportation. In order to reduce the damage caused by the falling volcanic ash, the ash cloud should be monitored because it provides significant information such as the moving velocity, heading, and covering area of the falling volcanic ash.

The ash cloud can be detected by the *in situ* measuring method, the indirect observation method, and the empirical method. The *in situ* measuring method requires installing the equipment in the volcanic area, such as RAdio Detecting and Ranging (RADAR), Light Detection and Ranging (LiDAR), and camera. It provides accurate information of the ash cloud, but the operation and maintainence costs of the equipment is high for just observing the crater only. The empirical method uses the atmospheric character of the local area, such as the mean temperature and wind, and the empirical formula (Oppenheimer, 1998). This method requires the weather database constructed for long periods.

The indirect method is comparatively less accurate than the *in situ* measuring method, but it is cost-effective. For example, the imagery taken on the satellite is one of the most powerful data that we can use in the indirect method. It observes a large area and monitors inaccessible areas. There are two types of satellites orbiting the Earth, the polar and geostationary satellites. The altitude of the polar orbit satellite is relatively lower such as 700–900 km, than the geostationary satellite which is orbiting higher than 20,000 km. The imagery taken by the polar orbit satellite is targeting the entire earth surface and has high resolution. On the other hand, the imagery taken by the geostationary satellites covers the identical area every time. It has relatively low resolution. If we are able to use these two types of satellite together, the results can provide the complementary information, compared to when we use only one type of satellite imagery (Zaksek et al., 2013).

We use two types of satellite imageries to extract ash cloud information for the Sakurajima volcano erupted on May 21, 2015.

1. Data set

We use the imagery taken on the Communication, Ocean and Meteorological Satellite (COMS) launched by the Korean government, and the Landsat-8 imagery provided by the United State Geological Survey (USGS). The COMS is the geostationary satellite and the Landsat-8 is the polar orbit statellite. Table 1 includes the detailed information of each satellite.

Table 1. The summary of the geostationary (COMS) and polar orbit (Landsat-8) satellites

Satellite	COMS	Landsat 8
Orbit Type	Geosynchronous	Polar orbital
Band	1. Visible 2. Shortwave 3. Water vapor 4. Thermal Infrared 1 5. Thermal Infrared 2	1. Coastal/Aerosol 2. Blue 3. Green 4. Red 5. Near Infrared 6. Shortwave infrared-1 7. Shortwave infrared-2 8. Panchromatic 9. Cirrus 10. Long wavelength Infrared-1 11. Long wavelength Infrared-2
Resolution	Bands 1-4: 4km Band 5: 1km	Bands 1-7,9: 30 m Band 8: 15 m Bands 10-11: 100 m
Acquisition Interval	15 minute	16 day
Altitude	36,000 km	705 km

2. Method

In order detect the ash cloud and analyze the information such as the velocity and heading, we follow the procedure described in Figure 1. The procedure consists of five steps: (1) finding the polar and geostationary satellite data based on the Volcano Ash Advisory Center's (VAAC) information, (2) preprocessing such as image importing, atmospheric

correction, and topographic correction, (3) generating the Normalized Difference Temperature Index (NDTI), (4) transforming each projection to Universal Transverse Mercator (UTM) coordinate, (5) extracting ash cloud information (velocity, direction, coverage, and height).

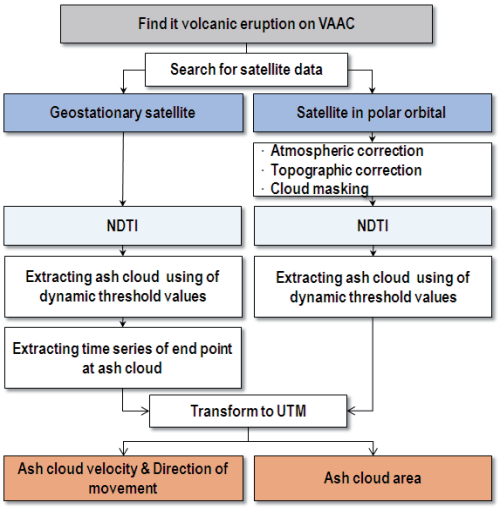

Figure 1. The procedure to generate the information of ash cloud.

The area of ash cloud is determined by counting the pixels of the detected ash cloud. The velocity of ash cloud is estimated by tracking the end of the detected ash cloud using the sequential images. In case of the height, there are five ways to determine it. These are based on the brightness temperature, wind correlation, shadow, RADAR and LiDAR, and video (Richards, 2006). We used the shadow method in using the high-resolution satellite image. The cloud height based on shadow method can be determined by the following equation:

$$H = L_s / \tan Z \qquad \ldots\ldots\ldots\ldots\ldots \quad (1)$$

where H is a cloud height, L_s is a shadow length, and Z is a sun zenith angle (Prata and Grant, 2001).

In order to use the shadow method to estimate the height of ash cloud, the topographic correction is necessary because the shadow looks shorter than real in the mountain area. We use the Advanced Spaceborne Thermal Emission and Reflection Radiometer (ASTER) Global Digital Elevation Model (GDEM) for the topographic correction. The shadow method is appropriate for a sunny day, but has limitations because it depends on the weather and solar azimuth angle.

3. Results and conclusion

Based on the Landsat-8 and COMS, we extracted the ash cloud of the Sakurajima, Japan erupted on May 21, 2015. The Landsat-8-derived NDTI image shows the ash cloud clearly as shown in Figure 2(a), but the COMS-derived NDTI image is less clear as shown in Figure 2(b). The height and size of ash cloud are determined from the NDTI taken from Landsat-8 because it is very accurate and has high resolution. On the other hand, the velocity and heading of ash cloud are estimated from the NDTI from COMS because it takes imagery every 15 minute as mentioned above.

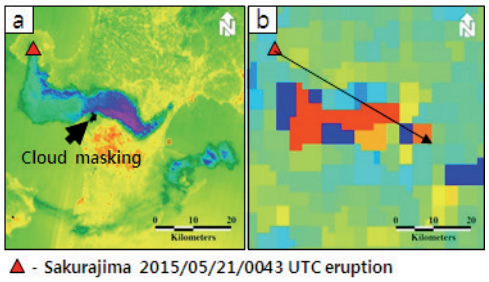

Figure 2. NDTI images from Landsat-8 (a) and COMS (b).

The determined height of ash cloud is 3.7 km, ash cloud direct toward the southeastward direction, and the determined mean velocity is 5.9 m/s. We conclude that the method of extracting ash cloud and such an information works well in case of the Sakurajima volcanic eruption in 2005. In the future work, the algorithm will be applied to other test sites to verify the performance. The information such as coverage, height, velocity, and direction extracted from the ash cloud will contribute to analyze and mitigate the volcanic hazard.

Acknowledgments

This study was supported by "Research and Development for KMA Weather, Climate, and Earth system Services (NIMS 2016-3100)" of National Institute of Meteorological Sciences. We used Landsat-8 data from the Earth Explorer archive provided by the USGS.

References

Oppenheimer, C., 1998. "Review article: Volcanological applications of meteorological satellites," International Journal of Remote Sensing 19: 2829–2864.

Zaksek, K., Hort, M., Zaletelj, J., and Langmann, B., 2013. "Monitoring volcanic ash cloud top height through simultaneous retrieval of optical data from polar orbiting and geostationary satellites," Atmospheric Chemistry and Physics 13: 2589–2606.

Richards, M.S., 2006. Volcanic Ash Cloud Height Using the MODIS CO_2-Slicing Algorithm, Univercity of Wisconsin, Madison.

Prata, A.J., and Grant, I.F., 2001. "Determination of mass loadings and plume heights of volcanic clouds from satellite data," CSIRO Atmospheric Research Technical Paper 48: pp. 1–38.

Abrupt and Cyclic Paleoclimatic Changes Since the Last Glacial Maximum Recorded in Maar Lake Xiaolongwan, Northeastern China

Guoqiang Chu[1,*], Qing Sun[2], Manman Xie[2], Yuan Lin[2], Yabin Shan[2], Qingzen Zhu[1], Deke Xu[1], Youliang Su[1], Patrick Rioual[1], and Jiaqi Liu[1]

[1]*Key Laboratory of Cenozoic Geology and Environment, Institute of Geology and Geophysics, Chinese Academy of Sciences, Beijing, China*
[2]*National Research Center of Geoanalysis, Beijing, China*
*Corresponding author E-mail: chuguoqiang@mail.igcas.ac.cn

Keywords: annually laminated sediment, compound-specific $\delta^{13}C$ values, paleoclimatic changes

Sudy area is located in northeastern China and is under the influence of the East Asian monsoonal climate (Figure 1). In summer, subtropical monsoon rainfall (Meiyu in Chinese, Changma in Korean, and Baiu in Japanese) is mainly associated with the northward shift of the western Pacific subtropical high (WPSH) from June to September. Meanwhile, the Okhotsk High (a semipermanent high pressure zone) forms and intensifies over the Sea of Okhotsk, brings vapor (cold and wet air, the Northeast Monsoon) to northeastern China, contributing to increasing summer precipitation (Wang, 1992). About 60% of the mean annual precipitation of ~770 mm falls between June and August.

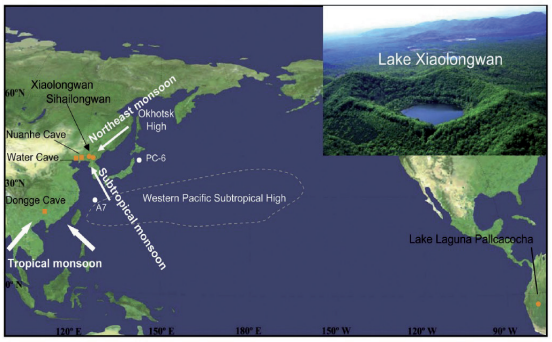

Figure 1. Map showing the location of Lake Xiaolongwan and paleoclimatic records discussed in the text. The solid arrows indicate the dominant direction of the summer monsoon and winter monsoon, modified from Liu (2010). Orange circles: Lake records (Lake Xiaolongwan in this study and Lake Laguna Pallcacocha) (Rodbell et al., 1999). Orange squares: Cave records (Wang et al., 2005; Tan, 2007; Wu et al., 2012). White circles: marine cores A7 (Sun et al., 2005) and PC-6 (Minoshima et al., 2007).

The maar lakes in northeastern China have been recognized as ideal sites for the preservation of paleoclimatic archives, and the subjects of numerous studies focused on paleoclimatic and paleoenvironmental changes (Mingram et al., 2004; Schettler et al., 2006; Parplies et al., 2008; Stebich et al., 2009; Chu et al., 2014; Xu et al., 2014; Gao et al., 2016).

We present an *n*-alkane and compound-specific carbon isotope record of the past 20 ka from the annually laminated sedimentary sequence of Lake Xiaolongwan, northeastern China. The *n*-alkane distribution suggests that Lake Xiaolongwan has undergone a shift from an oligotrophic state with low algal production and little emergent/submerged macrophytes in the Last Glacial Maximum, to a eutrophic state with high algal production and abundant emergent/submerged macrophytes since the middle Holocene. In this forested region, where the vegetation is dominated by C3 plants, the long-chain *n*-alkanes (C_{27}-C_{31}) are predominantly derived from leaf wax lipids. The compound-specific $\delta^{13}C_{27\text{-}31}$ value is sensitive to effective precipitation, and therefore represents a useful indicator of regional monsoonal precipitation. The variation of compound-specific carbon isotopic values in the middle- and short-chain alkanes was mainly regulated by lake productivity and the accumulating organic pool through time. Spectral analysis on the $\delta^{13}C_{27\text{-}31}$ time series reveals significant periodicities of 87–89, 205–212, 1020–1050, and 1750–2041 years during the Holocene. On the centennial timescale, the quasi-periodicities around 88 and 210 years suggest a strong link between solar activity and monsoon rainfall. In the Last Glacial Maxiumu and deglacation, the $\delta^{13}C_{27\text{-}31}$ time series and other proxies indicate cold-dry climatic conditions during the Last Glacial Maximum, a cold Heinrich event, a warm-dry Bølling-Allerød, and a cold-wet Younger Dryas. The synchroneity between the biomarker time series in Lake Xiaolongwan and the Chinese stalagmite $\delta^{18}O$ records suggest that monsoonal changes are coupled with high latitude atmosphere-ocean processes. Regionally, the North Pacific may have played an important role for both decadal climatic variability and abrupt changes during the glacial/interglacial transition.

Acknowledgments

This study was supported by the Research Program of China (973 Program, 2010CB950201), the Strategic Priority Research Program of the Chinese Academy of Sciences (Grant No. XDA05080400), and the National Natural Science Foundation of China (Grant no. 41371219).

References

Gao, Q., Rioual, P., Chu, G., 2016. Lateglacial and early Holocene climatic fluctuations recorded in the diatom flora of Xiaolongwan maar lake, NE China. Boreas, 45: 61–75.

Mingram, J., Allen, J.R.M., Brüchmann, C., Liu, J., Luo, X., Negendank, J.F.W., Nowaczyk, N., Schettler, G., 2004. Maar- and crater lakes of the Long Gang Volcanic Field (N.E. China) d overview, laminated sediments, and vegetation history of the last 900 years. Quat. Int. 123–125, 135–147.

Minoshima, K., Kawahata, H., Ikehara, K., 2007. Changes in biological production in the mixed water region of the northwestern North Pacific during the last 27 kyr. Palaeogeogr. Palaeoclimatol. Palaeoecol. 254, 430–447.

Parplies, J., Lücke, A., Vos, H., Mingram, J., Stebich, M., Radtke, U., Han, J., Schleser, G.H., 2008. Late glacial environment and climate development in northeastern China derived from geochemical and isotopic investigations of the varved sediment record from Lake Sihailongwan (Jilin Province). J. Paleolimnol. 40, 471–487.

Schettler, G., Mingram, J., Liu, Q., Stebich, M., Dulski, P., 2006. East-Asian monsoon variability between 15,000 and 2000 cal. yr BP recorded in varved sediments of Lake Sihailongwan (northeastern China, Long Gang volcanic field). Holocene 16, 1043–1057.

Stebich, M., Mingram, J., Han, J.T., Liu, J.Q., 2009. Late Pleistocene spread of (cool-) temperate forests in northeast China and climate changes synchronous with the North Atlantic region. Glob. Planet. Change 65, 56–70.

Sun, Y., Oppo, D.W., Xiang, R., Liu, W., Gao, S., 2005. Last deglaciation in the Okinawa Trough: subtropical northwest Pacific link to Northern Hemisphere and tropical climate. Paleoceanography 20, PA4005.

Tan, M., 2007. Climatic differences and similarities between Indian and East Asian Monsoon regions of China over the last millennium: a perspective based mainly on stalagmite records. Int. J. Speleol. 36, 75–81.

Wang, Y., 1992. Effects of blocking anticyclones in Eurasia in the rainy season (Meiyu/Baiu season). J. Meteorol. Soc. Jpn. 70, 929–951.

Wang, Y.J., Cheng, H., Edwards, R.L., He, Y.Q., Kong, X.G., An, Z.S., Wu, J.Y., Kelly, M.J., Dykoski, K.A., Li, X.D., 2005. The Holocene Asian Monsoon: links to solar changes and North Atlantic climate. Science 308, 854–857.

Wu, J.Y., Wang, Y.J., Cheng, H., Kong, X.G., Liu, D.B., 2012. Climate of the Past Stable isotope and trace element investigation of two contemporaneous annually laminated stalagmites from northeastern China surrounding the “8.2 ka event”. Clim. Past 8, 1497–1507.

Xu, D., Lu, H., Chu, G., Wu, N., Shen, C., Wang, C., Mao, L., 2014. 500-year climate cycles stacking of recent centennial warming documented in an East Asian pollen record. Sci. Rep. 4, 3611.

The 2015 Surtseyan Eruption of Hunga Ha'apai-Hunga Tonga, South Pacific

Shane J. Cronin[1,*], Manuela Tost[1], Marco Brenna[1], Simon Barker[1], Murray Ford[1], Ian Smith[1], Sisi Tongaonevai[2], and Taaniela Kula[2]

[1]*School of Environment, University of Auckland, Auckland, New Zealand*
[2]*Geology Unit, Natural Resources Division, Ministry of Lands and Natural Resources, Nuku'alofa, Tonga*
*Corresponding author E-mail: s.cronin@auckland.ac.nz

A month-long eruption from mid-December 2014 built an emergent tuff-cone island, between the existing islets of Hunga Tonga and Hunga Ha'apai, 65 km NW of the capital of Tonga. The "Hunga" volcano is one of several historically active, shallow submarine to emergent volcanoes regularly spaced along the Tonga volcanic arc. Syn-eruptive photos and videos, along with visiting the new subaerial pyroclastic cone provided a rare opportunity to investigate models of emergent volcanism and sample the latest magma of the Tongan arc. Rapid coastal and surface-runoff erosion redistributed tuff to rapidly reshape the newly formed volcanic cone to form beaches allowing landing on the island. The first notice of this eruption was 19 December 2014, with steam-rich plumes first seen from Nukualofa on 30 December 2014. A 6-km high eruption was noted on 12 January 2015, leading to several days of flight cancellations. At this stage vigorous hydromagmatic eruptions were witnessed at close hand, with the production of a new island well in progress. On 17 January 2015, steam plumes were >10 km and by 24 January, the eruption was over. The events produced a new island of unconsolidated lapilli tuff over ~7 days, reaching up to 120 m above sea level and roughly 2 km in diameter. The cone is made up of unconsolidated, moderately sorted lapilli tuff beds of 20–100 cm thickness, interbedded with more poorly sorted variants 5–30 cm thick and richer in fine ash. The lower cone is dominated by fall deposits and jetted deposits with planar fabric and bedding, with some evidence for sliding and localized shear. The upper part of the cone is made up of thinner, finer-grained beds with a greater proportion of poorly sorted planar-bedded fall units and cross-bedded surge deposits. The sequence is dominated by angular juvenile pyroclasts, mainly, weakly to moderately vesicular, aphyric basaltic-andesite scoria lapilli. The initial conclusions from these deposits is that fragmentation was driven by both magmatic-gas expansion and magma-water interaction in an emergent setting as magma was ejected onto the shallow sea floor. Higher reported eruption columns were correlated with the vent becoming contained within a lake/crater wall. Subsequently, as the vent shallowed, magma eruption rates or gas content diminished, single eruptive bursts produced lower volumes of tephra, forming thinner beds of more highly fragmented pyroclasts.

Preeruption History of Silicic Magma Beneath the Tengchong Volcanic Field: A Textural and Mineral Geochemical Study of the Tengchong Drill Core

Leilei Ding*, Jiaqi Liu, Lei Zhang, Chunqing Sun, Jinliang Gao, Zhihui Cheng, Maoliang Zhang, and Zhengfu Guo

Institute of Geology and Geophysics, Chinese Academy of Sciences, Beijing, China
*Corresponding author E-mail: dingleilei@mail.iggcas.ac.cn

Keywords: Tengchong, magma chamber, magma mixing

About 269.5 m of dacites, pyroclastic rocks, and fluvial sediments were drilled in the Tengchong Volcanic Field (TVF), western China, which was a joint research project with Chinese Continental Scientific Drilling Project (CCSD). Volcanic rocks from the drilled core preserve petrological information that reflects the magmatic processes before eruption. The upper part of the drilling, volcanic rocks of layer I are as much as 82.7 m thick, while the lower part (layer II) is 186.8 m thick. Volcanic rocks in layer II have more pyroclastic layer than layer I. Zircon U-Pb dating age of 0.33 Ma (layer I) and 0.68 Ma (layer II) likely imply two stages of the magma eruption. And the later eruption (0.68 Ma) in Tengchong volcanic activity is strongest based on the previous study. The dacites from layer I and II have similar mineral assemblages: enstatite, clinopyoxene, plagioclase, hornblende, and ilmenite. The electron probe data of phenocrysts from the two layers show that the dacites were formed through mixing three magma that were different in composition and phenocryst assemblages: basaltic andesite, with Mg-rich orthopyroxene and An-rich plagioclase; andesite, with Mg-poor orthopyroxene and clinopyroxene, hornblende and netural plagioclase; and dacite, with albite plagioclase. Besides, the cumulophyric clots in dacite were witness of intermediate magma for mixing. Therefore, the dacites were formed by magma mixing processes involving three discrepancy end-member magma compositions. However, the distribution of An-poor plagioclase in the two layers show that layer II have more albite plagioclase than layer I. Thus, we deduced that the dacites from layer I were formed by mixing larger proportion of basaltic magma. More basaltic magma filling may be the key factor leading to the largest volcanic activity in Tengchong. Honeycomb texture observed in plagioclase phenocrysts in the two layers may be due to the growth in a rapidly cooling melt, and the smaller grain size in groundmass may also indicate a shorter timescale for their growth in a rapid risen. Thus, the mixing magma was withdrawn to the conduit, and it was mixed by three different mama compositions.

Acknowledgments

We thank Ting Li and Yutao Sun for their assistance in the field trip and helpful discussion. And this work was jointly supported by the Chinese Ministry of Science and Technology (Sinoprobe-05-03) and Paleoclimate record from lake sediments in Changbai Mountain over the past Millennia (41472320).

References

Ban, M., Sagawa, H., Miura, K. and Hirotani, S., 2008. Evidence for a short-lived stratified magma chamber: petrology of the Z-To5 tephra layer (c. 5.8 ka) at Zao volcano, NE Japan. Geological Society, London, Special Publications, 304(1): 149–168.

Barbey, P., Ayalew, D. and Yirgu, G., 2005. Insight into the origin of gabbro-dioritic cumulophyric aggregates from silicic ignimbrites: Sr and Ba zoning profiles of plagioclase phenocrysts from Oligocene Ethiopian Plateau rhyolites. Contributions to Mineralogy and Petrology, 149(2): 233–245.

Kawamoto, T., 1992. Dusty and honeycomb plagioclase: indicators of processes in the Uchino stratified magma chamber, Izu Peninsula, Japan. Journal of Volcanology & Geothermal Research, 49(3–4): 191–208.

Hule and Rio Cuarto Maars, Costa Rica: Assessing Our Own Resources for a Collective Good

Eliécer Duarte

Volcanological and Seismological Observatory of Costa Rica (OVSICORI). Universidad Nacional, Heredia, Costa Rica
E-mail: eduarte@una.ac.cr

Keywords: maar, Costa Rica, Hule

Hule maar (10 21 20N, 84 12 59W, 760 m.a.s.l., 21 m deep) is located 10 km north of Poás Volcano while Rio Cuarto maar (10.350N, 84. 222W, 360 m.a.s.l, 66 m deep) is located only 4 km north of Hule. Such distal maars end the north fracture zone of which Poás massif is the main and current volcanic feature formed by some 25 kms, trending N-S, along other superficial volcanic shapes.

The main morphological features of the area is constituted by a large caldera, formed about 3000 years ago (Melson et al., 1988), representing the remnants of a former twin volcano of which only the southern cone, the Cerro Congo, still exists. Three lakes are situated within the caldera: Laguna Hule, the largest one, Laguna Congo, and Laguna Bosque Alegre. At least two events of water lake overturn have been witnessed and reported by nearby settlers in the last 30 years, including sudden color changes and death of fish and birds (OVSICORI-UNA, 1996).

Hule maar is a nearly circular depression (2.2 × 1.7 kms) occupying a basin with three water bodies around two nested pyroclastic cones. Some recent lava flows may be related to such cones and radiocarbon dating fixes Hule formation to some 6000 years ago. Waters combined may amount up to 7M m^3 of fresh drinkable water.

Figure 1. General view of Hule Maar seen from the east rim.

On the other hand, Rio Cuarto is the deepest lake considered in Costa Rica (71 m) extending some 40 hectares at 400 m.a.s.l. It is surrounded by altered natural forest, pasture land, and plantations dedicated to ornamental plants. Being part of the Caribbean basin receives from 5 to 7 m of rain a year. Due to this location in the northern plains showers may extend evenly year round changing water quality and conditions in these water bodies frequently. It is almost circular and stands approximately 40 m above the surroundings, in a greater alluvial plain. With a diameter of some 700 × 500 m.

Its steep inner walls have basalt to andesite lava flows that are heavily altered due to severe tropical weather conditions. Above these lava flows are chaotic fallout and pyroclastic surge layers due probably to the initial phreato-magmatic explosions through the preexistent layers of sediments and lava flows. Its large basin holds approximately 15.1M m^3 of fresh, neutral water with a steady temperature ranging from 25°C to 30°C. It is not clear why this maar did not have additional eruptions to construct a volcano as there are many polygenetic volcanoes in its surroundings in similar geological and geomorphological conditions.

One of the main reasons to study this lake was several reports, from neighbors, about unexplained mixing causing fish death (probably limnic eruptions). Such mixing is produced when lower layers are capable of sustaining important levels of toxic gases (namely, CO_2), that might be suddenly released. Witnessed death of fish could be explained by depletion of oxygen during such reported events. Similarly, aquatic micro- and macrofauna may die for this reason or due to rapid poisoning.

A geochemical sampling was carried out working on different levels from the surface (0 m) to its deepest point (71 m). In every selected level samples were taken for acidity, main, minor, and trace element chemical composition, dissolved organic compounds, gas content, isotopic composition, and main gas compounds (CO_2 y CH4). Furthermore, several dozens of samples were

collected in a vertical fashion along the deepest profile of this lake. Samples are being processed by researchers from the University of Florence and data will be available in the near future.

Figure 2. General view of Rio Cuarto Maar seen from the south rim.

Temperature profile indicates absence of thermal stratification although increasing acidity with depth suggests compositional stratification due to bacterial activity. Chemical and isotopic analysis may shed light on several issues or even confirm some of these preliminary indications.

Mixing events that may occur preferably during periods of heavy rain and erosion may act as a natural control over the potential overaccumulation of gases at the bottom. Such mechanism may contribute to diminish risk to fishermen, neighbors, and visitors that often enjoy the area.

Our talk will depict the nature of the forming volcanic activity from the exposed inner and outer walls. It will also show geomorphological and vegetation characteristics of these unusual volcanic features in order to illustrate the value of natural resources contained in both depressions. Both maars are poorly exploited, tourism wise, giving us conditions to propose alternative ways for more and better recreational use.

Moreover, details about the water characteristics and its potential for human consumption will be given in order to provide suggestions for surroundings communities and other users.

Acknowledgments

The author is thankful to the Universidad Nacional authorities for their support, to MICITT for partial funding support, and for those workmates at OVSICORI that, in one way or another, have supported my work. To Franco Tassi, Orlando Vaselli, and Francesco Bergamaschi (University of Florence, Italy) for sharing their time and expertise in our campaign at Rio Cuarto and other volcanoes and maars.

References

Alvarado, G. 2000. Los volcanes de Costa Rica. Geologia, historia y riqueza natural. Editorial UNED. San Jose, Costa Rica.

Haberyan, K. et al. 2003. Basic limnology of fifty one lakes in Costa Rica. Rev. Biologia Tropical. V51, N1, San Jose, marzo.

Tassi, F., Vaselli, O., Fernández, E., Duarte, E., Martínez, M., Delgado Huertas, A., Bergamaschi, F. 2009. Morphological and geochemical features of crater lakes in Costa Rica: an overview. J Limnol 68(2):1–13.

The Formation Mechanism and Distribution of Volcanic Hydrocarbon Reservoirs in China

Jinliang Gao and Jiaqi Liu

Institute of Geology and Geophysics, Chinese Academy of Sciences, Beijing, China
*Corresponding author E-mail: gaojinliang@mail.iggcas.ac.cn

Keywords: volcanic, hydrocarbon, reservoirs

Volcanic hydrocarbon reservoirs are distributed widely in sedimentary basins in China (Feng, 2008; Liu and Meng, 2009; Zou et al., 2008). Volcanic rocks have changed from "forbidden area" to "target area" in exploration. There are mainly intermediate rocks and acidic rocks in east China which primarily developed in intracontinental rift settings during Jurassic to Cretaceous and Paleogene to Neogene, and intermediate rocks and basic rocks in west China which developed in intracontinental rift and island-arc environment duiring Carboniferous to Permian.

The volcanism in sedimentary basins in China can promote the formation of high-quality source rocks and the biogenic hydrocarbon generation process. The role of volcanic activity effects on organic matter into hydrocarbon is mainly to supply catalyst and thermal energy (Zhu et al., 2007). Volcanogenic zeolite and olivine and transition metals in hydrothermal liquid can be a catalyst of organic matter into hydrocarbon (Mango, 1992). The thermal effect of volcanic activity has a dual function on organic matter hydrocarbon generation, which can accelerate the maturation of immature source rocks and hydrocarbon generation, also can make mature source rocks overmature or destroy oil and gas reservoir formed earlier (Chen et al., 1989).

The origin of natural gas hosted in volcanic reservoirs can be both biogenic and abiogenic (Dai et al., 2001). In the volcanic reservoirs in China, most of the hydrocarbon has been proved as organic derivation, and a few alkane gas and nonhydrocarbon gas are inorganic derivation. The origin of hydrocarbon can be distinguished with isotopes such as C and He.

The volcanic reservoirs are chiefly composed of rhyolite, dacite, andesite, basalt, and pyroclastic rocks in China (Luo et al., 1999). It can be classified into "5 facies and 15 subfacies" with respect to lithification mechanism and reservoir significance (Figure 1) (Wang et al., 2003). In general, felsic sequence starts with explosive facies, and intermediate, basic sequence starts with effusive facies. Reservoir spaces of volcanic rocks are composed of primary pores, secondary pores, and fissures (Figure 2). Upper part of effusive facies, loose intercalation in between explosive facies, and inner subfacies of extrusive facies are the main targets for hydrocarbon exploration in China because of their good porosity and permeability. It is indicated that secondary reservoir space which includes dissolved pores, structural fractures, and weathered fractures makes a dominant contribution to the improvement of volcanic reservoir capacity. The property of volcanic reservoirs is affected by several factors, such as lithology and lithofacies, eruption environment, tectonics, and diagenesis.

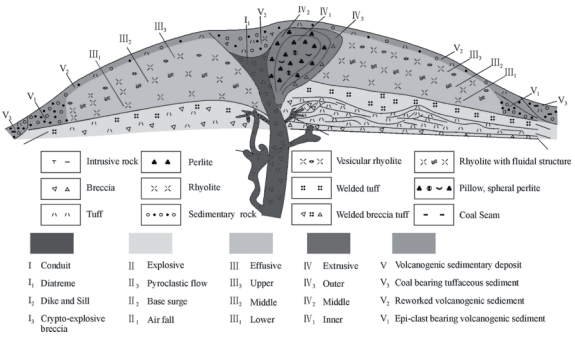

Figure 1. Facies model of the Mesozoic acidic volcanic rocks in the Songliao Basin.

Besides being reservoirs, volcanic rocks can also be good cap rocks (Fu et al., 2010). After volcanic ash falls into water, it will inflate and form layers of bentonite or mudstone with bentonite which may become excellent cap rocks. While mudstone is lacking of sealing abilities in the mid-shallow part of basins, unaltered massive basalts generally are rather better cap rocks. Some layered intrusive rocks may also be good cap rocks, for example, the Lin 8 oil trap in Huimin depression of Bohai Bay Basin, north China. In the deep part of Xujiaweizi depression of Songliao Basin, two types of volcanic rocks have been found to be cap rocks including the pyroclastic type and lava type.

The migration of hydrocarbon predominantly relies on faults and crusts of weathering in the volcanic hydrocarbon system in China. The features of faults control the distance and period of vertical migration while the area of crusts of weathering

controls the distance of lateral migration and the scale of hydrocarbon accumulation.

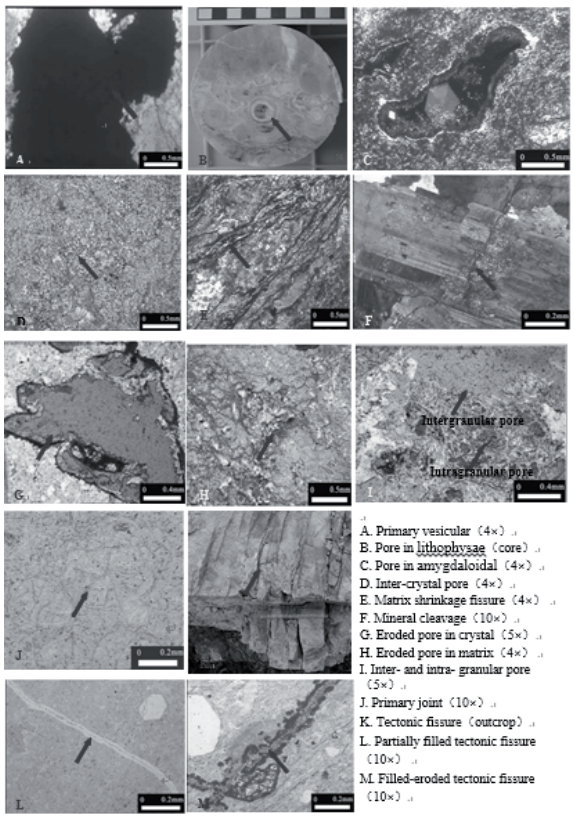

Figure 2. Volcanic reservoir space types.

By the comparison between industrial gas wells and other wells, advantages of forming high production gas include reservoir space diversity, high porosity, good source rocks, anticlinal /faulted anticline traps, and the vertical migration pathway. The reservoir forming effects will be poor once one of the conditions above is absent. For example，although having good source rocks，DB10 well only gains low producing gas because of unitary reservoir spaces and poor porosity-permeability. SS1 well has good porosity-permeability and diversiform reservoir spaces while its source rocks is poor, it does not gain industrial gas.

Under the control of all factors, the volcanic hydrocarbon accumulation chiefly develops in certain positions, including the top of volcanic cycles, unconformity surfaces, and areas near deep-seated faults. The volcanic hydrocarbon reservoirs in east China are lithologic and sturctural-lithologic reservoirs and those in west China belong to stratigraphic reservoirs.

References

Chen, R.S., He, S., Wang, Q.L., et al., 1989. A preliminary discussion of magma activity on the maturation of organic matter-taking Geyucheng-Wenan area of Hebei province as an example (in Chinese with English abstract). Petroleum Expoloration and Development 16: 29–38.

Dai, J.X., Shi, X., Wei, Y.Z., 2001. Summary of the abiogenic origin theory and the abiogenic gas pools (fields) (in Chinese with English abstract). Acta Petrolei Sinica 22: 5–10.

Feng, Z.Q., 2008. Volcanic rocks as prolific gas reservoir: A case study from the Qingshen gas field in the Songliao Basin, NE China. Marine and Petroleum Geology 25: 416–432.

Fu, G., Hu, M., Yu, D., 2010. Volcanic cap rock type and evaluation of sealing gas ability: An example of Xujiaweizi depression (in Chinese with English abstract). Journal of Jilin University (Earth Science Edition) 40: 237–244.

Liu, J.Q., Meng, F.C., 2009. Hydrocarbon generation, migration and accumulation related to igneous activity (in Chinese with English abstract). Natural Gas Industry 29: 1–4, 129.

Luo, J.L., Zhang, C.L., Qu, Z.H., 1999. Volcanic reservoir rocks: A case study of the Cretaceous Fenghuadian suite, Huanghua basin, eastern China. Journal of Petroleum Geology 22: 397–416.

Mango, F.D., 1992. Transition metal catalysis in the generation of petroleum and natural gas. Geochimica et Cosmochimica Acta 56: 553–555.

Wang, P.J., Chi, Y.L., Liu, W.Z., et al., 2003. Volcanic facies of the Songliao basin: Classification, characteristics and reservoir significance (in Chinese with English abstract). Journal of Jilin University (Earth Sciences Edition) 33: 449–456.

Zhu, D.Y., Jin, Z.J., Hu, W.X., et al., 2007. Effect of igneous activity on hydrocarbon source rocks in Jiyang sub-basin, eastern China. Journal of Petroleum Science and Engineering 59: 309–320.

Zou, C.N., Zhao, W.Z., Jia, C.Z., et al., 2008. Formation and distribution of volcanic hydrocarbon reservoirs in sedimentary basins of China (in Chinese with English abstract). Petroleum Exploration and Development 35: 257–271.

Eruptive Process and Internal Structure of the Songaksan Tuff Ring, Jeju Island, Inferred from Componentry Analysis of Pyroclasts

Sun Young Go[1,*], Gi Bom Kim[1], Jong Ok Jeong[2], and Young Kwan Sohn[1]

[1]*Department of Geology, Gyeongsang National University, Jinju, Republic of Korea*
[2]*Central Instrument Facility, Gyeongsang National University, Jinju, Republic of Korea*
*Corresponding author E-mail: igo@gnu.ac.kr

Keywords: tuff ring, componentry analysis, diatreme

Songaksan, Jeju Island, Korea, is a basaltic tuff ring with a scoria cone and ponded lava within the crater produced by a 3.8 ka phreatomagmatic eruption in a coastal setting (Sohn 1996; Figure 1). Componentry and geochemical analyses of ash-size tephra from four units (A–D) of the Songaksan rimbeds were carried out to understand the eruption processes.

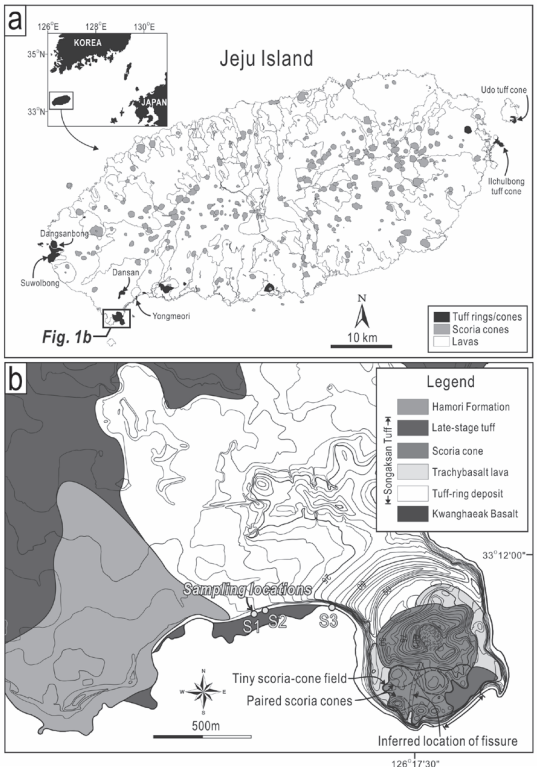

Figure 1. (a) Simplified geologic map of Jeju Island, showing outlines of lava flows and distribution of monogenetic volcanic landforms. Inset shows the location of Jeju Island. (b) Detailed geologic and topographic map of the Songaksan tuff ring. S1 and S2 are sampling locations for componentry analysis, and S3 for source verification of accidental lithic blocks. Modified after Sohn et al. (2002) and Sohn and Park (2004).

Glassy or juvenile grains are classified into sideromelane, tachylite, and intermediate grains based on BSE images of polished sections. Accidental materials include crystalline basalt fragments derived from 0 to 50 m in depth, tuff fragments from 50 to 150 m in depth, and quartz crystals and metasedimentary rock fragments from deeper levels.

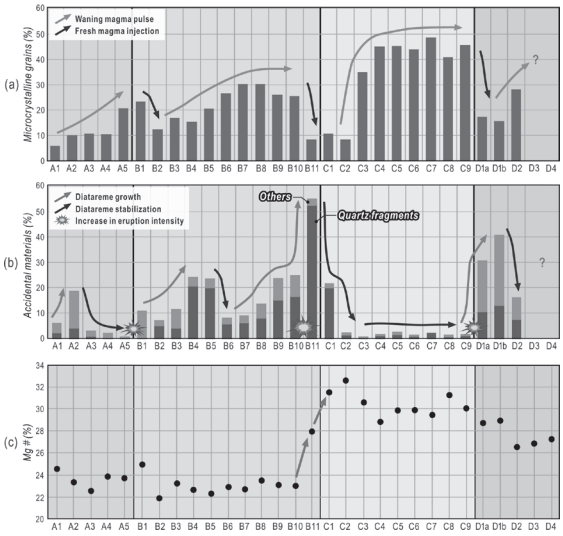

Figure 2. Vertical variations of the componentry of Songaksan tuff ring deposits. (a) The proportion of tachylite (+intermediate grains) relative to sideromelane changes abruptly near the unit boundaries, suggesting that the four units of the rimbeds, distinguished by colors in the field, represent four pulses of magma ascent. (b) The proportion of accidental materials relative to juveniles, showing a marked contrast between units A and C (accidental-poor) and units B and D (accidental-rich). (c) The variation of $Mg^{\#}$ of sideromelane glass, showing an abrupt change across the boundary between units B and C. Note: $Mg^{\#} = (MgO/(MgO + FeO))*100$.

The analysis shows that the ratio of tachylite to sideromelane grains generally increases within individual units (Figure 2a), suggesting four pulses of magma rise during the tuff-ring eruption (Taddeucci et al., 2004; Sable et al., 2006). Analysis of the ratio of accidental to juvenile

materials together with the ratio of shallow to deep-derived accidentals (Figure 2b) shows that Unit A is marked by generally low accidental content consisting dominantly of shallow-derived lithics, implying shallow-seated explosions following incipient cratering (Figures 3a–c). Unit B, characterized by a high accidental content of deep-derived lithics, especially at the top of the unit, suggests powerful deep-seated explosions (Tchamabe et al., 2015) and diatreme growth followed by a final eruption that probably emptied the diatreme structure (Figures 3d and e). Unit C has an extremely low accidental content, suggesting that the magma interacted with free water inside a stabilized diatreme rather than with wet sediment or interstitial water within the substrate (Figure 3f). Unit D has a high accidental content with rare deep-derived lithics, suggesting additional diatreme growth till the cessation tuff ring eruption (Figures 3g and h).

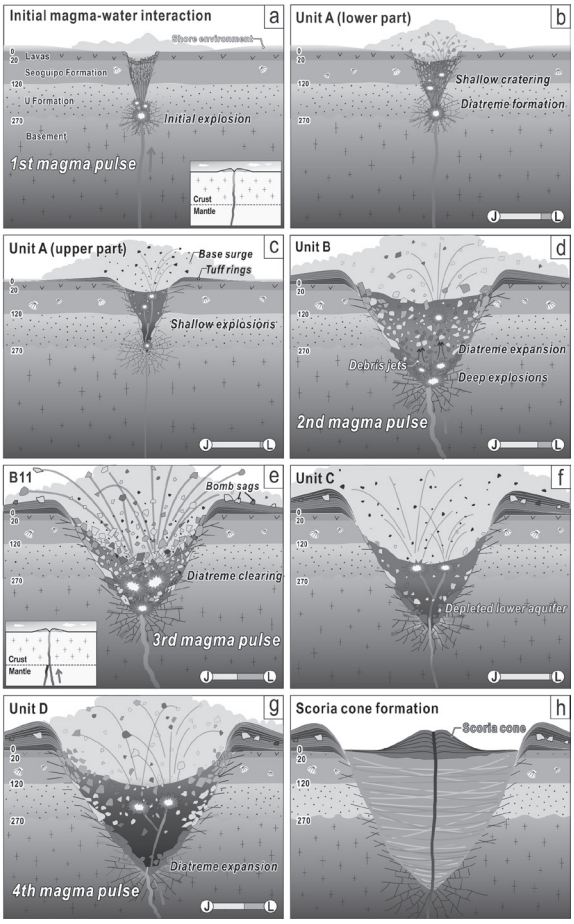

Figure 3. Cartoons showing the evolution and growth of the Songaksan tuff ring and its diatreme.

The transition between Unit B and Unit C is coincident with the change (Figure 2b) of sideromelane glass composition (Mg#), suggesting the arrival of a new magma batch by the end of Unit B eruption (Brenna et al., 2011; Ahn et al., 2015). Possibly, the ascent of new magma might have triggered the climactic eruption that maximized the excavation of diatreme-fill lithics at the end of Unit B.

Furthermore, we expect that the volume ratio of accidental materials from different substrata could be an aid to the estimation and approximation of the size and the morphology of the Songaksan diatreme.

References

Ahn, U. S., Sohn, Y. K., Yoon, Y. S., Ryu, C. K., Jeong, J. O., & Kang, C. W. (2015). Geochemical fingerprinting of basaltic glass in tephra deposits underlying the human footprints-bearing strata in Jeju Island, Korea: Provenance of tephra and age of the human footprints. Journal of the Geological Society of Korea. 51(2), 105–126.

Brenna, M., Cronin, S. J., Nemeth, K., Smith, I. E., & Sohn, Y. K. (2011). The influence of magma plumbing complexity on monogenetic eruptions, Jeju Island, Korea. Terra Nova, 23(2), 70–75.

Sable, J. E., Houghton, B. F., Del Carlo, P., & Coltelli, M. (2006). Changing conditions of magma ascent and fragmentation during the Etna 122 BC basaltic Plinian eruption: evidence from clast microtextures. Journal of Volcanology and Geothermal Research, 158(3), 333–354.

Sohn, Y. K., & Park, K. H. (2004). Early-stage volcanism and sedimentation of Jeju Island revealed by the Sagye borehole, SW Jeju Island, Korea. Geosciences Journal, 8(1), 73–84.

Sohn, Y. K., Park, J. B., Khim, B. K., Park, K. H., & Koh, G. W. (2002). Stratigraphy, petrochemistry and Quaternary depositional record of the Songaksan tuff ring, Jeju Island, Korea. Journal of Volcanology and Geothermal Research, 119(1), 1–20.

Sohn, Y. K. (1996). Hydrovolcanic processes forming basaltic tuff rings and cones on Cheju Island, Korea. Geological Society of America Bulletin, 108(10), 1199–1211.

Taddeucci, J., Pompilio, M., & Scarlato, P. (2004). Conduit processes during the July–August 2001 explosive activity of Mt. Etna (Italy): inferences from glass chemistry and crystal size distribution of ash particles. Journal of Volcanology and Geothermal Research, 137(1), 33–54.

Tchamabé, B. C., Ohba, T., Kereszturi, G., Németh, K., Aka, F. T., Youmen, D., ... & Hell, J. V. (2015). Towards the reconstruction of the shallow plumbing system of the Barombi Mbo Maar (Cameroon) Implications for diatreme growth processes of a polygenetic maar volcano. Journal of Volcanology and Geothermal Research, 301, 293–313.

From Regional Geopark to a UNESCO Global Geopark: Community Initiative with Strong Scientific Support to Evaluate the Geoheritage and Cultural Values at Ihumātao, South Auckland, New Zealand

Ilmars Gravis and Károly Németh*

Volcanic Risk Solutions, Institute of Agriculture and Environment, Massey University, Palmerston North, New Zealand
*Corresponding author E-mail: k.nemeth@massey.ac.nz

Keywords: geosite, scoria, maar

Monogenetic volcanic fields carry great geoheritage values, especially if their historic eruptions influenced human societies and are reflected in oral and written history, and artifactual historical remains of such event(s). Volcanic fields consist of few to over hundreds of volcanic centers erupted in numerous events, and usually spanning tens of thousands of years. Eruptions commonly recur in cycles of over hundreds of years; hence, the volcanic landforms of a single field can show various stages of erosion and vegetation cover, making monogenetic volcanic fields visually attractive landscapes. The Auckland Volcanic Field (AVF) in the North Island of New Zealand is one of the youngest basaltic volcanic fields in New Zealand, active since about 250 ka BP. The volcanic field displays a high geodiversity, as most of its volcanic eruptions were influenced in some degree by phreatomagmatism as rising magma interacted explosively with the shallow aquifers and some surface waters (Kereszturi et al. 2014). While the volcanic field has been the subject of intense scientific research in recent years, especially in relation to volcanic hazard and risk management and forecasting, relatively little has been done so far to document and evaluate the geoheritage values of the region, especially with the goal of developing successful geoeducational and geotouristic programs. Recently, an application has been lodged for adding AVF to the UNSECO World Heritage List, in spite of the general lack of evaluation of their geosites throughout the AVF as a whole. Even with a well-established geosite inventory of the AVF volcanic field demonstrating its **outstanding universal values (OUV)** based on its natural phenomena, establishing validity as a World Heritage site may prove to be a difficult task, as monogenetic volcanic fields contain the most common types of volcanoes on Earth.

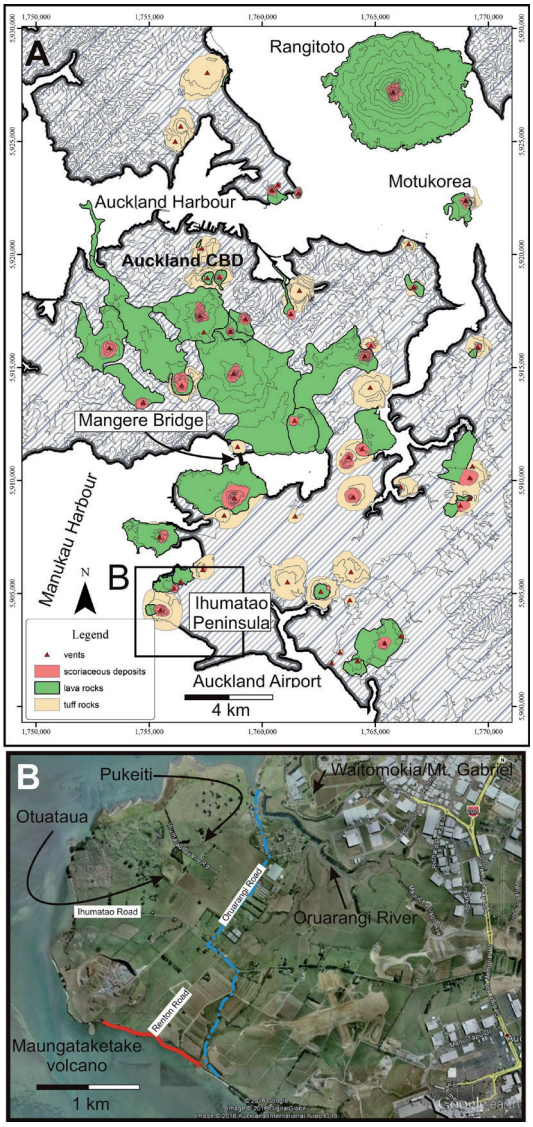

Figure 1. Map of the Auckland Volcanic Field shows the various types of volcanoes (A) and Ihumatao Peninsula (B).

Here, we argue for a more conservative approach to promoting the volcanic geoheritage of the AVF (Figure 1), by first establishing a local or regional geopark first that may later act as a catalyst to expand this idea through other communities located in the territory of the AVF. A systematic and thorough program in the future is expected to provide enough information and experience to bid for the AVF UNESCO Global Geopark status, or if the outstanding universal values are clearly demonstrated even for the UNESCO World Heritage status. The Ihumātao Peninsula is the home of well exposed and highly accessible volcanic features demonstrating a high geodiversity, offering itself as a reflection of the Auckland Volcanic Field on a miniature scale. It could be viewed as a hub of geosites showing many possible volcanic features seen elsewhere in the AVF, all within one discrete and easily accessible region.

In particular, the Ihumātao Peninsula, and the wider Mangere area, is a region where periods of alkaline basaltic volcanic activity have produced numerous volcanic features over the Quaternary Period. These features include tuff deposits, maar craters, lava flows, and scoria cones. In several areas the results of interacting eruptive processes may still be viewed in an area well served by infrastructure due to its proximity to an urban center. Auckland is well known for being a rapidly growing city (~1.4 million) developed on top of a still active monogenetic volcanic field, a fact which also contributes to the accessibility of the volcanic field.

To date considerable focus has been directed at the AVF from a scientific research and hazards management perspective. However, prior to a proposal for designation as a UNESCO world heritage site for values as a natural and cultural landscape, there has been no systematic effort to scientifically assess and research the value of the AVF as a whole, using models that have been applied in an international context.

It is proposed that the Ihumātao Peninsula and contiguous areas of South Auckland are an ideal region to assess suitability and refine assessment models. Due to the unbroken history of human occupation and cultivation in this area, it is acknowledged that cultural values in this area are particularly important, and it provides an ideal site for suitability of geosite assessment models with relation to cultural and societal values as they may be influenced by geography.

Figure 2. World class exposure of a tuff ring sequence with base surge demolished trees at Maungataketake.

In addition, this region may provide ideal for designation as a geopark or part of a broader Auckland-wide geopark, allowing protection, education, and celebration of values held in high regard by a diverse range of communities. Clearly definable geographical boundaries, volcanic features within close proximity of each other, and extremely strong connections with the local Māori community are factors that further reinforce the suitability of this area.

It is envisaged that designation of the AVF as a UNESCO World Heritage site, could take several years. In contrast, the formation of a “regional” geopark at Ihumātao could be driven primarily from a community level, while still providing effective protection for an area with a long history of threats from urban encroachment and industrial development. Additionally, this could be the first “geopark” of its type in Auckland, celebrating both the geological history of the land, and placing it alongside cultural history of the land in a position of equal importance.

References

Kereszturi G, Nemeth K, Cronin SJ, Procter J, Agustin-Flores J (2014) Influences on the variability of eruption sequences and style transitions in the Auckland Volcanic Field, New Zealand. Journal of Volcanology and Geothermal Research 286:101–115.

Fluxes and Genesis of Greenhouse Gases Emissions from Typical Volcanic-Geothermal Fields in China

Zhengfu Guo[1,*], Maoliang Zhang[1,2], Zhihui Cheng[1,2], Lihong Zhang[1], and Jiaqi Liu[1]

[1]*Institute of Geology and Geophysics, Chinese Academy of Sciences, Beijing, China*
[2]*University of Chinese Academy of Sciences, Beijing, China*
*Corresponding author E-mail: zfguo@mail.iggcas.ac.cn

Keywords: greenhouse gases, flux, deep carbon cycle

Deep-seated carbon could be transported from Earth's interior into atmosphere by volcanic activities, which play an important role in geologic carbon degassing and its effects on global climate and environment. In addition to volcanic eruptions, quiescent volcanoes could also release large amounts of magma-derived CO_2 into the atmosphere. Therefore, quantitative studies on evaluating the contribution of volcanic activities to rising of atmospheric CO_2 concentration are critical, especially in the context of global warming. Cenozoic volcanic activities are mainly distributed in two tectonic domains, i.e., the Pacific tectonic domain (e.g., Changbaishan volcanic field) and the Thethys tectonic domain (e.g., Tengchong volcanic field), which have great potential to release huge amounts of carbon into the atmosphere.

During the past few years, we have estimated the fluxes of greenhouse gases released from typical volcanic-geothermal fields (e.g., Changbaishan, Tengchong, Wudalianchi, and Yangbajing) in China using closed chamber method and gas-water chemistry methods. It is indicated that the total flux of greenhouse gases (referring mainly to CO_2) from the studied volcanic fields is ca. 8.13×10^6 t a^{-1} (Guo et al., 2014), taking up about 6% of the total CO_2 flux from global volcanoes. Additionally, total output of greenhouse gases released from Cenozoic volcanic fields in the Pacific tectonic domain may be lower relative to those of Cenozoic volcanic fields in the Thethys tectonic domain, suggesting difference in volatile recycling mechanism at different types of tectonic settings.

Magma-derived volatiles from the Pacific tectonic domain (as represented by Changbaishan and Wudalianchi in NE China; Zhang et al., 2011, 2015) and the Thethys tectonic domain (as represented by Yangbajing and Tengchong in SW China; Cheng et al., 2012, 2014; Zhang et al., 2014) display different signatures on flux of greenhouse gases and gas geochemistry. In details, volcanic gases from the Thethys tectonic domain are characterized by higher degree of crustal contribution in mantle source and their transportation in the crust (e.g., low $^3He/^4He$) than those of the Pacific tectonic domain (e.g., high $^3He/^4He$), indicating different tectonic settings and mechanisms of magma evolution between oceanic subduction zone and continental subduction zone.

References

Cheng, Z., Guo, Z., Zhang, M., Zhang, L., 2012. CO_2 flux estimations of hot springs in the Tengchong Cenozoic volcanic field, Yunnan Province, SW China. Acta Petrologica Sinica 28, 1217–1224 (in Chinese with English abstract).

Cheng, Z., Guo, Z., Zhang, M., Zhang, L., 2014. Carbon dioxide emissions from Tengchong Cenozoic volcanic field, Yunnan Province, SW China. Acta Petrologica Sinica 30, 3657–3670. (in Chinese with English abstract).

Guo, Z., Zhang, M., Cheng, Z., Zhang, L., Liu, J., 2014. Fluxes and genesis of greenhouse gases emissions from typical volcanic fields in China. Acta Petrologica Sinica 30, 3467–3480 (in Chinese with English abstract).

Zhang, L., Guo, Z., Zhang, M., Cheng, Z., 2014. Study on soil micro-seepage gas flux in the high temperature geothermal area: an example from the Yangbajing geothermal field, South Tibet. Acta Petrologica Sinica 30, 3612–3626 (in Chinese with English abstract).

Zhang, M., Guo, Z., Cheng, Z., Zhang, L., Guo, W., Yang, C., Fu, Q., Wen, X., 2011. Greenhouse gases flux estimation of hot springs in Changbaishan volcanic field, NE China. Acta Petrologica Sinica 27, 2898–2904 (in Chinese with English abstract).

Zhang, M., Guo, Z., Sano, Y., Cheng, Z., Zhang, L., 2015. Stagnant subducted Pacific slab-derived CO_2 emissions: insights into magma degassing at Changbaishan volcano, NE China. Journal of Asian Earth Sciences 106, 49–63.

Identification of the Optimal Spatial Unit for Process-Based Terrain Analysis in Mt. Changbai (Baekdu) Volcanic Region

Qiuhong Jin*, Yoosoon An, and Soojin Park

Department of Geography, Seoul National University, Seoul, Korea
*Corresponding author E-mail: qhj84@snu.ac.kr

Keywords: Mt. Changbai volcanic topography, surface curvature, upslope contributing area

Mt. Changbai (Baekdu) volcanic region, which distributes across Sino-Korean border, is one of the most unique landscapes for Korean and northeast Chinese in their historical, cultural, and ecological context. According to the historical records, about six volcanic eruptions have occurred (Choi et al., 2013). The impact of these eruptions affected not only Korea and northeast China, but also northeast Japan. The landform of this volcanic region that has been made by these eruptions is an unusual landscape in Korean Peninsula. This morphological characteristic may affect geomorphological, geochemical, and ecological processes. Therefore, geomorphological and hydrological process-based terrain analyses are needed for understanding environmental condition of this region. Despite the importance of terrain analysis in this region, however, there has been minimal research regarding terrain research in this area. For most part, recent geomorphological research in this region has tended to center around the description of the geomorphological landscape and estimation of the impact of the disasters caused by volcanic eruption.

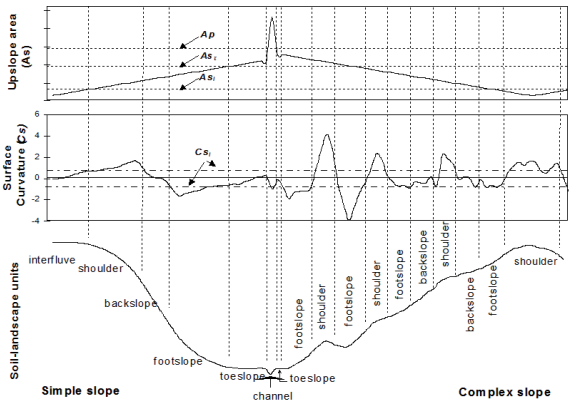

Figure 1. Quantitative terrain analysis method in catena concept by Park et al. (2001).

In geomorphological studies, various quantitative and classification methods have been developed by using Digital Elevation Model (DEM) (Vitek et al., 1996; Park et al., 2001; Park, 2004). In order to understand geomorphological process and ecosystem in this region, this study applies a simple process-based terrain characterization model that is based on the catena approach (Park et al., 2001). This concept was introduced by Milne (1936) to explain soil-geology-topography. Afterwards, Conacher and Dalrymple (1977) adopted the catena concept and established "nine-unit landscape unit (NULM)" for developing this concepts. This model remains one of the most widely accepted concepts both in geomorphology and pedology (Park et al., 2001). As NULM is just a descriptive approach for understanding pedogeomorphological relationship, however, quantitative methods were needed due to development of GIS and DEM (Park and Burt, 2002; Park, 2004). In order to overcome this limitation, Park et al. (2001) developed a quantitative method which is based on the catena concept, GIS and DEM. This model consists of two topographical indices and can classify landscape units by using the relationship between two indices (Figure 1). The first index is surface curvature (CS) which reflects magnitude of slope gradient and curvature of three-dimensional surface forms (Park et al., 2001). The second index is upslope contributing area (AS), which means the total catchment area above a point on the landscape (Park et al., 2001).

The study site is shown in Figure 2. The landform of this area, which consists of complicated origin cone-shape volcanos, is similar to low-gradient one cone-shape volcano. Although this area is the source of the three main rivers in this region (Yalu River, Tumen River, and Songhua River), drainage divide is not clear in this area. As the spatial unit of the Park et al.'s (2001) terrain model and any other terrain analysis approach is mainly based on the drainage basin reflecting the sediment cycle system, uncertainty of the drainage divide can be a problem for detecting the natural process of these areas. On account of this reason, we wonder whether basin unit is proper to analyze topographical characteristic in this region. Therefore, this study aims to compare the analyzing results that are based on basin unit and on alternatives to identify optimal unit for this study region.

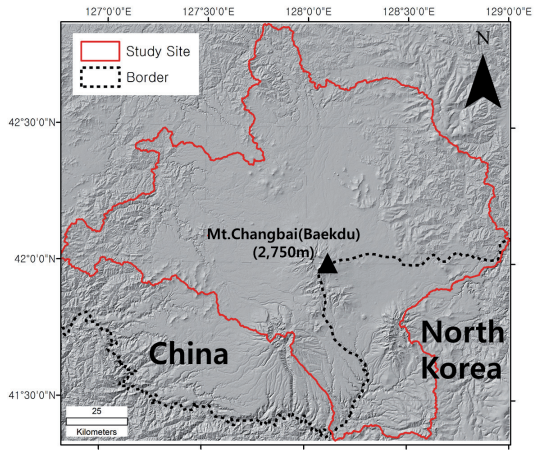

Figure 2. Location of study site and landform (hillshade).

In this study, Shuttle Radar Topography Mission (SRTM) 1 arc-second DEM from the United States Geological Survey published in 2015 are used. We set and use typical small-scale drainage basin and "mountain" unit, which share same forming process, for terrain analysis. And we compared these results of analysis.

The patterns of results seem to be almost the same. However, we could find much difference between the results of each cell (Table 1). Only 47.8% area of each results are same, other area shows slope unit class difference. Moreover, the area of backslope by using mountain unit shows much more than that by using drainage basin units. We guess this result shows overestimation in drainage basin unit results, which is caused by uncertainty of the drainage divide. These overestimates imply the error of terrain classification could happen when we apply drainage basin unit in volcanic region like this study site. Therefore, we conclude mountain unit is the optimal spatial unit in the study area and could be the best option for terrain analysis in volcanic region.

This study is the preliminarily study for understanding pedogeomorphological process and ecosystem structure of the study site. We expect that our findings of this research can contribute to method for terrain analysis and understanding ecological processes. However, follow-up study of the optimal spatial unit for terrain analysis in volcanic region is required.

References

Choi, E.K., Kim, S.W., Lee, Y. C., Lee, K. H., and Kim, I.S., 2013, Analyzing the Disaster Vulnerability of Mt. Baekdusan Area Using Terrain Factors, Journal of Korean Earth Science Socieity, 34(7): 605–614 (in Korean).

Conacher, A.J., and Dalrymple, J.B., 1977, The Nine Unit Landsurface Model : An Approach to Pedogeomorphic Research, Geoderma, 18: 1–153.

Milne, G., 1935, Some Suggested Units of Classification and Mapping, Particularly for East African Soils. Soil Research 4: 183–198.

Park, S.J., McSweeney, K., and Lowery, B., 2001, Prediction of Soils Using a Process Based Terrain Characterisation. Geoderma 103: 249–272.

Park, S.J., and Burt, T.P., 2002, Identification and characterization of pedogeomorphological processes on a hillslope using an indirect gradient analysis. Soil Science Society of America Journal 66: 1897–1910.

Park, S.J., 2004, A Geomorphological Classification System to Characterize Ecological Processes Over the Landscape, Journal of the Korean Geographical Society, 39(4):495–513.

Vitek, J.D., Giardino, J.R., and Fitzgerald, J.W., 1996, Mapping Geomorphology: A Journey from Paper Maps, Through Computer Mapping to GIS and Virtual Reality, Geomorphology, 16: 233–249.

Table 1. Cell to cell comparison between analysis by using basin unit and by using mountain unit. The bold results mean the area is of the same results of each unit. The red results mean most different area between them.

Area(Unit : ha)		Analysis by using mountain unit							
Analysis by using drainage basin unit	Slope Unit	Summit	Shoulder	Backslope	Footslope	Toeslope 1	Toeslope 2	Channel	Total
	Summit	**34347.2**	17211.69	42866.55	830.61	6634.44	455.22	796.86	103142.52
	Shoulder	24799.77	**113042**	82683.54	4632.21	18825.39	1576.08	242.46	245801.25
	Backslope	33064.47	39943.98	**285488.01**	23556.96	81438.57	17101.8	3987.18	484580.97
	Footslope	1573.38	5848.83	49535.1	**38549.79**	17674.11	32907.69	5044.77	151133.67
	Toeslope 1	6596.28	10250.73	63953.01	3756.87	**133168.5**	21185.37	2814.03	241724.79
	Toeslope 2	617.04	1377.45	23810.67	16238.34	39043.89	**62444.88**	5035.5	148567.77
	Channel	1373.58	240.21	8341.29	4786.83	12555	11225.43	**16374.78**	54897.12
	Total	102371.7	187914.7	556678.17	92351.61	309339.9	146896.47	34295.58	**1429848.09**

Uranium Deposits of Paleonecks of the Peripheral Zones of the Great Xingan Volcanic Plutonic Belt: Indicators of Large Ore Clusters

Vadim Khomich[1,*], Hongquan Yan[2,*], Yang Yanchen[2], and Natalia Boriskina[1]

[1]*Far East Geological Institute, Far East Branch of Russian Academy of Sciences, Vladivostok, Russia*
[2]*Geological Survey Institute of Jilin University, Jilin, China*
*Corresponding author E-mail: khomich79@mail.ru, hongquanyan@126.com

Keywords: uranium, deposits, criteria

Combination of the uranium ore occurrences and deposits, revealed in the outer and flank zones of the Great Xingan volcanic plutonic belt (GXVPB), is one of the notable characteristics of the contiguous territories of South-East Russia (Trans-Baikal region), East Mongolia (Dornod), and North China (Yinshan-Liaohe). In the Trans-Baikal-Mongol-North China uranium-bearing province, common are the hydrothermal, hydrogenic, and polygenic uranium deposits of different geological and mineral-geochemical types and a wide age (from Archean to Neogene and Quaternary period) interval of the formation (Shatkov et al., 1999).

Among them, of the greatest industrial value, are the hydrogenic-bedded pitchblende deposits in the Neogene-Quaternary gray-colored (with the dispersed coaly matter) beds overlapped by plateau-basalts (Vitim or Amalat types); polygenic-veined beta-uranotil-apatite deposits in zones of the clay-zeolite transformations of the Late Mesozoic rare-metal leucogranites (Chikoi type); and hydrothermally metasomatic streak-vein-stockwork fluorine-molybdenum-uranium (fluorite-jordisite-pitch) deposits in the Jurassic-Cretaceous volcanoplutonic structures (VPS) and taphrogenic basins (Streltsovka and Olov types). Volcanite occurrences of the Streltsovka type are of exclusive industrial importance as a real and potential source of uranium in the Russian Federation, Mongolia, and China. However, the natural resource of the nodes of concentration of the volcanite type deposits has not been discovered in full measure in the region. In our opinion, it is because the role of the deep-seated geodynamics in the formation of large nodes and districts of concentration of uranium mineralization has not been taken into account sufficiently (Khomich et al., 2016). The most known uranium-ore clusters (UOC) of the Russian Federation (Streltsovka), Mongolia (Dornod), and North China (Guyuan and others) are located above the frontal and flank (SW) areas of the slab stagnated in the mantle transitional zone. The nodes show in much one-type sections of the coeval (J_3-K_1) sedimentary-volcanogenic deposits. Similar is aslo the composition of the Archean-Proterozoic granitoid-metamorphic formations of the UOC basement belonging to the Kerulen-Argun superterrane (Streltsovka, Dornod) or to the northern marginal part of the Sino-Korean craton (Guyuan and others). In each of the sited districts there have been also revealed the ore occurrences and deposits of Pb, Zn, and fluorite, and in the terrigenous depressions of the periphery—the uranium hydrogenic deposits.

The uranium-bearing VPS of the contiguous territories of the Russian Federation, Mongolia, and China are characterized by a rather complicated structure with the availability of the horst dome-like uplifts and contiguous with them calderas and local depression subsidences, controlled by faults of various kinds. On the area of such uplifts, the paleocenters of volcanic eruptions are concentrated, represented by necks, extrusions, and subvolcanic bodies of porphyric, breccia, fluidal, and spherulitic varieties of the rocks of the moderately acid and acid composition. Some of the paleonecks contain the uranium mineralization, and other enclose or control the placement of uranium ore clusters (Zherlovoe, Krasnyi Kamen, Yugo-Zapadnoe, Dalnee, and others in Streltsovka ore cluster (SOC); Nemer, Mardaingol in Dornod ore cluster (DOC); Daguanchang and others in Guyuan ore cluster (GOC)). The main portion of its large and rich accumulations has been revealed in the depression subsidences in the surrounding of the horst-dome uplifts (Malo-Tulukuev, Streltsovka, Tulukuev, and others in SOC; Gurvanbulak, Dornod in DOC) and in the rocks of the VPS basement (Antaeus, Argun in SOC). Unfortunately, the same ones remain to be found in the DOC and GOC. On the area of the latter and as well as of the whole Yinshan-Liaohe subprovince (North China), the presence of the yet not revealed large uranium occurrences, similar to those explored in the SOC and DOC, is thought to be quite probable. This suggestion is supported by the following facts: the restriction of the F-Mo-U mineralization of Zhangmajing deposit to the subvolcanic body of rhyolite-porphyry (extrusion of fluidal rhyolites) in the dome marginal part; the

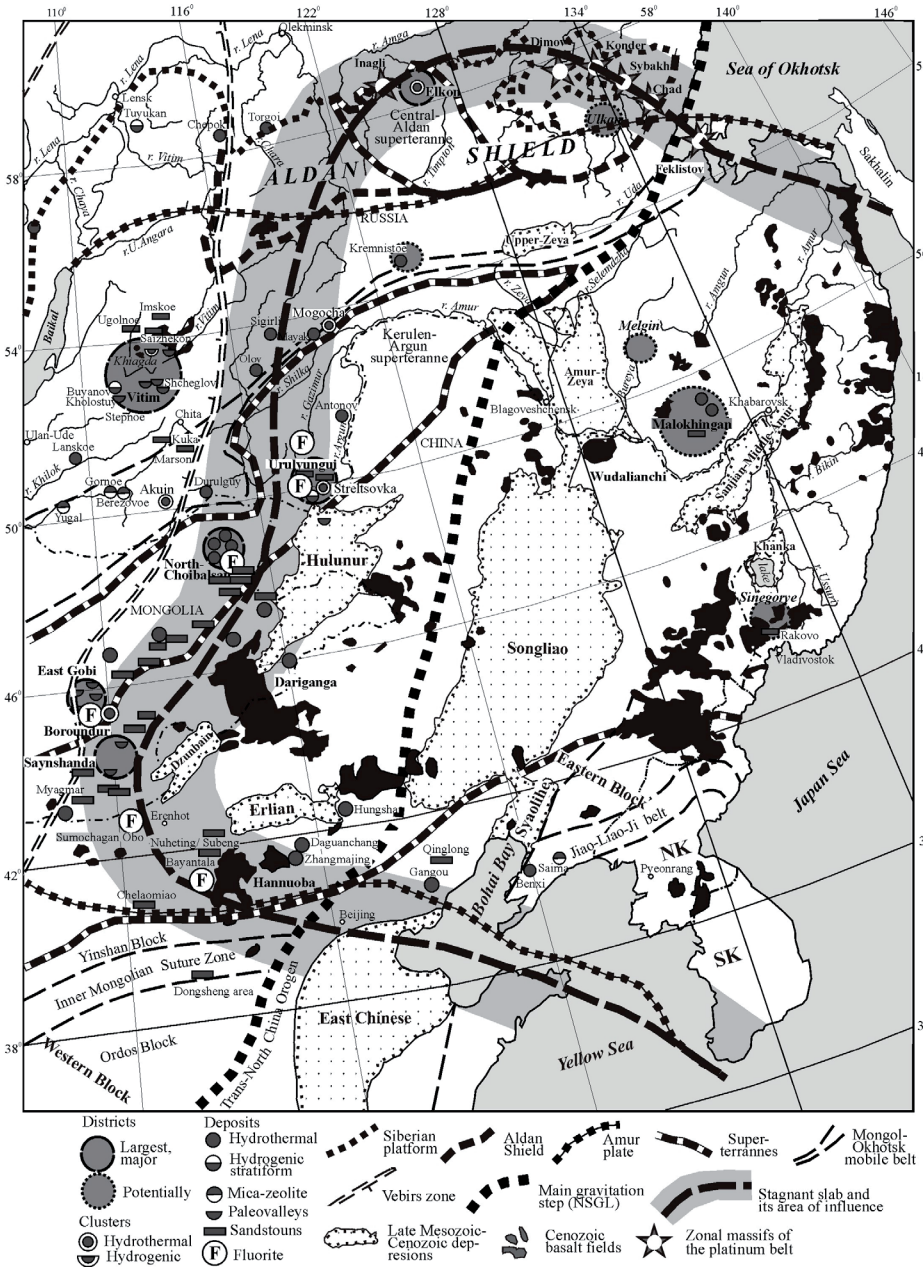

Figure 1. Location of the largest unique and others uranium districts of Southeast Russia and East Mongolia. After (Khomich et al., 2016) with additions and modifications.

presence of large fluorite (Sumochagan Obo, Obotu), and Pb and Zn (Caijiaying) deposits, as well as several hydrothermal uranium deposits (Hungshan and others in Guyuan-Duolun district and Qinglong Ore Field in East Yanshan-Liaohe) among the terrigenous-volcanogenic beds of the southern flank of the GXVPB; and at last the occurrence of the uranium hydrogenic deposits (Nuheting and Subeng, Bayantala Sag, Chelaomiao, Donosheng, and others) among the terrigenous beds of the VPS periphery.

References

Khomich, V.G., Boriskina, N.G., Santosh, M., 2016. Geodynamic framework of large unique uranium orebelts in Southeast Russia and East Mongolia. Journal of Asian Earth Sciences 119: 145–166.

Shatkov, G.A., Terent'ev, V.M., Pinskii, E.M., Shor, G.M., 1999. Metallogenic division of the Amur geoblock due with the problems forecasting industrial types of uranium mineralization in the East Russia (in Russian). Regionalnaya geologiya i metallogeniya 8: 35–46.

Bubble-Pocket Structure in the Millennium Pumice: A New Finding by the Korean-Chinese Cooperative Volcanic Research Group

Gi Bom Kim[1,*], Jiaqi Liu[2], Shane J. Cronin[3], Jong Ok Jeong[4], Youn Soo Lee[5], and Young Kwan Sohn[1]

[1]*Department of Geology, Gyeongsang National University, Jinju, Republic of Korea*corona@snu.ac.kr or gbkim42@gmail.com
[2]*Institute of Geology and Geophysics, Chinese Academy of Sciences, Beijing, China*
[3]*School of Environment, The University of Auckland, Auckland, New Zealand*
[4]*Central Instrument Facility, Gyeongsang National University, Jinju, Republic of Korea*
[5]*Geological Research Division, Korea Institute of Geoscience and Mineral Resources (KIGAM), Daejeon, Korea*
*Corresponding author E-mail: corona@snu.ac.kr, gbkim42@gmail.com

Keywords: millennium eruption, pumice, vesicle

Mt. Baekdusan (also referred to as Changbaishan in China) is an intraplate stratovolcano, where a powerful Plinian eruption around 1000 years ago (the Millennium eruption) produced a huge volume of tephra (~100 km^3 and ~25 km^3 in DRE) equivalent to the volcanic explosivity index (VEI) of 7 (Horn and Schmincke, 2000). Since 2014, as a precursory study for the Korean-Chinese cooperative volcanic research of the Baekdusan volcano, textural and geochemical analyses on the Millennium pumice have been carried out.

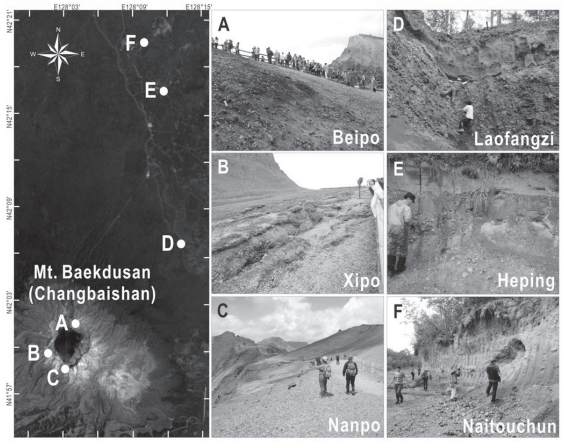

Figure 1. Map and field photographs showing the locations of sampling sites and deposit features of the Millennium pumice. Millennium pyroclasts are found as air-fall deposits on the caldera-rim sites (A–C) and secondary deposits (may be lahar deposits) on the medial to distal sites (D and E) to the north from the volcano (Wei et al., 2007).

For the analyses, fresh pumice samples were collected from air-fall deposits of three different sites on the caldera rim, and from medial to distal tephra deposits to the north away from the volcano (Figure 1). The pumice samples were first analyzed by means of X-ray computerized microtomographic (CT) technique so as to verify 3D interrelationship between glass matrix, crystals, and vesicles. Afterward, polished sections were prepared for further scanning electron microscopic imaging and electron probe microanalysis of glass groundmass and crystals.

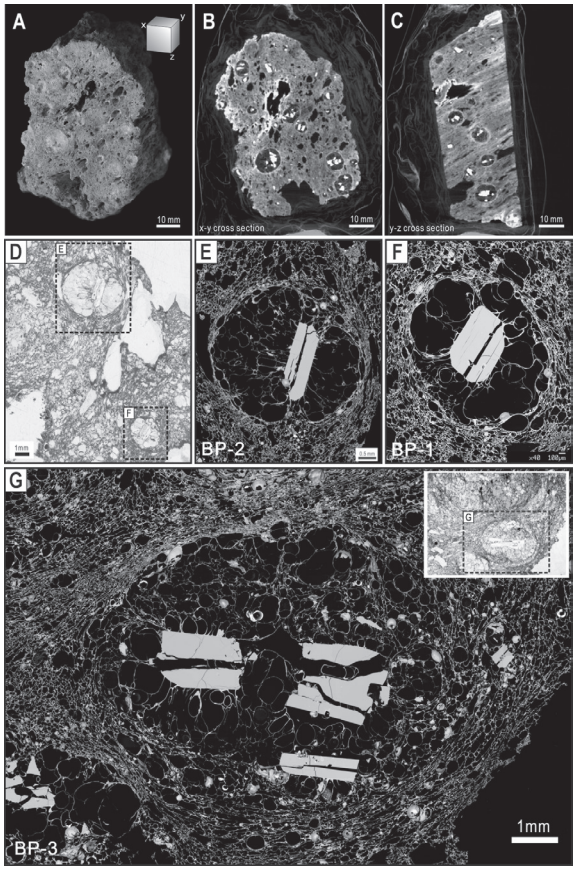

Figure 2. Photograph image of a Millennium pumice sample (sample no. GB17-1) (A), and selected CT images of the sample in *x*–*y* (B) and *y*–*z* (C) cross-sections. *Note that the domains colored white, gray, and black represent crystal, matrix, and vesicle, respectively. Photo-scanned thin section image of the sample GB17-1 (D), and BSE images showing details of bubble pockets and fractured sanidine crystals therein (E and F). (G) Another bigger sized bubble pocket structure showing jigsaw-like fractured sanidine crystal and the internal network of thin bubble film.

One of the important findings of our study is a specific vesicle structure, entitled hereafter "bubble pocket," a unique textural character of the Millennium pumice (Figure 2). The bubble pocket refers to a single, enclosed, near-spherical space (a few tens of micrometers to over 1 cm in diameter) within pumice, that is marked by an internal network of submillimeter-size bubbles with delicate glass film (<10 μm in thickness) of bubble wall. Every single bubble pocket contains fragmented sanidine and/or CPX crystals (Figures 2A–C), situated at the center of the pocket in a jigsaw-puzzle-like manner (Figures 2E–G). In 2D sections from CT analysis, the contrastingly dark color of bubble pockets compared to the bright outer domain (Figures 2B and C) suggests significantly higher porosity of those pockets compared with the host material outside. In addition, the intact spherical shape of the bubble pockets in stark contrast to the sheared vesicle texture in the host material (Figure 2C) implies that the histories of bubble growth and shear deformation were differential between inside and outside the pockets.

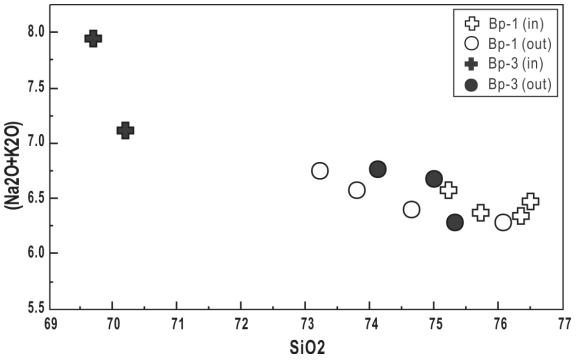

Figure 3. Diagram showing total alkali versus Sio2 composition of the glass inside and outside bubble pockets. In the Bp-3, glass composition inside the bubble pocket is more mafic and richer in total alkali contents compared with the outside. On the other hand, Bp-1 does not present evident contrast in composition. For the samples, see Figures 2D–F.

Detailed investigation on the bubble pocket structure arises several important implications as follows:

(1) In a few samples, bubble pockets, elongated in a manner similar to the sheared host material, implies that the pockets are not likely a posteruptive structure
(2) Almost intactly preserved glass film network within bubble pockets suggests that they were generated at the latest stage of magma ascending, thereafter the magma was not deformed by shear.
(3) Radially arranged stretched bubbles around the crystal imply that the magma adjacent to the crystal was isotropically expended till the times of abrupt quenching by magma fragmentation.
(4) Thin glass film on the surface of crystals suggests that heterogeneous bubble nucleation was not likely to happen in this case.
(5) There exists a subtle difference of major-elements composition of glass matrix between inside and outside the bubble pockets (Figure 3), which implies that the origin of the melt within bubble pockets could be different from the host melt outside the pockets.

There have been a few studies on pumice texture reporting vesicle, glass, and crystal textures (i.e., broken crystals with transverse glass fiber and radial-arranged vesicles) similar to those of the Millennium pumice (e.g., Giachetti et al., 2010; Miwa and Geshi, 2012). However, such an example of perfect separation between domains in pumice with distinct physical and textural properties has never been reported before. At the present state of our understanding about the bubble pocket structure, it is hard to draw a conclusion on its fundamental control. For now, we just assume that the unique bubble texture of the Millennium pumice is a result of the extreme viscosity increase with late-stage degassing in compositionally heterogeneous rhyolitic magma.

We expect that our new findings contribute to better understanding toward degassing and fragmentation processes in magma with extremely high silica content, as well as to identifying the Millennium tephra at various places on the Earth.

Acknowledgments

We specially appreciate the Chinese Academy of Science (CAS) for all logistic helps and academic advices during the field excursions in 2014 and 2015.

References

Horn, S., and Schmincke, H.-U. 2000. Volatile emission during the eruption of Baitoushan Volcano (China/North Korea) ca. 969 AD, Bulletin of Volcanology 61: 537–555.

Hurwitz, S., and Navon, O. 1994. Bubble nucleation in rhyolitic melts: Experiments at high pressure, temperature, and water content, Earth and Planetary Science Letters 122: 267–280.

Giachetti, T., Druitt, T.H., Burgisser, A., Arbaret, L., and Galven, C. 2010. Bubble nucleation, growth and coalescence during the 1997 Vulcanian explosions of Soufriere Hills Volcano, Montserrat, Journal of Volcanology and Geothermal Research 193: 215–231.

A Sedimental Record from a Maar on the Pleiku Volcanic Field in the Central Highland of Vietnam

Hiroyuiki Kitagawa[1,*], Dang Phong Xuan[2], Akira Hayashida[3], and Lai Vinh Cam [2]

[1]*Institute of Space-Earth Environmental Research, Nagoya University, Nagoya, Japan*
[2]*Institute of Geography, Vietnamese Academy of Science and Technology, Hanoi, Vietnam*
[3]*Faculty of Science and Engineering, Doshisha University, Kyo-tanabe, Japan*
*Corresponding author E-mail: hiroyuki.kitagawa@nagoya-u.jp

Keywords: Pleiku volcanic field, paleohydroclimate, SE Asia monsoon

It is important to understand rainfall changes across South China and Southeast Asia (hereafter referred to as "continental Southeast Asia"). A change in the summer rainfall in the region can affect the lives of more than a billion people by impacting agriculture, hydroelectric generation, industrial development, and even basic human life. The summer rainfall in this region is generally influenced by the activity of the Asian summer monsoon which is subdivided into two subsystems: the Indian Ocean (southwestern) summer monsoon (ISM) and the East Asia summer monsoon (EASM).

The meteorological observation, theoretical and modeling studies, and paleoclimatic archives have suggested that the summer rainfall in continental Southeast Asia has significantly changed on the temporal and spatial scales (Turner and Annamalai, 2012). The processes controlling the summer rainfall in this region are complex and rainfall is impacted not only by the Asian summer monsoon, but also by global climatic phenomena (Christensen et al., 2013) such as to the El Niño Southern Oscillation, the Indian Ocean Dipole, the Atlantic Meridional Overturning Circulation, the movement of the Intertropical Convergence Zone, and the SST anomalies in the equatorial eastern Pacific. Investigators are awaiting rainfall records covering a wider area to help them better clarify the changes of the Asian summer monsoon.

The Vietnamese central highland (VCH, between 12° N and 15° N and 107° E and 109° E, Figure 1) is located in the eastern edge of continental Southeast Asia, where it is in convergence zone of the Asian summer monsoon (Wang et al., 2006; Wang and Lin, 2002; Chen and Yoon, 2000; Conroy and Overpeck, 2011). High-temporal resolution hydroclimatic records from VCH are thought to be crucial for comprehending the Asian summer monsoon rainfall, as little other hydroclimatic data from the continental Southeast Asia are available (Cook and Jones, 2012; Wohlfarth et al., 2012).

More than 20 maars and dried maars are distributed on the Pleiku volcanic field on VCH (e.g., Hoàng et al., 2013). We presumed that the maar status inferred from the biogeochemical properties (TOC, TN, C/N, and FTIR spectra) of these maar sediments was expected to be useful for assessing the long-term changes of the Asian summer monsoon rainfall in the past. In this study, we performed high-resolution biogeochemical profiles of a sediment core from a semidried maar on Pleiku volcanic field to provide clear evidences of the hydroclimatic changes on the eastern edge of continental Southeast Asia going back to the late Pleistocene.

Figure 1. Pleiku volcanic field, the central highland of Vietnam (asterisk).

We have investigated hydroclimatic variability dating back to the late Pleistocene by performing a high-resolution analysis of the biogeochemical properties (TOC, TN, C/N, and FTIR spectra) of a

sediment core from a semidried maar on the Pleiku volcanic field in the central highland of Vietnam, an area situated on the eastern edge of continental Southeast Asia. The record identified two marked shifts in biogeochemical properties at 10.6 and 6.5 ka BP (1 ka = 1000 calibrated ^{14}C years BP). The shift to a wetter condition began at about 10.6 ka BP delaying by about 1000 years after the onset of the Holocene (11.7 ka BP), and was in-phase to southeastern China and antiphase to southwestern China and other regions in continental Southeast Asia. While the shift to a drier climatic condition took place after the middle of Holocene (around 6.5 ka BP), which is consistent with hydroclimate reconstructions from broad areas across continental Southeast Asia. It may be necessary to closely ascertain in the differences in relative contributions of the East Asia and Indian Ocean monsoon rainfalls between the late Pleistocene and the Holocene.

Acknowledgments

This work was part of a bilateral jointed research program (FY2013-2015) funded by the Vietnam Academy of Science and Technology (VAST.HTQT.NHATBAN.01/13-15) and the Japanese Society for the Promotion of Science (JSPS), and with partial support from the Ministry of Education, Science, Sports and Culture, Grant-in-Aid for Scientific Research (A), 2013-2016 (25241007, Hiroyuki Kitagawa). We would like to thank the local government of Gai Lai province in Vietnam for kindly supporting our field survey and providing information.

References

Chen TC, Yoon JH. 2000. Interannual variation in Indochina summer monsoon rainfall: Possible mechanism. Journal of Climate 13: 1979–1986.

Christensen, JH. et al. 2013. Climatic Change 2013. The Physical Science Basis, Working Group I Contribution to the Fifth Assessment Report of the International Panel on Climatic Changes (eds Stocker et al.) Ch. 14, pp. 1217–1308, Cambridge University Press.

Conroy JL, Overpeck, JT. 2011. Regionalization of present-day precipitation in the greater monsoon region of Asia. Journal of Climate 24: 4073–4095.

Turner AG, Annamalai H. 2012. Climate change and the South Asian summer monsoon. Nature Climate Change 2: 587–595.

Cook CG, Jones RT. 2012. Palaeoclimate dynamics in continental Southeast Asia over the last 30,000 cal yrs BP. Palaeogeography, Palaeoclimatology, Palaeoecology 339–341: 1–11.

Wang, B. 2006. The Asian Monsoon. Springer/Praxis Publishing Co., New York, pp. 787.

Hoàng N, Flower MFJ, Chí CT, Xuân, PT, Quý, HV, Sơn, TT. 2013. Collision-induced basalt eruptions at Pleiku and Buôn Mê Thuột, south-central Viet Nam. Journal of Geodynamics, 69: 65–83.

Wang B, Lin H, 2002. Rainy season of the Asian-Pacific summer monsoon. Journal of Climate 15: 386–398.

Wohlfarth B, Wichuratree K, Inthongkaew S, Fritz SC, Blaauw M, Reimer PJ, Chabangborn A, Löwemark L, Chawchai S. 2012. Holocene environmental changes in northeast Thailand as reconstructed from a tropical wetland. Global and Planetary Change 92–93: 148–161.

In the Land of Maar Lakes and Volcanoes: Geology as a Driver of Tourism!

Werner Klöckner[1], Andreas Schüller[1], and Martin Koziol[2]

[1]*Vulkaneifel UNESCO Global Geopark*
[2]*Maarmuseum Manderscheid (www.maarmuseum.de) maarmuseum@t-online.de*

From Bad Bertrich on the Moselle up to Goldberg volcano near Ormont on the Belgian border, in the northwest of Rhineland-Palatinate, there is a landscape that is not found anywhere else in the world, extending diagonally across the Eifel region.

There is no active volcano here, but the former volcanic action has left spectacular traces and made the area a textbook of geological history. When another eruption will occur is something we do not know. The geological conditions for this are still there, and the volcanologists are in agreement that volcanic activity has only made a pause; it has not been extinguished.

But it is not only geologists and volcano researchers from around the world for whom the "**West-Eifel volcanic field**" is a popular destination for research and science. Also, from a tourist perspective the name "**Vulkaneifel**" has attracted the attention of many visitors. Volcanic cones, mineral water springs, a unique concentration of natural phenomena, and especially the funnel-shaped maar lakes are centers of attraction in this landscape situated in the heart of Europe. With the famous "**Daun-Maars**" and the volcanic system "**Mosenberg-Volcanic group with Meerfeld-Maar**," the Vulkaneifel boasts of two geological sites that have been highlighted as "**Germany's most important Geotopes**."

The region has set itself the task of linking together the geological sciences and tourism, and thereby transmitting impulses to a variety of areas, whether gastronomy, art, culture, sport, or leisure. With a stronger focus on the geological heritage of the countryside yet without losing sight of the integrity of the living world, the **Vulkaneifel UNESCO Global Geopark** would like to make a contribution to the sustainable development of the region.

The remit of the **Vulkaneifel UNESCO Global Geopark** is defined not in the sense of "nature conservation" looking backwards, but looking ahead. Nature and landscape are to be protected and developed in the geopark in such a way that simultaneously the economic survival of the people living there is permanently protected. In a market, however, sustainable economy and trading does not happen automatically. Globalization often destroys existing sustainable economic models. It has rather to be promoted among consumers and producers, and through politics. For **Vulkaneifel UNESCO Global Geopark** this means: If it wants to achieve its sustainable goals, there has to be a targeted engagement in favor of sustainable economy and for sustainable regional development.

Nature park and geopark work is regional management in a broad and comprehensive sense. It is about bundling together in the area of the geopark all resources from business and industry, society, culture, environment, and politics, under the single overall concept of "sustainable regional development."

For the **Vulkaneifel UNESCO Global Geopark** it makes sense, against the background of demographic change, to formulate its work in such a way that it leads to an improvement of the economic, ecological, and social situation in the rural Eifel region. Nature park and geopark work, and its financing by the province, the communities, and industry, are to be understood as an investment in a future-oriented infrastructure that will benefit the coming generations. The synergistic combination of geotouristic valorization and marketing of our volcanic landscapes with the regional development potential of a geopark under the sponsorship of **Natur- und Geopark Vulkaneifel GmbH** thereby represents a special opportunity.

Figure 1. Map of the “Vulkaneifel UNESCO Global Geopark” with the western part of the “German volcano route.”

Volcano Activity Monitoring of the NIMS Using Remote Sensing Data

Won-Jin Lee*, Yoon-Ho Choi, Sun-Cheon Park, DukKee Lee, and Jong-Ho Lee

National Institute of Meteorological Sciences, Jeju, Republic of Korea
*Corresponding author E-mail: wjleeleo@korea.kr

Keywords: remote sensing, volcanic activity monitoring

Conventional volcanic studies using seismometers, leveling, gravity meters, etc. are still important tools for understanding the volcano activity. At the same time, technical advances of remote sensing has allowed to analyze volcano behavior in terms of both spatial coverage and temporal patterns, albeit its distant access. Especially, interpretation of deformation data (e.g., InSAR: Synthetic Aperture Radar Interferometry) and thermal observation (e.g., thermal infrared images) allowed to significantly improve the precursor monitoring of volcanic eruption.

Even though there is no active volcano on the Korean Peninsula, some volcanoes, such as Mt. Baekdu (Changbaishan in China), Sakurajima, Mt. Aso, etc., have the possibility to cause damage in the peninsula through ash dispersion. Therefore, National Institute of Meteorological Sciences has studied volcano activity using remote sensing techniques such as InSAR, thermal imagery, and visible imagery. In this paper, we introduce NIMS effort and techniques to monitoring volcano activity using remote sensing data.

1. Characteristics of remote sensing images

There are many different types of satellite images. Most usable ones for the research on volcanic eruption precursor are SAR and infrared images. From these two sensors we can produce time-series deformation pattern and surface temperature changes. On the other hands, visible satellite images are limited to monitoring volcano because light is required for imaging. Therefore, these images are only useful when the sun is shining on the volcanic area. Table 1 describes advantages and disadvantages of satellite remote sensing data.

2. Volcanic monitoring step

Table 1 shows that each sensor has its own characteristics and we should used them appropriately. Therefore, to monitor volcanic activity effectively, we are using all of the remote sensing images in step. We assume three steps and role of each satellite sensor.

(1) Preeruption step

From preeruption step, the most important role of NIMS is monitoring volcanic activity and precursor of eruption. To achieve the objective, SAR and infrared images are valuable dataset because it can produce deformation and heat changes of the surface. We have developed time-series deformation technique such as Permanent Scatterers Interferometry (Ferretti, 2000) and Small BAseline Subset algorithm (Berardino, 2002), as well as land surface temperature algorithm such as mono-window, single-channel, and split-window. These techniques will help to assess volcanic activity.

Table 1. The summary of advantages and disadvantages of remote sensing images

Sensor	Advantages	Disadvantages
SAR	· All weather acquisition · Day and night acquisition · 2D deformation generation	· Geometry distortion · Speckle noise · Low acquisition rate
Infrared image	· Day and night acquisition · Measure heat	·Weather problem ·Low precision
Visible Image (Polar orbit)	· High resolution · Good readability	·Weather problem · Low acquisition rate
Visible Image (geostationary)	· Good readability · Variety band Composition · High acquisition rate	· Low resolution

(2) Eruption step

During volcanic eruption, the most important behavior is monitoring volcanic ash dispersion and response to the disaster. To mitigate hazard risk, we use polar orbit satellite image, which observes a large area and also monitors inaccessible areas. Moreover, it can monitor ash direction, time, and velocity by short temporal resolution. Deformation measurements derived by InSAR technique also provide useful information by magma source and volume change modeling. These magma changes are important factor about expectation of eruption duration time, volcanic explosivity index, etc.

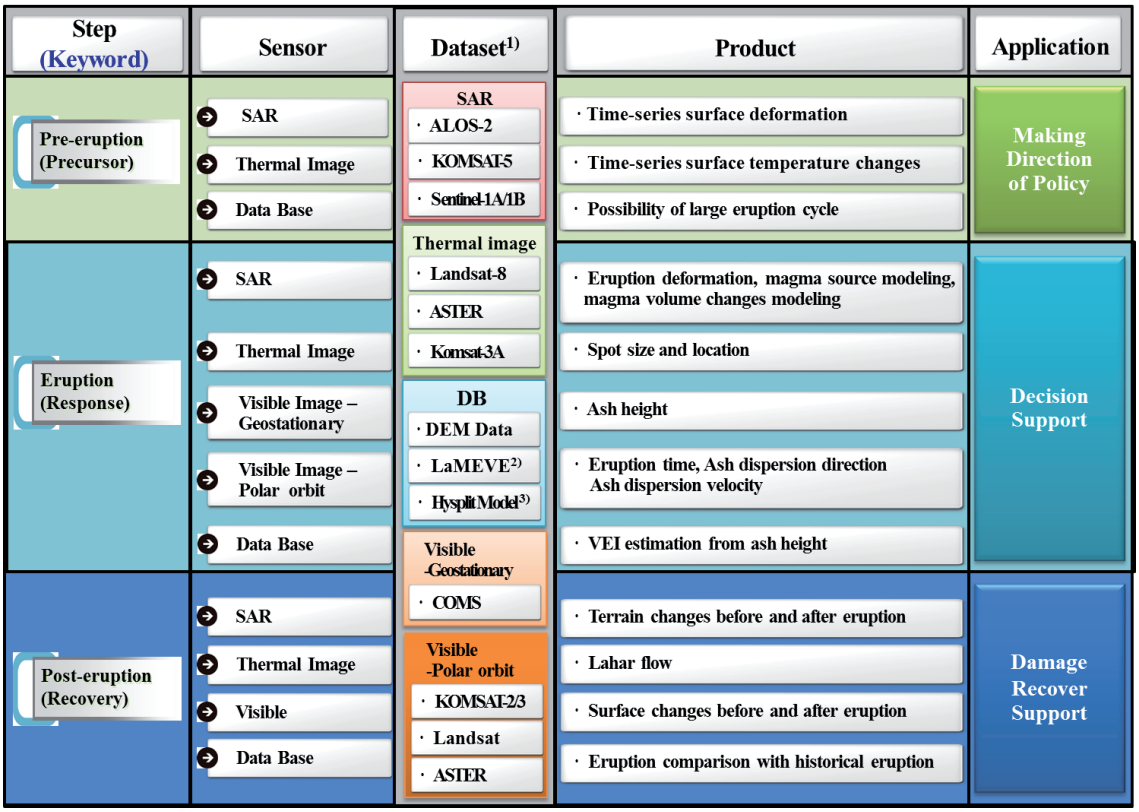

Figure 1. Remote sensing data for different eruption step.
[1)]Available datasets for free.
[2)]Large magnitude explosive volcanic eruptions (Crosweller et al., 2012).
[3)]Ash dispersion simulation model using meteorological data.

(3) Posteruption step

After volcanic eruption, damage recovery is necessary as soon as possible. In this step, visible remote sensing data are useful because it can produce change detection map using(?) reflective spectral change with high resolution. Also, Digital Elevation Model comparison with before and after eruption provides useful terrain change information. Figure 1 shows product generation step using remote sensing data. Not only remote sensing data, but external database such as historical volcanic eruption records, meteorological data for ash dispersion simulation, volcanic location, etc. are required. This database also will include *in situ* data such as GPS, leveling, tiltmeter, and volcanic gas around hot-spring data.

3. Conclusion

In this paper, we introduce our volcanic monitoring effort using remote sensing data. It still needs to upgrade and develop techniques to analyze volcanic activity. However, using the remote sensing data, it can support effectively and rapidly in policy direction, decision, and damage recovery.

Acknowledgments

This study was supported by “Research and Development for KMA Weather, Climate, and Earth system Services (NIMS 2016-3100)” of National Institute of Meteorological Sciences.

References

Berardino, P., Fornaro, G., Lanari, R., and Sansoti, E. (2002). A new algorithm for surface deformation monitoring based on small baseline Differential SAR Interferograms, IEEE Transactions on Geoscience and Remote Sensing, 40(11), 2375–2383.

Crosweller, et al., (2012). Global database on large magnitude explosive volcanic eruptions (LaMEVE), Journal of Applied Volcanology.

Ferretti, A., Prati, C., and Rocca, F. (2000). Non-linear subsidence rate estimation using permanent scatterers in differential SAR interferometry, IEEE Transactions on Geoscience and Remote Sensing, 38(5), 2202-2.

Review of the Late Cenozoic Tectonics of the Northeast Asia

Youn Soo Lee[1,*] and Jiaqi Liu[2,*]

[1]*Geological Research Division, Korean Institute of Geoscience and Mineral Resources, Daejeon, Korea*
[2]*Institute of Geology and Geophysics, Chinese Academy of Sciences, Beijing, China*
*Corresponding author E-mail: leeys@kigam.re.kr, liujq@mail.iggcas.ac.cn

Based on the existing geological and geophysical results, we provide an insight into Late Cenozoic tectonic and volcanic evolution in the Northeast Asia within extensional tectonic domain, linked to the reconstruction of the plate tectonics: collision of India-Eurasia plates, opening of the East Asia, and collision between the Eurasia-North America (NE Japan)-Pacific-Philippine plates.

Large volumes of volcanic flows (LVFs) are widely distributed in East Asia. Seismic tomography researches reveal that a low-velocity anomaly structure beneath Manchuria to East Sea (Japan Sea) region is placed on the deep mantle transition zone, interpreting increasing of instability by dehydration process from the stagnant Pacific oceanic slab. In the low-velocity anomaly structure, detailed geophysical results confirmed possible existences of local magma chambers: for example, Baekdu-Changbai and Ulleung volcanoes. The direct evidence is the lack of dehydration hypothesis from the ocean slabs.

The LVFs appear along major faults, such as Tan-Lu fault system, Baikal rift, and East Sea spreading axes. The only dehydration hypothesis by Pacific slab cannot explain the whole LVF activity, such as to Baikal rift (more than 3000 km), because the Pacific slab subside down to lower mantle beneath the Manchuria.

We suggest two mechanisms: (1) The initial formation of the LVFs occurred along the lithospheric fault systems that are associated to Mesozoic to Cenozoic collision and deformation in mosaic blocks of the Northeast Asia. The collision and crustal erosion may be responsible for the asthenosphere upwelling along the systems. (2) The dehydration process from oceanic subduction slab may facilitate to sustain magma chamber system in Manchuria to East Sea region.

The Gas Chemical and Rare Gas Isotope Compositions of Two Volcanic Rock Samples from Wudalianchi, China

Liwu Li*, Yan Liu, Chunhui Cao, Jian He, and Lantian Xing

Key Laboratory of Petroleum Resources, Gansu Province/ Key Laboratory of Petroleum Resources Research, Institute of Geology and Geophysics, Chinese Academy of Sciences, Lanzhou, PR China
*Corresponding author E-mail: llwu@lzb.ac.cn

Keywords: gas compositions, noble gas isotope, Wudalianchi rock

Studies have indicated that there are a large number of volatile components in many kinds of minerals or rocks, such as H_2O, CO_2, CH_4, H_2, CO, N_2, O_2, and C_2H_6. These volatile components play an important role in the evolution of the earth's interior fluid. For example, exchange of material and energy among rocks or minerals, chemical reaction with rocks or minerals, to change its elements and isotopic composition, and to change the mechanical properties of rock or mineral. Wudalianchi volcanic group is one of China's most young volcanic groups, volcanic activity can be divided into the Pleistocene and the Holocene stages, each has erupted several times. The gas chemical and rare gas isotope compositions may help us to understand the mantle and tectonic evolutions about this volcanic group.

Degassing experiments were carried out on two samples from Wudalianchi. One is Yaoquanshan volcano lava and another is Huoshaoshan volcano lava. First, about 5 g (0.5–1.5 cm in diameter) of each sample was put into a high vacuum electromagnetic broken and crushed for 2 min, then the pressure and the compositions of released gas were analyzed. Second, 0.2 g (0.18–0.5 mm in diameter) of each sample was step heated in a high vacuum quartz tube, each step heated for about 50 min, then the pressure and the compositions of released gas were analyzed. Third, about 0.35 g (0.18–0.5 mm in diameter) of each sample was heated from 300°C to 1100°C, and the rare gas abundances and isotope compositions of released gas were analyzed by a noble mass spectrometer with a preparation system.

The pressure of gas released from rock is measured by a diaphragm gauge. In the whole process, the pressure of gases is less than 300 Pa and H_2O should mostly be in gaseous state. The chemical compositions of gas released from rock are test by a gas chromatograph (GC) and a quadrupole mass spectrometer (QMS) at the same time. The GC uses a pulsed discharge detector (PDD) made by VICI Co. Ltd. The type of QMS is QMG220 made by Pfeiffer Vacuum Co. Ltd. The noble mass spectrometer with the preparation system is made by Nu instrument Co. Ltd.

The quantity of gas released by crushing is small (<1 μl, STP), less than three times of blank sample (about 0.6 μl, STP). Gas chromatography and mass spectrometry show the main components are N_2, H_2, and CH_4. CO_2 or H_2O may be absorbed in the rock for the temperature outside the broken is less than 50°C.

As for step heating, a quartz tube was heated in vacuum to 1000°C for >1 h, then cool down for test. The test procedure for the blank is the same as a real sample. After a test and the quartz tube cool down, the rock was found glued on the tube, this means the rock is melted at the last step. The compositions are present in Figure 1. From Figure1, the two rocks have similar degassing pattern. The main components are H_2O, CO_2, H_2, and CO, followed by little CH_4 and N_2. The atomic fraction of oxygen (Xo) is presented in Figure 2. Xo is about 0.5 for each heating step of the two samples. By comparing the gas compositions and the atomic fractions of oxygen with other researches (e.g., Goncharov et al., 2012; Zhang and Duan, 2009), it seems that the equilibrium pressure of the upper mantle is 3.37–1.27 GPa, the primary magma comes from 80–100 km, and the magma temperature is equivalent to 959°C–1127°C at the study area (Shao and Zhang, 2008).

The noble gas abundances and isotope compositions of released gas were analyzed for Yaoquanshan volcano lava sample (Y01) and Huoshaoshan volcano lava sample (H01) as shown in Table 1. Each sample is tested twice with different weight (0.32-–0.42 g). Although the repeatability is poor, each R/Ra is ≥1, where the R and Ra are $^3He/^4He$ of sample and that of air, respectively. These data suggest that the volatiles originate from the mantle. The average $^3He/^4He$ of the four samples is 2.2 Ra, in the range of 2–3 Ra of bubbling gases discharging from cold springs in the study area (Xu et al., 2013). The $^3He/^4He$ ratio of Y01 is higher than that of H01, and according to Zhao et al. (2014), Y01 erupted earlier than H01, which agree with that the early volcano

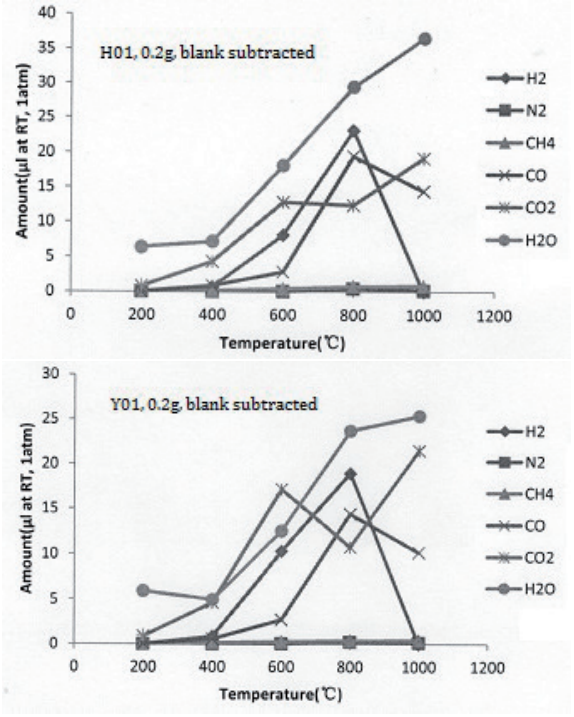

Figure 1. The chemical compositions of gases released by step heating Huoshaoshan volcano lava sample (H01) and Yaoquanshan volcano lava sample (Y01) at room temperature (RT) and 1 atm.

magmatic source is deeper than the late volcano magmatic source (Shao and Zhang, 2008). The average $CO_2/^3He$ ratios are 1.05×10^{12} for Y01 and 3.39×10^{12} for H01, far higher than that of bubbling

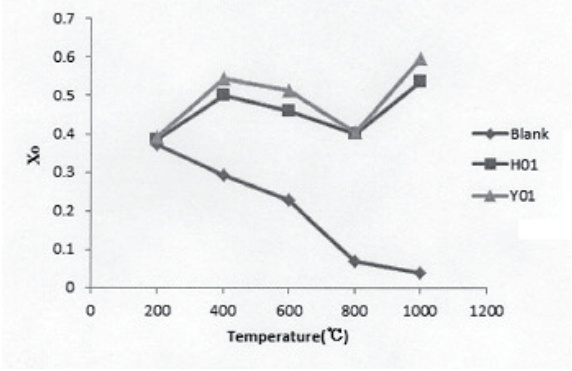

Figure 2. Xo of each step calculated from composition data. Xo is the atomic fraction of oxygen which is defined as $Xo = n_O/(n_O + n_H)$, where n_O and n_H are the moles of oxygen and hydrogen atoms in the fluid phase, respectively (Huizenga, 2001; Zhang and Duan, 2009).

gases discharging from cold springs in the study area (Xu et al., 2013). We guess that the ^3He in magma may lose faster than CO_2 or carbonate may be captured during magma upwelling. Other noble gas data are presented for advance research. It is interesting that Xe/Ar ratios are much higher than that of air.

Acknowledgments

This study is supported financially by NSF of China (No.41473062) and the Key Laboratory Project of Gansu Province (Grant No.1309RTSA041).

Table 1. Chemical and isotope compositions of noble gases of volcano rocks from Wudalianchi

	Weight (g)	He ($\times 10^{-9}$ ml/g)	Ar ($\times 10^{-5}$ml/g)	$^3He/^4He$ ($\times 10^{-6}$)	$^{40}Ar/^{36}Ar$	$^4He/^{20}Ne$	Kr/Ar ($\times 10^{-5}$)	Xe/Ar ($\times 10^{-5}$)
Y01	0.415	9.00	1.95	4.83	326	6.4	7.65	7.69
	0.321	15.6	2.21	3.27	324	9.2	6.94	5.98
H01	0.408	6.43	2.04	2.93	322	2.7	7.68	6.62
	0.355	5.29	1.89	1.40	317	2.7	8.42	5.57
Blank		0.16	0.10	0.00	233	1.0	20.6	2.83
Air				1.40	295.5	0.318	12.2	0.931

The data of blank and air are also shown; we suppose the weight of blank is 0.35 g. The volume is calculated at RT and 1 atm.

References

Goncharov, A. G., Ionov, D. A., Doucet, L. S., Pokhilenko, L. N. 2012. Thermal state, oxygen fugacity and C-O-H fluid speciation in cratonic lithospheric mantle: New data on peridotite xenoliths from the Udachnaya kimberlite, Siberia. Earth and Planetary Science Letters 357–358: 99–110.

Huizenga, J. M. 2001. Thermodynamic modelling of C–O–H fluids. Lithos 55: 101–114.

Shao, J. A., Zhang, W. L. 2008. The evolving rift belt-Wudalianchi volcanic rock belt (in Chinese with English abstract). Earth Science Frontiers 15(6): 241–250.

Xu, S., Zheng, G. D., Nakai, S., Wakita, H., Wang X. B., Guo, Z. F. 2013. Hydrothermal He and CO_2 at Wudalianchi intra-plate volcano NE China. Journal of Asian Earth Sciences 62: 526–530.

Zhang, C., Duan, Z. H. 2009. A model for C–O–H fluid in the Earth's mantle. Geochimica et Cosmochimica Acta 73: 2089–2102.

Zhao, Y. W., Li, N., Fan, Q. C., Zou, H. B., Xu, Y. G. 2014. Two episodes of volcanism in the Wudalianchi volcanic belt, NE China: Evidence for tectonic controls on volcanic activities. Journal of Volcanology and Geothermal Research 285: 170–179.

The Gas Geochemical Response of Magma Evolution of Changbaishan Tianchi Volcanic Region

Ting Li[1,*], Jiaqi Liu[2], Qingfu Yang[1], and Xiaodong Pan[1]

[1]*Earthquake Administration of Jilin Province, Changchun, China*
[2]*Key Laboratory of Cenozoic Geology and Environment, Institute of Geology and Geophysics, Chinese Academy of Sciences, Beijing, China*
*Corresponding author E-mail: liting198952@qq.com

Keywords: Changbaishan Tianchi volcanic area, isotope, volcanic activity

Magma migrates upward, together with energy transmission and fluid (H_2, CH_4, H_2O, N_2, H_2S, CO_2, HCl,SO_2, and rare gases, etc.), to the surface before a vulcanian eruption or magma activity. Since gases are easy-moving, they migrate to the surface more rapidly than magma, carrying great amounts of important information of deep magma (Shangguan, 2008).

The temperatures of the 9th and 15th Julong hot springs have risen synchronously by 3°C since May, 2010. Moreover, altitude of the northern slope of the Tianchi volcano cone decreased about 12.72 mm, whereas it increased by around 4 mm/a before 2009. Hence, Guoming Liu et al. (2011) thought that Changbaishan Tianchi volcano entered a primitive perturbation episode while Jiandong Xu et al. (2012) argued that it was caused by the filling of magma from deep magma system to shallow chamber. On the other hand, the latest geochemical data lacks to demonstrate the dynamic condition of Changbaishan Tianchi volcanic region. In this abstract we report the gas compositions of Julong and Jinjiang hot springs in Changbaishan Tianchi volcanic region from 1999 to 2013. The values of $\delta^{13}C_{CO2}$(PDB), $\delta^{18}O_{CO2}$(PDB), and $^3He/^4He$ ratios of the emitted gas from the 9th and 15th Julong hot springs, and the 1st and 2nd Jinjiang hot springs are measured in June, 2014 as well.

Gas samples from Julong and Jinjiang hot springs were collected using prevacuum gas gathering method which is internationally accepted (Giggenbach and Goguel, 1989; Newell, 2008; Zhang, 2011; Kulongoski, 2013). All the gas samples were stored in evacuated aluminum foil bags. We analyzed the gases in the Gas Geochemical Lab in Lanzhou Center for Oil and Gas Resources, Institute of Geology and Geophysics, CAS.

At last three points were concluded:

(1) The main component of Julong and Jinjiang hot spring is CO_2 (＞80%). Compared to Julong, Jinjiang spring releases more gases that are correlating to volcanic activity, such as CO_2, He, and CH_4 and less gases relating to air, for N_2 and O_2.

(2) The temperature contents of He, CO_2, and $^3He/^4He$ ratio of Julong spring, 71.1°C, 7×10^{-6}, 83.02%, and 3.92 Ra, are lower than historic values. However, those values of Jinjiang spring are 58.3°C, 133×10^{-6}, ＞94.06%, and 5.81 Ra, higher than previous 2 years. In one word, the temperatures contents of He, CO_2, CH_4, H_2, and $^3He/^4He$ ratios of Julong and Jinjiang spring are relatively stable, close to those from 1999 to 2003, when Changbaishan Tianchi volcano was calm.

(3) According to the gas combinations released from the springs around Tianchi volcano—the ratios of $\delta^{13}C_{CO2}/^3He$, $^{20}Ne/^4He$–$^3He/^4He$, we consider that the sources of both springs are a mixture of mantle and crust. The gas emitted from Jinjiang spring is little contaminated by air, containing many materials from mantle and few from crust, while the gas released from Julong spring are the opposite. Comparing with the previous research, the supply of mantle materials below Julong spring decreases, on the other hand, it is mainly supplied by crust, which means Julong spring can less reflect the activity of Tianchi volcano. But Jinjiang spring obviously releases mantle-sourced gases much, which shows the replenishment of mantle-sourced magma below the spring is rich.

Acknowledgments

We are grateful to the teachers in the labs of Lanzhou Center for Oil and Gas Resources, Institute of Geology and Geophysics, CAS and upperclassmen that helped during field sampling and experiments. Last but not the least, the Changbaishan volcano observatory supported us with their historical monitoring data.

References

Giggenbach, W. F., and Goguel, R. L. 1989. Methods for the Collection and Analysis of Geothermal and Volcanic Water and Gas Samples, Chem. Div., Dep. of Sci. and Ind. Res., Petone, New Zealand.

Kulongoski, J. T. et al., 2013. Volatile fluxes through the Big Bend section of the San Andreas Fault, California: Helium and carbon-dioxide systematics . Chemical Geology, 339: 92–102.

Liu, G. M., Yang, J. K., and Wang, L. J., 2011. Analysis of Tianchi volcano in Changbai Mountain, NE China. Global Geology, 14(1): 44–53.

Newell, D. L., 2008. Aqueous and isotope geochemistry of mineral springs along the southern margin of the Tibetan plateau: Implications for fluid sources and regional degassing of CO_2. Geochemistry, Geophysics, Geosystems, 9(8).

Shangguan, Z. G., Wu, C. Z., 2008. The geochemical characteristics of the magma derived gases in dormant volcanic zones in China. Acta Petrologica Sinica, 11: 2638–2646.

Zhang, M. L., 2011. Advances of research on greenhouse gases degassing from volcanic fields. Advances in Earth Science, 26(12): 1235–1247.

Study on Volcanoes and Maars in China

Jiaqi Liu[1]*, Jing Wu[1], Guoqiang Chu[1], Qiang Liu[1], Zhengfu Guo[1], Jingtai Han[1], Patrick Rioual[1], Jorg F.W. Negendank[2], Achim Brauer[2], Jens Mingram[2], Chunqing Sun[1], Lei Zhang[1], Jiali Liu[1], Shuangshaung Chen[1], Leilei Ding[1]

1 Key Laboratory of Cenozoic Geology and Environment, Institute of Geology and Geophysics, Chinese Academy of Sciences, Beijing, China
2 Helmholtz Centre Potsdam, German Research Centre for Geosciences GFZ, Section 5.2 Climate Dynamics and Landscape Evolution, Potsdam, Germany
*Corresponding author E-mail: liujq@mail.iggcas.ac.cn

Keywords: Cenozoic volcano, Changbaishan, maars in China

Even no fascinating volcanic eruptions occurred in China in modern time, there are many Cenozoic volcanoes and volcanic rocks almost distributed in the whole country, especially in the eastern continental margin and the southwestern Tibetan Plateau. Most volcanic activities took by central eruptions with basaltic magma and formed monogenic volcanoes and lava flows, of which the Neogene basalts usually located in high terraces and the Quaternary basalts distributed in valleys. The dominant volcanic rocks in China are continental intraplate basalts with high alkali in the eastern continental margin, and trachyte-basalt, shoshonite with high potassium in the Tibetan Plateau.

The Changbai Volcano is a huge composite volcano with some 12×10^3 km^2 area and hundreds of volcanic cones on the boundary between China and North Korea covering 41°–42.5° latitude north and 127°–129° longitude east. It is among the largest active and dangerous volcanoes on the globe. It has a series of volcanic rocks from basalt, trachyte to pantellerite, and obsidian with large volume of tephra and was built by basaltic flow as lava plateau, trachytic cones, and pyroclastic deposits covering on the top of these mountains and other places from the Early Miocene to the recent.

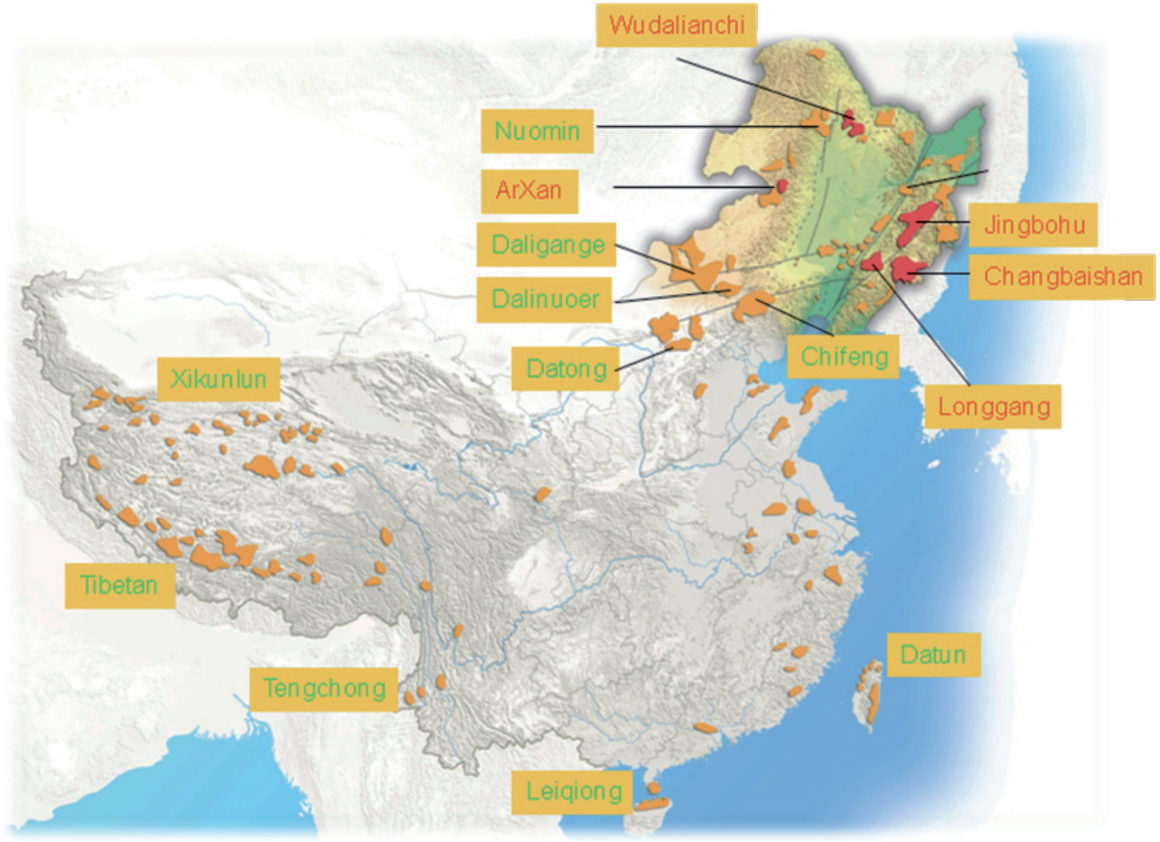

Figure 1. Distribution of the main volcanoes in China.

The volcanic eruptions in China can be simply divided into 10 episodes from the late Cretaceous to present, which correspond to volcanic eruptive frequencies around the Pacific Ocean. The upsurges of volcanic activities occurred during the middle Miocene and middle Quaternary. During this period, the volcanic activities occurred in the northeast China were as strong as those in Japan.

There are not only a large number of Cenozoic volcanoes, but also some active volcanoes in China, such as Wudalianchi, Arxan, Jingbohu, Changbaishan, Longgang, Taiwan, Hainan, Tengchong, the West Kunlun, and others, of which the Changbai Volcano is the largest one which erupted several times until 1903 AD including a large Plinian eruption with about VEI 7 in 1014–1019 AD by historical records and 940–941 AD by ice-chronology. The most recent volcanic eruption in China took place in Ashi volcano in the West Kunlun Mountains in May 27, 1951. Other active volcano(s) can also be found in other areas. Latent volcanic eruptions may also exist.

The volcanisms that occurred in the East Asia continental margin were related to the East Asian continental rifting system and the subduction of the Pacific plate underneath the Asian continent. The volcanisms usually developed from the center of rifting (graben) to the flanks in pace with the rifting evolution and accompanied by transition in magma type from calc-alkaline to alkali basalts. The volcanisms that occurred in the Tibetan Plateau might have resulted from the collision between Indian and Eurasian plates or postcollisional setting.

Accompanying frequent volcanisms, a large number of maars and maar lakes developed in the volcanic fields from the tropic to the temperate zones in China. The oldest maar edifice with 125 Ma age can be found in the Cretaceous in Yixian County, the West Liaoning Province, and other old maars with ~13 Ma are located in Shanwan, Shandong Province. Most maars and maar lakes occurred in the Quaternary and distributed in three main regions: Leiqiong volcanic field in South China, Longgang volcanic field to be called Chinese Eifel in Jilin Province near the Changbai Volcanoes, and Arxan volcanic field located in Daxing'an range of Inter Mongolia. The different maar (lake) has different geological background and different environment, so they can record various paleoclimatic and paleoenvironmental information. We have done many drilling works and got several long cores and short freeze cores from Huguangyan Maar Lake in the tropic Leizhou Peninsula, South China, and from Sihailongwan and other maar lakes in Longgang and Arxan volcanic fields since 1997.

After core opening and sampling, the sediment samples were analyzed by multiple methods including dating, varves, tephra, chemistry, pollen, and others, and more data dealing with paleoclimatic and paleoenvironmental indexes were obtained. Based on those indexes and good sediment sequence with varve and tephra layers, we established high resolution time sequences and identified some climatic change cycles and events.

Even no excellent varves can be found in Huguangyan Lake sediments, but it was none the less possible to establish a high-resolution time series through past 40–78 ka by AMS ^{14}C ages and paleomagnetic measurements. It revealed that the East Asian monsoon have rich records in the tropic zone. The paleoclimatic and paleoenvironmental variations in the tropical zone were corresponded to solar activity in different time scales and were different from those occurred in high latitude Greenland. In millennium scale, there were strong climatic varied frequencies in tropical zone during the last deglaciation and Holocene with 11 events at least, even interglacial stages within the last glacial period, and no obvious variations in the glacial period from 38 to 16 ka BP. On the contrary, in the high latitude Greenland, the strong climatic varied frequencies occurred in the last glacial period, and relative stable climate occurred in the Holocene.

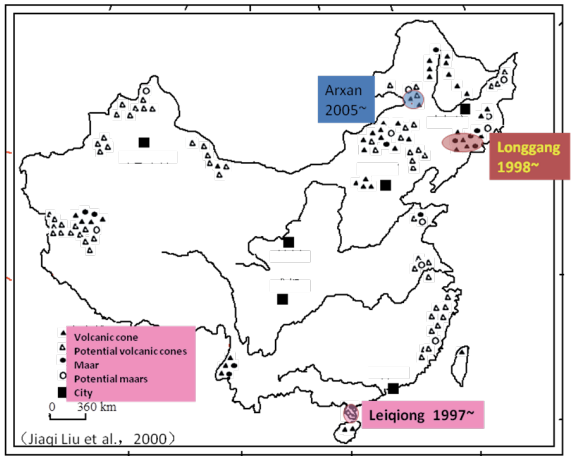

Figure 2. Distribution of the maars in China and starting researching time.

Implication of Heavy Mineral Distribution Based on U-Pb Dating of Detrital Zircons by Using LA-ICP-MS as a Tool for Provenance Analyses in Sediments of Jurassic/Cretaceous Paleodrainage Connections between Porcupine–Rockall–Orphan–Flemish Pass (PROF) Basins

Afsoon Moatari-Kazerouni* and Paul Sylvester

[1]*Department of Geosciences, Texas Tech University, Lubbock, Texas*
*Corresponding author E-mail: afsoon.moatari@gmail.com

In order to determine the extent to which deposition of Jurassic hydrocarbon source rock mudstone units and lower Cretaceous sandstone reservoir units along the Ireland-Newfoundland conjugate margins (Porcupine-Rockall-Orphan-Flemish Pass (PROF) basins) is the result of regional, large-scale versus local, small-scale paleodrainage systems, and the implications for their quality, thickness, and distribution.

Provenance analyses are a powerful tool for assessing the origin and dispersion of material in ancient and modern fluvial and marine sediments. Provenance-specific heavy minerals (e.g., zircon, rutile, tourmaline) provides information about potential regional or long distance transport paths, current flows, as well as depositional centers for the released sediments.

Petroleum exploration of the offshore deep-water basins of the Ireland-Newfoundland conjugate margin (Williams et al., 1999) is expensive and risky. An improved knowledge of the regional geology of the offshore would allow more effective evaluation of the hydrocarbon potential of the region. An aspect of the offshore geology in need of particular study is the nature and geological history of basement uplifts and their contributions to the supply of sedimentary detritus to source and reservoir units in the basins.

This project builds on recent studies of the principal investigator and his colleagues working on the provenance of Jurassic/Cretaceous siliciclastic units along the Ireland-Newfoundland conjugate margin. The goal is to determine if key, hydrocarbon source and reservoir, Jurassic/Cretaceous units in the Porcupine and Rockall basins on the Ireland margin and in the Orphan and Flemish Pass basins on the Newfoundland margin were deposited by the same paleodrainage systems. Common sediment supply routes likely would have been geographically extensive, with headlands on known continental margins surrounding the North Atlantic, and perhaps forming thick, laterally continuous siliciclastic units prior to tectonic readjustments. The alternative possibility is that the critical hydrocarbon source and reservoir units of the North Atlantic conjugate margin formed from detritus derived from more local, smaller scale drainage systems on basement uplifts in the offshore. Local sediment supplies may have produced hydrocarbon source and reservoir units with more variable thickness and quality between and within offshore basins. Determining which of these two possibilities more accurately describes the Jurassic/Cretaceous evolution of the Porcupine-Rockall-Orphan-Flemish Pass basins would be an important advancement for North Atlantic exploration strategies.

There have been few previous studies of provenance of Jurassic and Cretaceous units on the

Newfoundland conjugate margin. Lowe et al. (2011) reported that clastic material entering the northern Flemish Pass Basin during the Tithonian to Berriasian was connected to transport systems reaching west, as far as 400–500 km, including from Avalonia. The eastward-directed input of bed-load material into the basin resulted in the concentration of sandstone units along its western margin, with deteriorating reservoir grade toward the east, with the likely deposition of equivalent sandstones in the adjacent East Orphan Basin. In addition, McDonough et al. (2010) recognized sources from the continental basement of Flemish Cap and Iberia during the late Jurassic to early Cretaceous.

Enachescu et al. (2010) proposed that the source of hydrocarbons on the conjugate margins of the North and Central Atlantic is widespread, organic-rich Kimmeridgian-aged mudstone that predominantly had a restricted marine source in the Grand Banks basins.

Magoon et al. (2005) described the hydrocarbon source rock in the Jeanne d'Arc Basin as having a marine facies (Egret Member of the Rankin Formation) in the west and a terrigenous facies (Kimmeridgian source rock) in the east, the latter being thicker and younger, with more siliciclastic sediment, including the Tempest sandstone.

Monogenetic Volcanoes: A Useful Term for Small Volcanoes

Károly Németh

Institute of Agriculture and Environment, Volcanic Risk Solutions, Massey University, Turitea Campus, New Zealand
E-mail: k.nemeth@massey.ac.nz

Keywords: volcanic field, scoria, phreatomagmatism

Complex volcanological researches applying the source-to-surface model to dispersed volcanism revealed several key elements of the eruption style, volcanic architecture, degradation, and interaction with the background sedimentation of small and short-lived volcanoes (monogenetic volcanoes). There have also been several attempts to redefine and evaluate the suitability and use of the term monogenetic to volcanic processes and volcano types. Monogenetic volcanoes viewed as volcanoes that erupt only once during their eruptive history in spite that their eruption may follow numerous distinct eruptive phases controlled/influenced by systematically or randomly changing magma discharge rates, fluctuation of external versus internal influences on the eruption styles, and commonly repeated cyclic periods controlled by complex threshold parameters may alter specific eruption styles (e.g., magmatic versus phreatomagmatic) (Németh and Kereszturi, 2015). One of the most common aspects of monogenetic volcanoes is that they are small and resulted from eruption of low volume of magma. While there is no specific value attached to define a volcano monogenetic on the pure basis of their edifice and DRE volumes, the general preconception is that monogenetic volcanoes are "small." This definition, however, is probably one of the most fundamental roots of arguments around the definition of monogenetic volcanoes as their sizes can only be measured directly until they are intact. A typical monogenetic volcano is less than <0.5 km^3 while their tephra rarely cover larger areas than 1000 km^2, while the total magma involvement in their eruption is less than 0.1 km^3 DRE. The problem starts with applying the monogenetic definition to a volcanic succession that is dissected and has no real link to their original volcano morphology. In such occasion, the only geological information available is the rock units that may carry information to establish volcanic stratigraphy, and hence the potential volcano morphotype they belong to. In this presentation, a general model will be provided in context of the evolution of knowledge about small volcanoes.

Figure 1. Complex tuff ring of Brown Island (Motokorea) from Auckland shows great variety of eruptive product as a result of changes in eruption styles without any significant time break between events.

Figure 2. Complex maar (Tower Hill, Australia) crater rim similar to Brown Island with no easy to recognize unconformity surfaces indicating no significant time gap between eruptive phases.

The most common process-driven definition we can apply to name a volcano monogenetic is that the duration of the eruption forming these small volcanoes is usually shorter than the solidification time required for freezing their feeding system. This definition is, however, not excluding fluctuation of the magma rise rate and flux allowing magma batches traveling to the surface and to be involved in various eruption styles. Recent studies showed that even multiple deep melt sources or evolving melt conditions are commonly recorded as key features in the volcanic successions of a small volcano. The common feature, however, of these examples is that the overall eruptive volume of the

volcano is still at least a magnitude less than a typical polygenetic volcano.

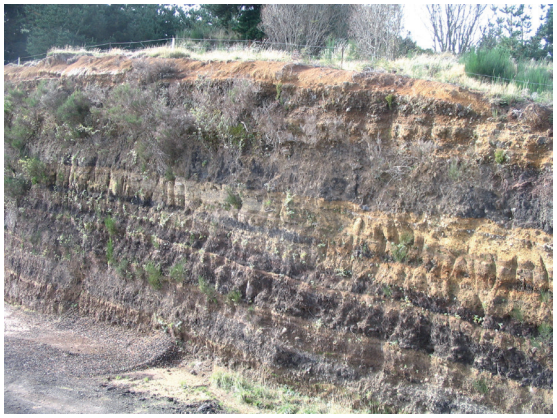

Figure 3. Ohakune is a small volcano with phreatomagmatic influence on the Strombolian/Hawaiian style eruptions.

It has also been demonstrated that the small overall eruptive volume is the key to allow the eruptions influenced in various level by external conditions such as the eruptive environment (low lying versus highland), aquifer conditions (confined versus unconfined), country rock types (hard versus soft), and climatic conditions. In a schematic view, if very low volume of magma rises to the surface these external conditions can make dominant effect on the eruption style, while increasing magma volumes can cause a gradual changes in the eruption styles in the course of the eruption generating an overwhelmingly complicated volcanic stratigraphy that will be composed of pyroclastic beds that are texturally very different (Figures 1 and 2). So far no systematic study has been performed to explore the pyroclasts texture and their link to these eruption style changes. Analyzing the eruption sequences of Auckland's 53 volcanoes and their geographical locations in respect to the country's rock geology, it was possible to define a relatively simple equation to express the probability of eruption style transitions in function of the country's rock geology (Kereszturi et al. 2014). Conversely, external controlling parameters on magma fragmentation and eruption styles have a greater effect on volcanoes produced by smaller volumes of melt (Figure 3). Fantastic example has been documented from the Harrat Rahat, where the smallest preserved scoria cones show phreatomagmatic base (Figure 4) resulted by a short initial influence at the start of the eruption (Murcia et al. 2015).

Large monogenetic volcanoes also exist and they are commonly the result of multiple explosive eruption along a fissure or across a slurry filled crater zone resulting in compound volcanoes such as Purrumbete maar in Australia (Jordan et al. 2013).

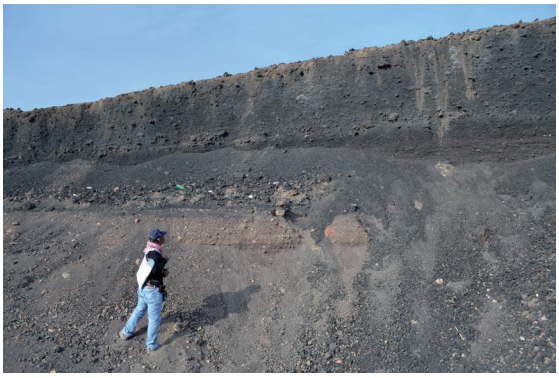

Figure 4. The Al-Du'aythah volcanic cones from Saudi Arabia are examples how the small magma output-dominated vents can be influenced externally.

The number of vents, their dominated eruption styles, and the eruptive volume together will determine the complexity of the small volume volcano. In typical small eruptions time gaps inferred between eruptive phases are short and the number of eruptive episodes is far less than a typical polygenetic volcano. Monogenetic volcanoes are diverse in their eruption styles, volume, and duration that can make their appearance complex. Here we present numerous examples to demonstrate the complexity of monogenetic volcanism and provide a critical model of how we can better understand the Earth's most common form of volcanism.

References

Jordan SC, Cas RAF, Hayman PC (2013) The origin of a large (> 3 km) maar volcano by coalescence of multiple shallow craters: Lake Purrumbete maar, southeastern Australia. J Volc Geotherm Res 254:5–22.

Kereszturi G, Nemeth K, Cronin SJ, Procter J, Agustin-Flores J (2014) Influences on the variability of eruption sequences and style transitions in the Auckland Volcanic Field, New Zealand. J Volc Geotherm Res 286:101–115.

Murcia H, Nemeth K, El-Masry NN, Lindsay JM, Moufti MRH, Wameyo P, Cronin SJ, Smith IEM, Kereszturi G (2015) The Al-Du'aythah volcanic cones, Al-Madinah City: implications for volcanic hazards in northern Harrat Rahat, Kingdom of Saudi Arabia. Bull Volc 77(6).

Németh K, Kereszturi G (2015) Monogenetic volcanism: personal views and discussion. Int J Earth Sci 104(8):2131–2146.

Geoheritage Values of Monogenetic Volcanic Fields: A Potential UNESCO World Heritage Site in the Arabian Peninsula

Károly Németh[1,*] and Mohammed Rashad Moufti[2]

[1]*Volcanic Risk Solutions, Institute of Agriculture and Environment, Massey University, Palmerston North, New Zealand*
[2]*Geohazards Research Center, King Abdulaziz University, Jeddah, Kingdom of Saudi Arabia*
*Corresponding author E-mail: k.nemeth@massey.ac.nz

Keywords: geosite, scoria, maar

The term geoheritage derives from the word heritage, which means something that has been transmitted from the past, or has been handed down by tradition. To evaluate geoheritage, three factors should be taken in to account: (1) the scale, (2) the scope, and (3) the significance of the site (Brocx and Semeniuk 2007). The uniqueness of a site is dependent on the scale in which it is measured. Expressing the geoheritage value of a site needs an appreciation of its scope; does the site represent causal processes (e.g., process-oriented features) and/or does it offer insights for Earth's development (e.g., product-oriented). Geoheritage sites can be further graded by separating the (1) international, (2) state, or (3) regional significance of the sites.

Short-lived and small monogenetic volcanoes are easy to access; their eruptive products are on a "human scale" and, therefore, they can be used to demonstrate volcanic processes without major challenges for educators or visitors. Monogenetic volcanic fields hence either active or ancient are excellent locations to transmit information to visitors about volcanic eruptive processes and volcanic hazards. Recent recognition of volcanic geoheritage studies of the role of volcanic hazard education is expressed by the newly formed IAVCEI Commission on Volcanic Geoheritage and Protected Volcanic Landscapes.

Monogenetic volcanic fields can carry great geoheritage value if (a) their historic eruptions influenced human societies, (b) they have high aesthetic value, or (c) they are used as reference areas to describe unique volcanic processes. However, it is difficult to demonstrate their outstanding universal values (OUV) based on their natural phenomena. As monogenetic volcanic fields host the most common volcano types on Earth (Németh and Kereszturi 2015), it is difficult to demonstrate their high OUV. Here we argue that in spite of monogenetic volcanoes being common they can carry OUV as required for a successful UNSECO World Heritage application; however, their features need to be demonstrated from a holistic perspective. While a single scoria cone can hardly be characterized by high OUV, the same scoria cone if it is influenced by cultural development or scientific knowledge advances it may be associated with high OUV. The main geoheritage value, however, is in the geodiversity of the volcanic fields. These volcanoes resulted from short-lived eruptions variably influenced by the magma's internal physical-chemical parameters and the environmental factors (type and availability of external water) (Németh and Kereszturi 2015). Hence, there are "simple" low geodiversity and "complex" high geodiversity volcanic fields. Geodiversity could be used as a strong argument to define the volcanic field's OUV.

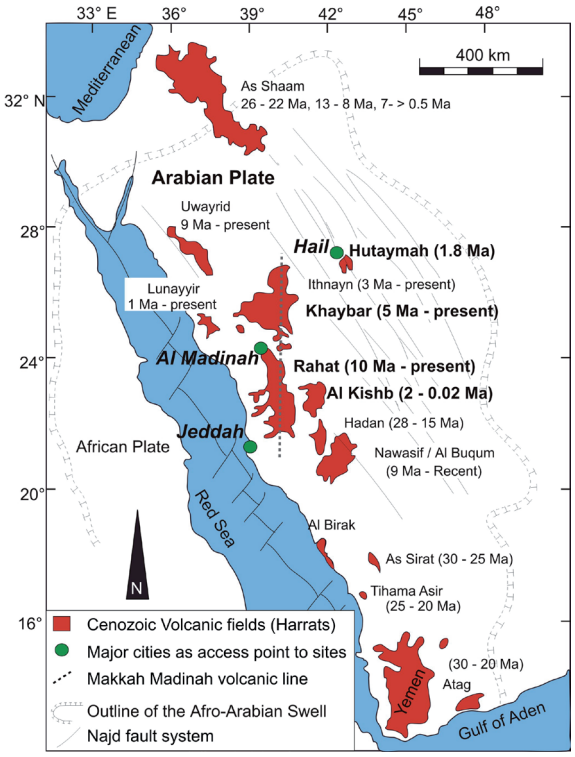

Figure 1. Major volcanic fields of the Western Arabian Peninsula.

The Arabian Peninsula is the home of superbly exposed and accessible volcanic fields with high

geodiversity, offering itself as a global hub of geosites showing every possible volcanic feature we know from volcanic fields (Moufti and Németh 2013).

In particular, Western Saudi Arabia is a region where long-lived dispersed alkaline basaltic intracontinental volcanic activity has produced numerous volcanic fields in the past 10 My. Five recently studied distinct volcanic fields, spanning a North to South axis over 1500 km in length, represent continental rift-related dispersed volcanism that is probably the largest monogenetic intracontinental volcanic province on Earth with the highest geodiversity we are aware of.

Harrat Rahat is one of the largest mature volcanic fields in the Arabian Peninsula located near the Holy City of Al Madinah (Figure 1). In addition, the location also carries cultural heritage. **Harrat Kishb** is a bimodal volcanic field and has been active since 2 Ma, having its latest eruptions 4.5–2 ka (Camp et al. 1992). Harrat Kishb hosts two geoheritage sites with high scientific, cultural, or aesthetic values such as the Al Wahbah maar crater and the Aslaj volcano. **Harrat Hutaymah** is a field located ~70 km to the SE of Hail city (Figure 1). The abundance of tuff rings and maars (Figure 2) makes Harrat Hutaymah different from other harrats by hosting the largest number of phreatomagmatic volcanoes across the Arabian Peninsula. **Harrat Khaybar** north of Al Madinah City is a young volcanic field, having at least two sites suspected to be as young as a few thousands of years. Jebel Quidr lava shield with a central cone dominates the field with its extensive lava fields and ash plains. Harrat Khaybar is also the home of the "*White Mountains*": Jebel Bayda and Jebel Abyad as felsic tuff rings and lava domes (Figure 3). **Harrat Al Birk** is in the south close to Yemen with its coastal location providing unique landscape impression. The eolian sand-covered maars in this region provide evidence that phreatomagmatism took place in time when water was available in this currently arid region.

The volcanic fields in Saudi Arabia with their high scientific, cultural, and aesthetic value and exceptional geodiversity are inferred to fulfil the OUV needed for an acceptance in the UNESCO World Heritage site list.

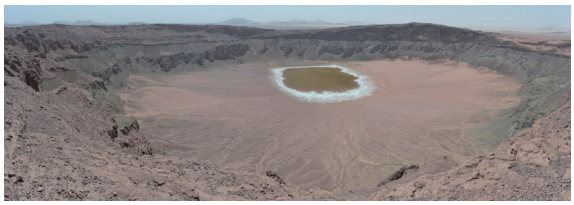

Figure 2. Harrat Hutaymah maar geotope.

Figure 3. Jebel Bayda felsic tuff ring geotope.

References

Brocx M, Semeniuk V (2007) Geoheritage and geoconservation - history, definition, scope and scale. Journal of the Royal Society of Western Australia 90:53–87.

Camp VE, Roobol MJ, Hooper PR (1992) The Arabian Continental Alkali Basalt Province .3. Evolution of Harrat Kishb, Kingdom of Saudi-Arabia. Geological Society of America Bulletin 104(4):379–396.

Moufti MR, Németh K (2013) The intra-continental Harrat Al Madinah Volcanic Field, Western Saudi Arabia: a proposal to establish Harrat Al Madinah as the first volcanic geopark in the Kingdom of Saudi Arabia. Geoheritage 5(3):185–206.

Németh K, Kereszturi G (2015) Monogenetic volcanism: personal views and discussion. International Journal of Earth Sciences 104(8):2131–2146.

A Relation between the GRACE-Derived Geoid Variation and Regional Magmatic Activities around the Volcanic Area

Chang Whan Oh[1,*], Young Seok Chang[2], Sung Chan Choi[3], Deok Su Lee[2], and Seung Hwan Lee[1]

[1]*Department of Earth and Environmental Sciences and The Earth and Environmental Science System Research Center, Chonbuk National University, Jeonju, Republic of Korea*
[2]*Research Institute of GN Co., Seoul, Republic of Korea*
[3]*Institute für Geowissenschaften, Abtlg. Geophysik, Christian-Albrechts-Universität zu Kiel, Kiel, Germany*
*Corresponding author E-mail: ocwhan@jbnu.ac.kr

Keywords: GRACE, geoid, magmatic activity

In recent decades, it has been confirmed that the change of gravity data in the volcanic area can provide valuable data on subsurface mass redistribution associated with volcanic activity throughout systematic microgravity studies over some 20 active volcanoes in Central America, Iceland, Italy, Japan, Papua New Guinea, and the United States (e.g., Rymer, 1994; Carbone et al., 2006, 2007). The gravity change in volcanic area is partially due to concurrent ground elevation but there are residual gravity changes after correction for elevation changes in many volcanic areas (Williams-Jones and Rymer, 2002). The residual gravity changes are considered to be related to magma movements in subsurface magma chambers, feeder systems, and vents or water table variations. In general, the smallest residual gravity changes are associated with eruptions from volatile-poor basaltic vents and at extensional rift zones, whereas the highest residual values occur at explosive, subduction-related stratovolcanos built from volatile-rich andesitic magma suggesting that the change of residual gravity is related to the amount of volatility in magma, which decreases the density of magma (Rymer, 1994).

In most volcanos, there are magma chambers at depth below 10 km which supply new magma to shallow magma chamber within 5 km depth. In some volcanos, very large magma chamber below 10 km was identified (e.g., magma chamber under Baegdu volcano, 160 × 120 km^2; Choi et al., 2013) indicating that the regional gravity change due to the activity of magma under the volcano can be detected using the Gravity Recovery and Climate Experiment (GRACE) satellite, which can measure gravity change with resolution of 150 × 150 km in average. However, no study has been done to detect gravity change related to magma activity under volcano using the Gravity Recovery and Climate Experiment satellite.

The GRACE temporal gravity variation is generally expressed in the form of spherical harmonic coefficients of the gravity and its derived Equivalent-Water-Height (EWH). In particular, the GRACE-derived EWH data (GEHW) are mainly utilized for monitoring hydrological applications in relation to ice-sheet mass balance, sea revel rise, ocean circulation, and water storage in the Earth's system. This study offers a hypothesis suggesting that the temporal GEWH variation (ΔGEWH) observed in the regional volcanic area is related not only with the Terrestrial-Water-Storage changes (ΔTWS) as an external factor but also with the time-dependent density variation (ΔDV) associated with the density change of magma chamber and surrounding rocks. This is well identified in several volcanos such as Kusatsu and Baegdu volcanos in Japan and Korea, respectively. In the two areas, during the time of activation of magma chamber with seismic activities, the ΔGEWH became lower than normal condition but there are no change in precipitation pattern indicating that the ΔGEWH decrease occurred due to the magma activity which caused the density decrease related to the increase of volatile component with increasing temperature of magma chamber by newly supplied magma. From that point of view, the relation can be expressed by an equation as like as ΔGEWH = ΔTWS + ΔDV. From this equation we can calculate ΔDV by subtracting ΔTWS from ΔGEWH (ΔDV = ΔGEWH – ΔTWS).

However, there are problems in calculating ΔTWS from precipitation because it is difficult to transfer the precipitation data into ΔGEWH especially in the area with heavy rainfall related to typhoon such as Kirishima and Ontake areas in Japan and it is difficult to get precipitation data in many remote volcanic areas. To overcome this problem, Fourier analysis on ΔTWS and ΔEWH in volcanic areas in Japan and Korea, is carried out to investigate the relationship between both datasets. ΔTWS is de-trended by subtracting a linear-regressed line to remove long periodic trends in order to avoid estimation fails due to nonperiodic signal before the Fourier transformation. The results of Fourier analysis on both ΔEWH and

ΔTWS at each volcanic area show 12-month period spectral peaks clearly. The peaks clearly show that there is the annual ΔEWH variations due to the ΔTWS variation related to monsoon and/or dry seasons in the volcanic area. The EWH peaks with periods less than 12-months are also expected to be affected by precipitation and other variation on the surface. Therefore, in this study, the EWH peaks with period shorter than 24 months are removed under the assumption that they are not related to magma activity beneath the surface.

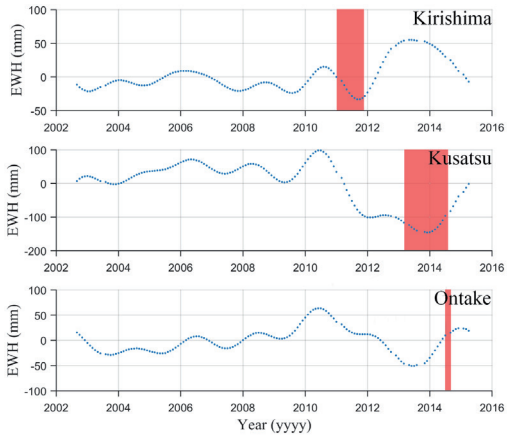

Figure 1. The ΔEWH variations form which ΔTWS variations are removed in the Kirishima, Kusatu, and Ontake volcanic areas. The red rectangles indicate the time of eruption or seismic activity related to magma activity.

The EWH variations after removing peaks with periods longer than 24 months from three volcanos in Japan show that volcanic activities are correlated with the time of minimum EWH fluctuations. Numerous eruptions and explosions at Kirishima volcano had been reported between January and September 2011 with large seismicity, and the minimum anomaly of EWH in this region is overlapped with the eruption period. Even though no eruption occurred at Kusatsu volcano, large seismicity and hydrothermal emissions related to magma activities occurred during the period with negative anomalies below –100 mm. The explosion of Ontake volcano occurred after 1 year from the minimum anomaly of EWH and seems to be affected by the magma activity in the neighboring Kusatsu volcano. These data suggest that the magma activity can be detected by the GRACE satellite and the magma activity can occur at the time when ΔGEWH reached the minimum value or somewhat later than the time with minimum value.

Acknowledgement

This study was carried out as the project “Satellite-derived Gravity Modeling in Mt. Baekdu” supported by Korean Meteorological Administration (CATER 2012-5062).

References

Daniele Carbone, Luciano Zuccarello, Gilberto Saccorotti, Filippo Greco, 2006. Analysis of simultaneous gravity and tremor anomalies observed during the 2002–2003 Etna eruption. Earth and Planetary Science Letters 245: 616–629.

D. Carbone, G. Budetta, F. Greco, L. Zuccarello, 2007. A data sequence acquired at Mt. Etna during the 2002–2003 eruption highlights the potential of continuous gravity observations as a tool to monitor and study active volcanoes. Journal of Geodynamics 43: 320–329.

Glyn Williams-Jones, Hazel Rymer, 2002. Detecting volcanic eruption precursors: a new method using gravity and deformation measurements. Journal of Volcanology and Geothermal Research 113: 379–389.

Hazel Rymer, 1994. Microgravity change as a precursor to volcanic activity. Jounal of Volcanology and Geothermal Research 61: 311–328.

Sungchan Choi, Chang-Whan Oh, H.-J. Götze, 2013. Three-dimensional density modeling of the EGM2008 gravity field over the Mount Paekdu volcanic area. Journal of Geophysical Research: Solid Earth 118: 1–17.

The Depth of Magma Chambers during the Eruption of Baekdu Volcano

Chang Whan Oh[1,*], Seung Hwan Lee[1], Youn Soo Lee[2], Seung-Gu Lee[2], and Jiaqui Liu[3]

[1]*Department of Earth and Environmental Sciences and The Earth and Environmental Science System Research Center, Chonbuk National University, JeonjuRepublic of Korea*
[2]*Geological Research Division, Korean Institute of Geoscience and Mineral Resources, Daejeon, Korea*
[3]*Institute of Geology and Geophysics, Chinese Academy of Sciences, Beijing, China*
*Corresponding author E-mail: ocwhan@jbnu.ac.kr

Keywords: magma chamber, depth, Baekdu Volcano

Baekdu Volcano is a 2750-m high stratovolcanic cone with a prominent caldera and rests on a basaltic shield and plateau situated on the North Korea-China border. The basement of the basaltic shield and plateau consists of Archean to middle-late Proterozoic metamorphic rocks, Paleozoic strata, and predominantly Mesozoic granite. Baekdu Volcano has been an active volcano since the Oligocene and is still regarded as a high-risk volcano, having provided one of the planet's largest eruptions in the past 2000 years (Yun et al., 1993; Xu et al., 2012).

The volcanic history of Baekdu Volcano can be divided into four stages based on age data, eruption style, and magma compositional changes (Wei et al., 2007) as follows (from the oldest to the youngest): (i) preshield plateau-forming eruptions, (ii) basalt shield formation, (iii) construction of a trachytic composite cone, and (iv) explosive ignimbrite forming eruptions. In the first stage, a fissure eruption produced basalts from the Oligocene to the Miocene (28–13 Ma). A preshield plateau was formed by these basalts. The basalt plateau became deeply eroded, forming valleys that were filled with lava flows during the shield-forming eruptions of the Pliocene and early Pleistocene (4.21–1.70 Ma). Fissure and central eruptions occurred together during the shield-forming eruptions. In the third stage, the trachytic composite volcano, with a diameter of 20–30 km and a height of 650 m, formed during the Pleistocene (0.61–0.09 Ma). In this stage, magma changed to an acidic melt to produce alkali trachyte, trachytic tuff, tuff breccia, alkali rhyolite, and obsidian. The latest stage has been characterized by explosive ignimbrite-forming eruptions during the Holocene, producing trachytic pumice, ash tuff, welded tuff, and tuff breccia. The ash produced in this stage has reached as far as the East Sea (Sea of Japan) and Japan. During this stage, a caldera formed at the top of Baekdu Volcano. The Holocene eruptions occurred between 1690 BP and AD 1702 (Yun et al., 1993). The largest eruption, which had a 35-km high column and produced comenditic ignimbrite around the volcano, took place at circa AD 935 (Yun et al., 1993; Xu et al., 2012).

To study the Moho depth and subsurface crustal structures within the volcanic area, two wide-angle reflection and refraction seismic survey profiles were conducted: one along a south-north line including Baekdu Volcano and another along a west-east line crossing the northern part of the volcanic area. The surveys were performed by the Research Center of Exploration Geophysics (now the Geophysical Exploration Center) of the China Seismological Bureau (now the China Earthquake Administration) (Tang et al., 1998). Previous results of deep seismic soundings along the two seismic lines allowed four layers with magma chambers to be identified. The crustal thickness varies from 31 km in the area north of the caldera lake to about 40 km directly under Baekdu Volcano. The magma chambers were represented by a series of LVZs (Low Velocity Zones) beneath Baekdu Volcano between 10 km depth and the Moho (Zhang et al., 2002a, 2002b). Here, the *P*-wave velocity is approximately 2–4% slower than that in the surrounding crust. The lateral extents of the other LVZs decrease with increasing depth (Tang et al., 1998; Zhang et al., 2002a, 2002b). Recently, Magma chamber at 5 km is also predicted to lie beneath Baekdu Volcano (Choi et al., 2013).

A total of 7 trachytic, 1 comendite, and 1 pumice samples were collected from the Baekdu Volcano in 2015 to study the depth of magma chambers which produced volcanic eruption during the formation of composite volcano part of the Baekdu Volcano. Nine collected samples are divided to five rock types, Xiaobaishan trachyte (66 Xiaobaishan trachyte 01, 67 Xiaobaishan trachyte 02), Lower trachyte (71 BP1571), Middle trachyte (63 Middle trachyte), Upper trachyte (65 Upper trachyte 01, 68 Upper trachyte 02, 70 XP1560), Comendite (64 BP1569), and Pumice (69GB/P1 Pumice). We carried out EPMA analysis on minerals whole rock analysis, to calculate depth of magma chambers for the trachytic composite part of Baekdu Volcano. Amphiboles and clinopyroxenes were analyzed to use amphibole geobarometer (Ridolfi and Renzulli, 2012) and

clinopyroxene geobarometer (Putirka et al., 2003). However, unfortunately we could not calculate the depth of magma chamber using amphibole because amphibole geobarometer can be used for amphibole with MgO component higher than 0.5 but all analyzed amphibole's MgO components were lower than 0.5. Therefore, clinopyroxene and whole rock geochemistry data were used to calculate pressure conditions of magma chambers under Baekdu Volcano. Note that 12 clinopyroxenes analyzed in four samples show Hedenbergite composition. The following clinopyroene geobarometer (Putirka et al., 2003) was used to calculate the depth of magma chambers.

$$P(\text{kbar}) = -88.3 + 2.82\times10^{-3}T(\text{K})\ln\left[\frac{[\text{Jd}^{\text{cpx}}]}{[\text{Na}^{\text{liq}}\text{Al}^{\text{liq}}(\text{Si}^{\text{liq}})^2]}\right] + 2.19\times10^{-2}T(K) - 25.1\ln[\text{Ca}^{\text{liq}}\text{Si}^{\text{liq}}] + 7.03[\text{Mg}^{\text{liq}}] + 12.4\ln[\text{Ca}^{\text{liq}}]$$

Equation. 1 – Equation to calculate pressure(P).

T(K) : Kelvins, Jd^{CPX} : mole fraction of Jadeite in Clinopyroxene, Mg^{liq} : $MgO^{liq}/(MgO^{liq} + FeO^{liq})$

The clinopyroxene geobarometer can be used for clinopyroxene with jadeite component. According to the calculation results using eight clinopyroxenes with jadeite component, two magma chambers are expected to have existed at 8.7–12.7 kbar and 3.7–4.1 kbar indicating the depth of two magma chambers are 10 and 27~30 km, respectively. These depth of magma chambers are similar to the first and fourth magma chambers figured out from the seismic survey suggesting that the magma chambers under the Baekdu Volcano may have existed since the trachyte composite cone stage of Baekdu Volcano.

Table. 1. Calculated pressure (depth) conditions of magma chambers for trachytes in Baekdu Volcano

Rock	CPX (Analysis number)	*P*(kbar)
70 XP1560	70-003	9.8
	70-007	12.7
63 middle trachyte	63-002	3.7
	63-003	3.9
	63-004	4.1
71 BP1571	71-002	8.9
	71-006	10.5
66 Trachyte01	66-001	8.7

Acknowledgments

This study was carried out as the project "A study of volcanic rocks, eruptive stratigraphy and geophysics of Baekdusan volcano" supported by Korean Institute of Geoscience and Mineral Resources.

References

Choi, S., H.-J. Goetze, U. Meyer, and DESIRE Group, (2011). 3-D density modelling of underground structures and spatial distribution of salt diapirism in the Dead Sea Basin, Geophys. J. Int., 184, 1131–1146, DOI:10.1111/j.1365-246X.2011.04939.x.

Ridolfi, F., and A. Renzulli, (2012). Calcic amphiboles in calc-alkaline and alkaline magmas: thermobarometric and chemometric empirical equations valid up to 1,130□ and 2.2 GPa. Contribut. Mineral. Petrol. DOI: 10.1007/s00410-011-0704-6.

Putirka, K. D., H. Mikaelian, F. Ryerson, and H. Shaw, (2003). New clinopyroxene-liquid thermobarometers for mafic, evolved, and volatile-bearing lava compositions, with applications to lavas from Tibet and the Snake River Plain, Idaho. Am. Mineralogist. DOI: 10.2138/am-2003-1017

Tang, J., M. Ma, and R. Liu, (1998). The electric structure of Tianch volcano area by magnetotelluric exploration and recent seismicity, in The Recent Eruptions of the Tianchi Volcano in Changbaishan, edited by R. Liu, H. Wei, and J. Li, pp. 108–123, Science Publishers, Beijing, China (in Chinese).

Wei, H., Y. Wang, J. Jin, L. Gao, S.-H. Yun, and B. Jin, (2007). Timescale and evolution of the intracontinental Tianchi volcanic shield and ignimbriteforming eruption, Changbaishan, Northeast China, Lithos., 96, 315–324.

Xu, J., G. Liu, J. Wu, Y. Ming, Q. Wang, D. Cui, Z. Shangguan, B. Oan, X. Lin, and J. Liu, (2012). Recent unrest of Changbaishan volcano, Northeast China: A precursor of a future eruption?, Geophys. Res. Lett., 39, L16305, doi:10.1029/2012GL052600.

Yun, S. H., C. K. Won, and M. W. Lee, (1993). Cenozoic volcanic activity and petrochemistry of volcanic rocks in the Mt. Paekdu area, J. Geol. Soc. Korea, 29(3), 291–307 (in Korean).

Zhang, C., X. Zhang, J. Zhao, B. Liu, J. Zhang, Z. Yang, Y. Hai, and G. Sun, (2002a). Crust-mantle structure of the Changbaishan Tianchi volcanic region and its vicinity: An exploratory study and inferences, Chin. J. Geophys., 45, 862–871.

Zhang, X.-K., C.-K. Zhang, J.-R. Zhao, Z.-X. Yang, S.-L. Li, J.-S. Zhang, B.-F. Liu, S.-X. Cheng, G.-W. Sun, and S.-Z. Pan, (2002b). Deep seismic sounding investigation into the deep structure of the magma system in Changbaishan-Tianchi volcanic region, Acta Seismol. Sin., 15(2), 143–151.

Distinction of Magnetic Fabrics Produced by Primary Pyroclastic Processes and Contemporaneous Storm-Reworking Processes in a Coastal Tuff Ring, Jeju Island, Korea

Mi Eun Park[1,*], Chanwoo Sohn[1], Hyeongseong Cho[2], and Young Kwon Sohn[1]

[1]*Department of Geology, Gyeongsang National University, Jinju, Korea*
[2]*Department of Geological Sciences, Pusan National University, Busan, Korea*
*Corresponding author E-mail: testify@gnu.ac.kr

Keywords: magnetic fabric, basaltic tuff, storm reworking

Measurement of magnetic fabrics has been used to resolve the mechanisms of sediment transport and deposition and to distinguish between different depositional conditions (Rees, 1961, 1966; Rees et al., 1968; Hamilton and Rees, 1970). Magnetic shape factor (q-value), which is a measure of the strength of magnetic lineation, L (degree of long-axis alignment of magnetic grains), produced by tangential shear stress, relative to magnetic foliation, F (degree of short-axis alignment), produced by gravity force (Rees and Woodall, 1975), has been especially useful for sedimentological interpretations. Imbrication angle of the magnetic foliation plane, β, and the corrected degree of anisotropy, P_J, defining the relative strength of the magnetic fabrics, are also useful parameters for the evaluation of the relationship between depositional processes and magnetic fabric (Taira, 1989; Park et al., 2013).

Magnetic fabrics were measured for the samples collected from the medial-to-distal rimbeds of the Songaksan tuff ring, which erupted ca. 3.8 ka ago in the southwestern margin of Jeju Island, Korea. The deposits comprise mainly thin-bedded and undulatory- to parallel-bedded tuff emplaced by dilute and waning pyroclastic surges and attendant ash fall (Chough and Sohn, 1990). Several units of reworked tuff were newly identified in the middle of the rimbeds, characterized by trough and low-angle cross-stratification with common scour surfaces and intercalating mud drapes, suggesting a combined action of wave and tide during a raised sea level, which was caused most likely by a storm surge event that lasted a few days during the eruption of the tuff ring.

The measurement of magnetic fabrics from the primary and reworked deposits shows that the former have subhorizontal magnetic foliation with low q-values and imbrication angle, characterized by oblate to weakly triaxial fabric shape, whereas the latter are characterized by imbricated triaxial fabric shape with higher values of shape factor and imbrication.

We interpret that the dilute and waning suspension currents (i.e., pyroclastic surges) in the medial-to-distal reach resulted in horizontal (foliated) magnetic fabric because of deposition in a gravitational stress-dominated regime. On the other hand, the storm-reworked deposits have imbricated (lineated) magnetic fabric indicating stronger tangential shear stress exerted by the storm waves. They also have either onshore- (NE- to SE-directed) or offshore-directed (NNW- to SSW-directed) maximum magnetic susceptibility axes (k_1) (Figure 1).

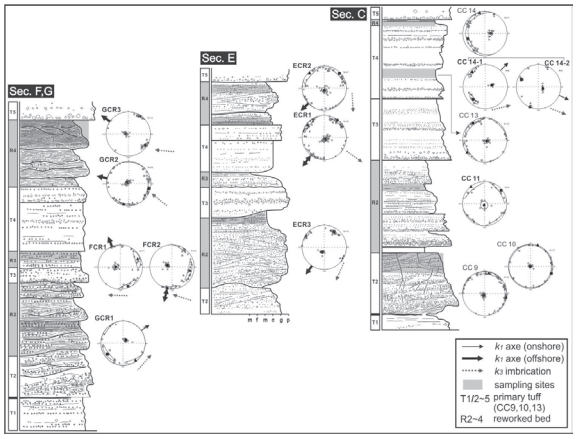

Figure 1. Magnetic fabrics and associated stratigraphic logs from the medial-to-distal rimbeds of Songaksan tuff ring.

Magnetic fabrics of ECR2 and GCR3 (unit R4) with higher values of q, Pj, L, and F within the "current" field of the q-β diagram and ECR1 and GCR2 with low q and β were probably produced in a surf zone (inner rough facies of Clifton et al., 1971) with variable wave activity and offshore-directed current component. Onshore-directed (NE and SE) magnetic fabrics for CC14 with larger imbrication angles may represent cross-shore sediment transport by swash in the foreshore (inner planar facies) (Clifton et al., 1971).

Magnetic fabrics for FCR1 and 2 (unit R3) with higher β within "turbulent suspension" field are attributed to highly unsteady wave in the surf zone.

Magnetic fabrics of GCR1 and CC11 (unit R2) with lower values of q and β suggest settling from stagnant or turbulent suspension during slack water phase, whereas the offshore-directed magnetic fabric for ECR3 (R2) with higher q, β, and L is considered to be affected by tidal effect (ebb) during waxing storm surge (Figure 2).

The $E_{12}(D)$ and $E_{12}(I)$ (the arithmetic mean of the k_1-k_2 semiangles of the confidence ellipses around declination and inclination values, respectively) describe how well lineated or foliated the axes are at the site scale (Ort et al., 2014). Reworked tuffs show $5° < E_{12}(I) < 13°$ and $8° < E_{12}(D) < 38°$, the same as primary tuffs (Figure 2D). Therefore, careful examination of various parameters of magnetic anisotropy for storm-reworked bed is expected to support the proposal.

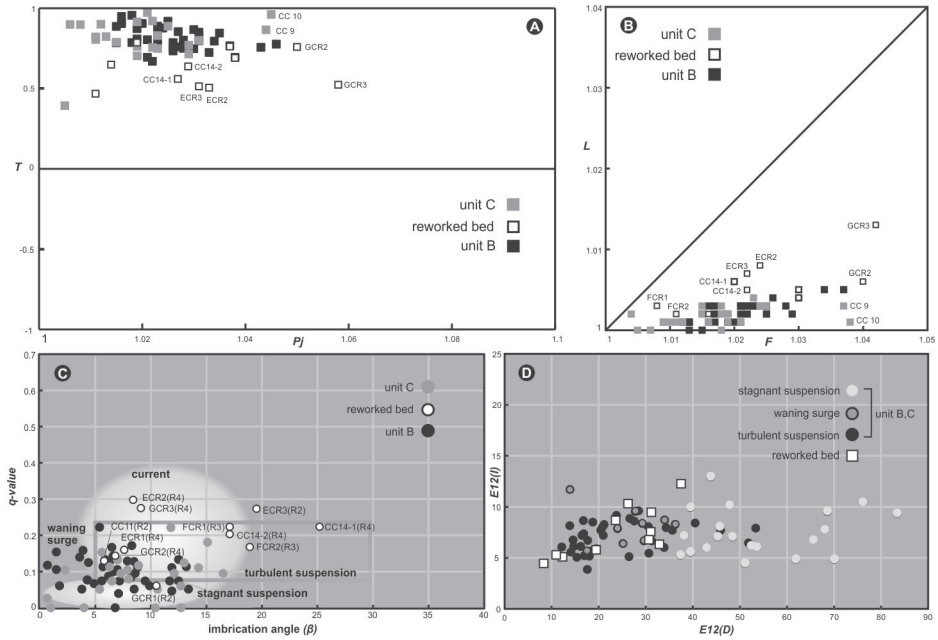

Figure 2. Correlation between the rimbeds of the Songaksan tuff ring and their intercalated storm-reworked deposits plotted on the *T*-*Pj*, *L*-*F*, *q*-*β*, and $E_{12}(I)$–$E_{12}(D)$ diagrams.

Acknowledgments

This work was supported by the Mid-career Researcher Program to Y. K. Sohn (No. 2014R1A2A1A11053516) through the National Research Foundation of Korea funded by the Ministry of Education.

References

Chough, S. K., and Sohn, Y. K., 1990, Depositional mechanics and sequences of base surges, Songaksan tuff ring, Cheju Island, Korea: Sedimentology, 37, 1115–1135.

Clifton, H. E., Hunter, R. E., and Phillips, L., 1971, Depositional structures and processes in the non-barred high-energy nearshore: Journal of Sedimentary Petrology, 41(3), 651–670.

Hamilton, N., and Rees, A. I., 1970, The use of magnetic fabric in paleocurrent estimation, in Runcorn, S. K., ed., Palaeogeophysics: New York, Academic Press, pp. 445–464.

Ort, M. H., Newkirk, T. T., Vilas, J. F., and Vazquez, J. A., 2014, Towards the definition of AMS facies in the deposits of pyroclastic density currents: Geological Society, London, Special Publications, 396(1), 205–226.

Park, M. E., Cho, H., Son, M., and Sohn, Y. K., 2013, Depositional processes, paleoflow patterns, and evolution of a Miocene gravelly fan-delta system in SE Korea constrained by anisotropy of magnetic susceptibility analysis of interbedded mudrocks: Marine and Petroleum Geology, 48, 206–223.

Rees, A. I., 1961, The effect of water currents on the magnetic remanence and anisotropy of susceptibility of some sediments: Geophysical Journal International. -, 1966, The effect of depositional slopes on the anisotropy of magnetic susceptibility of laboratory deposited sands: The Journal of Geology, 856–867.

Rees, A. I., Von Rad, U., and Shepard, F. P., 1968, Magnetic fabric of sediments from the La Jolla submarine canyon and fan, California: Marine Geology, 6(2), 145–178.

Rees, A. I., and Woodall, W. A., 1975, The magnetic fabric of some laboratory deposited sediments: Earth and Planetary Science Letters, 25, 121–130.

Taira, A., 1989, Magnetic fabrics and depositional processes, in Taira, A., and Masuda, F., eds., Sedimentary Facies in the Active Plate Margin: Tokyo, Terra Scientific Publishing Company, pp. 43–80.

Control of Volcanism in Asia by Transtensional Zones: Change of Sources at a Lithosphere–Asthenosphere Boundary Layer in the Wudalianchi Field, China

Sergei Rasskazov[1,2,*], Irina Chuvashova[1,2], Yi-min Sun[3], Chen Yang[3], Zhenhua Xie[3], Zhenxing Fang[3], Jinghua Wang[3], Tatiana Yasnygina[1], and Tatiana Chikisheva[1,2]

[1]*Institute of the Earth's Crust of Russian Academy of Science, Siberian Branch, Irkutsk, Russia*
[2]*Irkutsk State University, Irkutsk, Russia*
[3]*Institute of Volcano and Mineral Spring, Heilongjiang Academy of Science, Wudalianchi, Heilongjiang, China*
*Corresponding author E-mail: rassk@crust.irk.ru

Keywords: potassic rocks, transtension

Transtension is a system of stresses that tends to cause oblique extension, i.e., combined extension and strike slip (Neuendorf et al., 2011). Syn-volcanic transtensional deformations of the lithosphere may provide two possible scenarios for control of magmatic processes. One assumes ascending sublithospheric melts, which mark the permeable lithosphere in transtension area without melting lithospheric material. Products of volcanic eruptions in such a zone show only sublithospheric mantle material. Components of magmatic liquids do not reveal any connection to a lithospheric structure. Another scenario yields a direct control of melting in lithospheric sources in evolving transtensional structure. In this case, spatial-temporal change of lithospheric and sublithospheric components is a direct indication of the evolving transtensional zone.

Activity of echelon volcanic fields, controlled by north-south or west-east transtensional structures, is indicative for specific tectonically active areas of Asia. For instance, volcanism is characteristic of transtensional segments of the Baikal Rift Zone. In the north-south Kamar segment, volcanism is constrained between 18 and 12 Ma, in the west-east Muya-Udokan segment, it was displayed in the Udokan volcanic field in the last 14 Ma, and in the north-south Tsipa-Muyakan segment in the Vitim volcanic field in the range of 16.0–0.6 Ma (Rasskazov et al., 2013). A transtension of the lithosphere is well pronounced also in the Eastern Hangay area, Central Mongolia. To the south of this ridge, in Valley of Lakes, en echelon character of west-east volcanic structures was exhibited at 32–31 Ma. At the ridge and north of it, volcanism occurred in west-east left-lateral transtensional segments in the time interval from 17.0 to 8.0 Ma. Between the Eastern and Central Hangay, the right-lateral north-south Chulutyn transtensional segment was reactivated in the range of 9.6–2.1 Ma (Rasskazov et al., 2012). There are nonvolcanic transtensional segments (such as Rel-Verkhniyangarsk in the Baikal Rift Zone). Some seismically active strike slips (e.g., Bolnay) have no effect on the configuration of volcanic fields and might reflect shallow displacement of crustal tectonic blocks.

Lateral movements widely developed along north-south faults in East Asia (e.g., Tan-lu, Sakhalin-Hokkaido, Tsushima, and Central Sikhote-Alin). Right- and left-lateral displacements in some of these faults, however, are controversial (Jolivet et al., 1994.; Rasskazov et al., 1998; Gilder et al., 1999; Zhang et al., 2003). In this paper, we present arguments in favor of common transtensional nature of lithospheric-derived melting anomaly of the Wudalianchi volcanic zones that extends north-south over 230 km at the northern circuit of the Songliao basin, northeast China.

The basin subsided from the Middle Jurassic to Paleogene. Potassic rocks from the Wudalianchi zone, dated back to the Pliocene and Quaternary (Guide book…, 2010; Zhao et al., 2014), show stepwise widening of K_2O contents along this zone from the Erkeshan volcanic field (5.6–5.8 wt.%) through Wudalianchi (3.2–6.0 wt.%) and Keluo (4.0–7.0 wt.%) to the Xaogulihe volcanic field (2.0–9.5 wt.%). In the Quaternary rocks from Wudalianchi, K_2O concentrations range from 4.8 to 6.0 wt.% with its relative decrease in rocks at the beginning and end of volcanic evolution. Initial lava flows with K_2O contents 3.9–5.2 wt.% erupted along the Laoshantou-Old Gelaqiushan north-south locus from 2.5 to 2.0 Ma and in the final cone of the Huoshaoshan volcano, erupted in 1721, dropped to 3.2 wt.%.

Volcanism displays background activity, irregular in time and space, and propagating activity, characterized by temporal shift of volcanic edifices. Background eruptions occurred between 1.3 and 0.8 Ma at the South Gelaqiushan volcano and along the west-east locus of the Lianhuashan, Yaoquanshan, West Jaodebushan, and West Longmenshan

volcanoes. In the last 0.6 Ma, three groups of volcanoes erupted: Western (North Gelaqiushan, Lianhuashan, Jianshan-Jiamshanzi), Central (Wohushan, Bijiashan, Laoheishan, Huoshaoshan), and Eastern (Weishan, East Jaodebushan, Xiaogoshan, West and East Longmenshan, Molabushan). Background eruptions continued in the Western and Eastern groups, whereas the Central group displayed stepwise shift of activity from the southwest to the northeast. Such a regular volcanic evolution was accompanied with a relative reduction of K_2O abundances in final eruption products of the Huoshaoshan volcano.

From a comparative analysis of K_2O, other major oxides, and trace elements in rocks of early and late eruption phases in the Central group of volcanoes, we infer that rocks were compositionally almost similar to the background ones in edifices of the first volcano (Wohushan) were partially close to the background rocks and partly differed from them in edifices of the second and third volcanoes (Bijiashan, Laoheishan), and were significantly different from the background rocks in the cone of the fourth volcano (Huoshaoshan).

We suggest that magma generation under the Wudalianchi volcanic field was controlled by developing transtension of a layer at the base of the lithosphere that divided and shielded sources of underlying homogeneous sublithospheric convective mantle and the overlying enriched heterogeneous lithosphere. The sublithospheric magma source had $^{87}Sr/^{86}Sr = 0.7052$ (Rasskazov et al., 2011), sources of the boundary shielding layer the same and lower Sr-isotopic ratios, and sources of the overlying region the same and higher ones. The development of transtension governed time and space of locally introduced convective mantle component through the boundary shielding layer on background of melting enriched mantle material above the latter.

The 2.5–2.0 Ma local eruptions of sublithospheric liquids, derived from the axial part of the north-south zone of transtension, were followed with the 1.3–0.8 Ma background melts from a wider transtensional segment of the enriched lithospheric region. Afterwards, in the past 0.6 Ma, background melting of the enriched lithosphere sharply outlined edge portions of the transtensional segment, whereas simultaneous local sublithospheric melting propagated along a crack originated within the boundary shielding layer due to concentrating tectonic forces at the central portion of the transtensional segment.

Acknowledgments

This presentation was prepared in the Chinese-Russian Wudalianchi-Baikal Research Center on recent volcanism and environment.

References

Guide book for field mission to Wudalianchi National Park, China, 2010. Prepared by Wudalianchi National Park and Nature Management Committee Heilongjiang province, 50 p.

Gilder, S.A., Leloup, P.H., Courtillot, V., Chen, Y., Coe, R.S., Zhao, X., Xiao, W., Halim, N., Cogné, J-P., Zhu, R., 1999. Tectonic evolution of the Tancheng-Lujiang (Tan-Lu) fault via Middle Triassic to Early Cenozoic paleomagnatic data, J. Geophys. Res. 104: 15365–15390.

Jolivet, L., Tamaki, K., Fournier, M., 1994. Japan Sea opening history and mechanism: A synthesis. J. Geophys. Res. 99: 22 237–22 259.

Neuendorf, K.K.E., Mehl, J.P., Jr., Jackson, J.A., 2011. Glossary of geology. Fifth edition, revised. American Geosciences Institute, Alexandria, Virginia. 783 p.

Rasskazov, S.V., Logatchev, N.A., Ivanov, A.V., 1998. Correlation of Late Cenozoic tectonic and magmatic events of the Baikal Rift System with the events in the south-east of the Eurasian Plate. Geotectonics 4, 25–40.

Rasskazov, S.V., Chuvashova, I.S., Liu, J., Meng, F., Yasnygina, T.A., Fefelov, N.N., Saranina, E.V., 2011. Proportions of lithospheric and asthenospheric components in Late Cenozoic K and K–Na lavas in Heilongjiang Province, Northeastern China. Petrol. 19: 568–600.

Rasskazov, S.V., Chuvashova, I.S., Yasnygina, T.A., Fefelov, N.N., Saranina, E.V., 2012. Potassic and potassic–sodic volcanic series in the Cenozoic of Asia. Novosibirsk Academic Publishing House "GEO", 351 p.

Rasskazov, S.V., Yasnygina, T.A., Chuvashova, I.S., Mikheeva, E.A., Snopkov, S.V., 2013. The Kultuk Volcano: spatial-temporal change of magmatic sources at the western terminus of the South Baikal basin between 18 and 12 Ma. Geodyn. Tectonophys. 4: 135–168. doi: 10.5800 / GT2013420095.

Zhang, Y. Q., Shi, W., Dong, S. W., 2003. Strike-slip and extensional tectonics of the Tan-Lu fault zone (eastern China) from the Cretaceous to Cenozoic. EGS - AGU - EUG Joint Assembly, Abstract #1949.

Zhao, Y.-W., Li, N., Fan, Q.-C., Zou, H., Xu, Y.-G., 2014. Two episodes of volcanism in the Wudalianchi volcanic belt, NE China: Evidence for tectonic controls on volcanic activities. J. Volcanol. Geothermal Res. 285: 170–179. dx.doi.org/10.1016/j.jvolgeores.2014.08.016.

The Architecture and Shallow Conduits of Laki-Type Pyroclastic Cones: Insights into a Basaltic Fissure Eruption

P. Reynolds[1,*], R. J. Brown[2], T. Thordarson[3], and E. W. Llewellin[2]

[1]*Centre for Tectonics, Resources and Exploration (TRaX), Australian School of Petroleum, North Terrace, Adelaide, Australia*
[2]*Science Labs, Department of Earth Sciences, Durham University, Durham, UK*
[3]*Faculty and Institute (Nordvulk) of Earth Sciences, University of Iceland, Reykjavík, Iceland*
*Corresponding author E-mail: peter.reynolds@adelaide.edu.au

Keywords: spatter cone, fissure, conduit

Basaltic fissure eruptions can manifest a range of eruptive activity from Hawaiian, through strombolian, to violent strombolian (Valentine and Gregg 2008). Large magnitude fissure eruptions have also been linked to global mass extinction (Brown et al. 2014 and references there-in), as plumes associated with unusually large (>1 km high) lava fountains may have injected gases into the stratosphere. The fissures are commonly overlain by cone rows composed of spatter cones and ramparts, scoria cones and half-cones, tuff cones and hybrids thereof (e.g., Thordarson and Self 1993; Sumner 1998). The internal architecture of these cones provides a host of volcanological evidence that can be used to derive information relating to eruption dynamics such as column height, mass flux, and duration (e.g., Parfitt and Wilson 1999). Additionally, the geometry of their conduits plays a role in governing eruption dynamics (e.g., Keating et al. 2008). However, the internal architecture of the cones and their feeder dikes are often poorly exposed as they are buried by deposits from later stages of the eruption (e.g., the 1783–1785 Laki eruption; Thordarson and Self 1993).

This study details the spatial and temporal development of a spatter cone, scoria half-cone, and their feeder dike (Figure 1) emplaced during the 6−8 ka Rauðuborgir-Kvensöðul (R-K) basaltic fissure eruption in Iceland. This eruption occurred within an active graben. Glacial floods have subsequently dissected the cones and their feeder dike, revealing a near-complete record of the vent-proximal erupted products. Geological mapping and detailed stratigraphic logging are used to unravel the eruption chronology.

The R-K feeder dike widened in the upper 40 m of the subsurface to form a localized conduit beneath the spatter cone. Two mechanisms for conduit widening are proposed for the R-K fissure eruption: country rock removal (e.g., Keating et al. 2008 and references there-in); and elastic deformation (e.g., Valentine and Groves 1996). Country rock removal occurred early in the eruption, evidenced by abundant armored clasts with country rock-clast cores toward the base of the R-K volcanic succession. However, the country rock clasts only account for a conduit of 100 m^3 volume; significantly smaller than the observed conduit size (8000 m^3). Therefore, conduit widening is thought to have occurred via an additional method besides brittle deformation. Elastic deformation may have been triggered by the intrusion of the R-K dike along a fault plane, and/or may have been related to syn-eruptional development of the graben within which the fissure is located. Propagation of the dike to the surface resulted in the production of abundant pāhoehoe lava.

The scoria half-cone was constructed immediately after emplacement of the lava by a fountain ~100 m in height, as indicated by ballistic calculations. The abundance of welding and absence of grain avalanching within the half-cone is typical of Hawaiian-style eruptions (Valentine and Gregg 2008). We infer that rapid variations in pyroclast size and welding result from pulsing of the fountain (e.g., Valentine and Gregg 2008). Pyroclasts were stripped from the fountain by north-westerly winds, favoring southeast accumulation of the fissure. The half-cone is inferred to have spread laterally, resulting in faulting. Blocks of scoria are inferred to have collapsed into the faults, as observed during the 1991 Hekla eruption and on the upper flanks of Pu'u Ō'ō, Hawaii (Heliker and Mattox 2003).

The spatter cone formed after 4−8 months had elapsed, and could have been constructed within 3 hours. The size and distribution of components pyroclasts indicate the spatter cone was constructed beneath a fountain ≤50 m in height; smaller than that during construction of the half-cone. Thus, the fountain height is inferred to have decreased during the eruption, as observed in contemporary examples (Thordarson and Self 1993). The decreased fountain height is attributed to a decreased exsolved gas content late in the eruption. The abundance of welding within the spatter cone is typical of Hawaiian-style activity. Cone construction was dominated by the ballistic ejection of clasts and secondary flow of reconstituted spatter. The spatter

cone is breached at its base by a bocca which formed late in the eruption.

The cones are of comparable dimensions and structure to those formed during the 1783−1785 Laki eruption (e.g., Thordarson and Self 1993). These cones may effuse lavas, as evidenced by the bocca observed at the base the R-K spatter cone. Our observations indicate that the spatter cones form beneath low (<100 m) fountains which produce spatter-rich deposits. These deposits feed rootless flows which may drain back into the vent and/or feed the lava flow field. We highlight the diversity of cones produced during fissure eruptions, and discuss how the cones link to the underlying feeder dike. These observations can be used to identify vent-proximal locations in other settings, and link their deposits with processes observed in contemporary eruptions.

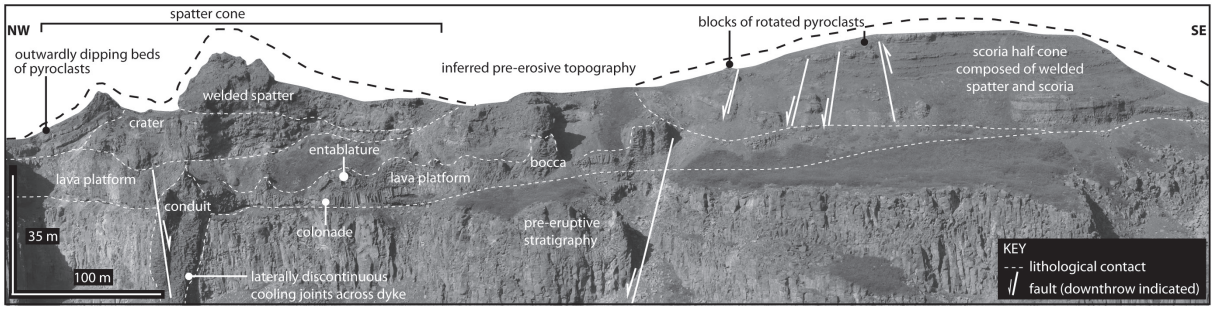

Figure 1. Field photo of the R-K spatter cone, scoria half-cone, and their feeder dike.

References

Brown RJ, Blake S, Thordarson T, Self S (2014) Pyroclastic edifices record vigorous lava fountains during the emplacement of a flood basalt flow field, Roza Member, Columbia River Basalt Province, USA. Geologic Soc Am Bull 126(7–8):875–891.

Heliker C, Mattox T (2003) The first two decades of the Pu'u 'O'o-Kupaianaha eruption: chronology and selected bibliography. US Geol Surv Prof Pap 1676:1–28.

Keating G, Valentine G, Krier D, Perry F (2008) Shallow plumbing systems for small-volume basaltic volcanoes. B Volcanol 70:563–582.

Thordarson T, Self S (1993) The Laki (Skaftár Fires) and Grímsvötn eruptions in 1783–1785. B Volcanol 55:233–263.

Parfitt EA, Wilson L (1999) A Plinian treatment of fallout from Hawaiian lava fountains. J Volcanol Geoth Res 88:67–75.

Sumner JM (1998) Formation of clastogenic lava flows during fissure eruption and scoria cone collapse: the 1986 eruption of Izu-Oshima Volcano, eastern Japan. Bulletin of Volcanology 60:195–212.

Thordarson T, Self S (1993) The Laki (Skaftár Fires) and Grímsvötn eruptions in 1783–1785. B Volcanol 55:233–263.

Valentine GA, Groves KR (1996) Entrainment of country rock during basaltic eruptions of the Lucero Volcanic Field, New Mexico. J Geol 104:71–90.

Valentine GA, Gregg TKP (2008) Continental basaltic volcanoes — Processes and problems. J Volcanol Geoth Res 177:857–873.

A Review on Diatom Records of Environmental Change in Maar Lakes of the Long Gang Volcanic Field (Northeast China)

Patrick Rioual[1*], Luo Wang[1], Guoqiang Chu[1], Qiang Gao[1], Jingtai Han[1], Anson W. Mackay[2], Jens Mingram[3], Virginia N. Panizzo[3], Zhongyan Zhang[1], and Jiaqi Liu[1]

[1]*Institute of Geology and Geophysics, Chinese Academy of Sciences, Beijing, China*
[2]*Environmental Change Research Centre, Department of Geography, University College London, London, United Kingdom*
[3]*Helmholtz Centre Postdam GFZ German Research Centre for Geosciences, Potsdam, Germany*
*Corresponding author E-mail: prioual@mail.iggcas.ac.cn

Keywords: diatoms, varves, paleolimnology

There are eight maar lakes in the Longgang volcanic field (LGVF) with water depths ranging between 15 and 127 m (Mingram et al. 2004). These lakes are sensitive to climate and environmental change owing to their characteristic morphology such as a small catchment area and limited inflow/outflow (Marchetto et al. 2015). Moreover, they often provide seasonally laminated sediments that can be used to establish precise chronologies (Chu et al. 2005; Chu et al. 2009).

Among the various proxy records derived from the sedimentary profiles of the Long Gang maar lakes, diatoms are very promising. This is because diatoms are outstanding indicators of limnological conditions, are a very diverse group of microscopic algae, including numerous species new to science (e.g., Rioual et al. 2013, 2014), preserved well and abundantly in the sediment, and respond almost instantly to changes in the environment.

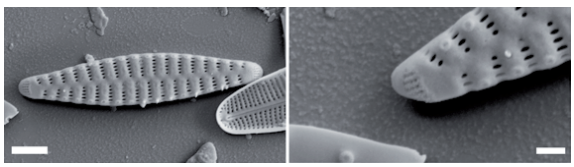

Figure 1. SEM photographs of *Staurosira longwanensis*, a diatom species new-to-science described from Lake Sihailongwan (Rioual et al. 2014).

In this presentation, we review the diatom studies (published and unpublished) that focus on the sedimentary records from three of these maar lakes. These studies cover short (the last 100 years) and/or long (the last 50,000 years) time spans.

The diatom record from Lake Erlongwan spans the past 1000 years (Wang et al. 2012). The composition and abundance of the diatom assemblages, especially the ration of planktonic/benthic species, reflect the relative lengths of the ice cover and ice-free seasons, which are linked to changes in temperature. Three intervals were identified by their diatom assemblages and correspond within dating uncertainties to the Medieval Warm Period (MWP), the Little Ice Age (LIA), and the twentieth-century warming trends. The diatom assemblages from Erlongwan exhibit sensitive response to changes in seasonal conditions. The diatom record suggests that during the MWP the duration of summer was longer, while the spring and autumn were shorter than during the twentieth century.

In the recent sedimentary record of Lake Xiaolongwan, the increase in the planktonic diatom *Discostella woltereckii* after ca. 1980 AD is also interpreted as a response to increased mean annual temperature trends. These temperature trends may be manifested as changes in ice cover persistence, a longer growing season and/or increased DOC at Lake Xiaolongwan as such conditions give planktonic species a competitive advantage (Panizzo et al. 2013).

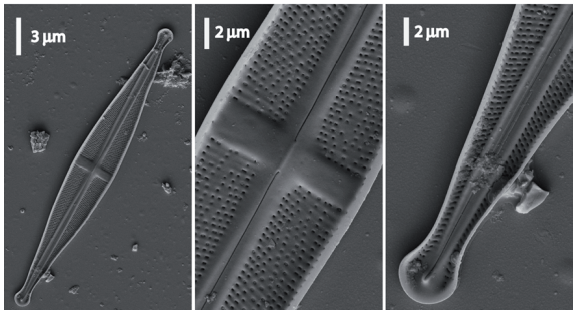

Figure 2. SEM photographs of *Stauroneis lacusvulcani,* a species new-to-science found in Lake Xiaolongwan (Rioual et al. (2013).

Further back in time, but from the same lake, Gao et al. (2016) found distinct diatom responses to Lateglacial and early Holocene climate change between ~20 and ~10 ka. The diatom assemblages reveal a complex interplay between direct climate effects on the seasonal lake conditions (timing of ice cover break-up, water column mixing, and thermal stratification), catchment-mediated effects on the concentrations of nutrients, and dissolved organic carbon and, possibly, biotic interactions between the different algal groups present in the phytoplankton of Lake Xiaolongwan (diatoms, Chrysophyceae and

Dinophyceae). Remarkably, two diatom assemblage zones characterize the Younger Dryas at Lake Xiaolongwan, suggesting a bipartite division of this stadial event as in several records from eastern Asia (Liu et al. 2013) and Europe (Lane et al. 2013).

The longest sedimentary record retrieved so far from one of the LGVF maar lakes is that from Lake Sihailongwan that spans the last 60,000 years. In Sihailongwan diatom record, cold events are characterized by a decrease in the productivity of planktonic diatoms and high relative percentages of benthic species. Most of the cold events identified in the oxygen isotopes records from the Greenland ice core (GISP2) and the Hulu cave stalagmites from China are also observed in the diatom record of Lake Sihailongwan, especially the percentages of benthic diatoms. However, the magnitude of the cold and warm episodes is often difficult to assess using the diatom record. The most pronounced cold events identified in the Sihailongwan diatom sequence appear to be coeval with the Greenland stadial events GS1 (Younger-Dryas), GS2, GS3, and GS8.

In conclusion, these studies illustrate the potential of diatoms to answer various scientific questions especially on the climate variability since the late Pleistocene and over the Holocene, on the development of these lake ecosystems and on the impact of recent anthropogenic activities on these lakes.

Acknowledgments

The various studies presented here were supported by the National Basic Research Program of China (973 Program), The ‘Strategic Priority Research Program’ of the Chinese Academy of Sciences, the National Science Foundation of China (grant no 41320104006).

References

Chu, G., Liu, J., Schettler, G., Li, J., Sun, Q., Gu, Z., Hu, H., Liu, T.S. 2005. Sediment fluxes and varve formation in Sihailongwan, a maar lake from northeastern China. Journal of Paleolimnology 34, 311–324.

Chu, G., Sun, Q., Wang, X., Li, D., Rioual, P., Liu, Q., Han, J., Liu, J. 2009. A 1600 year multiproxy record of paleoclimatic change from varved sediments in Lake Xiaolongwan, northeastern China. Journal of Geophysical Research 114, D22108.

Gao, Q., Rioual, P., Chu, G., 2016. Lateglacial and early Holocene climatic fluctuations recorded in the diatom flora of Xiaolongwan maar lake, NE China. Boreas 45: 61–75.

Lane, C. S., Brauer, A., Blockley, S. P. E., Dulski, P. 2013. Volcanic ash reveals time-transgressive abrupt climate change during the Younger Dryas. Geology 41, 1251–1254.

Liu, D., Wang, Y., Cheng, H., Kong, X., Chen, S. 2013. Centennial-scale Asian monsoon variability during the mid-Younger Dryas from Qingtian Cave, central China. Quaternary Research 80, 199–206.

Marchetto, A., Ariztegui, D., Brauer, A., Lami, A., Mercuri, A. M., Sadori, L., Vigliotii, L., Wulf, S., Guilizzoni, P. 2015. Volcanic lake sediments as sensitive archives of climate and environmental change. In Rouwet, D., Christenson, B., Tassi, F. & Vandemeulebrouck, J. (eds.): Volcanic Lakes, Advances in Volcanology, 379–399. Springer-Verlag, Berlin.

Mingram, J., Allen, J.R.M., Brüchmann, C., Liu, J., Luo, X., Negendank, J.F.W., Nowaczyk, N., Schettler, G. 2004. Maar- and crater lakes of the Long Gang Volcanic Field (N.E. China) – overview, laminated sediments, and vegetation history of the last 900 years. Quaternary International 123–125, 135–147.

Panizzo, V.N., Mackay, A.W., Rose, N.L., Rioual, P., Leng, M.J. 2013. Recent palaeolimnological change recorded in Lake Xiaolongwan, northeast China: climatic versus anthropogenic forcing. Quaternary International 290–291, 322–334.

Rioual, P., Gao, Q., Peng, Y., hu, G. 2013. *Stauroneis lacusvulcani* sp. nov. (Bacillariophyceae), a new diatom from volcanic lakes in northeastern China. Phytotaxa 148, 47–56.

Rioual, P., Morales, E.A., Chu, G., Han, J., Li, D., Liu, J., Liu, Q., Mingram, J., Ector, L. 2014. *Staurosira longwanensis*sp. nov., a new araphid diatom (Bacillariophyta) from Northeast China. Fottea, Olomouc 94, 91–100.

Wang, L., Rioual, P., Panizzo, V. N., Lu, H., Gu, Z., Chu, G., Yang, D., Han, J., Liu, J., Mackay, A. W. 2012. A 1000-yr record of environmental change in NE China indicated by diatom assemblages from maar lake Erlongwan. Quaternary Research 78, 24–34.

Impact Volcanism of El'gygytgyn Crater (Central Chukotka, Russia): Problems of Genesis

Vladimir G. Sakhno[1,*] and Guoming Liu[2]

[1]*Far East Geological Institute, Far Eastern Branch – Russian Academy of SciencesVladivostok, Russia*
[2]*Changbaishan Volcano Observatory, Earthquake Administration of Jilin Province, Antu, China*
*Corresponding author E-mail: v_sakhno@mail.ru

Keywords: impactites, impact volcanism, crater El'gygytgyn

In Central Chukotka in Northeast Russia there is El'gygytgyn Crater Lake, 175 m deep and 12 km wide. The crater is in the basin about 17 km in diameter with steep underwater walls. On the El'gygytgyn basin slopes and beyond it, the impact rocks—impactites, impact glasses, breccias of impactites with volcanic fragments of rocks of different composition, and bombs of glass—were found. Extensive investigations of geological structure of El'gygytgyn caldera, petrological-geochemical study, and isotopic investigations were carried out, and geochronology of impactites, breccias of impactites, and glasses was studied with different methods.

Findings of impactites and impact glasses in the explosive structures of the Earth attract the attention of researches due to their specific formation. The commonly accepted idea exists of the impactites as rocks whose formation is related to the impact metamorphism that comes into being when cosmic bodies fall onto the Earth's surface.

Most of the researchers explain the findings of the silica high-bar phases in them by their cosmic origin. It is agreed that such structures (astroblemes) in which the impactites and impact breccias were found, are Popigeiskaya, Zhamanshin, Karskaya, and other (Masaitis, Selivanovskaya, 1975; Impactites, 1981). The El'gygytgyn Lake crater has been assigned to them.

Nevertheless, other ideas are available that on the petrological-geochemical and geological data suggest such "*astroblemes*" to be of endogenous origin (Marakushev et al., 1993; Belyi, 2010; Sakhno, 1999).

Extensive petrological-geochemical and isotopic investigations of the El'gygytgyn crater impact rocks are very important for solving the problems of their origin. We have conducted widespread investigations using modern instrumental methods: U-Pb (SHRIMP-II) dating on zircons, Re-Os isochrones determination of age, $^{187}Os/^{188}Os$ isotope ratio, REE spectra, petrochemical composition, content of the reduced gases (H_2, CH_4, etc.), determination of isotopic composition $^{3}He/^{3}He$, Sm/Nd, and composition of PGE (Re and others elements) in rocks and helium and argon isotopes in glass (Sakhno, Prasolov, 2014).

Based on the analyses of the obtained data, the following conclusions can be made:

(1) One of the geological criteria is the regularities of spatial-temporal localization of the structure and duration of its development. According to U-Pb (SHRIMP) isotope dating, the Upper-Anadyr dome rise, in whose center there is El'gygytgyn crater, has been forming over a long period of time—several tens of millions of years (Sakhno et al., 2010). This is good evidence for its endogenous origin. (Figure 1)

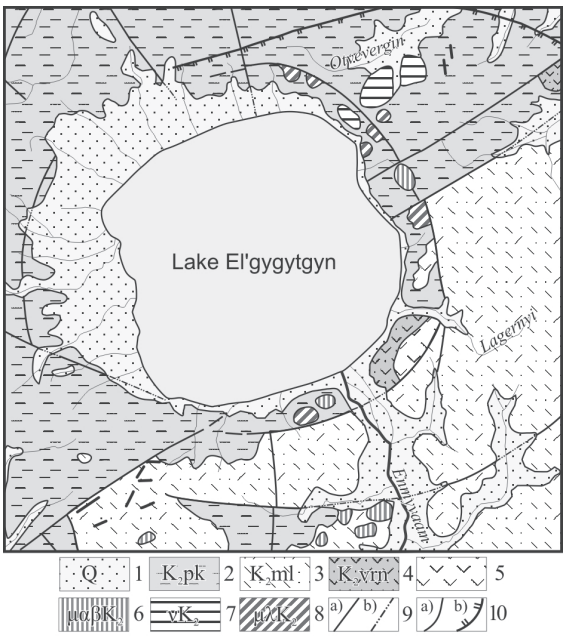

Figure 1. Scheme of geological structure of the crater basin of the El'gygytgyn Lake (with the use of materials (Niessen et al., 2007; Geological map F Gup. 2012 and with the authors' additions).
1 – River flood plains; 2 – Pykarvaamskaya suite; 3 – Melguvaamskaya suite; 4 – Voroninskaya suite; 5 – Ergyvaamskaya suite; 6 – Koekvunkaya suite; 7 – Extrusions of the gabroids; 8 – Extrusions and dikes of the granites; 9 – Faults: transregional (a), etc.; 10 – Faults: of the arched, etc.

(2) The most rigorous criterion for the proof of the cosmic or endogenous origin of the crater is the presence or absence of significant amounts of

meteoritic matter. Data on the content of high-siderophile elements and on the Re-Os ratio in the volcanic rocks of the Upper-Anadyr Rise ("target") and in the rocks "impactites," as possible products of a cosmic impact, have not been confirmed (Sakhno et al., 2011).

(3) Isochronous Re-Os isotope dating showed two stages of the melt formation. The melts then were erupted by a powerful explosion that does not correspond to the instancy of the structure formation.

(4) U-Pb isotope dating on zircons made it possible to establish that the "impactite" glasses (O-1454/1a) were generated at various depths from the protolith, and from them the ignimbrite melts of the Voronenskaya suite were fused (a depth of these ignimbrite formation is 6.5–8.5 km) (Belyi, 2010). The glasses (O-1454/1d, O-1454/7, and others were generated at a great depth from the protolith composed of rocks of the Early Paleozoic-Neoproterozoic folded basement (Figure 2).

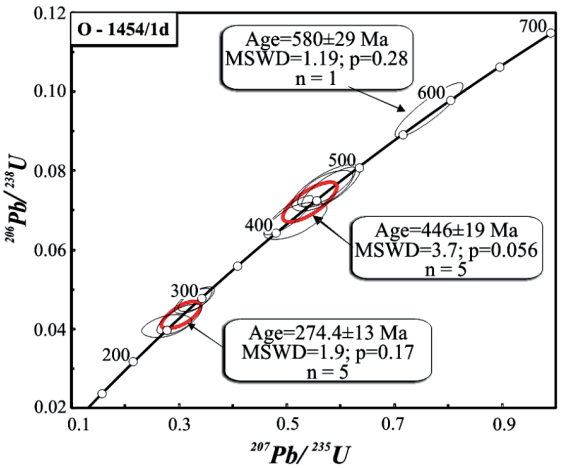

Figure 2. Results of SHRIMP dating of zircons from impactites of El'gygytgyn Lake.

(5) The thesis of the nonisochemical nature of the melts, which is repeatedly cited by the supporters of the cosmic nature of El'gygytgyn caldera (Impactites, 1981; and others), is not confirmed by the results of the study of both rock-forming oxides, and micro- and rare-earth elements with rare exception. Rare exceptions are explained by degassing through explosive bursts.

(6) And finally, drilling to the entire depth of the bottom sediments in the center of El'gygytgyn crater, performed by the Russian-German-American expedition in 2009, has not revealed the tagamite melts characteristic for the craters of a cosmic impact, as the supporters of this hypothesis supposed (Niessen et al., 2007; and others).

Data given above and the results of investigations, carried out using the precision methods, show that the endogenous nature of El'gygytgyn crater is most probable. In the history of the planets and the Earth there were long periods of the interrupted-pulsation development of the structures of a central type that is connected with the stability of the deep-seated power-generating centers on the boundary of the outer core (layer "D") and lower mantle producing a thermal plume which was a carrier of high-energy fluids initiating the impactogenic volcanism. The plume emersion and phase transformations at different levels in the mantle result in a downfall above the central rise, explosions, and crater formation. This process is possible under conditions of the being extended Earth.

References

Belyi V.F., 2010. Impactite Generation in the El'gygytgyn Basin, Northeast Russia as a Volcanic Phenomenon. On Petrography and geochemistry of the Impactites. Volcanology and Seismology, 3, 3–18.

Impactites, 1981. Edited by A.A. Marakushev. Moscow: MGU Publishing House, 240 pp.

Marakushev A.A., Bogatyrev O.S., Fenogenov A.N., 1993. Impactogenes and volcanism. Petrology, 1(6), 577–595.

Masaitis V.L., Selivanovskaya T.V., 1975. Popogai meteoritic crater. Zapiski Vsesoyuznogo Mineralogicheskogo Obshchestva (Transactions of the All-Union Mineralogical Society), CXVI(4), 52–59.

Niessen F., Gebhardt A.C., Kopsch C., Wagner B., 2007. Seismic investigation of the El'gygytgyn impact crater lake (Central Chukotka, NE Siberia): preliminary results. Journal of Paleolimnology, 3. 49–63.

Sakhno V.G., 1999. Mantle fluids and genesis of explosion and impact circum structures. problems of impact volcanism. Journ. Confer. EUG-10. Strasbourg, France. Cambridge Publ. Abstr. V. 008:4k/12:H2. 778.

Sakhno V.G., Polin V.F., Akinin V.V., 2010. The diachronous formation of the Enmyvaam and Amguema-Kanchalan volcanic fields in the Okhotsk-Chukotka Volcanic Belt (NE Russia): Evidence from isotopic data. Doklady RAN (Reports of RAS), 434, 1172–1178.

Sakhno V.G., Krymsky R.S., Glushkova O.Y., 2011. Impactites of El'gygytgyn crater: isotopic dating by U-Pb (SHRIMP) and Re-Os methods. Special features of their micro- and RRE- element composition and $^{187}Os/^{188}Os$ isotopy (Central Chukotka, Russia). Doklady Earth Sciences, 441, 1637–1644.

Sakhno V.G., Prasolov E.M., 2014. Helium and argon isotopes in glasses of the Elgygytgyn Crater, Central Chukotka, and Their Origin. Doklady Earth Sciences, 454, 16–20.

Maar structures in Perşani Volcanic Field, SE Transylvania, Romania: A Revised Volcanological Study

Ioan Seghedi[1,*], Alexandru Szakács[1,2], and Răzvan-Gabriel Popa[1,3]

[1]*Institute of Geodynamics, Romanian Academy, Bucharest, Romania*seghedi@geodin.ro
[2]*Department of Environmental Sciences, Sapientia University, Cluj-Napoca, Romania*
[3]*Institute of Geochemistry and Petrology, Zürich, Switzerland*
*Corresponding author E-mail: seghedi@geodin.ro

Keywords: Perşani Mountains, monogenetic Na-alkalic volcanoes, maar

The Perşani Mountains' basaltic field is a NNE-SSW elongated area (ca. 22 × 8 km) and consists of 21 monogenetic volcanic centers (cinder cones, tuff-rings, and maars) (Seghedi and Szakács, 1994). The eruptions took place in six episodes between 1220 and 683 ka (Seghedi et al., submitted). Most of the volcanoes are clustered along and at the intersection of faults, so it may be presumed that tectonics closely controls the space-time evolution of volcanic activity. The monogenetic volcanoes were rapidly constructed on hard basement formations represented mainly by Miocene rhyolitic tuffs and by Mesozoic sedimentary rocks. Most of them started with a phreatomagmatic explosive phase. The hydromagmatic processes resulted from the interaction of ascending magma with the aquifers hosted by older tuffs, sandstones, conglomerates, and limestone generating several maars and tuff-ring edifices. The Bârc volcano is the largest one and it was generated during the third episode (1060 ka). It is a 2.25 km wide tuff ring that evolved into a maar. The subsequent effusive phase filled the maar with a lava lake. Finally, the lavas breached the NE side of the tuff ring and flowed northward for ~1.5 km (Figure 1).

Fântâna maar volcano has also erupted in the third episode in a pure phreatomagmatic event (Figure 2). Based on the lithology of the ejected clasts, it suggests that the fuel-coolant interaction occurred at a depth of ca. 150 m. The two maars generated in the third episode expulsed the largest volume of mantle xenoliths, including spinel lherzolites and (garnet) pyroxenites.

The other maar volcanoes, Dîlma West and Pietrele, erupted in the sixth episode (683 ka). Both maars were filled by scoria cones and by subsequent lava flows. Pietrele volcano has one lava flow that extends from a sill injection, while Dîlma West erupted three lava flows. There is a connection between the erupted volumes and the ages of maar structures: the largest volume of Bârc maar and the smallest Fântana maar are recorded in the third episode and intermediate volume-maars (Dîlma West and Pietrele) in the sixth episode.

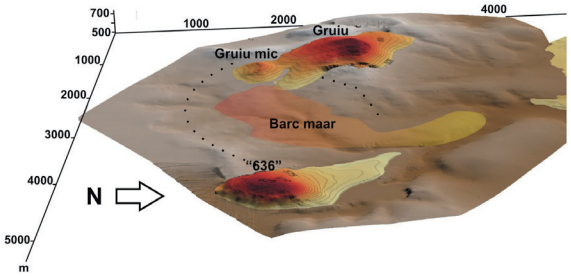

Figure 1. 3D view of Bârc maar generated in the third episode, showing the crater lava lake breaching the edifice toward N. The volcano is bordered by the Gruiu and Gruiu mic volcanoes (forth episode) to the west and "636" volcano (fifth episode) to the east.

Figure 2. Base surge and fall-out phreatomagmatic deposits at the rim of Fântâna maar, including ejected limestones.

Acknowledgments

The research was funded through CNCS – UEFISCDI, project number PN-II-ID-PCE-2012-4-0137.

References

Seghedi I., Szakács A., 1994. Upper Pliocene to Quaternary basaltic volcanism in the Perşani Mountains, Romania. Rom. J. Petrol. 76: 101–107

Seghedi I., Popa R.-G., Panaiotu G., Szakács A., Pécskay Z., submitted. Short-lived eruptive episodes during construction of a Na-alkalic basaltic field (Perşani Mountains, SE Transylvania, Romania). Bull. Volcanol.

Paleo-environmental and Geological Controls on Late Pleistocene Phreatomagmatism in the Lacustrine Zacapu Basin (Michoacán, Mexico)

Claus Siebe*, Pooja Kshirsagar, Marie-Noëlle Guilbaud, and Sergio Salinas

Departamento de Vulcanología, Instituto de Geofísica, Universidad Nacional Autónoma de México, Ciudad de México, México
*Corresponding author E-mail: csiebe@geofisica.unam.mx

Keywords: maars, Michoacán, phreatomagmatism

The active Mexican Volcanic Belt (MVB) stretches across central Mexico for ~1200 km in an E-W direction from the Gulf of Mexico to the Pacific Ocean. This volcanic arc is related to the subduction of the oceanic Cocos and Rivera Plates underneath the continental North American Plate. It consists of Late Tertiary to Quaternary volcanoes and traverses the southern part of the *Mexican Altiplano*, a highland characterized by normal faulting and horst-and-graben structures. The basins resulting from this extensional regime are/were often occupied by extensive (but shallow) lakes. Another particularity of the MVB is the abundance of scoria cones and other types of monogenetic volcanoes, which outnumber by several orders of magnitude the much larger strato-volcanoes. Although the exact causes responsible for their great number (>3000) are still unknown, their high frequency of occurrence must be sought in the peculiar geometric configuration of the subduction zone, namely, the relatively low subduction angle and its consequences on the physical-chemical conditions prevailing in the mantle wedge.

The largest concentration of monogenetic volcanoes in the MVB occurs in the Michoacán-Guanajuato Volcanic Field (MGVF), where the arc reaches a maximum width of ~300 km. This 40,000 km^2 area hosts more than 1000 monogenetic scoria cones (including the historical Jorullo and Paricutin volcanoes), ~300 medium-sized volcanoes (mostly shields, but also domes), fewer isolated small viscous lava flows and domes, and rare maars (Hasenaka and Carmichael, 1985; Guilbaud et al., 2012). A recent inventory of monogenetic phreato-magmatic volcanoes (maars, tuff-rings, tuff-cones) in the MVB, revealed the occurrence of only 88 such volcanoes (3% of all monogenetic vents) within the entire arc (Siebe and Salinas, 2014) and that many of them are found clustered in only a few of the many intermontane basins in the *Mexican Altiplano*.

On the other hand, maars are the second most common type of volcanic vents encountered on Earth and their formation requires two basic ingredients: water (surficial or ground) and a small batch of magma (Lorenz, 2007). From the above it becomes clear that optimal conditions for maar formation are usually not met in the MVB, despite of the relative availability of ground water (abundance of lacustrine basins) and ascending low volume magmas required to fuel this type of eruptions.

One of these basins, the Zacapu basin (Figure 1) is located within the boundaries of the MGVF and hosts three Late Pleistocene phreatomagmatic andesitic monogenetic volcanoes, namely, El Caracol (~cal 32,300 BP), Alberca de los Espinos (~cal 29,000 BP), and Alberca de Guadalupe (~cal 25,300 BP). They were studied by us in greater detail (Siebe et al., 2012; Ksirsagar et al., 2015, 2016) with the aim of determining the unusual geological setting and hydrological environment that favored their formation.

While scoria cones in the MGVF are usually situated on higher ground, the three phreato-magmatic craters in the Zacapu all formed at hydrologically favorable locations. They all sit on highly permeable old (>1 Ma) lava flows that form the strongly faulted and slightly elevated areas that are adjacent to the former shores of the lacustrine flat. One of these, Alberca de Guadalupe, was entirely phreatomagmatic throughout its eruption. It is located in a narrow valley bordered on one side by a ~N-S alignment of domes including the high-elevation El Zirate volcano and on the other side by the C. Picacho Gendo shield (Figure 1). The hydraulic gradient is high in this area and subterranean water supply to the eruption site was optimal. The other two craters display Strombolian fallout layers prevailing at the top of the stratigraphic sequences indicating that the water supply dropped during the course of the activity. In the case of El Caracol, the eruption even turned magmatic toward its end producing lava flows. Interestingly, all three craters formed either shortly before or at the beginning of the Last Glacial Maximum (LGM), which occurred between 26,500–19,000 cal BP (Clark et al., 2009). It seems that annual precipitation in central Mexico was relatively

high during this period promoting saturation of aquifers and, hence, the formation of maars. If so, other maars in central Mexico should also have ages falling within this time frame.

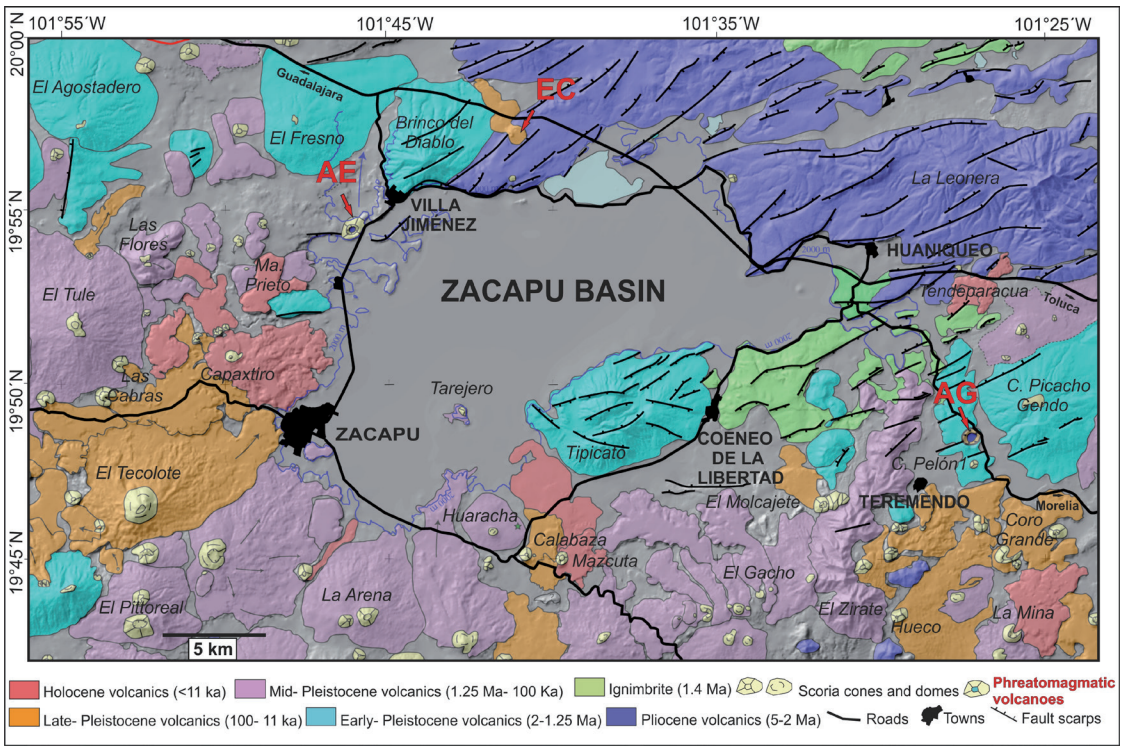

Figure 1. Geological map of the Zacapu basin surrounded by Pliocene-Holocene volcanic highlands disrupted by NE-SW trending normal faults. Late Pleistocene phreatomagmatic vents El Caracol (EC), Alberca de Guadalupe (AG), and Alberca de los Espinos (AE) are also indicated. Areas left in gray have extensive young sedimentary cover.

Acknowledgments

Project funded by CONACYT-167231 and 152294 and UNAM-DGAPA IN-101915 and IN-105615 granted to C. Siebe and M.N. Guilbaud. P. Kshirsagar was funded by a UNAM-DGAPA postdoctoral fellowship 2013-2015.

References

Clark, P.U., Dyke, A.S., Shakun, J.D., Carlson, A.E., Clark, J., Wohlfarth, B., Mitrovica, J.X., Hostetler, S.W., McCabe, A.M., 2009. The last glacial maximum. Science 325 (5941): 710–714.

Guilbaud, M.N., Siebe, C., Layer, P., Salinas, S., 2012. Reconstruction of the volcanic history of the Tacámbaro-Puruarán area (Michoacán, México) reveals high frequency of Holocene monogenetic eruptions. Bulletin of Volcanology 74(5): 1187–1211.

Hasenaka, T., Carmichael, I.S.E., 1985. The cinder cones of Michoacán-Guanajuato, central Mexico: their age, volume and distribution, and magma discharge rate. Journal of Volcanology and Geothermal Research 25: 105–124.

Kshirsagar, P., Siebe, C., Guilbaud, M.N., Salinas, S., Layer, P.W., 2015. Late Pleistocene Alberca de Guadalupe maar volcano (Zacapu basin, Michoacán): Stratigraphy, tectonic setting, and paleo-hydrogeological environment. Journal of Volcanology and Geothermal Research 304: 214–236.

Kshirsagar, P., Siebe, C., Guilbaud, M.N., Salinas, S., 2016 (in press). Geological and environmental controls on the change of eruptive style (phreatomagmatic to Strombolian-effusive) of Late Pleistocene El Caracol tuff cone and its comparison with adjacent volcanoes around the Zacapu basin (Michoacán, México). Journal of Volcanology and Geothermal Research.

Lorenz, V., 2007. Syn-and posteruptive hazards of maar-diatreme volcanoes. Journal of Volcanology and Geothermal Research 159: 285–312.

Siebe, C., Guilbaud, M.N., Salinas, S., Chedeville-Monzo, C., 2012. Eruption of Alberca de los Espinos tuff cone causes transgression of Zacapu lake ca. 25,000 yr BP in Michoacán, México. 4IMC Conference, Auckland, NZ. Abstract volume 131A. Geoscience Society of New Zealand Miscellaneous Publication, pp. 74–75.

Siebe, C., Salinas, S., 2014. Distribution of monogenetic phreatomagmatic volcanoes (maars, tuff-cones and tuff rings) in the Mexican Volcanic Belt and their tectonic and hydrogeologic environment. IAVCEI-5IMC-meeting, Querétaro (Mexico), Abstracts volume, pp. 183–184.

Siebe, C., 1986. On the possible use of maars and cinder cones as palaeoclimatic indicators in the closed basin of Serdán-Oriental, Puebla, México. Journal of Volcanology and Geothermal Research 28: 397–400.

How Small Scale Basaltic Volcanic Systems Behave: A Geochemical Perspective

Ian E. M. Smith

School of Environment, University of Auckland, Auckland, New Zealand
E-mail: ie.smith@auckland.ac.nz

Keywords: basalt, geochemistry, monogenetic

Small-scale basaltic magmatic systems are the most widespread manifestation of magmatic activity of planet Earth and occur in all of the major tectonic environments; they are characteristically expressed at the Earth's surface as fields of small monogenetic cones. Although the compositions of monogenetic volcanoes in volcano fields are dominantly basaltic there is wide variation within this spectrum from strongly silica-undersaturated nephelinites through basanites and alkali basalts to subalkaline transitional and tholeiitic basalts .

The geochemical character of monogenetic volcano fields is in part related to their specific tectonic setting which includes intraplate (e.g., Eastern Australia, northern New Zealand), extension (e.g., central Europe, Arabia), and subduction associated (e.g., Mexico, Japan) settings; many fields have unique characteristics. Important underlying factors for the development of small-scale volcanic systems are small magma volumes, episodic eruption of discrete magma batches, and a crustal environment that allows the passage and escape of small magma volumes through the crust.

Although the observed compositions of volcanoes in each of the intraplate, extensional, and subduction-related tectonic environments overlap, there are some distinct trends. In intraplate and extensional tectonic settings, compositions are more commonly undersaturated to strongly undersaturated in terms of silica compared with those in subduction-related settings where compositions tend toward silica oversaturation.

The chemical compositions of small basaltic cones show a remarkable variety despite the small volumes of magma represented by individual eruptive centers. Compositional trends are revealed by detailed sampling of eruption sequences representing periods of eruption that range from months to years to decades. A first order observation is the correlation between the chemical composition of erupted material and the size of the cone they constitute indicating a close link between magma source and their surface manifestation as volcanic cones (McGee et al., 2015).

A second characteristic observation is of a remarkably systematic pattern of compositional variation correlated with stratigraphy and observed as variation in composition from relatively evolved compositions at the beginning of an eruption sequence to primitive compositions at the end. However, the detailed features of these patterns point to a variety of different processes

A simple pattern described by Smith et al. (2008) is attributed to near-source crystal fractionation on the magma conduit walls during extraction of the magma from its source. This produces a fractionated magma column that rises within chilled margins (Figure 1). A second pattern described by McGee et al. (2012) is the initial eruption of magma representing a low melting temperature source component followed by a distinct magma composition representing melting of a higher melting temperature source component. More complex variants of these relatively simple patters have been described by Brenna et al. (2012) who document cases of mixing of distinct magma batches within a single monogenetic cone. Clearly, compositional variation in small-scale basaltic volcanoes can be the result of one or more of several distinct processes.

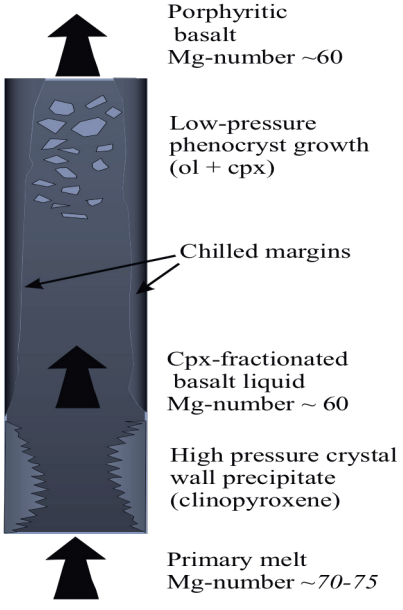

Figure 1. The model of near-source fractionation of clinopyroxene to produce a fractionated magma column (after Smith et al., 2008).

Several important concepts underlie an understanding of the role of small-scale basaltic magmatic systems in the wider framework of an evolving Planet Earth. The key aspects of the geochemistry of small basaltic systems are:

(1) Small monogenetic volcanoes can be described in terms of the eruption of a batch of magma that rises as a discrete body and is erupted within a confined time period. Magma batches may represent a single melting event but commonly they are shown to represent melts of more than one source component or mixtures of distinct melt batches, and a range of processes can occur within a single eruption (for example, mixing of sources, crystallisation of different minerals, variation in degrees of partial melting).

(2) The primary magmas observed in small-scale basaltic systems range from strongly silica-undersaturated nephelinites through basanites and alkali basalts to silica saturated and oversaturated transitional and tholeiitic basalts. Discrete evolutionary trajectories can be described as originating from this spectrum of primitive compositions (Figure 2).

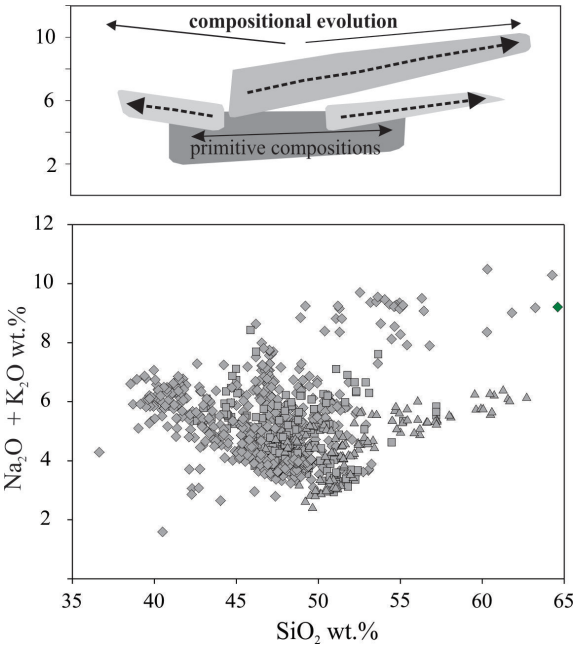

Figure 2. The range of compositions shown in representative small-scale basaltic volcanic fields from intraplate environments. In the upper part of the diagram compositional trajectories are indicated for primitive compositions (dark gray) and for several evolutionary trends (lighter shades).

(3) Source regions beneath volcanic fields are never homogeneous, and often more than two mantle components are involved in the genesis of a magma batch. Isotopic studies used in conjunction with more traditional geochemical modeling techniques have proven extremely useful in elucidating the details of an entire magmatic system.

(4) Most studies invoke small (sometimes <1%) degrees of partial melting of the source or sources.

(5) Tectonic setting (modern and ancient) can play a large part in the form and chemistry of a volcanic field.

(6) There is a strong correlation between magma volume and degree of silica saturation in primary magmas. Small magma batch volumes are characteristically more silica undersaturated compared with the larger volume transitional and tholeiitic compositions.

Despite the small volumes involved in individual magma batches, monogenetic volcano fields are the most widespread form of volcanism on Earth. Their small volumes require rapid ascent rates if the magmas are to reach the Earth's surface, and so their compositions carry the signature of the deep-seated processes that give rise to them. An important characteristic of "monogenetic" eruptions is that they show geochemical evidence for the isolation and preservation of magmatic processes, whether the melting event is composed of one magma batch or many. Tectonic setting is clearly a significant factor in the extent of differentiation of basalts in volcanic fields, but we suggest that this is not a defining factor in whether a volcanic center is "monogenetic" or not, rather that the isolation of the melting event and its subsequent evolution defines whether a field of individual, generally geochemically unique cones develops instead of a centralized system.

References

Brenna, M., Cronin, S.J., Smith, I.E.M., Sohn, Y.K., Maas, R. 2012. Spatio-temporal evolution of a dispersed magmatic system and its implications for volcano growth, Jeju Island Volcanic Field, Korea. Lithos**,** 148, 337–352.

McGee, L.E., Millet, M.-A, Smith, I.E.M., Nemeth, K., Lindsay, J.M. 2012. The inception and progression of a monogenetic eruption: Motukorea Volcano, the Auckland Volcanic Field, New Zealand. Lithos 155, 360–374.

McGee, L.E., Millet, M.-A, Beier, C., Smith, I.E.M., Lindsay, J.M. 2015.Mantle heterogeneity controls on small-volume basaltic volcanism. Geology 43, 551–554

Smith, I.E.M., Blake, S., Wilson, C.J.N., Houghton, B.F. 2008. Deep-seated fractionation during the rise of a small-volume basalt magma batch: Crater Hill, Auckland, New Zealand. Contributions to Mineralogy and Petrology 3155: 511–527.

Interpreting Compositional Variations in the Stratigraphic Sequences of Small-Scale Basaltic Volcanoes

Ian E. M. Smith*, Shane J. Cronin, and Marco Brenna

School of Environment, The University of Auckland, Auckland, New Zealand
*Corresponding author E-mail: ie.smith@auckland.ac.nz

Keywords: geochemistry, monogenetic, Auckland

A notable feature of small monogenetic volcanic cones is their systematic compositional variations. These variations are typically closely correlated with their stratigraphy and record changes in the composition of magma erupted at the Earth's surface as an eruption progresses. Generally, the compositional trends are from relatively evolved magmas in the initial stages of an eruption to relatively primitive toward the end. However, recent studies have revealed several other variation patterns indicating the operation of several processes. One of the reasons that these patterns are observed is that the magmas of monogenetic volcanoes are generally of small volume and they rise rapidly from their source without significant interaction with the crust.

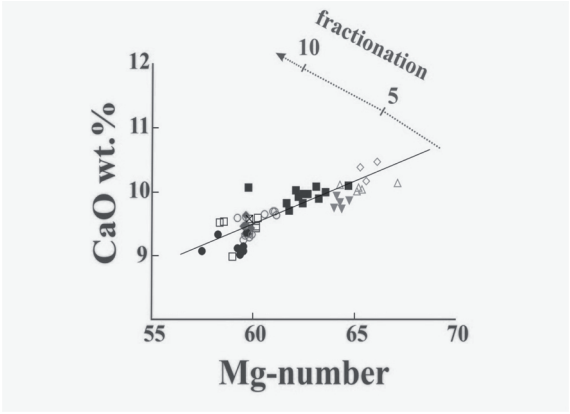

Figure 1. Compositional variation within a suite of samples from Crater Hill in the Auckland Volcanic Field (after Smith et al., 2008). Samples with low CaO content and Mg-number were erupted early and those with high values late in the eruption sequence. The upper curve describes a fractionation trajectory involving olivine and the lower curve describes fractionation of clinopyroxene from a primitive composition with a Mg-number of 70.

This study is based on detailed work on the small volcanoes of the Auckland Volcanic Field in northern New Zealand. Variation patterns that have been recognized within the volcanic cones of the Auckland Volcanic Field are:

(1) Systematic continuous variation in chemical composition from relatively evolved magmas erupted in the early stages of an eruption sequence to relatively primitive compositions erupted at the end (Figure 1). This is interpreted as the rise to the surface of a fractionated magma column. An example is Crater Hill in the Auckland Volcanic Field, and in this case the process of fractionation has been modeled as near-source side wall crystallization of clinopyroxene (Smith et al., 2008).

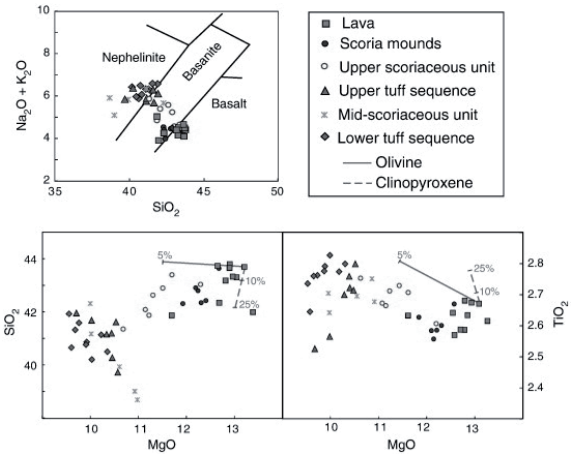

Figure 2. Compositional variation in the Motukorea Volcano eruptive sequence. Two distinct compositions are represented and there are a few samples which appear to represent mixtures. Early eruptives are relatively alkaline. Fractional crystallization cannot explain the relationship between the two compositions and both are relatively high in MgO. (after McGee et al., 2012).

(2) Eruption of a succession of different compositions both of which have relatively primitive chemical compositions. This has been explained by the successive melting of a heterogeneous source. Early eruptives are of magmas generated by melting of a low melting

point component in a mantle source. Once this different component and produces a different magma composition, e.g., Motukorea, in the Auckland Volcanic Field (McGee et al., 2012).

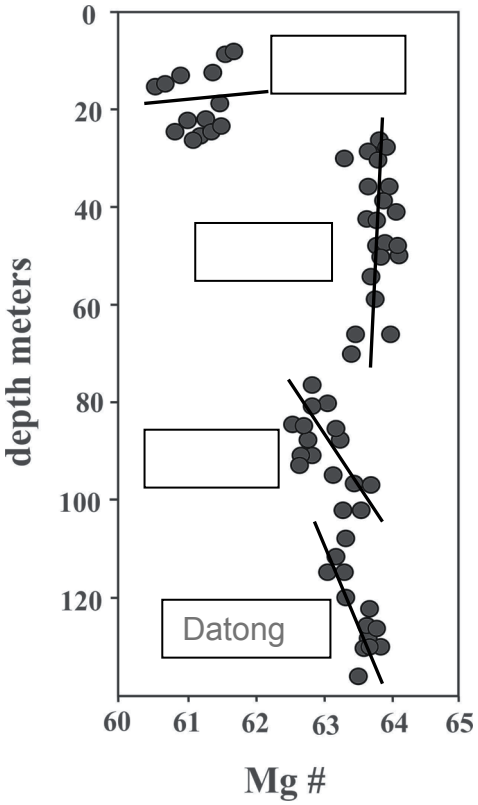

Figure 3. Variation in the composition of samples collected from a core drilled through a lava flow succession on Rangitoto Volcano in the Auckland Volcanic Field (after Linell et al., 2016). Four discrete compositions are present. Although the final stage may be explained by fractionation from an earlier composition the variation in the lower part of the sequence appear to represent processes related to the extraction of magmas from their source.

(3) Eruption of a relatively small magma volume followed after a short but distinct time interval by a second larger magma volume with a distinct composition. In this case the initial magma is typically more alkaline than that erupted later, e.g., Rangitoto in the Auckland Volcanic Field (Needham et al., 2011). This pattern has been explained by the rise of a smaller volume of magma generated deeper in the system triggering instability and melting of a larger source volume at shallower levels.

(4) Eruption of several distinct magma compositions in an essentially continuous succession, e.g., Linell et al. (2016). This has been observed in a suite of samples collected from a core through a lava flow sequence on Rangitoto Volcano in the Auckland Volcanic Field (Figure 3). Although not yet fully interpreted, the different compositions observed are not readily interpreted as due to fractional crystallization of observed olivine phenocrysts and it is suggested that they represent variations in the extraction process that produces the magmas from their mantle source.

The compositional trends that have been observed in volcanoes of the Auckland Volcanic Field are relatively simple patterns that involve discrete magma batches. More complicated patterns have been observed elsewhere in basaltic systems in which magma batches have mixed during their rise toward the surface to produce complex compositional mixtures. Typically, these are characteristic of volcanic systems involving larger volumes of magma.

References

Linnell, T., Shane, P., Smith, I., Augustinus, P., Cronin, lumes of magma.S., Lindsay, J. and Maas, R., 2016. Long-lived shield volcanism within a monogenetic basaltic field: The conundrum of Rangitoto volcano, New Zealand. Geological Society of America Bulletin: B31392. 31391.

McGee, L.E., Millet, M.-A., Smith, I.E.M., Németh, K. and Lindsay, J.M., 2012. The inception and progression of melting in a monogenetic eruption: Motukorea Volcano, the Auckland Volcanic Field, New Zealand. Lithos, 155(0): 360–374.

Needham, A.J., Lindsay, J.M., Smith, I.E.M., Augustinus, P. and Shane, P.A., 2011. Sequential eruption of alkaline and sub-alkaline magmas from a small monogenetic volcano in the Auckland Volcanic Field, New Zealand. Journal of Volcanology and Geothermal Research, 201(1–4): 126–142.

Smith, I.E.M., Blake, S., Wilson, C.J.N. and Houghton, B.F., 2008. Deep-seated fractionation during the rise of a small-volume basalt magma batch: Crater Hill, Auckland, New Zealand. Contributions to Mineralogy and Petrology, 155(4): 511–527.

Sedimentary Record of a 4 ka B.P. Storm Event Preserved Within the Rimbeds of a Coastal Tuff Ring, Jeju Island, Korea

Chanwoo Sohn* and Young Kwon Sohn

Department of Geology, Gyeongsang National University, Jinju, Korea
*Corresponding author E-mail: paie23@gnu.ac.kr

Keywords: storm, tide, volcaniclastics

Volcaniclastic deposits can preserve unusually high-resolution records of earth-surface processes and environments due to extremely high aggradation rate. We provide a peculiar example of volcaniclastic sedimentation, which resulted from the interaction between a volcano (Songaksan tuff ring) and the sea.

The Songaksan tuff ring, located at the southwestern coast of Jeju Island, was produced by phreatomagmatic activity 4000 years ago when the sea level was almost identical to that at present. The rimbeds of the tuff ring, exposed mostly above sea level, were deposited by pyroclastic surges and attendant air fall in a subaerial condition. However, in the middle of the medial to distal rimbeds between ca. 2.9 and 6.2 m above sea level, four units of reworked or water-laid deposits (Unit R1–R4) are interbedded with primary tuffs.

Overall, the reworked units are lenticular and bounded by erosional surface (Figure 1). The deposits are well sorted and contain mm-thick to paper-thin mud laminae, suggesting winnowing and settling of fines in a subaqueous setting. Unit R1, found up to 2.9 m a.s.l., is trough cross-bedded. Unit R2, found up to 4.8 m a.s.l., consists of three subunits of graded and stratified deposits, showing wavy stratification, ripple cross-lamination, and parallel to subparallel lamination. Unit R3, found up to 6.2 m a.s.l., shows pinch and swelling structure. Unit R4, found up to 4.3 m a.s.l., is divided into three subunits, showing ripple cross-lamination or wavy stratification. A total of nine mud drapes are found within the reworked deposits, mainly along the unit/subunit boundaries.

Considering the duration of phreatomagmatic eruptions, which commonly last days to weeks, the reworking events are inferred to have taken place within hours to days. We negate the possibility of rainfall-induced reworking because of the occurrence of the reworked deposits beneath 6.2 m a.s.l. The reworking is thus inferred to have been caused by a marine process when the medial-to-distal rimbeds of the tuff ring was temporarily submerged under water because of a sea level rise by a few to several meters above fair weather sea level.

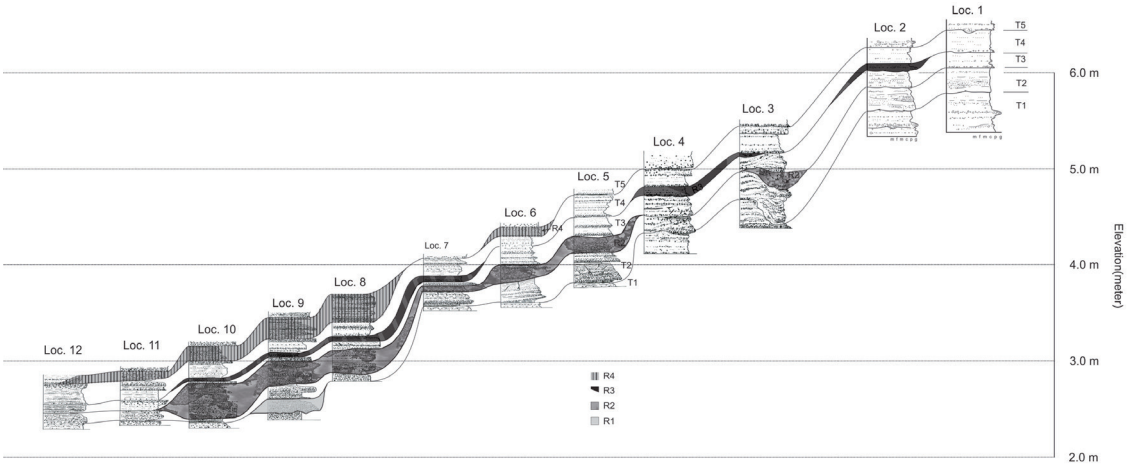

Figure 1. Correlation of columns of four reworked units (shaded units) within the medial-to-distal rimbeds of Songaksan. Primary tuff units have laterally continuous and craterward-thickening bed geometry, whereas the reworked units have laterally discontinuous bed geometry. Individual columns are vertically positioned according to the altitude data that were obtained by land-based Lidar terrain mapping.

We interpret that the sea level rise was caused by a storm surge. Intercalation of the four wave-reworked units within the primary tuff beds that were evidently deposited in a subaerial setting by PDCs

and air-fall indicates that there were alternations of subaerial and subaqueous conditions at the depositional site. We infer that the cyclic fluctuations of sea level were associated with tides, and that the four reworked units reflect ca. four cycles of tidal fluctuations during a ca. 2-day long storm surge event. Occurrence of reworked units at different altitudes suggests possible inequality of tide and/or waxing and waning of storm intensity. The possibility of a tsunami is ruled out because of the abundance of wave-generated structures, which are poorly developed in tsunami deposits, in spite of the occurrence of some structures that are known to be associated with tsunami deposits, such as mud drapes and soft deformation structures.

The storm deposit in Songaksan is regard as the most complete record of a paleostorm event ever reported, which could be preserved because of a contemporaneous eruption of a volcano in a coastal setting. Coexistence of some features that have previously been related with a tsunami event such as loading structures and mud drapes within the storm deposit necessitates a refinement of the depositional models of tsunamites and tempestites.

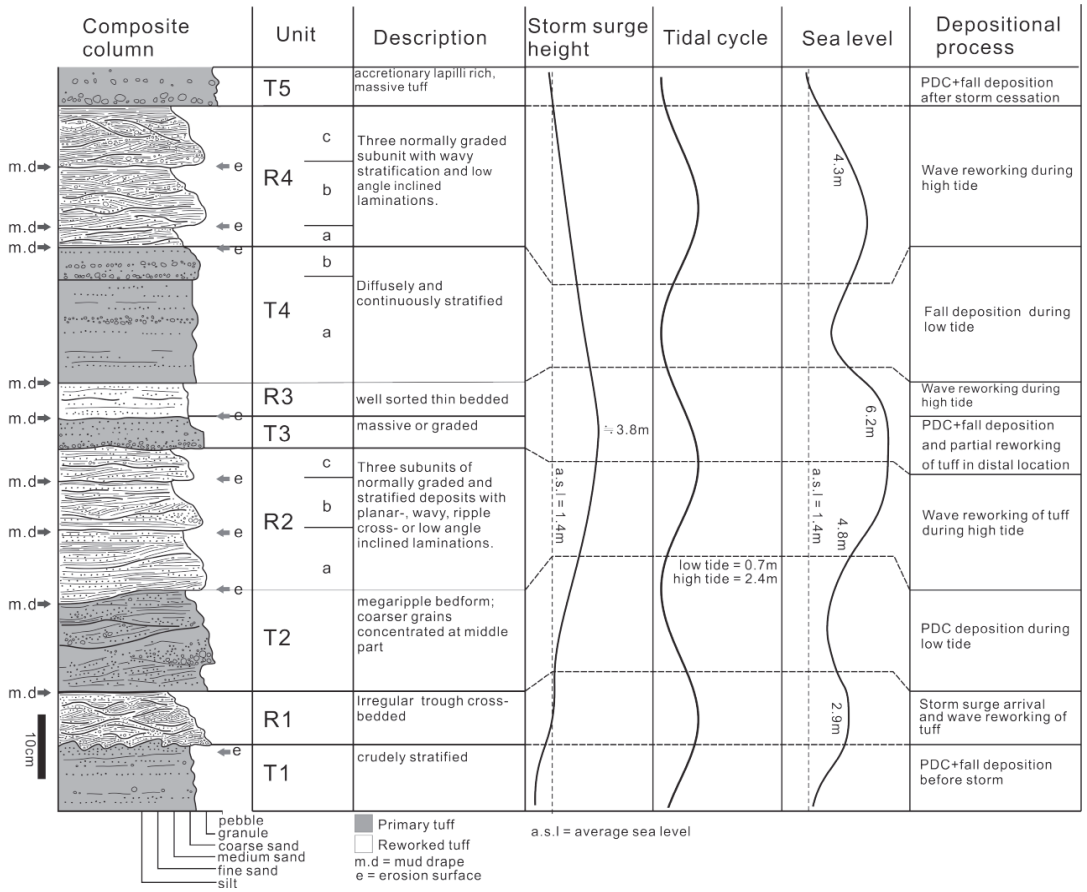

Figure 2. Composite column of the storm-reworked deposits within the primary tuff beds of the Songaksan tuff ring. The reworked deposits suggests a combined action of wave and tide during a raised sea level, which was caused most likely by a storm surge event that lasted a few days during the eruption of the tuff ring.

References

Hunter, R. E., & Clifton, E. H. (1982). Cyclic deposits and hummocky cross-stratification of probable storm origin in Upper Cretaceous rocks of the Cape Sebastian area, southwestern Oregon. Journal of Sedimentary Research, 52(1).

Clifton, H. E., Hunter, R. E., & Phillips, R. L. (1971). Depositional structures and processes in the non-barred high-energy nearshore. Journal of Sedimentary Research, 41(3).

Morton, R. A., Gelfenbaum, G., & Jaffe, B. E. (2007). Physical criteria for distinguishing sandy tsunami and storm deposits using modern examples.Sedimentary Geology, 200(3), 184–207.

Kortekaas, S., & Dawson, A. G. (2007). Distinguishing tsunami and storm deposits: an example from Martinhal, SW Portugal. Sedimentary Geology, 200(3), 208–221.

Sohn, Y. K., & Yoon, S. H. (2010). Shallow-marine records of pyroclastic surges and fallouts over water in Jeju Island, Korea, and their stratigraphic implications. Geology, 38(8), 763–766.

The First Tephra Evidence for a Late Glacial Explosive Volcanic Eruption in the Arxan-Chaihe Volcanic Field (ACVF), Northeast China

Chunqing Sun[1,*], Qiang Liu[1], Jing Wu[1], Károly Németh[2], Luo Wang[1], Yongwei Zhao[3], Guoqiang Chu[1], and Jiaqi Liu[1]

[1]*Key Laboratory of Cenozoic Geology and Environment, Institute of Geology and Geophysics, Chinese Academy of Sciences, Beijing, China*
[2]*Institute of Agriculture and Environment, Massey University, Palmerston North, New Zealand*
[3]*Institute of Geology, China Earthquake Administration, Beijing, China*
*Corresponding author E-mail: suncq@mail.iggcas.ac.cn

Keywords: tephrochronology, Arxan-Chaihe, MoonLake

5-mm thick tephra layer has been identified in the lacustrine sediments of Moon Lake in the Arxan-Chaihe volcanic field (ACVF) in Greater Khingan Mountains (NE China) identified on the basis of magnetic susceptibility anomaly (Figure 1).

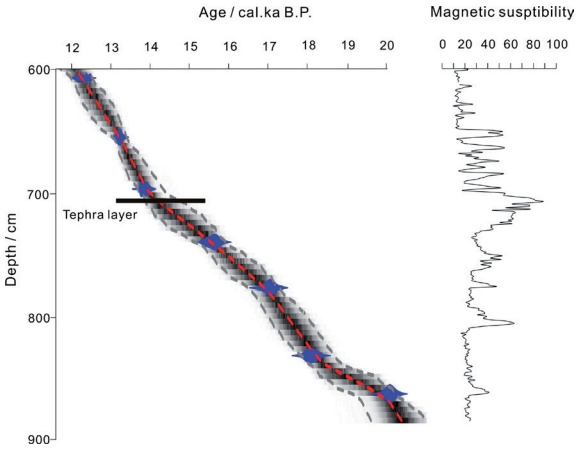

Figure 1. Age-depth model (age results were from Liu et al., 2010) and magnetic susceptibility of the sediment core at Moon Lake. Tephra layer locates at the positions of abnormal high level of magnetic susptibility. The age model was based on the Bacon software (Blaauw and Christen 2011).

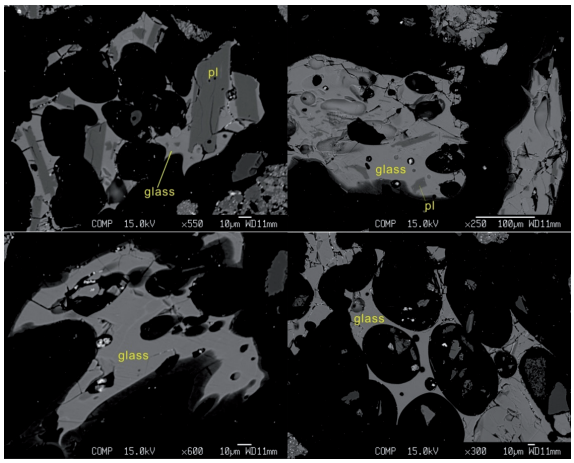

Figure 2. BSE (back scattering electron) map of the glass shards (glass) and plagioclase (pl) from the tephra at Moon Lake.

This tephra layer mainly consists of brown glass shards and minor amounts of plagioclase (Figure 2), olivine, and clinopyroxene. Major elements analysis on the glass shards and plagioclase illustrate that these glass shards show low concentration of K_2O similar to the eruptive products derived from post-Miocene volcanoes of the ACVF (Figures 3 and 4). The plagioclase composition from the tephra is also similar to the typical labradorite member of the ACVF (Zhao 2010). During late Pleistocene to Holocene, there were also extensive explosive eruptions in the Nuominhe volcanic field (NVF) near to the ACVF. But the geochemical characteristics of eruptive products from ACVF are significantly different from those chemical compositions derived from eruptive products from the NVF where volcanic eruptive products are mainly potassic in composition (Fan et al. 2015; Liu 1999). The compositional variations between ACVF and NVF are likely the results of different magmatic processes. Yanshan and Gaoshan volcanoes might have erupted during the late Holocene (Bai et al. 2005). Radiocarbon dating on the organic materials from the lacustrine sediments allows this tephra layer to be dated at ca. 14,200 cal yrs BP, which implies a previously unknown explosive eruption in the ACVF during the late Pleistocene.

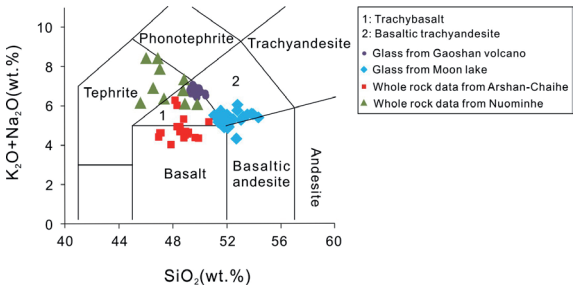

Figure 3. TAS diagram (Le Maitre et al. 1989) for comparing the glass data from Moon Lake and Gaoshan volcano, and the whole rock data from Nuominhe and Arxan-Chaihe volcanic fields. Whole rock compositions from local Arxan–Chaihe volcanic field and Nuominhe volcanic field were from Zhao (2010).

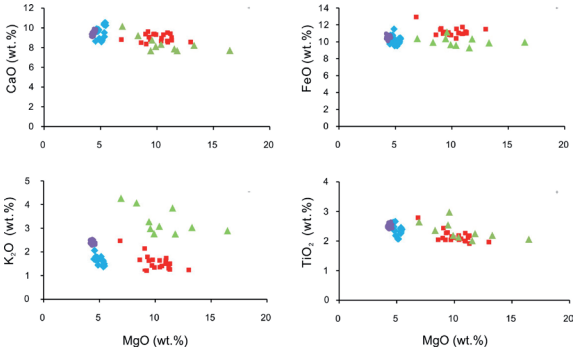

Figure 4. Major element compositions of glass shards from the tephra at Moon Lake and the whole rock compositions from local Arxan–Chaihe volcanic field and Nuominhe volcanic field. Data sources and symbols are same as Figure 3. The error bars (2δ) were calculated on the basis of analyzed results of secondary glass standard.

These results, for the first time, give a direct tephra record in this area, and suggest that future tephra and/or cryptotephra identifications in local sedimentary basins such as crater lakes of scoria cones and maars are very significant for dating the late Pleistocene-Holocene volcanic eruptions that can help to establish the volcanic activity of this volcanic field. This tephra layer also provides a potential tephrochronological marker layer which can be used to synchronize local sedimentary records during the climatically variable Late Glacial (Figure 5).

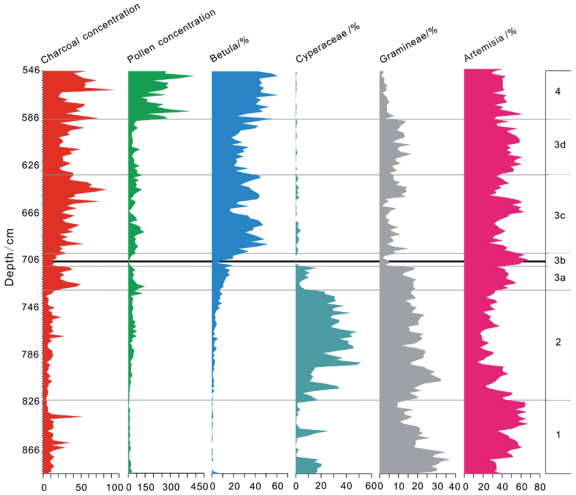

Figure 5. Climate changes and plant evolutions based on the pollen and charcoal records from Moon Lake sediment. The black line at 708 cm is the position of the tephra layer. Pollen and charcoal data were from Wu and Liu (2012, 2013), and the unit for the concentration of pollen and charcoal is 10^3 grains per gram.

Acknowledgments

This work was supported by the National Natural Science Foundation of China (Grant Nos. 40872206, 41272392, 41572353, and 41320104006). C. Sun would like to thank K. Jochum and B. Stoll for providing MPI-DING glasses. Huaiyu He and Zhengfu Guo (IGGCAS) are thanked for their kind suggestions on an early version of the manuscript. Qian Mao, Yuguang Ma, and Di Zhang are thanked for their help during EPMA analysis.

References

Bai, Z., Tian, M., Wu, F., Xu D., Li T., 2005. Yanshan, Gaoshan—Two active volcanoes of the volcanic cluster in Arshan, Inner Mongolia (In Chinese with English abstract). Earthquake Res. China 21(1): 113–117.

Blaauw, M., Christen, J.A., 2011. Flexible paleoclimate age-depth models using an autoregressive gamma process. Bayesian Anal. 6: 457–474.

Fan, Q., Zhao, Y., Chen, S., Li, N., Sui, J., 2015. Quaternary volcanic activities in the west of the Daxing'anling-Taihangshan gravity lineament (In Chinese with English abstract). Bull. Mineral. Petrol. Geochem. 34(4): 674–681.

Le Maitre, R.W., Bateman, P., Dudek, A., Keller, J., Lameyre, J., Le Bas, M.J., Sabine, P.A., Schmid, R., Sorensen, H., Streckeisen, A., Woolley, A.R., Zanettin, B., 1989. A Classification of Igneous Rocks and a Glossary of Terms. Blackwell Sciencific, Oxford.

Liu, Q., Li, Q., Wang, L., Chu, G., 2010. Stable carbon isotope record of bulk organic matter from a sediment core at Moon lake in the middle part of the Daxing'an Mountain range, northeast China during the last 21 ka (In Chinese with English abstract). Quat. Sci. 30(6): 1069–1077.

Liu, J., 1999. Volcano in China (In Chinese). Beijing: Science Press, 1–219.

Wu, J., Liu, Q., 2012. Pollen-recorded vegetation and climate changes from Moon Lake since Late Glacial (In Chinese with English abstract). Earth Sci. — J. China University Geosci. 37(5): 947–954.

Wu, J., Liu, Q., 2013. Charcoal-recorded climate changes from Moon Lake in Late Glacial (In Chinese with English abstract). Chin. J. Geol. 48(3): 860–869.

Zhao, Y., 2010. Study on geology and geochemistry of Quaternary volcanoes in the Da Hinggan Ling Mountains (In Chinese with English abstract). Institute of Geology, China Earthquake Administration, Beijing.

The Maar in the Leiqiong UNESCO Global Geopark

Kuiyuan Tao*, Zhenyang Wu, Wenzhao Huang, Libin Zhang, Muzhen Cai,Yuanwei Chen, Yusheng Jie, and Xiaomin Xun

Leiqiong UNESCO Global GeoPark Management Committee, Zhanjiang, China
*Corresponding author E-mail: hgy2819197@163.com

Keywords: maar, Leiqiong, popularization

Maar is an important composition of Leiqiong UNESCO Global Geopark geo-heritages, represented by Huguangyan Maar Lake (Figure 1). There are 15 more geological remains including maar-like Qingtongyang, Tianyang, Shuangchiling, Luojingpan (Figure 2), and Yingfengling surge tuff cone, etc.

Figire 1. The photograph of Huguangyan Maar Lake.

Figure 2. The photograph of Luojingpan Maar.

The magma explosion and lava eruption in Leiqiong Global Geopark not only recorded the history of volcanic eruption (Figure 3), but also recorded the changes of geological environment, which have significant value. Leiqiong maar geo-heritages need to strengthen scientific research, protection, and science popularization. Let the public understand the formation and significance of the maar, and raise the awareness of the protection of the whole people.

Figure 3. The photograph of outcrop of Yanghualing in Haikou.

Monogenetic Volcanism Influenced by Spatially and Temporally Confined Eruptive Environment Changes in a Coastal Setting

Rickus van Niekerk[1], Károly Németh[1,*], Gert Lube[1], and Zoltán Pécskay[2]

[1]*Volcanic Risk Solutions, Institute of Agriculture and Environment, Massey University, Palmerston North, New Zealand*
[2]*ATOMKI – Nuclear Research Centre of the Hungarian Academy of Sciences, Debrecen, Hungary*
*Corresponding author E-mail: k.nemeth@massey.ac.nz

Keywords: diatreme, hyaloclastite, Surtseyan

The Ngatutura Volcanic Field (NVF, North Island, New Zealand) comprises at least 16 basaltic centres (Figure 1) and forms part of a series of Late Cenozoic intraplate basaltic fields, all of which are found in a back-arc setting in the region (Briggs et al. 1989). At the western boundary of the NVF, the Ngatutura Bay Complex (NBC) offers extraordinary exposures of subsurface volcanic structures, lava flows, hyaloclastite, and a diatreme. The magma feeding these volcanoes has erupted through siltstones and sandstones of Jurassic age (Murihiku Terrane), and Tertiary siltstones, sandstones, and limestones (Oligocene Te Kuiti Group and Lower Miocene Waitemata Group). Fragments of these rocks are found as accidental lithics in many of the preserved volcanic successions. The vent locations of the NVF seem to follow Mesozoic or older structural elements, although no significant pattern on the age distribution of the eruptions has been noted. However, a general tendency of a northward younging of volcanism has been suggested and widely accepted, ranging from the older Alexandra Volcanics just south of the NVF being 2.74–1.6 Ma, NVF being 1.83–1.54 Ma while South Auckland being 1.56–0.51 and Auckland less than 0.3 Ma old (Briggs et al. 1990). New research on the Ngatutura Bay Complex in the western margin of the NVF sheds light on several concepts on understanding the time and space evolution of this volcanic field in a relatively narrow time slice and spatially confined area. The wide range of eruption styles, longevity of the volcanic complex, and intricate 3D architecture at the NBC show the complex nature of the volcanism at a typical "monogenetic" volcanic field.

The history of the NBC has been determined through detailed mapping and K-Ar dating of all the volcanic features exposed in a c. 250 m wide section (Figure 2), revealing at least two phases of volcanism. Interestingly, the total volcanic activity at this single locality spans nearly 1.7 million years, exceeding the duration of volcanism previously documented for the entire volcanic field (Briggs et al. 1989). The older eruptive phase is represented by a basaltic intrusion at the base of a diatreme (c. 3.4 Ma), and a prominent lava flow (c. 3.22 Ma), up to 40 m in thickness and comprising pillow lavas and rosette-style cooling fractures suggesting their submarine emplacement conditions. This indicates that some prediatreme intrusion and lava outflow took place first in this region. Lava flows outpoured during this phase were likely emplaced in shallow subaqueous conditions. The diatreme, along with the older intrusion at its base is located on the Ngatutura Fault, with dikes being intruded along the planes of two smaller extensional faults. The diatreme (c. 2.3 Ma) along with dikes A and B (1.8–1.7 Ma) and a lava pond (c. 1.83 Ma) is part of the younger phase of syn-sedimentary volcanism. These features are found within variably indurated marine strata. The intrusive features (lava pond, dikes A and B) all have peperitic margins. At the dikes the peperite is globular to sandy and up to several decimeters thick. The lava pond also comprises hyaloclastite sheets in some parts. Shortly after the diatreme and associated tuff ring formation the region is inferred to have been submerged again below shallow marine conditions demolishing the majority of the surface deposits of the maar-diatreme in a coastal environment. Subsequent magma intrusions invaded the gradually accumulating shallow marine sand and silt, partially invading it by a peperitic dike and sill that occasionally break through the sea floor feeding hyaloclastite sheets preserved in the top of the marine sedimentary succession. The time and space evolution of volcanic events in this <1 km^2 area suggests that the volcanism in this area record volcanic events over time periods that exceeds the time span previously recorded for the entire volcanic field, illustrating the need for a future resurvey of volcanic centers in the NVF to understand the timing of the volcanism. In addition, the changes from an older diatreme formation toward younger intrusive/extrusive processes clearly mark coeval synsedimentary volcanic processes where magma interacted with a shallow marine environment. This suggests that the paleoenvironment must have changed dramatically

in a short period of time allowing marine transgression to a broad coastal plain, thereby shifting coastal subaerial phreatomagmatic volcanism to be more shallow marine type producing hyaloclastite piles. This also suggests that such environmental change might have led to the development of fully Surtseyan conditions; however, the deposits are either not exposed or already eroded. The NBC shows very clearly how eruptive environment change can alter the forming of volcanic successions. This has implications to the active Auckland Volcanic Field, where a future sea level rise would increase the potential of phreatomagmatism and Surtseyan-style volcanism in the future.

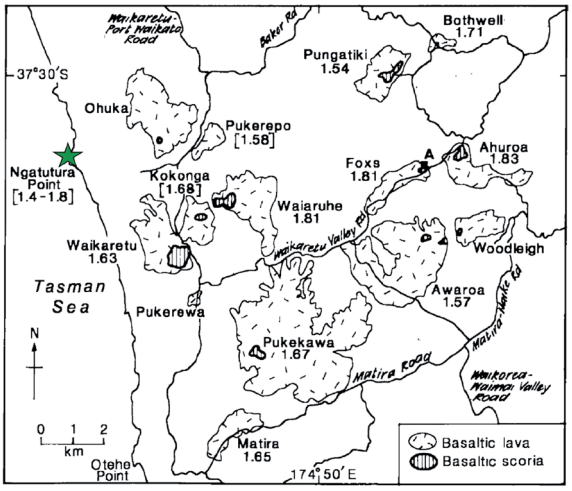

Figure 1. ap of the Ngatutura Volcanic Field with eruptive centers and some ages known from literature (Briggs et al. 1989). The eruptive ages of the entire field range between 1.8 and 1.4 Ma in general, based on previous data (Briggs et al. 1989).

References

Briggs RM, Itaya T, Lowe DJ, Keane AJ (1989) Ages of the Pliocene Alexandra and Ngatutura Volcanics, Western North-Island, new Zealand, and some geological implications. New Zealand Journal of Geology and Geophysics 32(4): 417–427.

Briggs RM, Utting AJ, Gibson IL (1990) The origin of alkaline magmas in an intraplate setting near a subduction zone - the Ngatutura-basalts, North island, New Zealand. Journal of Volcanology and Geothermal Research 40(1): 55–70.

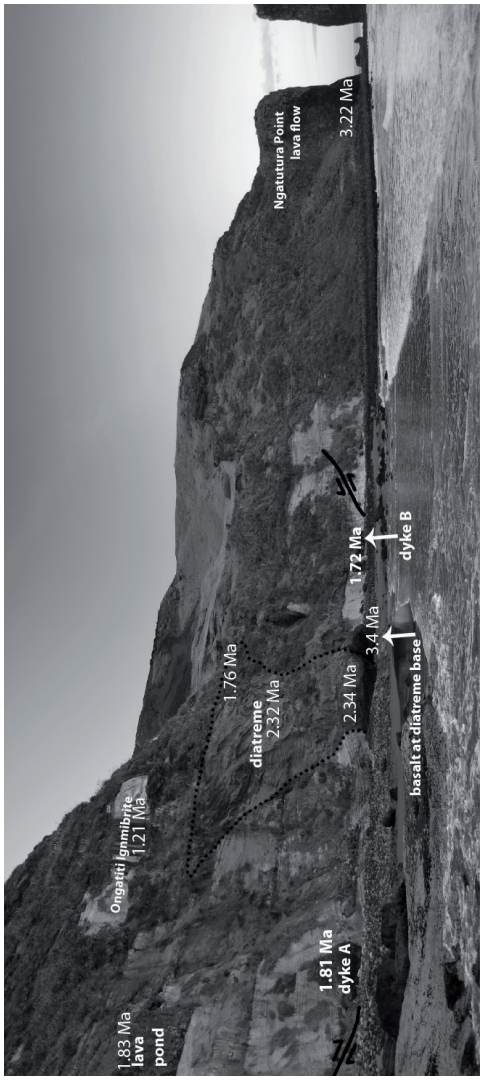

Figure 2. Coastal section of the NBC with newly obtained K-Ar ages.

Comparative Semiquantitative Assessment of the Geodiversity of Monogenetic Volcanoes

Max van Wyk de Vries[1] and Benjamin van Wyk de Vries[2]

[1]*Department of Geosciences, University of Edinburgh, Edinburgh, UK*
[2]*Laboratoire Magmas et Volcans, Universite Blaise Pascal, Clermont-Ferrand, France*
*Corresponding author E-mail: s1447108@sms.ed.ac.uk

Keywords: geodiversity, monogenetic, volcanoes

The development of semiquantiative methods for geoheritage assessment can allow for a more rigorous comparison of sites and between individual volcanoes and volcanic fields. This serves to highlight the relative value of a geosite, but can also provide fundamental information for comparative research into the nature of monogentic volcanism. Thus, both science and geoheritage benefit. There are opportunities open for applying such methods more widely, not only for monogenetic volcanoes but for other geological phenomena. Different geological sites require specifically adapted methods for geosite quantification. Volcanoes have particular geological and geomorphological expressions and so require their own specific geosite classification and quantification procedures. Monogenetic volcanoes require special treatment, as they are the world's most numerous and highly diverse class of volcano. Monogenetic volcanoes group into fields, and fields have diverse characteristics reflecting close relationships to the tectonic environment. Our recent experiences promoting the monogenetic volcanoes in the Chaîne des Puys–Limagne Fault UNESCO World Heritage ChdP-LF (2016) project have led to the development of a classification scheme that starts from the general large-scale tectonic environment, the root of all geodiversity. The branching classification from this essential root is like a Bayesian tree, acknowledging uncertainty in the decision process, and allowing for modification as more information comes available.

We provide examples of monogenetic volcanic fields in different tectonic environments and geomorphologic settings that illustrate how the classification descends from the global, through different geological environments, through "volcano," to individual volcanic geotypes and their features. The classification can become very complicated, and so as to not become meaningless, simplification and subjective strategic decisions are needed. One of these is to use indicators such as SiO_2 and volcano clustering (Figure 2).

We think this process is a useful exercise to improve the comparative analysis between sites, and can help avoid some of the pitfalls of subjective qualitative approaches.

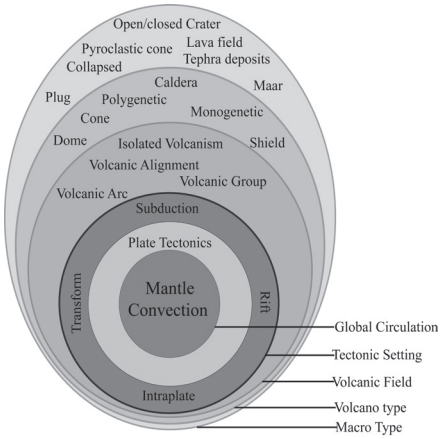

Figure 1. Diagram showing the classification scheme, originating from global Earth Processes of mantle convection and plate tectonics, to individual volcano types. This can be presented either pictorially, as shown here or by a branching diagram.

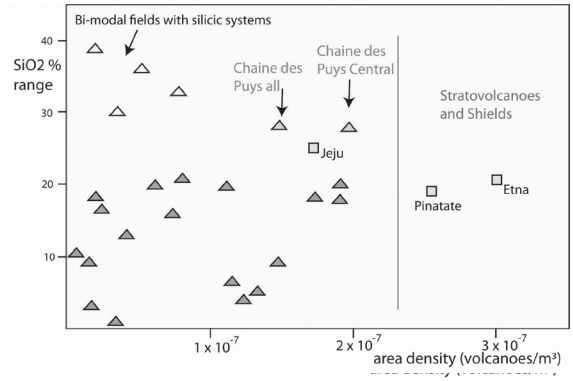

Figure 2. Plot of SiO % range against volcanic density. Silica range and distance between volcanic structures are both related in different ways to the tectonic environment.

The comparative analysis that we have undertaken for the UNESCO nomination has shown that there is a large diversity of monogenetic fields in different tectonic environments. If these volcanic fields are taken in combination with their tectonic features there is potential for a number of sites to be inscribed to World Heritage. This is a step toward

overcoming the current lack of appreciation for the diversity of geological sites and would enrich the World Heritage List.

References

ChdP-LF (2016), Additional information, Chaîne des Puys-Limgane Fault UNESCO nomination dossier, Conseil Departmental du Puy de Dome, pp. 279.

Merle O. (2011). A simple continental rift classification: Tectonophysics, 513, 88–95. doi:10.1016/j.tecto.2011.10.004.

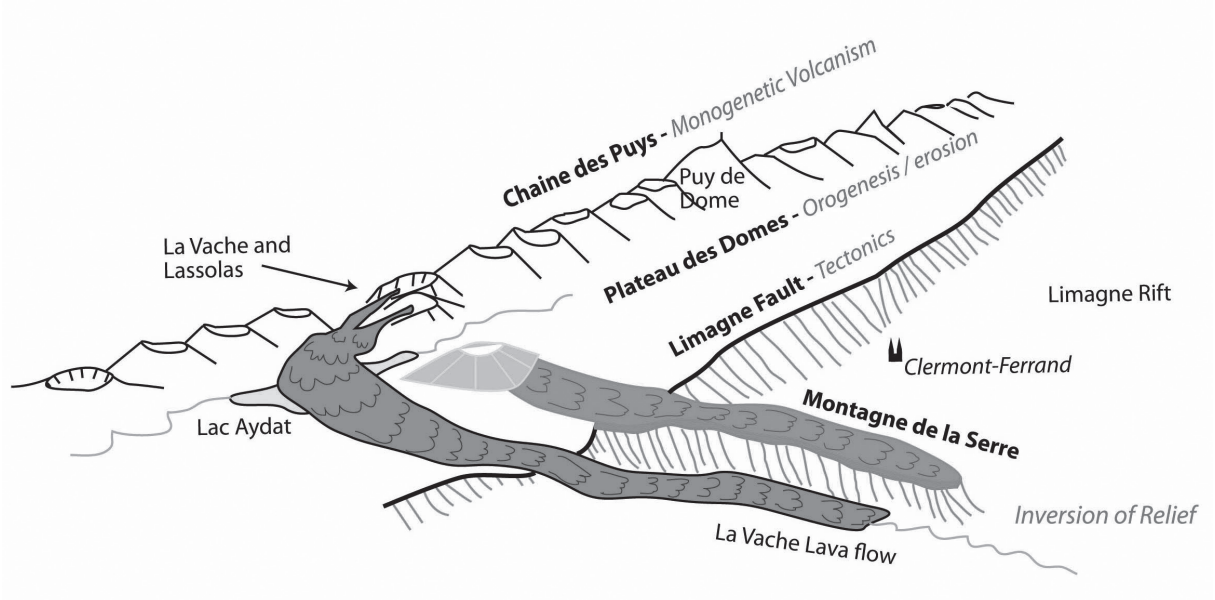

Figure 3. Sketch showing the main features of the Chaine des Puys–Limagne Fault project, where this holistic approach has laid the foundation of the tectonic , volcanic, and geomorphological context. The fault represents the main tectonic element linking to the Western European Rift—one of the two main mountain-related rifts of the world (Merle 2011). The plateau des domes is the basement of a former orogen. The parallel monogenetic alignment, links to the fault and provides a full range of volcanic types. The inverted relief provides anchors the fault and volcanic evolution in geological time.

Active Seabed Swelling and Mantle Degassing Processes: The Dynamics of Sprouting Volcanism in Coastal Areas

Guido Ventura[1,2,*], Salvatore Passaro[2], Stella Tamburrino[2], Mattia Vallefuoco[2], Franco Tassi[3,4], Orlando Vaselli[3,4], Luciano Giannini[3,4], Giovanni Chiodini[5], Stefano Caliro[6], Marco Sacchi[2], and Andrea Luca Rizzo[7]

[1]*Istituto Nazionale di Geofisica e Vulcanologia, Roma, Italy*
[2]*Istituto per l'Ambiente Marino Costiero, Consiglio Nazionale delle Ricerche, Naples, Italy*
[3]*Dipartimento di Scienze della Terra, Università di Firenze, Florence, Italy*
[4]*Istituto di Geoscienze e Georisorse, Consiglio Nazionale delle Ricerche, Florence, Italy*
[5]*Istituto Nazionale di Geofisica e Vulcanologia, Bologna, Italy*
[6]*Istituto Nazionale di Geofisica e Vulcanologia - Osservatorio Vesuviano, Naples, Italy*
[7]*Istituto Nazionale di Geofisica e Vulcanologia, Palermo, Italy*
*Corresponding author E-mail: guido.ventura@ingv.it

Keywords: seabed morphology and deformation, active degassing, unrest

The occurrence of submarine hydrothermal discharges in coastal areas implies a heat source (magma reservoir) within the continental crust and/or the mantle. These discharges may precede magma upraising through the uppermost level of the crust and, ultimately, eruptions and emplacement of volcanic seamounts (Jamtveit et al., 2004). Therefore, the recognition of (a) morphologies related to active deformation of the seabed and (b) gas emissions near densely inhabited coastal is of primary importance for an evaluation of possible volcanic eruptions at shallow depth.

Here, we present new bathymetric, seismic, water column, and geochemical data on a submerged, morphologically and structurally complex area affected by gas emissions located in the Gulf of Naples (Southern Italy), about 5 km offshore from Naples (about 1 million inhabitants).

The Digital Seafloor Model shows that the seabed south of the harbor of Naples is characterized by a 5.0 × 5.3 km uplift structure, locally known as Banco della Montagna (BdM) (Figures 1a and b). BdM develops between about 100 and 170 m depth and it is 15–20 m higher than the surrounding seafloor. The seabed shows a hummocky morphology due to 280 subcircular to elliptical mounds, 665 cones, and 30 pockmarks. The circularity [$C = 4\pi(\text{area}/\text{perimeter}^2)$] of the mounds decreases as the perimeter increases and their axial ratio (AR) ranges between 1 and 6.5 (Figure 2). Elongated mounds show a preferred N45°E ±15° strike and a second-order N145°E strike. We recognize 37 gas emissions from echo-sounder images and direct observations. The acoustic anomalies show vertically elongated shapes upraising from the seafloor sometimes arranged in "trains." The pH values above the discharge sites show a drop indicating local more acidic conditions. This testifies the involvement of acid fluids associated to the BdM degassing process.

The composition of the discharged gas is largely dominated by CO_2 with relevant concentrations of H_2S.

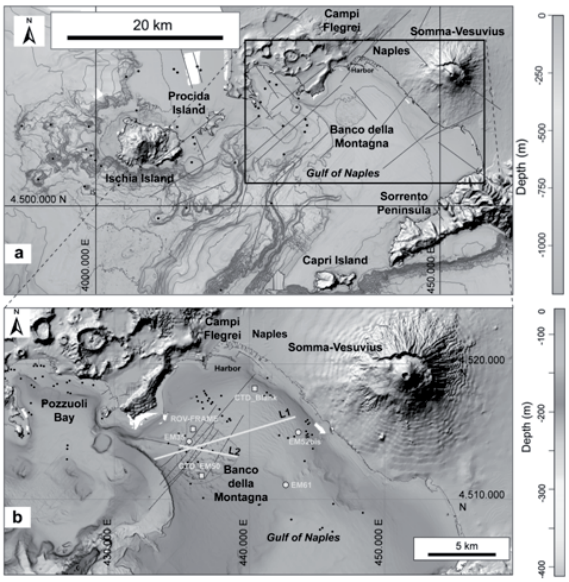

Figure 1. (a) Morphological and structural arrangement of the continental shelf and Gulf of Naples. (b) Bathymetry of the Gulf of Naples with the fluid vents (dots) and the trace of the seismic lines L1 and L2 reported in Figure 3.

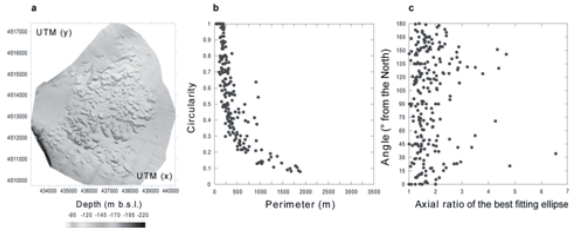

Figure 2. (a) Digital Seabed Model of BdM. (b) Perimeter versus circularity of the mounds. (c) Axial ratio versus angle (orientation) of the major axis of the best fitting ellipses encircling the mounds.

The R/Ra values indicate the presence of a significant fraction of mantle He. In the $CO_2/^3He$ versus $\delta^{13}C$ of CO_2 plot the BdM samples fall on the mantle-crust mixing line depicted by the neighbor active volcanoes of Ischia, Vesuvius, and Campi Flegrei (Figure 3).

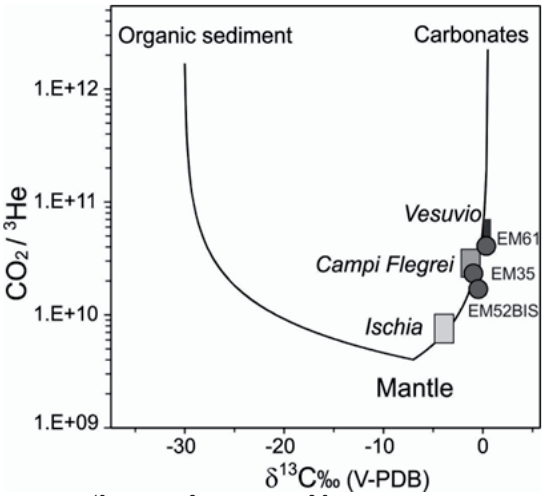

Figure 3. $\delta^{13}C$ of CO^2 versus $CO^2/^3He$ plot of the sampled gas (dots). The mixing lines between a mantle composition and the limestone and organic sediment and the composition of the Campanian volcanoes fumaroles are reported for comparison.

Seismic profiles crossing BdM (Figure 4) show that the seabed is characterized by two main layers: (a) the uppermost one with subparallel reflectors and lateral continuity; (b) the underlying layer shows a chaotic to transparent facies (mixed sediments and gas) with a columnar or hourglass shape, i.e., "pagodas." The top of this layer form the seabed mounds. Gravity cores collected on mounds show that the uppermost 40 cm consist of actual sands; the underlying succession is made up of these sands chaotically mixed with pumice fragments of the 12 ka old deposits of Campi Flegrei eruptions. The pagoda-like geometry testifies the intrusion of 12 ka old material in the uppermost, actual deposits. As for hydrate systems, the gas upraising is responsible for the formation of folds and faults affecting the sea bottom. Gas pressurization at depth is likely responsible for the formation of the km-scale BdM uplift. We applied a thin-plate mechanical model assuming that BdM is a circular thin plate. By selecting appropriate parameters, we obtain the pressure required for the uplift, which is 0.3 Pa, a value consistent with that estimated for seafloor doming processes in gas-hydrate basins (Barry et al., 2012). The buoyancy-controlled uprising of "pagodas" allows us to estimate the gas column height and the pressure required for the seafloor breaching. We obtain a gas column height of 245 m, and a pressure of 2.4 MPa, which accounts for the overpressure to form degassing vents. We conclude that a 25 km^2 wide uplift-like structure affected by active, mantle degassing processes and resulting from the emplacement of pagodas and mounds occurs in the Gulf of Naples few kilometers offshore from the harbor of Naples.

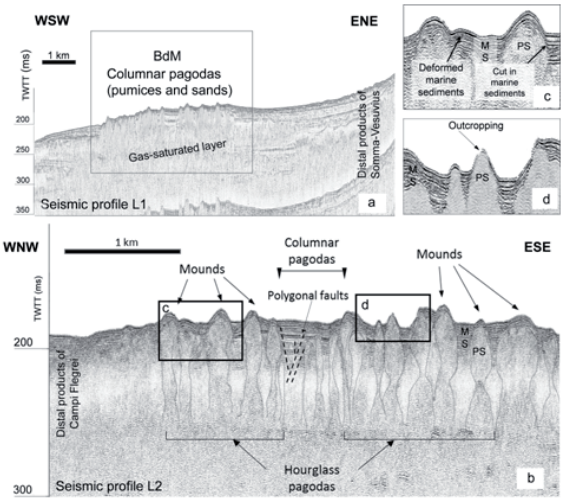

Figure 4. Mono-channel seismic profiles L1 (a) and L2 (b) (tracks in Figure 1b) showing the spatial arrangement of columnar shapes (pagodas); (c) and (d) detail of the deformations reported in (b).

At the present, the BdM features indicate a nonmagmatic unrest potentially foregoing embryonic volcanism, i.e., the early emission of magma and/or hot fluids. A monitoring activity should be implemented with the aim to analyze the evolution of the phenomena and detect the geochemical and geophysical signals indicative of a potential magmatic unrest.

Acknowledgments

We thank the *R/V Urania* crewmembers for the active collaboration and help.

References

Jamtveit, B., Svensen, H., Podladchikov, Y.Y., Planke, S., 2004. Hydrothermal vent complexes associated with sill intrusions in sedimentary basins. Journal Geological Society London 234: 233–241.

Barry, M.A., Bernard, B.P., Johnson, B.D., 2012. Gas domes in soft cohesive sediments. Geology 40: 379–382.

Passaro, S., et al., 2016. Seafloor doming driven by degassing processes unveils sprouting volcanism in coastal areas. Scientific Reports: 22448; doi:10.1038/srep22448.

How Empirical Models of Volcanic Eruption Features Depend on a Maar Record

Han-Fei Wang[1,*], Cheng-Zhi Wu[2], Song Sun[3], Wen-Hua Wang[3], and Jian Yi[3]

[1]*Departmemt of Computer Science and Technology, Nanjing University, Najing, China*
[2]*Monitoring Station of the Changbaishan-Tianchi Volcano, Earthquake Administration of Jilin Province, Erdaobaihe, China*
[3]*College of Earth Sciences, Jilin University, Changchun, China*
*Corresponding author E-mail: 17790005276@163.com

Keywords: Changbaishan-Tianchi volcano, models on eruption parameters, maar deposits

One of the widely used methods for determining bulk volumes of fallout deposits is using the observed (or inferred) relations (exponential decay) of thickness (T) with isopach area (A) and integrating under the lines of Ln T versus $\sqrt{A}$. These methods are dependent on accurate measurement data (or assumption) to extrapolate values of $\sqrt{A}$ as T approaches 0. In other words, the final results are extremely sentive to the critical margin values of the volcanic fall-out area.

Pyle (1989) proposed a widely used eruption volume estimation method by assuming segmentary exponential distribution of tephra thickness (T) over squire root of area $\sqrt{A}$. The tephra volume is calculated by integrating this formula over isopach area. Recently Bonadonna (2013) refactor Pyle's method and proposed his own empirical model by assuming Weilbull distribution of thickness over squire root of area $T = \theta_{th} \cdot \left(\frac{k}{\lambda_{th}} \right)^{n_{th}-2} \cdot \exp\left(- \left(\frac{k}{\lambda_{th}} \right)^{n_{th}} \right)$, and the tephra volume is calculated as $T = \int \theta_{th} \cdot \left(\frac{k}{\lambda_{th}} \right)^{n_{th}-2} \cdot \exp\left(- \left(\frac{k}{\lambda_{th}} \right)^{n_{th}} \right) dk^2$, where k refers to the squire root of isopach area. Both of these methods are based on thickness-areal relationship and sensitive to tephra thickness data, especially when T is small. Thus, the reliability of the field work data, reasonable assumption, and insightful understanding of these data are all necessary and crucial.

According to the previous studies of the Great Millennium eruption of Changbaishan-Tianchi volcano (also known as Baitoushan volcano), the western border is believed to be 40–60 km away from the ejecta vent, because no volcanic fall-out evidence is recognized further west to this outreach. While volcanic ash is found as far as 1400 km east to the volcanic vent across the Japan Sea and in the lakes of Japan islands (Machida and Arai 1983), the highly distorted shape of isopach was explained by the strong winds of winter monsoon. However, new discoveries in Sihailongwan Longgang Maar by Guo et al. (2005) and Sun et al. (2015) indicate that 120 km west to the vent, there are still volcanic ash deposits up to 2.5 cm in thickness from the Great Millennium eruption of Changbaishan-Tianchi volcano which suggest a much greater extension around the western margin of the volcanic area. This evidence is important for the volume estimation in two aspects.

First, this evidence reveals more details of the air fall-out in upwind direction of the Great Millennium eruption of Changbaishan-Tianchi volcano. Therefore, it redefines the western margin of this eruption and thus provides more accurate isopach data which volcanic volume estimation is highly dependent on.

Second, the volcanic fall-out in upwind direction also indicates a potential possibility of discovery of similar evidences in other directions especially in the cross-wind directions, such as north and south. Moreover, for volume estimation, we could safely assume that the northern and southern margin of this eruption could also be much more extended as the western margin has been already proven.

Thus, we rebuild the isopach as Figure 1 shows.

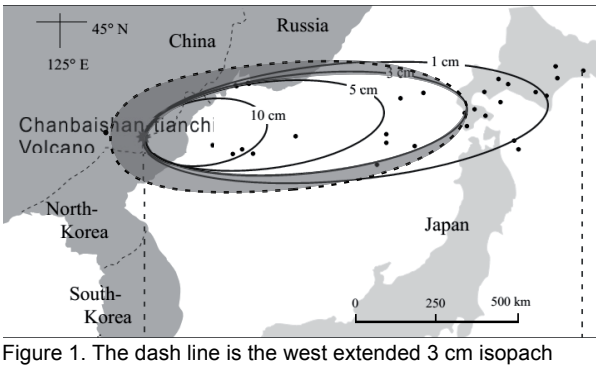

Figure 1. The dash line is the west extended 3 cm isopach line, and the shadow area is the increased area (modified after Horn 2000).

In conclusion, the isopach lines are greatly modified by a single but crucial data in Longgang Maar lake recognized by Guo et al. (2005) and Sun et al. (2015). This increases the final calculation results on the estimation of the eruption volume in a magnitude of about 10 km^3.

For further studies, more data is necessary for building a more accurate isopach. Although the new evidence makes the models improve a lot, it still needs more maar data to build a concrete and detailed isopach based preferably on direct coring and borehole collections.

References

Bonadonna Costanza, Costa Antonio (2013) Plume height, volume, and classification of explosive volcaniceruptions based on the Weibull function. Bull. Volcanol. 75: 742–760.

Guo, Z., Liu, J., Fan, Q., He, H., Sui, S., Chu, G., Liu, Q., Negendank, J.F.W. (2005) Source ofvolcanic ash in the sediments of Sihailongwan maar, NE China, and its significance (in Chinese with English abstract). Acta Petrologica Sinica. 21: 251–255.

Horn, S., Schmincke, H.U. (2000) Volatile emission during the eruption of Baitoushan Volcano (China/North Korea) ca. 969 AD. Bull. Volcanol. 61: 537–555.

Machida, H., Arai, F. (1983) Extensive ash falls in and around theSea of Japan from large late Quarternary eruptions. J. Volcanol. Geotherm. Res. 18: 151–164.

Pyle, D. (1989) The thickness, volume, and grainsize of tephrafall deposits. Bull. Volcanol. 51: 1–15.

Chunqing, S., Haitao, Y., Huaiyu, H., Lei, Z., Jinliang, G., Wenfeng, G., Shuangshuang, C., Qian, M., Qiang, L., Guoqiang, C., Jiaqi, L. (2015) New evidence for the presence of ChangbaishanMillennium eruption ash in the Longgang Volcanic Field, Northeast China. Gondwana Res. 28(1): 52–60.

New Evidence of Vegetation Change in Northeast China of Late Glacial Based on the stomata Record from Lake Moon

Jing Wu*, Qiang Liu, Luo Wang, Guoqiang Chu, and Jiaqi Liu

Key Laboratory of Cenozoic Geology and Environment, Institute of Geology and Geophysics, Chinese Academy of Sciences, Beijing, China
*Corresponding author E-mail: wujing@mail.iggcas.ac.cn

Keywords: crater lake, stomata, climate change

The forest zone system in China includes cold temperate conifer forest, temperate mixed conifer-deciduous forest, warm temperate deciduous forest, subtropical evergreen broadleaf forest, tropical rain forest, and so on (Zhou et al., 2002). Among such resourceful zonal forest types, the current cold-temperate boreal forests dominated by Larix gmelini in the Great Khingan Mountain Region, northeast China is not only one of the most important resources of timber in China (Zhou et al., 2002), but also one of the most significant regions for biomass carbon storage (Fang et al., 2001). Larch forest is well-known for its high volume, biomass and carbon storage, while little information was reported about the evolution history of this forest in China.

The Great Khingan Mountain range is located in the northern boundary of the the East Asian Summer Monsoon (EASM). In biogeography, this area is a boreal-temperate forest transition zone in north-south direction as a reaction of temperature gradient, and a woodland-to-grassland transition zone in east-west direction as a response to monsoonal rainfall extension. The vegetation evolution in the region might be sensitive to the rapid climate changes. It is expected that the vegetation history recorded in this region could capture the regional monsoon variations in response to large climatic changes during the last deglaciation (Wu et al., 2016). Here, we report a high-resolution stomata record from Lake Moon with aims to understand how the regional monsoonal climate responded to the shift in glacial/interglacial modes.

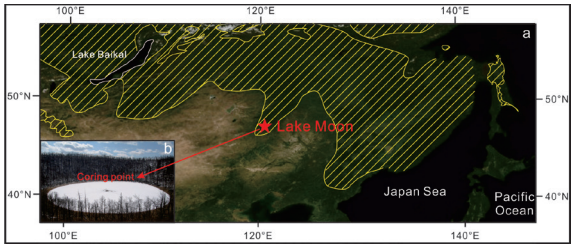

Figure 1. The locations of Lake Moon (a). The yellow shadow shows the region dominated by larch forest and the red arrow points to the location of coring point of Lake Moon (b).

Lake Moon (47°30′N, 120°52′E, 1190 m a.s.l) is one of the crater lakes within the Aershan-Chaihe Volcanic Field, Inner Mongolia, which is almost circular with 220 m diameter.

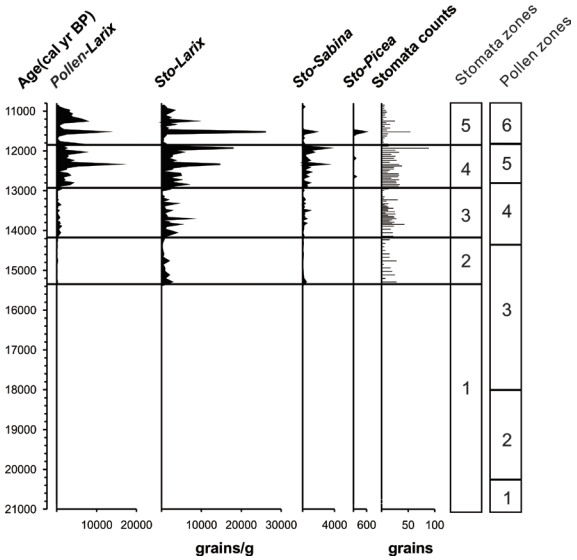

Figure 2. The diagram of *Larix* pollen and stomata concentration from Lake Moon with stomata and pollen zones.

According to the stomata record of Lake Moon, the forest existed since ca. 15.3 ka in study region dominated by *Larix* with a small quantity of *Sabina* and *Picea* (Figure 2). The onset of deglacial warming marked by the appearance of the larch forest at the beginning of the Stomata zone 2 is earlier than Bølling-Allerød (B-A) warm phases occurred at ca. 14.4 ka indicated by the pollen record at the beginning of Pollen zone 3. The finding implies that the index of the stomata maybe more sensitive to mark the existence of the coniferous forest, especially the larch forest, than pollen. The vegetation change from steppe/meadow to forest indicated by the stomata record at ca. 15.3 ka also signifies the local warming in northeast China is possibly earlier than the B-A warm phases according

to the $\delta^{18}O$ values of the ice cores from the Greenland. This onset of the first appearance event of larch forest is more synchronous with the first interstadial event of Lake Suigetsu based on the pollen record started at around 15.0 ka (Nakagawa et al., 2003). The first deglacial warming in East Asia in response to Northern Hemisphere summer insolation is earlier than the B-A warming caused by the intension of EASM linked to the thermohaline circulation of the ocean.

Acknowledgments

We thank Dr. Chunhai Li from Nanjing Institute of Geography and Limnology, Chinese Academy of Sciences on stomata counting. This research was supported by the National Natural Science Foundation of China (41572353; 41272392; 41202259; 41320104006; 41561144010).

References

Zhou, G., Wang, Y., Jiang, Y., Yang, Z. 2002. Estimating biomass and net primary production from forest inventory data: a case study of China's Larix forests. Forest Ecology and Management 169: 149–157.

Fang, J., Chen, A., Peng, C., Zhao, S., Ci, L. 2001. Changes in forest biomass carbon storage in China between 1949 and 1998. Science 292: 2320–2322.

Wu, J., Liu, Q., Wang, L., Chu, G.Q., Liu, J.Q. 2016. Vegetation and climate change during the last deglaciation in the Great Khingan Mountain, Northeastern China. PLoS ONE 11: e0146261.

Nakagawa, T., Kitagawa, H., Yasuda, Y., Tarasov, P.E., Nishida, K., Gotanda, K., Sawai, Y. 2003. Asynchronous climate changes in the North Atlantic and Japan during the last termination. Science 299: 688–691.

500-Year Climate Cycles Stacking of Recent Centennial Warming Documented in an East Asian Pollen Record

Deke Xu[1,2,*], Houyuan Lu[1,2], Guoqiang Chu[1], and Naiqin Wu[1]

[1]*Key Laboratory of Cenozoic Geology and Environment, Institute of Geology and Geophysics, Chinese Academy of Sciences, Beijing, China*
[2]*CAS Center for Excellence in Tibetan Plateau Earth Sciences, Beijing, China*
*Corresponding author E-mail: ccxudeke@mail.iggcas.ac.cn

Keywords: Arctic Oscillation/North Atlantic Oscillation, North Atlantic deep water, total solar irradiance

1. Introduction

Periodic climate changes on multidecadal to multicentennial scales induced by external and internal forcings are of importance not only for understanding the regional climate dynamic but also for assessing the contribution of anthropogenic forcing to the twentieth century warming (Mann et al., 2009; Moberg et al., 2005; Shen et al., 2013). Among these cyclic climate changes, the effect of the multicentennial scale solar variability is less certain. A ~500-year cycle in solar activity, inferred from global atmospheric $^{14}CO_2$ production variation (Stuiver and Braziunas, 1993) might have driven North Atlantic, North Pacific, and North America terrestrial climates (Chapman and Shackleton, 2000; Hu et al., 2003; Stuiver et al., 1995; Yu and Ito, 1999; Zhao et al., 2010). However, it remains to be seen whether this periodic paleoclimate changes is global or regional signals in the Holocene.

Recent studies based on global and regional climate records indicated that the warming of the past century is unprecedented and not relative to natural forcing but anthropogenic forcing (Ahmed et al., 2013; Marcott et al., 2013; Solomon et al., 2007). One of reasons for this controversy rising is that multicentennial periodic variability in regional climate changes in other places of the world, especially in East Asia, is still not well known due to the lack of long-term and high-resolution regional climate proxies. Although some work to date hints of multidecadal- to multicentennial-scale climate changes in East Asia have been revealed by high-resolution stalagmite (Tan et al., 2003; Zhang et al., 2008) and varved maar lake records (Chu et al., 2009), there has been no detailed study of ~500-year periodic climate variability to the extent that we know neither the patterns nor the mechanisms.

2. Site descriptions

Lake Xiaolongwan is located in Longwan National Forest Park at the northwest margin of Changbai Mountain chain of northeast China (Figure 1). The highest peak of Changbai mountain on the Chinese side is 2691 m asl. The climate conditions in the study region are controlled by East Asian monsoon system. Summer monsoon from mid-low latitude ocean brings warm and humid air mass to this region in summer, whereas winter monsoon controlled by Siberia High causes cold and dry climate in winter (Chu et al., 2008; Jiang et al., 2008).

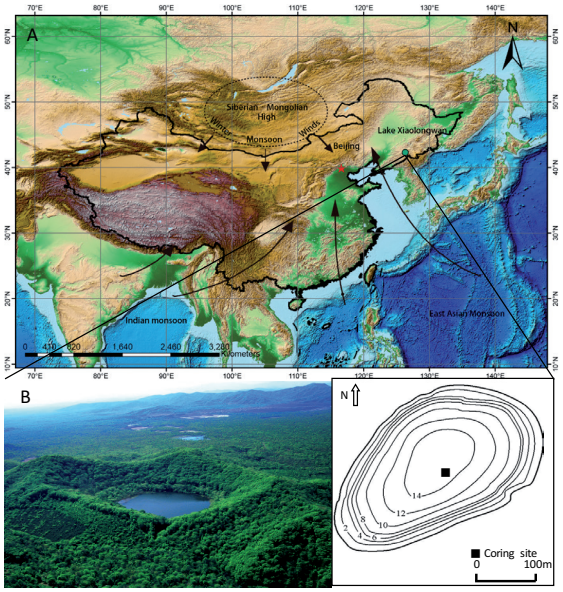

Figure 1. Overview maps of Lake Xiaolongwan showing locations of coring site.

3. Method

Pollen samples of 0.3 ± 0.05 g at 1 cm intervals with average resolution of 20 years from the same split cores were used. This interval was selected for thin section preparation for varve counting to ensure the best temporal correlation between the pollen and varve data. All samples were treated with KOH, HCl, HF, and a hot acetolysis mixture. Pollen preservation and concentration were great and an average sum of 652 (minimum 559, maximum 931) terrestrial pollen grains were counted for every sample. Previous studies using scanning electron and optical microscope, sediment

trap observation, and independent chronology method indicated that the varved sediments were most likely annually laminated (Chu et al., 2008).

In this study, the varve counting result showed that the upper 271 cm of this core contained a maximum of 5350 layers. Six radiocarbon ages were obtained from monospecific samples of bulk and leaf. ^{14}C ages were converted to calendar ages using CALIB 6.1 and IntCal09 data sets (Stuiver et al., 1998). The age model of the core from varve counting was supported by independent chronological control using radio nuclides analyses including ^{137}Cs, ^{210}Pb, and ^{14}C. The results using the two dating methods indicated that the varved maximum age of this core covered the interval from 3340 BC to 2005 AD.

4. Result and disscussion

Pollen percentages of dominant pollen types, such as temperate mixed deciduous and coniferous forest elements [*Pinus, Betula*, *Carpinus*, deciduous *Quercus* (*Quercus* D) and *Ulmus*] and herb taxa (*Artemisia*) showed significant changes from 3340 BC to 2005 AD (Figure 2). Among them, *Pinus*, *Betula*, and *Artemisia* exhibited an increase trend, while *Quercus* D, *Carpinus*, and *Ulmus* showed a decrease trend. Superimposed on these two trends were quasi-periodic changes in pollen percentages of those pollen types.

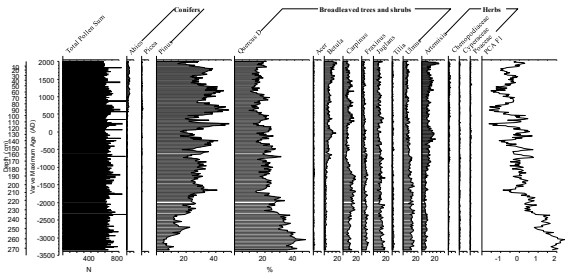

Figure 2. Pollen diagram of key pollen types from core Lake Xiaolongwan.

Pinus is the main component of temperate mixed deciduous and coniferous forest, whereas *Quercus* D is the constructive taxa of the broadleaved deciduous forest (Li et al., 2001; Zhao, 1980). In addition, the mountains within 5 km of the Lake Xiaolongwan, which ranges from ~500 to ~1000 m asl, are covered by temperate broadleaved forest, temperate mixed deciduous and coniferous forest, and their ecotone. Thus, the antiphase fluctuations between *Pinus* and *Quercus* D represent the ratio changes between coniferous and broadleaved plants in the forest community (Li et al., 2008; Sun et al., 2003) and dynamics of vertical vegetation belt in Changbai Mountain region (Herzschuh et al., 2006; Körner, 1998) (Figure 2).

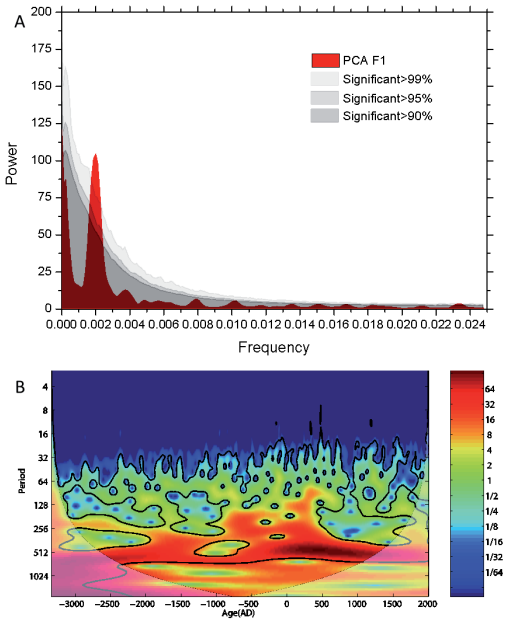

Figure 3. Characteristic PCA F1 periodicities.

A high abundance of *Pinus* and low PCA F1 scores suggest downward of temperate mixed deciduous and coniferous forest and thus cool climatic conditions, whereas a high proportion of *Quercus* D and high PCA F1 imply upward of temperate deciduous forest and thus a warm conditions.

The decreases of *Quercus* D component and PCA F1 (increases of *Pinus* component) indicated the cooling trend during the past 5350 years (Figure 2). In addition, the most striking feature is a series of multicentennial oscillations among *Pinus*, *Quercus* D, and PCA F1 during the cooling trend (Figure 2). *Pinus* component reaches its higher value, while *Quercus* D ratio and PCA F1 value drop to a low level around 2700 BC, 2200 BC, 1600 BC, 1200 BC, 900 BC, 600 BC, 300 BC, 200 AD, 700 AD, 1200 AD, and 1800 AD. Each PCA F1 and *Quercus* D ratio's lower value (*Pinus* higher value) interval is about 500 year. The regular 11 antiphase coupled fluctuations between *Pinus* and *Quercus* D existed throughout the past 5350 years. Furthermore, these oscillations seem rather regular during the past 5350 years.

We performed spectral and wavelet analysis on PCA F1 and spectral analysis on the percentage of *Pinus* and *Quercus* D (Figure 3) to determine their periods and periodic stabilities (Schulz and Mudelsee, 2002; Torrence and Compo, 1998). The spectra of PCA F1 reveal peaks at ~500-year period, significant at the 99% confidence level. The result of the wavelet analysis shows that 500-year quasi-periodic oscillations of PCA F1 are almost completely stable and dominant during the last 5350 years.

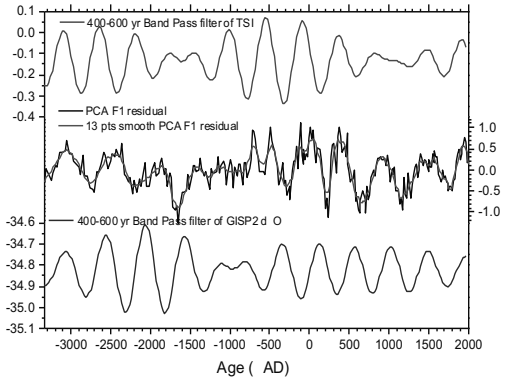

Figure 4. A comparison of climate proxy records from core Lake Xiaolongwan with other proxy records for Total Solar Irradiance and Greenland (GISP2) oxygen isotope ($\delta^{18}O$).

During the last millennia, two warm (800 ~ 1100 AD and 1830 ~ 2005 AD) and one cold (1550 ~ 1830 AD) periods (Figure 4) inferred from PCA F1 are almost in phase with the well-known Medieval Warm Period (MWP), Modern Warm Period (MCP), and Little Ice Age (LIA), respectively (Lamb, 1977). In the MCP, the abrupt rebound of PCA F1 is nearly synchronous with Greenland temperature (Stuiver et al., 1995) and TSI (Steinhilber et al., 2012; Stuiver and Braziunas, 1993) changes, and this warming phase lasts nearly 170 years (Figure 3). This recurrent warm phase would be ended within several decades according to the cyclic climate change in East Asia, if anthropogenic forcing were unconcerned. Thus, the coming of natural-forced ~250-year cooling phase could reduce the anthropogenic warming according to prediction of cyclic climate change in East Asia.

Thus, our study provides evidence for the influence of ~500-year solar variability on climate in East Asia. The solar variability associated with amplified AO/NAO and NADW anomaly could regulate land temperature variation over East Asia and trigger periodic vertical zonal vegetation change in Northeast Asia.

5. Conclusion

Our pollen record shows ~500-year cyclic vegetation and temperature oscillation in East Asia during the last five millennia. This result indicates that ~500-year cyclic climate change over East Asian still exists under anthropogenic forcing during the last century. Recent warm phase, which has lasted about 170 years, is most likely finished in several decades without regard to anthropogenic factors. In addition, this periodic climate change could reduce the man-made warming trend in the next two centennials in East Asia.

Acknowledgments

This study was supported by NSFC (41471166) and NBRPC (2015CB953801).

References

Ahmed, M., Anchukaitis, K.J., Asrat, A., et al., 2013. Continental-scale temperature variability during the past two millennia. Nature Geoscience 6, 339–346.

Chapman, M.R., Shackleton, N.J., 2000. Evidence of 550-year and 1000-year cyclicities in North Atlantic circulation patterns during the Holocene. The Holocene 10, 287–291.

Chu, G., Sun, Q., Rioual, P., et al., 2008. Dinocyst microlaminations and freshwater "red tides" recorded in Lake Xiaolongwan, northeastern China. Journal of Paleolimnology 39, 319–333.

Chu, G., Sun, Q., Wang, X., et al., 2009. A 1600 year multiproxy record of paleoclimatic change from varved sediments in Lake Xiaolongwan, northeastern China. Journal of Geophysical Research 114, D22108.

Herzschuh, U., Kürschner, H., Mischke, S., 2006. Temperature variability and vertical vegetation belt shifts during the last □50,000 yr in the Qilian Mountains (NE margin of the Tibetan Plateau, China). Quaternary Research 66, 133–146.

Hu, F.S., Kaufman, D., Yoneji, S., et al., 2003. Cyclic variation and solar forcing of Holocene climate in the Alaskan Subarctic. Science 301, 1890–1893.

Jiang, W., Leroy, S.A.G., Ogle, N., et al., 2008. Natural and anthropogenic forest fires recorded in the Holocene pollen record from a Jinchuan peat bog, northeastern China. Palaeogeography, Palaeoclimatology, Palaeoecology 261, 47–57.

Körner, C., 1998. A re-assessment of high elevation treeline positions and their explanation. Oecologia 115, 445–459.

Lamb, H.H., 1977. Climate history and the future. William Clowes & Sons Ltd, Methuen.

Li, J., Wu, B., Sheng, L., 2001. Jilin vegetation. Jilin Science Press, Changchun.

Li, Y., Xu, Q., Cao, X., et al., 2008. Pollen influx and surface pollen assemblage on the northern slope of Taibai Mountain. Geographical Research 27, 536–546.

Mann, M.E., Zhang, Z., Rutherford, S., et al., 2009. Global signatures and dynamical origins of the Little Ice Age and Medieval Climate anomaly. Science 326, 1256–1260.

Marcott, S.A., Shakun, J.D., Clark, P.U., et al., 2013. A reconstruction of regional and global temperature for the past 11,300 years. Science 339, 1198–1201.

Moberg, A., Sonechkin, D.M., Holmgren, K., et al., 2005. Highly variable Northern Hemisphere temperatures reconstructed from low- and high-resolution proxy data. Nature 433, 613–617.

Schulz, M., Mudelsee, M., 2002. REDFIT: estimating red-noise spectra directly from unevenly spaced paleoclimatic time series. Computers & Geosciences 28, 421–426.

Shen, C., Wang, W., Zeng, G., et al., 2013. Rates of global temperature change during the past millennium. Climate Research 57, 11–18.

Solomon, S., Qin, D., Manning, M., et al., 2007. Climate Change 2007 - The Physical Science Basis: Working Group I Contribution to the Fourth Assessment Report of the IPCC. Cambridge University Press, Cambridge.

Steinhilber, F., Abreu, J.A., Beer, J., et al., 2012. 9,400 years of cosmic radiation and solar activity from ice cores and tree rings. Proceedings of the National Academy of Sciences 109, 5967–5971.

Stuiver, M., Braziunas, T.F., 1993. Sun, ocean, climate and atmospheric 14CO2 : an evaluation of causal and spectral relationships. The Holocene 3, 289–305.

Stuiver, M., Grootes, P.M., Braziunas, T.F., 1995. The GISP2 [delta] 18O climate record of the past 16,500 years and the role of the sun, ocean, and volcanoes. Quaternary Research 44, 341–354.

Stuiver, M., Reimer, P.J., Bard, E., et al., 1998. INTCAL98 radiocarbon age calibration, 24,000-0 cal BP. Radiocarbon 40, 1041–1083.

Sun, X., Lou, Y., Tian, J., et al., 2003. Pollen record of surface sediments from vertical forest zones of Changbai Mountain, Northeast China and their relations to the modern vegetation. Acta Botanica Sinica 45, 910–916.

Tan, M., Liu, T., Hou, J., et al., 2003. Cyclic rapid warming on centennial-scale revealed by a 2650-year stalagmite record of warm season temperature. Geophysics Research Letters 30, 1617.

Torrence, C., Compo, G.P., 1998. A practical guide to wavelet analysis. Bulletin of the American Meteorological Society 79, 61–78.

Yu, Z., Ito, E., 1999. Possible solar forcing of century-scale drought frequency in the northern Great Plains. Geology 27, 263–266.

Zhang, P., Cheng, H., Edwards, R.L., et al., 2008. A test of climate, sun, and culture relationships from an 1810-year Chinese cave record. Science 322, 940–942.

Zhao, C., Yu, Z., Ito, E., et al., 2010. Holocene climate trend, variability, and shift documented by lacustrine stable-isotope record in the northeastern United States. Quaternary Science Reviews 29, 1831–1843.

Zhao, D., 1980. Vertical vegetation Zone in Changbai Mountain. China Forestry Publishing House, Beijing.

Geochemical Signatures of the Pinglin Tuff, Western Foothills, Central Taiwan: Constraints on Thinning of Continental Lithosphere before South China Sea Spreading

Mengming Yu[1,2,*], Chi-Yue Huang[1,3], Yi Yan[1], and Qing Lan[4]

[1]*Key Laboratory of Marginal Sea Geology, Guangzhou Institute of Geochemistry, Chinese Academy of Sciences, Guangzhou, China*
[2]*University of Chinese Academy of Sciences, Beijing, China*
[3]*Department of Earth Sciences, National Cheng Kung University, Tainan, Taiwan, Republic of China*
[4]*State Key Laboratory of Ore Deposits Geochemistry, Institute of Geochemistry, Chinese Academy of Sciences, Guiyang, China*
*Corresponding author E-mail: yumm@gig.ac.cn

Keywords: continental extension, initial seafloor spreading, South China Sea

The South China continental margin (SCCM) were progressively attenuated by developing series of pre-Oligocene rift basins, such as the Sanshui, Lianping, Heyuan, and Pearl River Mouth, and eventually seafloor spreading of the South China Sea (SCS) during the Oligocene and Early Miocene (Holloway, 1982; Taylor and Hayes, 1983). This attenuated process has also been witnessed by Cenozoic intraplate volcanism in the SCCM, which characteized by the Eocene IAT-like volcanic rocks had been nearly replaced by the pervading Miocene to Pliocene OIB-like basalts (Zhu et al., 2004; Wang et al., 2012; Huang et al., 2013c). Since there was an Oligocene magmatic quiescence in the SCCM (Zhu et al., 2004; Huang et al., 2013c), the SCS seafloor spreading during ~32–16 Ma probably have drained mantle melts of ancient metasomatized mantle origin that formed those Eocene IAT-like volcanic rocks (Huang et al., 2013c). However, until now lifespan of this ancient metasomatized mantle and especially its contribution to magma that crystallized ocean crust of the SCS is unclear. Since the Site U1435 of the IODP Expedition 349 failed to core old lavas of the SCS, volcanisms developed near the continent-ocean transition zone and erupted during the transition from rifting to early seafloor spreading stage of the SCS, which could act as great candidates.

The Pinglin tuff, which originally deposited on the continental slope basin and currently outcropped in the Western Foothills of central Taiwan, is uncomfortably overlain by the postrift sedimentary units of the SCS (Huang et al., 2012, 2013a, b; Lan et al., 2014). It may record a last volcanism before initial seafloor spreading. Here we report major trace elements and Sr-Nd-Pb isotopes data of tuff samples from the top of the Pinglin tuff layer, and then compare them with Eocene IAT-like intraplate volcanic rocks outcropped in Guangdong (Huang et al., 2013c), Taiwan Strait, and western Taiwan (Wang et al., 2012) to discuss mantle evolution before seafloor spreading of the SCS. The Pinglin tuff is grayish green and reddish brown in color, it shows fine-grained porphyritic texture, and contains glauconite grains. In the TAS plot, the PL-1 and PL-2 locate in the andesite area, whereas the PL-4 and PL-5 fall in dacite region after LOI corrected due to high LOI contents (5.67–9.81 wt.%). All show LREEs enrichment ($(La/Sm)_N$ = 1.8–4.3) and flat HREE pattern ($(Gd/Yb)_N$ = 1.0–1.2) after Chondrite is normalized. However, later two dacites display negative Eu abnormality, and the PL-2 apparently has low content REEs than others. In the incompatible elements pattern, all show LILEs enrichment and obviously negative Nb, Ta, and Ti abnormalities, and exhibit typical arc-like characteristics. Moreover, though part of them show distinct major and trace elements characteristics, Sr-Nd-Pb isotopes of all are relatively uniform with $^{87}Sr/^{86}Sr$ = 0.70620–0.70851, $^{143}Nd/^{144}$ Nd = 0.51261–0.51277, $^{206}Pb/^{204}Pb$ = 18.430–18.446, $^{207}Pb/^{204}Pb$ = 15.607–15.614, and $^{208}Pb/^{204}Pb$ = 38.634–38.661. Comparatively, Pb isotopic compositions are more uniform than Sr and Nd isotopes, which indicate the Pinglin tuff in this study share the same mantle source (Figure 1).

When comparing the Pinglin tuff with the Eocene IAT-like intraplate volcanic rocks exposed in Guangdong (Huang et al., 2013c), Taiwan Strait, and western Taiwan (Wang et al., 2012), it shows that they have the same trace element signatures. Moreover, Sr-Nd-Pb isotopes of the Pinglin tuff locate in the mantle evolution trend line defined by Eocene IAT-like and Miocene OIB-like intraplate volcanic rocks end members of the SCCM (Figure 1). All these features show the Pinglin tuff are congenic with Eocene IAT-like intraplate volcanic rocks exposed along the SCCM, which are generated by ancient metasomatized mantle source (Wang et al., 2012; Huang et al., 2013c). Since the Pinglin tuff is uncomfortably overlain by the SCS breakup-unconformity that represents initial seafloor

spreading (Huang et al., 2012, 2013a, b; Lan et al., 2014), it recorded magma characters of thinning of continental lithosphere nearly at initial seafloor spreading. Thus, we propose the ancient metasomatized mantle source beneath the SCCM was still alive nearly at initial seafloor spreading. And the SCS ocean crust crystallized during initial seafloor spreading stage may inherit IAT-like geochemical signatures.

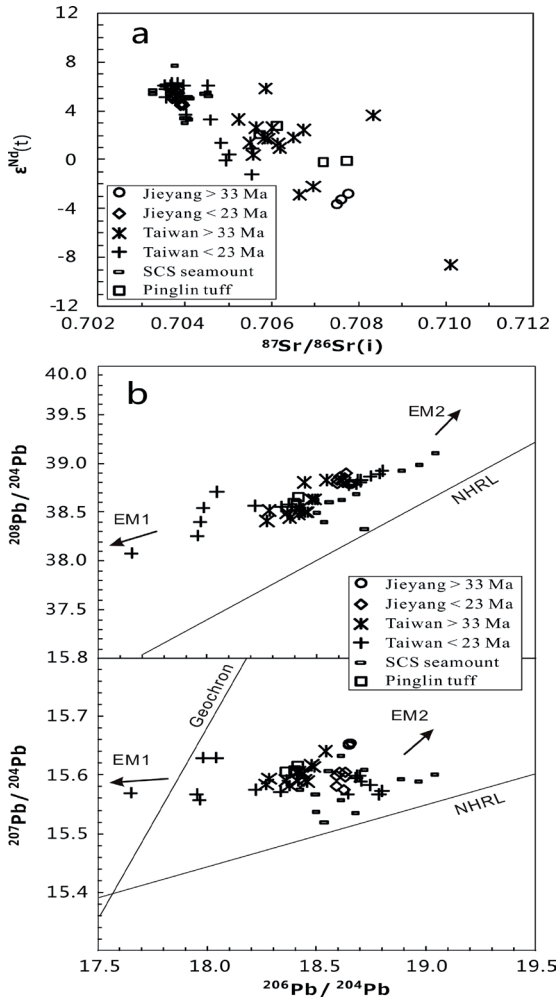

Figure 1. (a) Variation of $^{87}Sr/^{86}Sr$ - $\varepsilon_{Nd}(t)$; (b) $^{207}Pb/^{204}Pb$ and $^{208}Pb/^{204}Pb$ versus $^{206}Pb/^{204}Pb$ for the Pinglin tuff from central Taiwan. Data for the Jieyang volcanic rocks are from Huang et al. (2013c), the Taiwan basalts data cite from Wang et al. (2012) and Chung et al. (1995), and the SCS seamount basalts data are from Tu et al. (1992). The EM1, EM2, and NHRL are from Hart (1984).

Acknowledgments

This work is financially support by the National Natural Science Foundation of China (grant 41472093, U1505231, 41476036).

References

Chung, S.L., Jahn, B.M., Chen, S., Lee, T., Chen, C.-H., 1995. Miocene basalts in northwestern Taiwan: Evidence for EM-type mantle sources in the continental lithosphere. Geochimica et Cosmochimica Acta 59: 549–555.

Hart, S.R. 1984. A large-scale isotope anomaly in the southern hemisphere mantle. Nature 309: 753–757.

Holloway, N.H. 1982. North Palawan block, Philippines-Its relation to Asian mainland and role in evolution of South China Sea. AAPG Bulletin 66(9): 1355–1383.

Huang, C.Y., Chi, W.R., Yan, Y., Yang, K.M., Liew, P.M., Wu, M.S., Wu, J.C., Zhang, C. 2013a. The first record of Eocene tuff in a Paleogene rift basin near Nantou, Western Foothills, central Taiwan. Journal of Asian Earth Sciences 69: 3–16.

Huang, C.Y., Yen, Y., Liew, P.M., He, D.J., Chi, W.R., Wu, M.S., Zhao, M. 2013b. Significance of indigenous Eocene larger foraminifera Discocyclina dispansa in Western Foothills, Central Taiwan: A Paleogene marine rift basin in Chinese continental margin. Journal of Asian Earth Sciences 62: 425–437.

Huang, C.Y., Yen, Y., Zhao, Q., Lin, C.T. 2012. Cenozoic stratigraphy of Taiwan: Window into rifting, stratigraphy and paleoceanography of South China Sea. Chinese Science Bulletin 57(24): 3130–3149.

Huang, X.L., Niu, Y., Xu, Y.G., Ma, J.L., Qiu, H.N., Zhong, J.W. 2013c. Geochronology and geochemistry of Cenozoic basalts from eastern Guangdong, SE China: constraints on the lithosphere evolution beneath the northern margin of the South China Sea. Contributions to Mineralogy and Petrology 165(3): 437–455.

Lan, Q., Yan, Y., Huang, C.Y., Clift, P.D., Li, X., Chen, W., Zhang, X., Yu, M. 2014. Tectonics, topography, and river system transition in East Tibet: Insights from the sedimentary record in Taiwan. Geochemistry, Geophysics, Geosystems 15(9): 3658–3674.

Taylor, B., Hayes, D.E. 1983. Origin and history of the South China Sea basin. The Tectonic and Geologic Evolution of Southeast Asian Seas and Islands Part 2: 23–56.

Tu, K., Flower, M.J., Carlson, R.W., Xie, G., Chen, C.Y., Zhang, M., 1992. Magmatism in the South China basin 1. Isotopic and trace-element evidence for an endogenous Dupalmantle component. Chemical Geology 97: 47–63.

Wang, K.L., Chung, S.L., Lo, Y.M., Lo, C.H., Yang, H.J., Shinjo, R., Lee, T.Y., Wu, J.C., Huang, S.T. 2012. Age and geochemical characteristics of Paleogene basalts drilled from western Taiwan: Records of initial rifting at the southeastern Eurasian continental margin. Lithos 155: 426–441.

Zhu, B.Q., Wang, H.F., Chen, Y.W., Chang, X.Y., Hu, Y.G., Xie, J. 2004. Geochronological and geochemical constraint on the Cenozoic extension of Cathaysian lithosphere and tectonic evolution of the border sea basins in East Asia. Journal of Asian Earth Sciences 24(2): 163–175.

Characterizing and Tracing the Dust Sources of Lakes Sihailongwan and Huguang Maar in NE and SE China Over the Past 80 ka

Shikma Zaarur[1,*], Mordechai Stein[1,2], and Yigal Erel[1]

[1]*Institute of Earth Sciences, The Hebrew University of Jerusalem, Jerusalem, Israel*
[2]*Geological Survey of Israel, Jerusalem, Israel*
*Corresponding author E-mail: shikma.zaarur@mail.huji.ac.il

Keywords: maar lakes, dust, paleo-synoptics, Nd-Sr radiogenic isotopes

Desert dust is an important component of the global environmental-climate system; it travels long distances in the atmosphere and settles on Earths' surface. Arid continental regions (e.g., Sahara-Arabia desert belt, Gobi desert), referred to as accumulation basins, are the source of desert dust comprised of fine mineral particles. This dust can be lifted and blown by strong winds and circulate the atmosphere before settling in destination basins. The isotopic signature (e.g., $^{87}Sr/^{86}Sr$, εNd) of the dust source rocks is preserved in the particle and hence can be used to trace the source of the dust (accumulation basin). Because the dust is windblown and circulates the atmosphere, tracing the source provides means to studying past climate and hydrological conditions in the source basin and the paleo-synoptic conditions of dust transport (e.g., Grousset and Biscaye 2005). Deep-sea and lacustrine sediments serve as important archives for dust.

In this study, we analyze sediments from lakes Sihailongwan and Huguang Maar to establish the paleo-synoptic conditions that controlled dust transport from the central Asia deserts to the areas of NE and SE China during the MIS 5/4 transition (~80–70 ka BP), during MIS2 (~30–14ka BP), and during Termination T1 and the MIS2/1 transition (14–9 ka BP).

Sediment cores from the Sihailongwan and Huguang Maar lakes were obtained by the German-Chinese drilling project (Mingram et al. 2004; Zhu et al. 2013), and sediments were collected from around, and the vicinity of Lake Huguang Maar. The cores of these two lakes have been previously dated and their general composition had been characterized (Mingram et al. 2004; Zhu et al. 2013). In this study, we focus on the chemical and isotopic composition of the dust size particles (<70 μm) of the core sediments; our goal is to trace the dust sources.

The grain size distribution of each sediment sample is measured, and the different grain-size fractions are separated accordingly. We measure the chemical and isotopic compositions of the different fractions, as well as analyze their mineralogical composition.

Basalt, tuff, soils, and paleosols from the vicinity of Lake Huguang Maar are used to characterize the local signature and input into the lake sediments. In a previous study, Zhou et al. (2009) published isotopic values for bulk sediments in Lake Huguang Maar; based on their results, they estimated up to ~20% dust input into the lake. We compare the results of our measurements, to the values published by Zhou et al. (2009) (Figure 1). We find an overlap of the values in some of the materials and a hint to a mixing of two end members in the lake sediments; one is the composition of the local volcanic deposits, and the other has higher εNd and $^{87}Sr/^{86}Sr$ values. We additionally identify another distinct group of soils that has an isotopic signature that hints to a loess-like source from the Chinese Loess Plateau and the Tibetan Plateau (Yang et al. 2009).

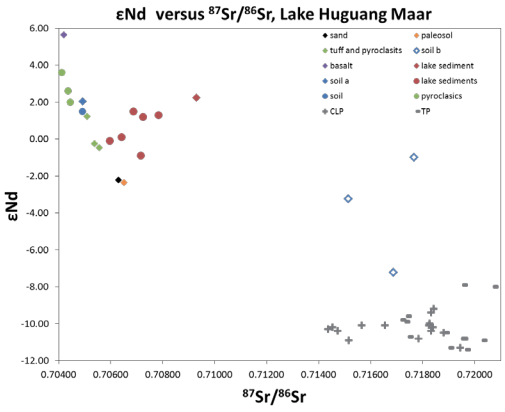

Figure 1. εNd versus $^{87}Sr/^{86}Sr$ of our bulk samples (diamonds) and from Zhou et al. (2009) (circles). The colors correspond to different materials, listed in the legend. Our samples overlap with those of Zhou et al. (2009). Three soil samples collected ~2 km from the lake have isotopic values that are distinct from the rest and might point to an additional endmember. The gray + and – symbols are materials from the Chines Loess Plateau (CLP) and the Tibetan Plateau (TP) (Yang et al. 2009).

Grain size analysis of these samples revealed that while the tuffs and paleosols are bimodal, the soils

and lake surface sediment samples have on average finer particles, and exhibit an additional particle size group at 0.2 μm. We separate these different fractions to characterize the mineralogy, chemistry, and isotopic composition of each group. Characterizing the fractions separately allows us to identify the dust fractions independently from the bulk sediment.

Our isotopic results suggest that there is an aeolian loess component to soils around Lake Huguang Maar. Ultimately, our goal is to use these chemical and isotopic signals on the core sediments to identify the dust sources to these lakes and use it as a tracer to study the paleo-synoptic evolution of the region.

Acknowledgments

We thank Jens Mingram and the GFZ team for their assistance and for providing us the core samples. We thank ISF-CAS 2235/15 for funding this study. We thank J. Liu, G. Chu, J. T. Han, J. Liu, and J. Wu for their help in sampling and discussing the research concept.

References

Grousset, F.E., and Biscaye, P.E. 2005. "Tracing dust sources and transport patterns using Sr, Nd and Pb isotopes." Chemical Geology 222 (3–4), 149–167. doi: 10.1016/j.chemgeo.2005.05.006.

Mingram, J., Schettler, G., Nowaczyk, N., Lou, X., Lu, H., Liu, J., and Negendank, J.F.W. 2004. The Huguang marr lake—a high resolution record of palaeoenvironmental and palaeoclimatic changes over the last 78,000 years from South China. Quaternary International 122, 85–107.

Yang, J., Li, G., Rao, W., and Ji, J. 2009. Isotopic evidences for provenanace of East Asian Dust. Atmospheric Environment 43, 4481–4490.

Zhu, J., Mingram, J., and Brauer, A. 2013. Early Holocene aeolian dust accumulation in northeast China record in varved sedminets from Lake Sihailongwan. Quaternary International 290–291, 299–312.

Zhou, H., Wang, B.-S., Guan, H., Lai, Y.-J., You, C.-F., Wang, J., and Yang, H.-J. 2009. "Constraints from strontium and neodymium isotopic ratios and trace elements on the sources of the sediments in Lake Huguang Maar." Quaternary Research 72(2), 289–300. doi: 10.1016/j.yqres.2009.06.005.

Magma-Derived CO_2 Emissions in the Tengchong Volcanic Field, SE Tibet: Implications for Deep Carbon Cycle at Intracontinent Subduction Zone

Maoliang Zhang[1,2,*], Zhengfu Guo[1], Yuji Sano[3], Lihong Zhang[1], Yutao Sun[1,2], Zhihui Cheng[1,2], and Tsanyao Frank Yang[4]

[1]*Institute of Geology and Geophysics, Chinese Academy of Sciences, Beijing, China*
[2]*University of Chinese Academy of Sciences, Beijing, China*
[3]*Atmosphere and Ocean Research Institute, University of Tokyo, Chiba, Japan*
[4]*Department of Geosciences, National Taiwan University, Taipei, Taiwan*
*Corresponding author E-mail: mlzhang@mail.iggcas.ac.cn

Keywords: soil CO_2 flux, deep carbon cycle, continental subduction zone

Active volcanoes at oceanic subduction zone have long been regard as important pathways for deep carbon degassed from Earth's interior, whereas those at continental subduction zone are poorly constrained. Large-scale active volcanoes, together with significant modern hydrothermal activities, are widely distributed in the Tengchong volcanic field (TVF) on convergent boundary between the Indian and Eurasian plates. They provide an important opportunity for studying deep carbon cycle at the ongoing intracontinent subduction zone. Soil microseepage survey based on accumulation chamber method reveals an average soil CO_2 flux of ca. 280 g m^{-2} d^{-1} in wet season for the Rehai geothermal park (RGP). Combined with average soil CO_2 flux in dry season (ca. 875 g m^{-2} d^{-1}), total soil CO_2 output of the RGP, and adjacent region (ca. 3 km^2) would be about 6.30×10^5 t a^{-1}. Additionally, we conclude that total flux of outgassing CO_2 from the TVF would range in $(4.48-7.05) \times 10^6$ t a^{-1}, if CO_2 fluxes from hot springs and soil in literature are taken into account. Both hot spring and soil gases from the TVF exhibit enrichment in CO_2 (>85%) and remarkable contribution from mantle components, as indicated by their elevated 3He/4He ratios (1.85−5.30 R_A) and $\delta^{13}C$-CO_2 values (−9.00% to −2.07%). He-C isotope coupling model suggests involvement of recycled organic metasediments and limestones from subducted Indian continental lithosphere in formation of the enriched mantle wedge (EMW), which has been recognized as source region of the TVF parental magmas. Contamination by crustal limestone is the first-order control on variations in He-CO_2 systematics of volatiles released by the EMW-derived melts. Depleted mantle and recycled crustal materials from subducted Indian continental lithosphere contribute about 45−85% of the total carbon inventory, while the rest of the carbon (about 15−55%) is accounted by limestones in continental crust. As indicated by origin and evolution of the TVF volatiles, mantle-derived magmas at continental subduction zone can act as important triggers for liberation of carbon stored in crustal carbonate rocks, which has the potential to be a complement to volatile recycling mechanism at subduction zones. Variations in He-Nd-Sr isotopes of magmas and volatiles from different types of plate boundaries suggests higher amounts of recycled materials for mantle wedge enrichment of continental subduction zone relative to that of oceanic subduction zone.

New Evidence for the Yellow River Intrusion into the Huaihe River

Lei Zhang[1,2,*], Xiaoguang Qin[1], and Jiaqi Liu[1]

[1]*Institute of Geology and Geophysics, Chinese Academy of Sciences, Beijing, China*
[2]*University of Chinese Academy of Sciences, Beijing, China*
*Corresponding author E-mail: zhanglei1921@163.com

Keywords: geochemical, provenance, intrusion, Yellow River, Huaibei Plain

The sediments of the Huaibei Plain in semihumid mid-eastern China represent valuable geological records with respect to eolian–fluvial interactions, depositional environments, and climate change in this region (Figure 1). Provenance is often reconstructed using sedimentary geochemistry methods. In this study, an 8-m core from Huainan and a set of loess samples from northern and southern China were analyzed for major, trace, and rare earth elements (REEs). Results were compared to determine the samples' provenance and to discuss the Yellow River intrusion into Huaihe River. The major, trace, rare earth elements contents, and grain size distribution were found to fluctuate widely in the 2–8 m section of the Huainan core and more narrowly closer to the surface (0–2 m). This suggests a provenance shift at a depth of 2 m. The TiO_2/Al_2O_3, SiO_2/Al_2O_3, Th/Nb, La/Nb values, and REE patterns in the upper core (0–2 m) are similar to those found in samples from the Chinese Loess Plateau (CLP) (Figure 2). These results suggest that the CLP in northern China is likely to be the primary origin of the upper part (0–2 m) of the Huainan core. The sediments may have been transported from the CLP to Huainan as Yellow River flood events, probably during the last deglaciation (13.2 ka) as a result of increased precipitation, along with glacier and snow melt in the upper reaches of the Yellow River catchment during this period. This suggests that the Yellow River may have migrated into the Huaihe River catchment much earlier than the earliest historical records (361 BCE) suggest. This result demonstrates that the influence of the Yellow River in the formation and shaping of the Huaibei Plain has been underestimated.

The implications of this would be profound with respect to the Chinese history.

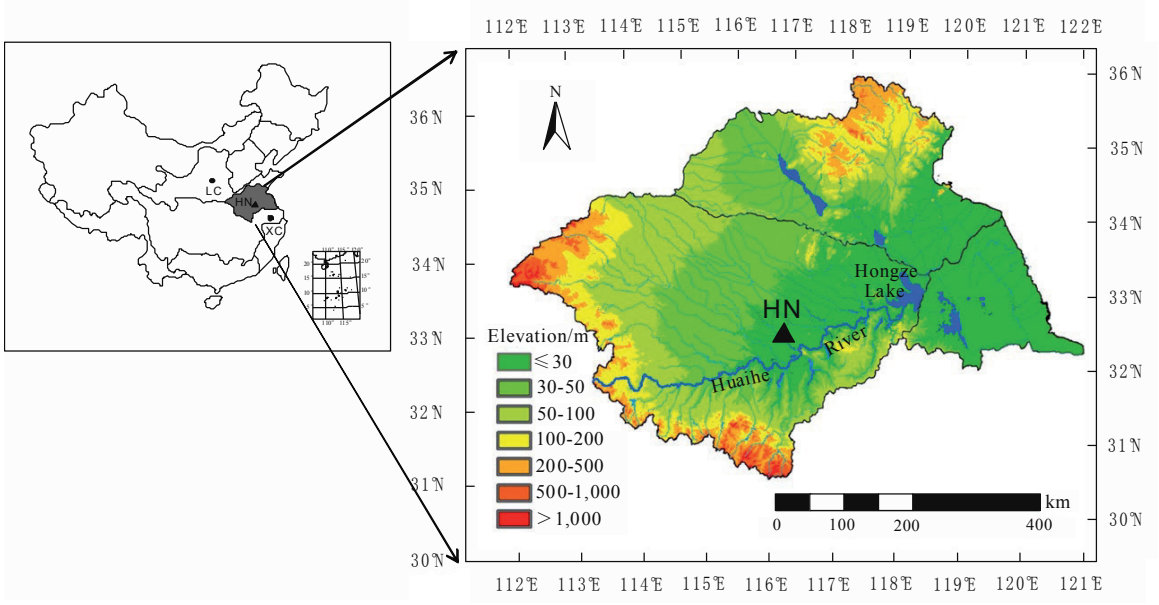

Figure 1. Digital elevation model of the Huaibei Plain. The solid black triangle indicates the core location. LC means Luochuan, XC means Xuancheng.

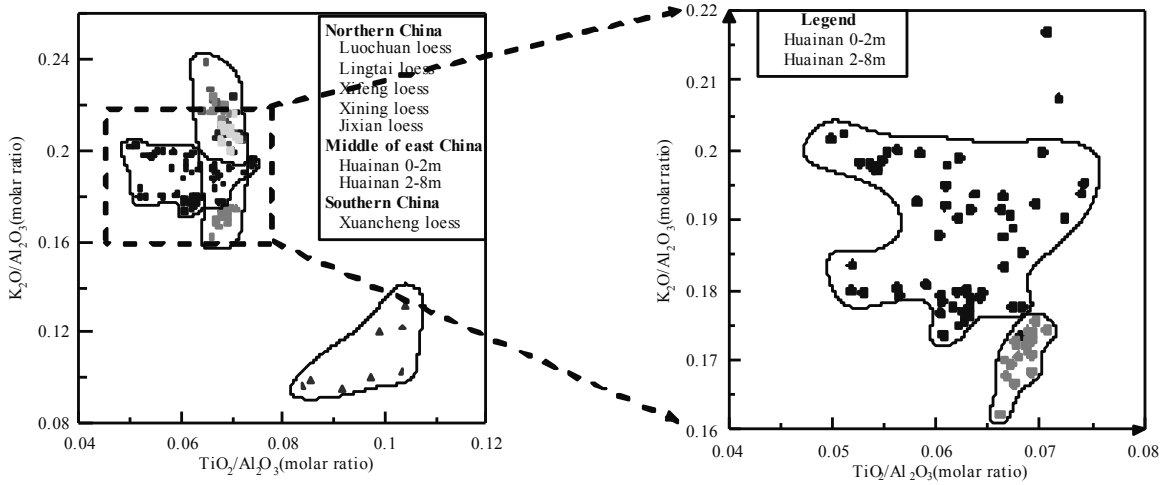

Figure 2. Cross-plots of K_2O/Al_2O_3 versus TiO_2/Al_2O_3 of Huainan core sediments from the Huaibei Plain, and loess from northern and southern China. Data for the Luochuan loess are from Gallet et al. (1996) and Xuancheng and Lingtai loess are from Qiao et al. (2011). Those for the Xining, Xifeng, and Jixian loess are from Jahn et al. (2001).

Acknowledgments

Financial support for this study was provided by the National Scientific Foundation of China (Grant Nos. 41372187, 41172158, 40472094 and 40024202), the Key Consultation Program of the Chinese Academy of Engineering (Study of Environment and Development of the Huaihe River Watershed), 973 Program (Grant No.2010CB950200), the Strategic Priority Research Program of the Chinese Academy of Sciences (Grant No. XDA05120502) and the Knowledge Innovation Program of the Chinese Academy of Sciences (Grant No. KZCX2-YW-Q1-03).

References

Gallet, S., Jahn, B.-M., Torii, M., 1996. Geochemical characterization of the Luochuan loess-paleosol sequence, China, and paleoclimatic implications. Chem. Geol.133, 67–88.

Qiao, Y., Hao, Q., Peng, S., Wang, Y., Li, J., Liu, Z., 2011. Geochemical characteristics of the eolian deposits in southern China, and their implications for provenance and weathering intensity. Palaeogeogr. Palaeoclimatol. Palaeoecol. 308, 513–523.

Jahn, B., Gallet, S., Han, J., 2001. Geochemistry of the Xining, Xifeng and Jixian sections, Loess Plateau of China: eolian dust provenance and paleosol evolution during the last 140 ka. Chem. Geol. 178, 71–94.

Study on C^{14} Age of Dawengquan Volcano in Longgang Volcano Area

Bo Zhao[1,*], Zhida Bai[2], Debin Xu[2], Hongmei Yu[1], Jiandong Xu[1], and Bo Pan[1]

[1]*Institute of Geology, China Earthquake Administration, Beijing, China*zhaobo@ies.ac.cn
[2]*China University of Geoscience, Beijing, China*
*Corresponding author E-mail: zhaobo@ies.ac.cn

Keywords: Dawengquan Maar volcano, C^{14} age, Longgang volcano area

Longgang volcano area is one of the typical monogenetic volcanic fields of Quaternary in China (Wei et al., 1999). Volcanic activities started in Neogene, and got its peak in Pleistocene (Fan et al., 2002; Bai et al., 2006). In AD 460, there was a basaltic explosive eruption (Liu et al., 2009). There are many Maar volcanoes and base-surge deposits, such as Dalongwan (DALW), Erlongwan (ELW), Sanjiaolongwan (SJLW), Sihailongwan (SHLW), Nanlongwan (NLW), Donglongwan (DLW), Longquanlongwan (LQLW), and Dawengquan (DWQ). This paper mainly presents our study of strata and chronology in DWQ volcano.

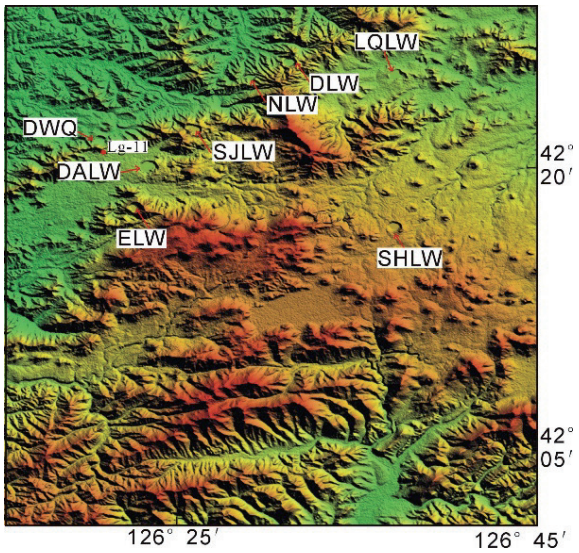

Figure 1. Distribution of Maar volcano in Longgang.

1. Strata of DWQ volcano

DWQ is a low rimmed volcano, which is located in the northeast of Jinchuan town. Characteristics of the volcanic strata near the crater are interlaying with coarse massive layer and fine thin layer in section Lg-11. There are lenticular structure, sag structure, and dune-like structure in base-surge deposits.

Under the base-surge deposits there are scoria. Median diameters (MdΦ) are –2.53. Sorting (σΦ) parameters are 0.95. Characteristics of grain size are moderately sorted. The origin of scoria is still not understood.

2. C^{14} age of DWQ volcano

Carbonized woods were found in both the base-surge deposits and scoria deposits. One age is 15,560 ± 50 BP in the base-surge deposits from DWQ which was tested by Beta laboratory in the United States. The result is close to the age of 15,965 ± 145 BP (Bai et al., 2006; Liu et al., 2009).

The other is 17,120 ± 145 BP in the scoria which was tested by C^{14} laboratory in the institute of Geology, China Earthquake Administration. There are two tephra layers in ELW lake (Liu et al., 2009), which is about 7.6 km away from DWQ. One layer's age is near the 16,997 BP, which is good fit to the age of carbonized woods in scoria.

According to the C^{14} dating result and strata among these volcanoes, volcano activity of this area is frequency in the Late Pleistocene. There are many volcanoes around the DWQ volcano, such as Dalongwan volcano, Sanjiaolongwan volcano, and Jilongdingzi volcano. It may be helpful for building the volcanic succession in this area.

References

Bai Zhi-Da, Xu De-Bing, Zhang Bing-liang, et al. 2006. Study on type and phase of Quaternary explosive volcanism in Longgang volcanic cluster (in Chinese). Acta Petrologica Sinica, 22(6): 1473–1480.

Fan Qi-Cheng, Sui Jian-Li, Liu Ruo-Xin, et al. 2002. Period of quanternary volcanic activity in Longgang area, Jilin Province (in Chinese). Acta Petrologica Sinica, 18 (4): 495–500.

Wei Hai-Quan, Liu Ruo-Xin, Fan Qi-Cheng, et al. 1999. Monogenetic volcanism in longgang volcano clusters(in Chinese). Geological Review, 45 (sup): 325–331.

Liu Jia-Qi, Chu Guo-Qiang, Han Jin-Tai, et al. 2009. Volcanic eruptions in the Longgang volcanic field, northerneastern China, during the past 15000 years. Journal of Asian Earth Sciences, 34: 645–654. doi:10.1016/j.jseaes.2008.09.005

Cenozoic K-Rich Adakitic Volcanic Rocks in the Hohxil Area: Lower-Crust Partial Melting in an Intracontinental Setting

Weigui Zhou*, Yu Guo, Jinwei Feng, Jingzhou Yang, and Baorong Luo

College of Earth Sciences, Chengdu University of Technology, Chengdu, China
*Corresponding author E-mail: zhouwg1990@163.com

Keywords: potassic volcanic rocks, lower crust, partial melting, Cenozoic

It is generally accepted that the Cenozoic potassic volcanic rocks of northern Tibet were derived from a lithospheric mantle source. Cenozoic rocks reported in Gangdisi (south Tibetan Plateau) have received attention because of the apparent absence of a contemporaneous proximal subduction zone. The Gangdisi area was in an arc setting from the Mesozoic to the early Tertiary, and an active collision zone between the Indian and Asian continents exists nearby, others have argued that these adakitic magmas could have originated by partial melting of subducted oceanic crust, involving incorporation of melts from sediments and mantle-wedge components (Qu et al., 2004). Thus, the origin of Cenozoic adakites in southern Tibet remains controversial.

Our study deals with a new adakite locality within the Tibetan Plateau and presents new geochemical and isotopic data to clarify the issue. Unlike the adakitic rocks in the Gangdisi region referred to here, the Cenozoic K-rich adakitic volcanic rocks in the Hohxil area of northern Tibet occur within an intracontinental setting, far removed from an active collision zone or an island-arc zone during the Cenozoic Era. They are geochemically similar to adakites produced by slab melting in subduction zones, except for their high K contents and other geochemical peculiarities discussed herein. A critical issue therefore is whether these Cenozoic rocks represent nonarc adakites, derived by partial melting of amphibolebearing eclogitic rocks in the lower crust. If so, they would be the first documented occurrence of adakitic magmatism not directly associated with subduction of oceanic crust and so would have important implications for models of adakite genesis.

The Tibetan Plateau constitutes a tectonic collage of continental blocks (terranes). From north to south, the three main east-trending continental blocks are Kunlun (Qaidam), Songpan-Ganzi (SG), and Qiangtang, all within the north-central Tibetan region (Figure 1A) (Yin and Harrison, 2000). The SG block, containing the Hohxil area, is bounded by the Anyimaqen-Kunlun-Muztagh suture to the north, and the Jinshajiang suture to the south (Yin and Harrison, 2000). It is generally accepted that suturing of the SG-Kunlun and SG-Qiangtang blocks occurred in pre-Jurassic time (Tapponnier et al., 2001), and consequently the SG and Kunlun blocks have been in an intracontinental setting since the Jurassic. Although volumetrically minor, Cenozoic volcanic rocks are widely distributed in the SG block (Figure 1A). Previous studies indicated that most are potassic to ultrapotassic in composition, and their eruption ages range from ca. 17–15 to 1 Ma (Turner et al., 1996; Zheng et al., 1996; Deng, 1998; Cooperet al., 2002). The K-rich adakitic volcanic rocks discussed here occur in the Hohxil area near the center of the SG block in northern Tibet (Figures 1A and B), and the available data indicate that intermediate to acidic volcanic rocks are dominant in the Hohxil area (Deng, 1998), whereas mafic volcanic rocks are common in the western SG block (Deng, 1998; Cooper et al., 2002).

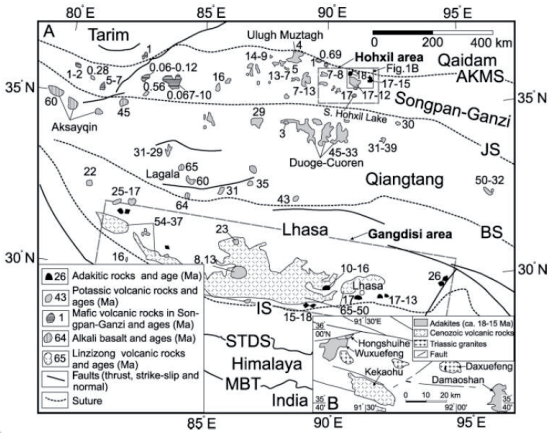

Figure 1. (A) Map of Tibetan Plateau showing major blocks and temporal-spatial distribution of Cenozoic volcanic rocks. (B) Simplified geologic map showing outcrops of magmatic rocks in Hohxil area, Songpan-Ganzi block, northern Tibet.

Our investigations and published data indicate that samples with adakitic compositional features (such as high Sr/Y ratios, high Sr concentrations, and low Y and heavy rare earth element [REE] contents) are confined to three sites (Hongshuihe, Wuxuefeng, and Damaoshan), all in the Hohxil area (Figure 1B). These Cenozoic adakitic volcanic rocks

are exposed either as large-scale lava flows or as small-volume lava domes. The Hongshuihe volcanic dome, for example, has an outcrop area of 2 km^2, whereas the Wuxuefeng and Damaoshan flows crop out over areas of 190 and 150 km^2, respectively. Individual lava flows and domes are typically 30–100 m thick. No Cenozoic basaltic rocks occur in association with the adakitic rocks in the Hohxil area (Figure 1B), but in the southern Hohxil Lake area (Figure 1A), small-volume (<1 km^2) olivine-bearing leucite foidites (SiO_2 = 43–45 wt%) have been discovered (Zheng et al., 1996; Data Repository Table DR2[1]), and dated to ca. 16.47 Ma ($^{40}Ar/^{39}Ar$ plateau age; Table DR1; see footnote 1).

Here, we report new chronological, geochemical, and isotopic data for the Miocene (ca. 18–15 Ma) K-rich adakitic volcanic rocks from the Hohxil area of the Songpan-Ganzi block in northern Tibet. We contend that these rocks were generated by partial melting of the mafic lower crust, in an intracontinental setting unrelated to subduction of oceanic crust.

The Hohxil rocks exhibit high Sr/Y and La/Yb ratios, high Sr and La contents, but low Yb and Y concentrations, similar to adakites formed by slab melting associated with subduction. However, their relatively low εNd values (22.09–24.58); high $^{87}Sr/^{86}Sr$ (0.7072–0.7075), Th/U, Th/Ba, and Rb/Ba ratios; and distinctive potassium enrichments (K_2O > Na_2O) are very different from the composition of typical adakites. In addition, those K-rich adakitic rocks with the highest SiO_2 contents (>61 wt%) exhibit the lowest $^{87}Sr/^{86}Sr$ ratios and highest εNd values and are the oldest Cenozoic volcanic rocks exposed in the Songpan-Ganzi block, suggesting that they were derived neither directly from a mantle source nor by differentiation of a shoshonitic magma. Taking into account the composition of lower-crustal mafic xenoliths in Tibet, as well as the tectonic and geophysical evidence, we conclude that the Hohxil adakitic magmas were produced by partial melting of amphibole-bearing eclogites with a K-rich mafic bulk composition, in the lower part (>55 km) of the thickened northern Tibetan crust. Partial melting of the lower crust may have been triggered by dehydration release of fluids from sedimentary materials in the southward-subducted continental lithosphere.

References

Cooper, K.M., Reid, M.R., Dunbar, N.W., and Mc-Intosh, W.C., 2002, Origin of mafic magmas beneath northwestern Tibet: Constraints from 230Th-238U disequilibria: Geochemistry, Geophysics, Geosystems, 11, 1065, doi: 10.1029/2002GC000332.

Deng, W.M., 1998, Cenozoic intraplate volcanic rocks in the northern Qinghai-Xizang plateau: Beijing, Geologic Publishing House, 180 p.

Qu, X.-M., Hou, Z.-Q., and Li, Y.-G., 2004, Melt components derived from a subducted slab in late orogenic ore-bearing porphyries in the Gangdese copper belt, southern Tibetan plateau: Lithos, 74, 131–148.

Tapponnier, P., Xu, Z.Q., Roger, F., Meyer, B., Arnaud, N., Wittlinger, G., and Yang, J.S., 2001, Oblique stepwise rise and growth of the Tibet plateau: Science, 294, 1671–1677.

Turner, S., Arnaud, N., Liu, J., Rogers, N., Hawkesworth, C., Harris, N., Kelley, S., van Calsteren, P., and Deng, W., 1996, Postcollision, shoshonitic volcanism on the Tibetan plateau: Implications for convective thinning of the lithosphere and the source of ocean island basalts: Journal of Petrology, 37, 45–71.

Yin, A., and Harrison, T.M., 2000, Geologic evolution of the Himalayan-Tibetan orogen: Annual Review of Earth and Planetary Sciences, 28, 211–280.

Zheng, X.S., Bian, Q.T., and Zheng, J.K., 1996, On the Cenozoic volcanic rocks in Hoh Xil district, Qinghai Province: Acta Petrologica Sinica, 12, 530–545.

Maar Lake Sediments and Their Potential for Environmental and Climate Reconstruction: A Global Review

Bernd Zolitschka

Institute of Geography, GEOPOLAR – Geomorphology and Polar Research, University of Bremen, Celsiusstr. Bremen, Germany, zoli@uni-bremen.de

Keywords: lacustrine sediments, crater lakes, maars, varves

During the last 50 years lacustrine sediment records have established as environmental and climatic archives throughout the continents. Although they are present in many different environmental settings, they are distributed irregularly on Earth and mainly occur in landscapes formed by two processes: crater lakes exist in volcanic and tectonically active zones, while glacial lakes predominate in areas under recent or Pleistocene glacial influence. Morphologically, both types of lakes have much in common: they can be rather deep and often are hydrologically closed, i.e., they are terminal lakes. However, differences exist: crater lakes are smaller with a round perimeter and a central deep basin, while glacial lakes are often larger with a complicated morphology and many tributaries. As influences of the (shorter) shoreline and the (smaller) catchment area are reduced, crater lakes provide a simpler depositional basin, which allows for an easier and more straightforward interpretation of their sediment record. Of all crater lakes, the monogenetic "maar" type is the most promising candidate for environmental and climatic reconstruction. Protected by steep and forested crater-wall slopes, these lakes tend to be sheltered against the influence of wind and thus often establish a stable stratification of the water column.

Selected maar lakes with prominent environmental and climatic records are introduced from such diverse regions as western Germany, southern Italy, northeastern China, the North Island of New Zealand, and southern Argentina.

If a maar lake has a rather small surface area with a considerable depth and if the protection from surrounding winds by the crater walls and a closed forest in combination with at least mesotrophic nutrient conditions exists, then the formation of a stratified water column is strongly supported. At least seasonal (holomixis) or even perennial (meromixis) anoxic conditions may establish at the sediment/water interface. Such lakes are ideal candidates for the development of annually laminated sediments (Zolitschka et al., 2015). These varved sediments enable unique and high-resolution analyses to be carried out, because the seasonal depositional signal is not destroyed by bioturbation. Moreover, preservation of varved sediments provides the opportunity to develop a varve chronology. Based on incremental dating it provides ages in calendar years. This internal time control is one of the best dating methods and makes a high-resolution and continuous age/depth relationship available. Finally, such a dataset provides easy access to sedimentation rates and, in combination with dry bulk density, sediment accumulation or flux rates can be calculated.

Today, the meaning of "varve" has expanded to include all annually deposited laminae in terrestrial, i.e., lacustrine (Zolitschka et al., 2015), and marine settings (Schimmelmann et al., 2016). Individual (sub)laminae in varved sediments typically express contrasting colors, differ in terms of their organic (Figure 1), chemical and/or mineralogical composition, and often also with regard to their grainsize. The various climatic and depositional conditions result in clastic, biogenic (Figure 1), and endogenic (evaporitic) varved sediments and their mixtures.

To establish a varve chronology, the annual character of laminations needs to be determined and verified in a multidisciplinary fashion. Sources and influences of possible errors in the varve chronology are best determined and constrained by repeated varve counts and the multiple dating approach, including radioisotopes, combination with tephrochronology (Lane et al., 2015; Wutke et al., 2015), and correlation with historically documented events (Kienel et al., 2013). A well-established varve chronology greatly enhances the scientific value of annually laminated archives by securely anchoring the wealth of multiproxy paleoenvironmental information in the form of a time series in calendar years for reliable multidisciplinary interpretations.

Varved sediment records provide accurate time control for a multitude of environmentally relevant sedimentary parameters and document the frequency and rates of change of annual to millennial climatic and environmental oscillations. Monitoring approaches like sediment trapping additionally provide detailed characterization of

modern sedimentary processes to enhance the reliability of mechanistic models of varve formation. Furthermore, the increasing availability of modern instrumental environmental and meteorological time series aids in rigorous calibration of environmental proxies from a local varve record, assesses statistical error margins, and enhances the validity of interpretations.

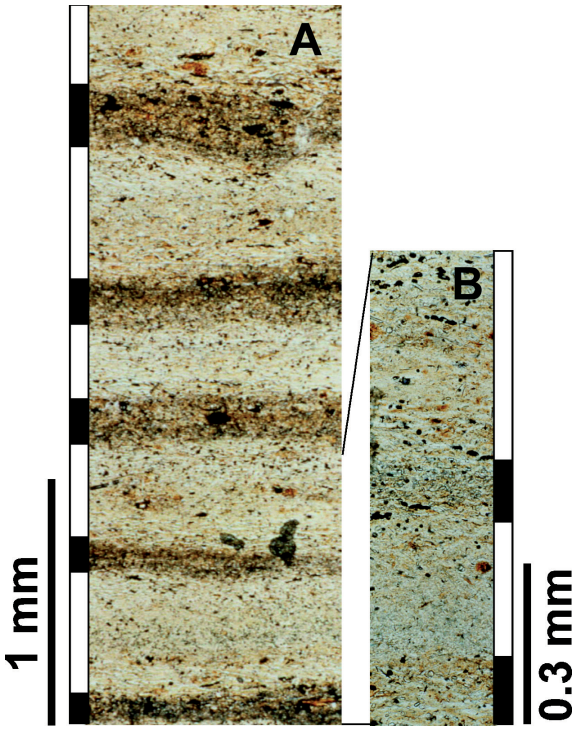

Figure 1. Biogenic varves from Holzmaar, Germany. Macroscopic (A) and microscopic (B) photographies of pale diatom-bloom layers (white bars) and dark organic-rich detritus (black bars). The macroscopic image covers 5 years and the microscopic image covers 2 years (Zolitschka et al., 2015).

Due to their exceptional high temporal resolution and in combination with their accurate "internal" time scale in calendar years, varved sediments are regarded as one of the most precious environmental archives. Records that are necessary to extend temporally limited instrumental climate records back in time and make available high-resolution reconstructions. Such data are necessary to better understand natural climate variations, like, e.g., temperature variations (Chu et al., 2012), the East Asian summer monsoon (Stebich et al., 2015), or the rising level of human impact on environmental systems during the Anthropocene as documented by, e.g., cultural eutrophication (Jenny et al., 2016) and soil erosion (Su et al., 2015).

References

Chu, G., Sun, Q., Wang, X., Liu, M., Lin, Y., Xie, M., Shang, W., Liu, J., 2012. Seasonal temperature variability during the past 1600 years recorded in historical documents and varved lake sediment profiles from northeastern China. The Holocene 22: 785−792. http://dx.doi.org/10.1177/0959683611430413

Jenny, J.-P., Francus, P., Normandeau, A., Lapointe, F., Perga, M.-E., Ojala, A.E.K., Schimmelmann, A., Zolitschka, B., 2016. Global spread of hypoxia in freshwater ecosystems during the last three centuries is caused by rising local human pressure. Global Change Biology 22: 1481–1489. http://dx.doi.org/10.1111/gcb.13193

Kienel, U., Vos, H., Dulski, P., Lücke, A., Moschen, R., Nowaczyk, N.R., Schwab, M.J., 2013. Modification of climate signals by human activities recorded in varved sediments (AD 1608-1942) of Lake Holzmaar (Germany). Journal of Paleolimnology 50: 561–575. http://dx.doi.org/10.1007/s10933-013-9749-z

Lane, C.S., Brauer, A., Martín-Puertas, C., Blockley, S.P.E., Smith, V.C., Tomlinson, E.L., 2015. The Late Quaternary tephrostratigraphy of annually laminated sediments from Meerfelder Maar, Germany. Quaternary Science Reviews 122: 192–206. http://dx.doi.org/10.1016/j.quascirev.2015.05.025

Su, Y., Chu, G., Liu, Q., Jiang, Z., Gao, X., Haberzettl, T. 2015. A 1400 year environmental magnetic record from varved sediments of Lake Xiaolongwan (Northeast China) reflecting natural and anthropogenic soil erosion. Geochemistry, Geophysics, Geosystems 16: 3053–3060. http://dx.doi.org/10.1002/2015GC005880

Schimmelmann, A., Lange, C.B., Schieber, J., Francus, P., Ojala, A.E.K., Zolitschka, B., 2016. Varves in marine sediments: A review. Earth-Science Reviews, in press. http://dx.doi.org/10.1016/j.earscirev.2016.04.009

Stebich, M., Rehfeld, K., Schlütz, F., Tarasov, P.E., Liu, J., Mingram, J., 2015. Holocene vegetation and climate dynamics of NE China based on the pollen record from Sihailongwan Maar Lake. Quaternary Science Reviews 124: 275–289. http://dx.doi.org/10.1016/j.quascirev.2015.07.021

Wutke, K., Wulf, S., Tomlinson, E.L., Hardiman, M., Dulski, P., Luterbacher, J., Brauer, A., 2015. Geochemical properties and environmental impacts of seven Campanian tephra layers deposited between 40 and 38 ka BP in the varved lake sediments of Lago Grande di Monticchio, southern Italy. Quaternary Science Reviews 118: 67–83. http://dx.doi.org/10.1016/j.quascirev.2014.05.017

Zolitschka, B., Francus, P., Ojala, A.E.K., Schimmelmann, A., 2015. Varves in lake sediments – a review. Quaternary Science Reviews 117: 1–41. http://dx.doi.org/10.1016/j.quascirev.2015.03.019

Volcanic, Climatic, and Anthropogenic Forcing Recorded in the Holocene Crater-Lake Sediments of Laguna Azul (Patagonia, Argentina)

Bernd Zolitschka[1,*], Michael Fey[1], Stephanie Janssen[2], Nora I. Maidana[3], Christoph Mayr[4,5], Sabine Wulf[6,7,8], Torsten Haberzettl[9], Hugo Corbella[10], Andreas Lücke[11], Christian Ohlendorf[1], and Frank Schäbitz[2]

[1]*Universität Bremen, Institut für Geographie, GEOPOLAR – Geomorphologie und Polarforschung, Bremen*
[2]*Universität zu Köln, Institute for Geography Education, Köln, Germany*
[3]*Universidad Nacional de Buenos Aires, Departamento de Biodiversidad y Biología Experimental, IBBEA (CONICET-UBA), Buenos Aires, Argentina*
[4]*Ludwig-Maximilians-Universität München, GeoBio-CenterLMU und Department für Geo- und Umweltwissenschaften, München, Germany*
[5]*Friedrich-Alexander-Universität Erlangen-Nürnberg, Institut für Geographie, Erlangen, Germany*
[6]*Helmholtz Zentrum Potsdam, Deutsches GeoForschungsZentrum, Potsdam, Germany*
[7]*Senckenberg Gesellschaft für Naturforschung, Biodiversität und Klima Forschungszentrum (BiK-F), Frankfurt/Main, Germany*
[8]*Institut für Geowissenschaften, Ruprecht-Karls-Universität Heidelberg, Heidelberg, Germany*
[9]*Friedrich-Schiller-Universität Jena, Institut für Geographie, Physische Geographie, Jena, Germany*
[10]*Museo Argentino de Ciencias Naturales Bernardino Rivadavia, Buenos Aires, Argentina*
[11]*Forschungszentrum Jülich, Institut für Bio- und Geowissenschaften, Jülich, Germany*
**Corresponding author E-mail: Germany*zoli@uni-bremen.de

Keywords: Southern Hemispheric Westerlies, lake-level fluctuations, tephra layers

Laguna Azul (Figure 1) is located 25 km N of the Strait of Magellan and 60 km W of the Atlantic Ocean in extra-Andean Southeastern Patagonia, Argentina (52°05' S, 69°35' W). This crater lake is part of the Pliocene to Late Quaternary Pali Aike Volcanic Field. Its volcanism is characterized by the eruption of alkali basaltic and basanitic magmas deposited on molasse-type sediments of the Late-Miocene Santa Cruz Formation and Plio-Pleistocene glaciofluvial sediments (Zolitschka et al., 2006; Ross et al., 2011; Coronato et al., 2013). The main crater exhibits a complex eruptive history of explosive and effusive volcanism with a pyroclastic ring wall of 850 m in diameter. The central depression (Figure 1) of the crater formed by gravitational collapse after phreatomagmatic explosions during an early (maar) stage of the eruption. Later a lava lake filled the depression and extensive magma production caused an overflow through a 30-m wide channel to the N creating proximal "pahoehoe" and distal "aa" lava (Corbella et al., 2009). Dating of the basalt flow related to the overflow of the lava lake resulted in a $^{40}Ar/^{39}Ar$ age of 0.01 ± 0.02 Ma (Corbella, 2002).

In the deepest part of the depression related to the Laguna Azul crater, a lake developed at the Pleistocene/Holocene transition with a maximum present-day water depth of 56 m (Figure 1). It is one of the very few permanent water bodies in the semiarid grass steppe of southeastern Patagonia.

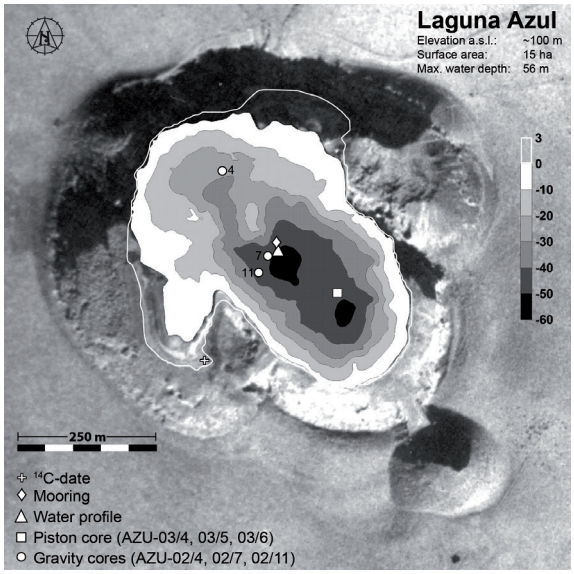

Figure 1. Aerial photography of Laguna Azul in southeastern Patagonia (Province of Santa Cruz, Argentina) with bathymetry, coring, and sampling locations.

Here we present a radiocarbon-dated sediment record from Laguna Azul including sedimentological, physical, and geochemical as well as pollen, diatom, and stable isotope data. The focus is directed to processes of sediment formation and their volcanic, climatic, and anthropogenic forcing factors.

Temperature, precipitation, and wind intensity of southern South America respond to the air-pressure gradient between polar and subtropical southern latitudes, to sea-surface temperatures of adjacent oceans, sea-ice and continental ice masses, as well as the pathway of the Southern Hemispheric Westerlies (SHW, Garreaud et al., 2009; Mayr et al., 2013). The resulting variations of the regional hydrological balance are recorded especially in sediments of closed lakes (Piovano et al., 2009) like Laguna Azul.

Multiproxy limnogeological investigations of the Holocene sediment record from Laguna Azul document a superior climatic control on the lacustrine system, i.e., position and intensity of the SHW. These climatic conditions influence local evaporation, precipitation, and insolation with impacts on the type of stratification of the water column and lake-level fluctuations. Altogether, these climatic influences lead to internal feedbacks on wave erosion along the lakeshore, algal communities, and trophic conditions as well as on authigenic mineral formation. Based on a gravity core with a millennial-long record (Mayr et al., 2005), we continue this interdisciplinary research approach and present a detailed environmental reconstruction documenting hydrological variability during the entire Holocene.

Volcanic influences on the sediments are evidenced by radiocarbon ages that are significantly older than their stratigraphical position would demand. They probably suffer from ^{14}C-depleted carbon as the result of volcanic CO_2 exhalations during the Lateglacial and the early Holocene. Human impact is restricted to the last ca. 150 years when it obscures the climatic signal. Additionally, two volcanic ash layers were detected, geochemically characterized, and identified. Their sources are Mt. Burney and a so far unknown volcano in the Northern Andean Volcanic Zone (NAVZ). These well-documented and well-dated events provide useful knowledge for updating the tephrostratigraphic framework in South America.

Acknowledgments

This is a contribution to the project “South Argentinean Lake Sediment Archives and modeling” (SALSA) funded within the framework of the German Climate Research Program (DEKLIM grants 01 LD 0034 and 0035) of the German Federal Ministry of Education and Research (BMBF). Additional financial support was provided by the German Science Foundation (DFG) in the framework of the Priority Program ‘ICDP’ (grants ZO 102/5-1, 2, 3).

References

Corbella, H., 2002. El campo volcano-tectónico de Pali Aike. In: Haller, M., ed., Geología y Recursos Naturales de Santa Cruz. Asociación Geológica Argentina, Buenos Aires: pp. 285–302.

Corbella, H., Ercolano, B., Tiberi, P., 2009. Laguna Azul: a unique volcanic lagoon in Pali Aike Holocene eruptive terrains, Patagonia Austral, Argentina. In: M.J. Haller, Massaferro, G.I., eds., Third International Maar Conference, 14–17 April 2009. Publicaciones Especiales, Resúmenes y Eventos. Asociación Geológica Argentina, Malargüe, Argentina, pp. 17–18.

Coronato, A., Ercolano, B., Corbella, H., Tiberi, P., 2013. Glacial, fluvial and volcanic landscape evolution in the Laguna Potrok Aike maar area, southernmost Patagonia, Argentina. Quaternary Science Reviews 71, 13–26.

Garreaud, R.D., Vuille, M., Compagnucci, R., Marengo, J., 2009. Present-day South American climate. Palaeogeography, Palaeoclimatology, Palaeoecology 281, 180–195.

Mayr, C., Fey, M., Haberzettl, T., Janssen, S., Lücke, A., Maidana, N.I., Ohlendorf, C., Schäbitz, F., Schleser, G.H., Struck, U., Wille, M., Zolitschka, B., 2005. Palaeoenvironmental changes in southern Patagonia during the last millennium recorded in lake sediments from Laguna Azul (Argentina). Palaeogeography, Palaeoclimatology, Palaeoecology 228: 203–227.

Mayr, C., Lücke, A., Wagner, S., Wissel, H., Ohlendorf, C., Haberzettl, T., Oehlerich, M., Schäbitz, F., Wille, M., Zhu, J., Zolitschka, B., 2013. Intensified Southern Hemisphere Westerlies regulated atmospheric CO_2 during the last deglaciation. Geology 41: 831–834.

Piovano, E.L., Ariztegui, D., Córdoba, F., Cioccale, M., Sylvestre, F., 2009. Hydrological variability in South America below the Tropic of Capricorn (Pampas and Patagonia, Argentina) during the last 13.0 ka. In: Vimeux, F., et al., eds., Past Climate Variability in South America and Surrounding Regions, Developments in Paleoenvironmental Research, 14: 323–351.

Ross, P.-S., Delpit, S., Haller, M.J., Németh, K., Corbella, H., 2011. Influence of the substrate on maar-diatreme volcanoes - an example of a mixed setting from the Pali Aike volcanic field, Argentina. Journal of Volcanology and Geothermal Research 201: 253–271.

Zolitschka, B., Schäbitz, F., Lücke, A., Corbella, H., Ercolano, B., Fey, M., Haberzettl, T., Janssen, S., Maidana, N., Mayr, C., Ohlendorf, C., Oliva, G., Paez, M.M., Schleser, G.H., Soto, J., Tiberi, P., Wille, M., 2006. Crater lakes of the Pali Aike Volcanic Field as key sites for paleoclimatic and paleoecological reconstructions in southern Patagonia, Argentina. Journal of South American Earth Sciences 21: 294–309.

ISBN 978-953-51-2540-2

INTECH
open science | open minds

INTECHOPEN.COM